ÇUKUROVA UNIVERSITY
INSTITUTE OF NATURAL AND APPLIED SCIENCES

PhD THESIS

Ahmet FERTELLİ

AIR-CONDITIONING SYSTEM WITH ICE THERMAL STORAGE

DEPARTMENT OF MECHANICAL ENGINEERING

ADANA, 2008

ÇUKUROVA ÜNİVERSİTESİ
FEN BİLİMLERİ ENSTİTÜSÜ

AIR - CONDITIONING SYSTEM WITH ICE THERMAL STORAGE

Ahmet FERTELLİ

DOKTORA TEZİ

MAKİNA MÜHENDİSLİĞİ ANABİLİM DALI

Bu Tez 14/07/2008 Tarihinde Aşağıdaki Jüri Üyeleri Tarafından Oybirliği/Oyçokluğu İle Kabul Edilmiştir.

İmza: …….....	İmza: ……...	İmza: ……...
Prof. Dr. Orhan BÜYÜKALACA	Prof. Dr.Tuncay YILMAZ	Prof. Dr. R. Tuğrul OĞULATA
DANIŞMAN	ÜYE	ÜYE

İmza: ……..	İmza: ……
Doç.Dr. Ertan BUYRUK	Doç. Dr. Hüseyin AKILLI
ÜYE	ÜYE

Bu Tez Enstitümüz Makina Mühendisliği Anabilim Dalında Hazırlanmıştır.

Kod No:

Prof. Dr. Aziz ERTUNÇ
Enstitü Müdürü

Bu çalışma Çukurova Üniversitesi Bilimsel Araştırma Projeleri Birimi tarafından desteklenmiştir.
Proje No: : MMF2006D31

Not: Bu tezde kullanılan özgün ve başka kaynaktan yapılan bildirişlerin, çizelge, şekil ve fotoğrafların kaynak gösterilmeden kullanımı, 5846 sayılı Fikir ve Sanat Eserleri Kanunundaki hükümlere tabidir

ABSTRACT

PhD THESIS

AIR - CONDITIONING SYSTEM WITH ICE THERMAL STORAGE

Ahmet FERTELLİ

DEPARTMENT OF MECHANICAL ENGINEERING
INSTITUTE OF NATURAL AND APPLIED SCIENCES
UNIVERSITY OF ÇUKUROVA

Supervisor : Prof. Dr. Orhan BÜYÜKALACA

Year : 2008, Pages: 173

Jury : Prof. Dr. Orhan BÜYÜKALACA

Prof. Dr. Tuncay YILMAZ

Prof. Dr. R. Tuğrul OĞULATA

Assoc. Prof. Dr. Ertan BUYRUK

Assoc. Prof. Dr. Hüseyin AKILLI

Performance characteristics of an-air conditioning system based on ice storage to cool a room located in the laboratories of Mechanical Engineering Department of Çukurova University were investigated. First, the behaviour of water during liquid-to-solid phase change process and effect of brine inlet temperature on ice formation inside the ice storage tank were investigated. In the second stage, effects of brine inlet temperature, air temperature at the inlet of the condenser and charging period on performance of the system were analyzed. Discharge experiments were also performed with two automatic control operating strategies.

The results of charging experiments showed that some mechanisms observed during the ice formation are important parameters for the system performance. Therefore, a parallel experimental system was constructed to investigate phase change phenomena around a horizontal tube and experiments were performed at three different brine inlet temperatures. A mathematical model was also developed to calculate the heat transfer process for phase change phenomenon around a horizontal tube.

Keywords: Ice thermal energy storage, phase change, nucleation, ice formation.

ÖZ

DOKTORA TEZİ

BUZ DEPOLAMALI BİR İKLİMLENDİRME SİSTEMİ

Ahmet FERTELLİ

ÇUKUROVA ÜNİVERSİTESİ
FEN BİLİMLERİ ENSTİTÜSÜ
MAKİNA MÜHENDİSLİĞİ ANABİLİM DALI

Danışman : Prof. Dr. Orhan BÜYÜKALACA
Yıl : 2008, Sayfa: 173
Jüri : Prof. Dr. Orhan BÜYÜKALACA
Prof. Dr. Tuncay YILMAZ
Prof. Dr. R. Tuğrul OĞULATA
Doç. Dr. Ertan BUYRUK
Doç. Dr. Hüseyin AKILLI

Bu çalışmada, Çukurova Üniversitesi Makine Mühendisliği Laboratuarlarında bir mahalin soğutulması için kurulan buz depolamalı iklimlendirme sisteminin performans karakteristikleri araştırılmıştır. İlk olarak, faz değişimi esnasında suyun davranışı ve aracı akışkanın depo giriş sıcaklığının buz oluşumuna etkisi araştırılmıştır. İkinci aşamada, depo girişindeki aracı akışkan sıcaklığının, yoğuşturucu girişindeki hava sıcaklığının ve şarj süresinin sistem performansı üzerine etkileri incelenmiştir. Ayrıca, iki farklı otomatik kontrol stratejisi kullanılarak deşarj deneyleri yapılmıştır.

Şarj deneylerinin sonuçları, buz oluşumu esnasında meydana gelen farklı aşamaların sistem performansını etkileyen önemli parametreler olduğunu göstermiştir. Bu nedenle, yatay tek bir boru üzerinde buz oluşumunu incelemek için yeni bir deney düzeneği kurulmuş ve bu deney düzeneği ile üç farklı aracı akışkan giriş sıcaklığında deneyler gerçekleştirilmiştir. Ayrıca boru etrafındaki faz değişimi için bir matematik model geliştirilmiştir.

Anahtar Kelimeler: Buz depolama, faz değişimi, çekirdekleşme, buz oluşumu.

ACKNOWLEDGEMENTS

I am truly grateful to my research supervisor, Prof. Dr. Orhan BÜYÜKALACA, for his encouragement, advice, invaluable guidance, understanding and support throughout the preparation of this thesis and during my graduate education.

Thanks are extended to Prof. Dr.-Ing Tuncay YILMAZ for providing valuable research advice, continuous support, his understanding and motivation during my thesis.

I would like to express my special thanks to Assoc. Prof. Dr. Ertan BUYRUK for his encouragement, help and support.

I also thank my special committee member, Prof. Dr. R. Tuğrul OĞULATA and Assoc. Prof. Dr. Hüseyin AKILLI for their support and many helpful suggestions.

I would also like to express my special thanks to head of the Mechanical Engineering Department of Çukurova University Prof. Dr. Beşir ŞAHIN for his help and support.

In addition, I want to express my sincere appreciation to all research assistants of the Mechanical Engineering Department of Çukurova University for their help, support and motivation, especially research assistants Ertaç HÜRDOĞAN, Arif ÖZBEK and Hasan SERİN. I also want to thank staff of Laboratories of Mechanical Engineering for their help and support, especially technicians Cevdet YILDIRIM and Veysel KAZAZ.

I would like to thank to my research assistant friend Cahit GURLEK for his continuous motivation.

Finally, I want to express my gratitude to my wife Tülay FERTELLİ, my lovely son Berkay FERTELLİ, my mother Bedriye FERTELLİ and my father Hüseyin FERTELLİ, each whom gave support, encouragement and love in my life and made this thesis possible.

TABLE OF CONTENTS **PAGE**

ABSTRACT……..……..... I

ÖZ ……..... II

ACKNOWLEDGEMENTS……...… III

TABLE OF CONTENTS……..... IV

LIST OF TABLES ….……... VI

LIST OF FIGURES…..……..... VII

NOMENCLATURE……..... XV

1. INTRODUCTION…….. 1

2. LITERATURE REVIEW..... 4

2.1. Ice Storage Systems…… 4

2.2. Phase Change of Water Around Tube……..... 13

3. MATERIAL AND METHOD..... 18

3.1. Historical Background……..... 18

3.1.1. Cool Storage and the Electric Utility …….. 20

3.2 Fundamentals of Cool Thermal Energy Storage …… 21

3.2.1. Chilled Water Storage…..……..... 22

3.2.2. Ice Storage…… 24

3.2.2.1. Ice Harvesting Systems…… 25

3.2.2.2. External Melt Ice-on-Coil Storage Systems…. 27

3.2.2.3. Internal Melt Ice-on-Coil Storage Systems….. 29

3.2.2.4. Encapsulated Ice …….. 33

3.2.3. Eutectic Salt Phase-Change Materials…….. 35

3.3. Operating and Control Strategies of CTES Systems…….. 37

3.3.1. Full Storage……... 38

3.3.2. Partial Storage……... 39

3.3.2.1. Partial-Storage Load Leveling Type…….. 39

3.3.2.2. Partial-Storage Demand Limiting Type……... 39

3.4. Experimental Study……. 42

3.4.1. Experimental Setup 1…… 42

3.4.1.1. Air Cooled Chiller…… 47
3.4.1.2. Ice Storage Tank……... 50
3.4.1.3. Air-Conditioned Room……. 52
3.4.1.4. Automatic Control System……... 54
3.4.1.5. Measurements Carried Out With Experimental Setup 1……... 58
3.4.2. Experimental Setup 2…… 61
3.4.2.1. Measurements Carried Out With Experimental Setup 2……... 64
3.4.3. Temperature Measurements…….. 68
3.4.4. Measurement of Brine Flow Rate……. 69
3.4.5. Measurement of Relative Humidity…….. 71
3.4.6. Data Logger System…….. 73
3.5 Mathematical Model for Ice Formation around the Tube……... 74
4. RESULT AND DISCUSSIONS……. 78
4.1. Results Obtained from Experimental Setup 1……. 78
4.1.1. Charging Tests…….. 78
4.1.2. Phase Change of Water……. 83
4.1.3. Nucleation Temperature and Nucleation Time……. 89
4.1.4. Effect of Brine Inlet Temperature on Phase Change of Water……. 97
4.1.5. Charging Performance…….. 110
4.1.6. Charging Period…… 121
4.1.7. Discharging Tests……..... 125
4.2. Results Obtained from Experimental Setup 2……..….. 140
5. CONCLUSIONS AND RECOMMENDATIONS……. 162
5.1. Conclusions…….. 162
5.2. Recommendations for Future Works……..…… 164
REFERENCES……..... 165
CURRICULUM VITAE…… 170
APPENDIX ……..... 171

LIST OF TABLES **PAGE**

Table 3.1.	Technical data for MHP 04P air-cooled water chiller……..	48
Table 3.2.	Technical data for water circuit kit ……..	50
Table 3.3.	Specifications of the ice storage tank constructed……	51
Table 3.4.	Specifications of the fan-coils installed……	53
Table 3.5.	Monitoring points for the Experimental System 1……	58
Table 3.6.	Specifications of the humidity transmitter …….....	72
Table 4.1.	Conditions of charging experiments…….	80
Table 4.2.	Conditions of charging experiments ……	97
Table 4.3.	Amount of cold energy stored and charge performance for all charging experiment……..	111
Table 4.4.	Conditions of experiments for effect of charging period……..	121
Table 4.5.	Effect of charging period on amount of energy stored and charging performance……..……..	122
Table 4.6.	Conditions of discharge experiments ……...	126
Table 4.7.	Conditions of phase change experiments……..	140

LIST OF FIGURES **PAGE**

Figure 3.1. Air cooling by circulating ice-cooled water…….. 19
Figure 3.2. Ice harvesting system ……... 26
Figure 3.3. External melt ice storage……... 28
Figure 3.4. Internal melt ice storage…… 30
Figure 3.5. Typical internal melt storage configuration…….. 32
Figure 3.6. Encapsulated ice containers…….. 34
Figure 3.7. Charge and discharge of encapsulated ice storage…… 34
Figure 3.8. Stacked eutectic salt storage container…….. 36
Figure 3.9. Full-storage operating strategy…….. 38
Figure 3.10. Partial-storage load leveling operating strategy…… 40
Figure 3.11. Partial-storage demand limiting operating strategy…….. 40
Figure 3.12. Ice storage air-conditioning system …….. 43
Figure 3.13. Schematic representation of the experimental setup 1 (Charging cycle)…… 45
Figure 3.14. Schematic representation of the experimental setup 1 (Discharging cycle)……... 46
Figure 3.15. Refrigerant flow diagram of the chiller for cooling mode…… 49
Figure 3.16. Schematic diagram of water circuit kit……. 50
Figure 3.17. Ice storage tank ……. 51
Figure 3.18. Coil distribution arrangement in the tank……. 52
Figure 3.19. Air-conditioned room ……..……. 53
Figure 3.20. Schematic representation of the automatic control of the experimental system (Fan control)…… 56
Figure 3.21. Schematic representation of the automatic control of the experimental system (Valve control)……..... 57
Figure 3.22. Measurement system on experimental setup 1……. 59
Figure 3.23. Water temperature measurement points in the ice storage tank 60

Figure 3.24. Connections of thermocouples to measure average temperatures…….. 61
Figure 3.25. Experimental system 2……..…….... 62
Figure 3.26. Schematic representation of the experimental setup 2…….. 63
Figure 3.27. Measurement stations along test tube……..... 64
Figure 3.28. Temperature measurement locations within the water…….. 65
Figure 3.29. Photographs of the ice formed around test tube at two different times……... 66
Figure 3.30. Post processing of photographs *a)* Original photograph *b)* First hipass filter *c)* Second hipass filter…….. 67
Figure 3.31. Schematic view of temperature measurement arrangement….. 68
Figure 3.32. Calibration curve for T/C'used…….. 69
Figure 3.33. Venturimeter…….. 70
Figure 3.34. Calibration curve of the flow rate…….. 71
Figure 3.35. Calibration curve for the humidity transmitter…….. 72
Figure 3.36. Data logger unit and the computer……..…….. 73
Figure 3.37. Schematic of ice formation process…….. 74
Figure 3.38. Variation of ice thickness obtained from model with time for different brine inlet temperatures…….. 77
Figure 4.1. Phase change during cooling processes of water inside the ice storage tank (Experiment 050407)……..……. 84
Figure 4.2. Variation of water temperature with time for sensible heat thermal storage processes around density inversion (Experiment 050407)…….…… 85
Figure 4.3. Variation of water temperature with radial distance at 1000. s during the experiment before density inversion (Experiment 050407)…….…… 85
Figure 4.4. Variation of water temperature with time for dendritic ice formation processes after density inversion, (Experiment 050407)……. 87

Figure 4.5. Variation of water temperature with radial distance at the beginning of nucleation, t_n =5279 s (Experiment 050407)….. 87

Figure 4.6. Nucleation times at the temperature measurement points inside the ice storage tank (Experiment 050407)…….. 88

Figure 4.7. Variation of water temperature with time for latent heat thermal storage process (Experiment 050407)…….. 88

Figure 4.8. Variation of water temperature with radial distance for 13196. s during the experiment (Experiment 050407)…….. 89

Figure 4.9. Variation of nucleation temperature with radial distance for *a)* $\overline{T}_{b,i}$ = -5.3 °C (200206) *b)* $\overline{T}_{b,i}$ = -5.1 °C (300306) *c)* $\overline{T}_{b,i}$ = -5 °C (030306)……. 90

Figure 4.10. Variation of nucleation temperature with radial distance for *a)* $\overline{T}_{b,i}$ = -4.9 °C (140606) *b)* $\overline{T}_{b,i}$ = -4.8 °C (190506) *c)* $\overline{T}_{b,i}$ = -4.7 °C (260606)……. 91

Figure 4.11. Variation of nucleation temperature with axial distance for *a)* $\overline{T}_{b,i}$ = -5.3 °C *b)* $\overline{T}_{b,i}$ = -5.1 °C *c)* $\overline{T}_{b,i}$ = -5 °C…… 93

Figure 4.12. Variation of nucleation temperature with axial distance for *a)* $\overline{T}_{b,i}$ = -4.9 °C *b)* $\overline{T}_{b,i}$ = -4.8 °C *c)* $\overline{T}_{b,i}$ = -4.7 °C…… 94

Figure 4.13. Nucleation time at the temperature measurement points inside the ice storage tank *a)* Experiment 2811S1 *b)* Experiment 2811S2……... 95

Figure 4.14. Variation of water temperature with time in the storage tank ($T_{b,s}$ = -4 ºC)…….. 98

Figure 4.15. Variation of brine temperature with time at the inlet and exit of the tank ($T_{b,s}$ = -4 ºC)…….. 98

Figure 4.16. Variation of air temperature with time at the inlet and exit of the condenser ($T_{b,s}$ = -4 ºC)……... 99

Figure 4.17. Variation of water temperature with time in the storage tank ($T_{b,s}$ = -5 ºC)…….. 100
Figure 4.18. Variation of brine temperature with time at the inlet and exit of the tank ($T_{b,s}$ = -5 ºC)…… 101
Figure 4.19. Variation of air temperature with time at the inlet and exit of the condenser ($T_{b,s}$ = -5 ºC)……... 101
Figure 4.20. Variation of water temperature with time in the storage tank ($T_{b,s}$ = -6ºC)……... 102
Figure 4.21. Variation of brine temperature with time at the inlet and exit of the tank ($T_{b,s}$ = -6 ºC)……... 103
Figure 4.22. Variation of air temperature with time at the inlet and exit of the condenser ($T_{b,s}$ = -6 ºC)……... 103
Figure 4.23. Variation of water temperature with time in the storage tank ($T_{b,s}$ = -7 ºC)…….. 104
Figure 4.24. Variation of brine temperature with time at the inlet and exit of the tank ($T_{b,s}$ = -7 ºC)……... 105
Figure 4.25. Variation of air temperature with time at the inlet and exit of the condenser ($T_{b,s}$ = -7 ºC)……... 105
Figure 4.26. Variation of water temperature with time in the storage tank ($T_{b,s}$ = -8 ºC)…….. 106
Figure 4.27. Variation of brine temperature with time at the inlet and exit of the tank ($T_{b,s}$ = -8 ºC)……... 106
Figure 4.28. Variation of air temperature with time at the inlet and exit of the condenser ($T_{b,s}$ = -8 ºC)……... 107
Figure 4.29. Variation of cumulative energy storage with time for $T_{b,s}$ = -4 ºC, -5 ºC, -6 ºC and -8 ºC……...…….. 108
Figure 4.30. Variation of charging performance with brine inlet temperature for $\overline{T}_{a,i}$ = 20-21 ºC…… 115
Figure 4.31. Variation of charging performance with brine inlet temperature for $\overline{T}_{a,i}$ = 23-24 ºC…… 115

Figure 4.32. Variation of charging performance with brine inlet temperature for $\overline{T}_{a,i}$ = 25 ºC…….. 116
Figure 4.33. Variation of charging performance with brine inlet temperature for $\overline{T}_{a,i}$ = 27 ºC……. 116
Figure 4.34. Variation of charging performance with brine inlet temperature for $\overline{T}_{a,i}$ = 28 ºC……..…….. 117
Figure 4.35. Variation of charging performance with brine inlet temperature for all air temperatures at the inlet of the condenser……..…….. 117
Figure 4.36. Variation of charging performance with air inlet temperature for $\overline{T}_{b,i}$ = -4.8 ºC…….…… 118
Figure 4.37. Variation of charging performance with air inlet temperature for $\overline{T}_{b,i}$ = -4.9 ºC…….…… 119
Figure 4.38. Variation of charging performance with air inlet temperature for $\overline{T}_{b,i}$ = -5.2 ºC and -5.3 ºC…….. 119
Figure 4.39. Variation of charging performance with air inlet temperature for all brine inlet temperatures…….. 120
Figure 4.40. Variations of the energy stored with charging period for 18 charging experiments…….…… 123
Figure 4.41. Variations of charging performance with charging period for 18 charging experiments…….……... 124
Figure 4.42. Variation of water temperature with time in the storage tank (Experiment 120706)…….…… 127
Figure 4.43. Variation of brine temperature with time at different measurement points (Experiment 120706)……..……... 128
Figure 4.44. Variation of air temperature with time for room and ambient (Experiment 120706)…….…… 129
Figure 4.45. Variation of relative humidity with time for room and ambient (Experiment 120706)…….…….. 130

Figure 4.46. Comparison of air conditions obtained during experiment with ASHRAE comfort zone (Experiment 120706)……. 130
Figure 4.47. Variation of water temperature with time (Experiment 090706)…….…. 131
Figure 4.48. Variation of brine temperature with time at different measurement points (Experiment 090706)……..... 132
Figure 4.49. Variation of air temperature with time for room and ambient (Experiment 090706)…….…… 133
Figure 4.50. Variation of relative humidity with time for room and ambient (Experiment 090706)…….…….. 134
Figure 4.51. Comparison of air conditions obtained during experiment with ASHRAE comfort zone (Experiment 090706)……. 134
Figure 4.52. Variation with time of cumulative energy extracted from room for two fan-controlled experiments…….……. 135
Figure 4.53. Variation of water temperature with time in the storage tank (Experiment 030906)…….…… 136
Figure 4.54. Variation of brine temperature with time at different measurement points (Experiment 030906)……..……... 137
Figure 4.55. Variation of air temperature with time for room and ambient (Experiment 030906)…….…… 138
Figure 4.56. Variation of relative humidity with time for room and ambient (Experiment 030906)…….…….. 138
Figure 4.57. Comparison of air conditions obtained during experiment with ASHRAE comfort zone (Experiment 030906)……. 139
Figure 4.58. Variation of water temperature with time at three measurement stations for $\overline{T}_{b,i}$ = -5.8 ºC (*a:* x/L = 0.1, *b:* x/L = 0.47, *c:* x/L = 0.86)…….. 141
Figure 4.59. Variation of water temperature with time at positions just above the test tube (thermocouple 3) for different axial measurement stations ($\overline{T}_{b,i}$ = -5.8 ºC)…….…… 143

Figure 4.60. Variation of nucleation time along tube for $\overline{T}_{b,i}$ = -5.8 ºC…… 143
Figure 4.61. Variation of ice thickness with time for top, bottom and sides of tube for $\overline{T}_{b,i}$ = -5.8 ºC (x/L= 0.1)……..... 144
Figure 4.62. Variation of ice thickness with time for top, bottom and sides of tube for $\overline{T}_{b,i}$ = -5.8 ºC (*a:* x/L= 0.23, *b:* x/L= 0.35, *c:* x/L= 0.47)……... 145
Figure 4.63. Variation of ice thickness with time for top, bottom and sides of tube for $\overline{T}_{b,i}$ = -5.8 ºC (*a:* x/L= 0.62, *b:* x/L= 0.74, *c:* x/L= 0.86)……... 146
Figure 4.64. Variation of water temperature with time at three measurement stations for $\overline{T}_{b,i}$ = -4.9 ºC (*a:* x/L = 0.1, *b:* x/L = 0.47, *c:* x/L = 0.86)…….. 148
Figure 4.65. Variation of water temperature with time at positions just above the test tube (thermocouple 3) for different axial measurement stations ($\overline{T}_{b,i}$ = -4.9 ºC)……..…. 149
Figure 4.66. Variation of nucleation time along tube for $\overline{T}_{b,i}$ = -4.9 ºC…… 149
Figure 4.67. Variation of ice thickness with time for top, bottom and sides of tube for $\overline{T}_{b,i}$ = -4.9 ºC (x/L= 0.1)……..…..... 150
Figure 4.68. Variation of ice thickness with time for top, bottom and sides of tube for $\overline{T}_{b,i}$ = -4.9 ºC (*a:* x/L= 0.23, *b:* x/L= 0.35, *c:* x/L= 0.47)……... 151
Figure 4.69. Variation of ice thickness with time for top, bottom and sides of tube for $\overline{T}_{b,i}$ = -4.9 ºC (*a:* x/L= 0.62, *b:* x/L= 0.74, *c:* x/L= 0.86)……... 152
Figure 4.70. Variation of water temperature with time at three measurement stations for $\overline{T}_{b,i}$ = -4.3 ºC (*a:* x/L = 0.1, *b:* x/L = 0.47, *c:* x/L = 0.86)……...……... 154

Figure 4.71. Variation of water temperature with time at positions just above the test tube (thermocouple 3) for different axial measurement stations ($\overline{T}_{b,i}$ = -4.3 ºC)…….. 155

Figure 4.72. Variation of nucleation time along tube for $\overline{T}_{b,i}$ = -4.3 ºC…… 155

Figure 4.73. Variation of ice thickness with time for top, bottom and sides of tube for $\overline{T}_{b,i}$ = -4.3 ºC (x/L= 0.1)……..... 156

Figure 4.74. Variation of ice thickness with time for top, bottom and sides of tube for $\overline{T}_{b,i}$ = -4.3 ºC (*a:* x/L= 0.23, *b:* x/L= 0.35, *c:* x/L= 0.47)…….. 157

Figure 4.75. Variation of ice thickness with time for top, bottom and sides of tube for $\overline{T}_{b,i}$ = -4.3 ºC (*a:* x/L= 0.62, *b:* x/L= 0.74, *c:* x/L= 0.86)…….. 158

Figure 4.76. Evolution of ice-water interface with time for different brine inlet temperatures (*a:* $\overline{T}_{b,i}$ = -4.3 °C, *b:* $\overline{T}_{b,i}$ = -4.9 °C, *c:* $\overline{T}_{b,i}$ = -5.8 °C)……..…….. 159

Figure 4.77. Influence of brine inlet temperature on ice thickness at x/L=0.47 …….. 160

Figure 4.78. Variation of nucleation time along tube for different brine inlet temperatures ……..…… 160

Figure 4.79. Comparison of ice thickness obtained from measurements and model for different brine inlet temperatures (*a:* $\overline{T}_{b,i}$ = -4.3 °C, *b:* $\overline{T}_{b,i}$ = -4.9 °C, *c:* $\overline{T}_{b,i}$ = -5.8 °C)……..... 161

Figure A.1. Density of aqueous solutions of ethylene glycol (vol. %)……. 172

Figure A.2. Specific heat of aqueous solutions of ethylene glycol (vol. %) 172

Figure A.3. Thermal conductivity of aqueous solutions of ethylene glycol (vol. %)…….. 173

Figure A.4. Viscosity of aqueous solutions of ethylene glycol (vol. %)….. 173

NOMENCLATURE

C : Specific heat (J / kg°C)

C_d : Flow coefficient

d : Diameter of throat of venturimeter (m)

h_{ew} : Latent heat of fusion (kJ / kg)

h : Heat transfer coefficient (W / m^2°C)

k_e : Thermal conductivity of ice (W / m°C)

k_w : Thermal conductivity of tube material (W / m°C)

L : Tube length (m)

M : Mass (kg)

m : Mass flow rate (kg / s)

P : Periphery (m)

Q_x : Heat transfer rate (W)

Q_d : Cooling energy recovered during discharging (kJ)

$Q_{s,b}$: Stored energy calculated from the brine (kJ)

$Q_{s,w}$: Stored energy calculated from the water (kJ)

W : Total energy consumed (kJ)

r : Radial coordinate

R : Radius of tube (m)

R_p : Thermal resistance for periphery (°C / W)

R_{po} : Thermal resistance for inner side of the tube and pipe wall (°C / W)

s_w : Thickness of tube wall (m)

s_e : Thickness of ice (m)

t : Time (s)

T : Temperature (°C)

$T_{b,s}$: Brine set temperature (°C)

$T_{b,i}$: Brine inlet temperature (°C)

$T_{w,i}$: Initial temperature of water (°C)

$T_{w,f}$: Final temperature of water (°C)

ΔP : Pressure difference

y : Axial coordinate

Greek letters

η : Performance

β : Ratio of diameters of venturimeter

ρ : Density (kg / m^3)

ϑ : Volumetric flow rate (m^3 / s)

Subscripts

b : Brine

d : Discharge

e : Ice

in : Inlet

ex : Exit

f : Final

i : Inner

n : Nucleation

o : Outer

w : Water

wm : Mean for tube wall

em : Mean for ice

teo : Theoretical

act : Actual

Superscripts

* : Dimensionless

$\bar{}$: Average

ABBREVIATIONS

CTES : Cold thermal energy storage

ITES : Ice thermal energy storage

TES : Thermal energy storage

PCM : Phase change material

1. INTRODUCTION

The world energy consumption is increasing rapidly, and the developed countries have become heavily reliant upon energy in all activities. It is well accepted now that electrical energy is the most versatile form of energy and its conservation will solve part of the world energy problems (Kahwaji, 2006). Furthermore, developing nations are facing the same situation as in the developed world: i.e., increasing summer electric peak demand, declining utility load factors and the reluctance to build large, base-load generation plants (Wendlad, 1990).

The components of electrical load in commercial buildings may be divided into chiller load, lights and other operating equipments. The chiller load represents the main varying part of the above-mentioned loads and its peak load usually coincides with the peak electrical demand, which leads to the consumption of high electrical energy during on-peak hours (Kahwaji, 2006). This requires the utility companies to bring additional, more costly generating sources on line to handle its increased demand. Moreover, since the cost of fuel for base-load generation is only a small fraction of the cost of fuel for fast response equipment used to meat peak loads, commercial users whose large air conditioning loads contribute to these added generating requirements are assessed an additional charge based on their highest on-peak demand for electricity. This is termed a “demand charge” and is based on kilowatt usage (Calmac, 1991). With the rise of energy prices, electric utilities escalated the demand charge to prevent their customers from consuming high electrical energy during on-peak hours.

The decade of the 1980s saw the birth, early growth and recognition of air-conditioning thermal storage technology as a solution to the increased peak demand on electricity (MacCracken, 1990). The concept of thermal storage as applied to cooling systems relies on replacing the large equipment designed to handle peak loads with smaller units, which will operate throughout the day, storing additional capacity during off-peak hours and using the stored capacity during on-peak periods. By producing cooling capacity during off-peak hours, the power demand is shifted from on-peak to off- peak periods resulting in demand charge savings.

These systems utilize a storage medium to store cooling produced during off-peak hours. The stored cooling is later used during peak hours to meet an air-conditioning or process-cooling load. Various media such as chilled water, ice, or phase-change-materials can be used to store cooling material (Dorgan and Elleson, 1993). Chilled water storage and ice storage are the most common storage designs. Ice storage tanks have much smaller volumes than chilled water tanks of the same cooling capacity.

A conventional vapor compression chiller or an industrial-grade ice-making unit is used to charge the storage tanks during off-peak hours. The chilled liquid from the storage tanks is circulated through the building's fan coils or a secondary heat exchanger during on-peak times for cooling.

Operating strategies for cool thermal energy storage systems are generally classified as either "full storage" or "partial storage", referring to the amount of cooling load transferred from on-peak period to off-peak. In full storage thermal energy storage strategy, the refrigeration equipment is of during on-peak hours, and all cooling load is provided from the storage that is charged during the off-peak period.

Although thermal energy storage systems for cooling were first used commercially in the 1940s and have gaining popularity in the USA and Europe in recent years, application of these systems are very limited in Turkey. Although there has been an interest in these systems in recent years, barriers still exist in Turkey regarding the application of these systems; such systems are not well known, and they are notorious for troublemaking. Another barrier is the lack of designers, contractors and operators who can properly design, install and operate these systems economically and reliably. Cool storage tanks, which are one of the key components in cool thermal energy storage systems, are not manufactured at all in the country. They are imported from abroad and this makes these systems economically unattractive.

Turkish Government has introduced a law on 25 December 1997 about electricity tariffs to shave the peak-load. According to the new law, the day is divided into three periods by electric utility (TEDAS): 17:00 to 22:00 (peak period),

22:00 to 06:00 (off-peak period), and, 06:00 to 17:00 (normal period). At the present time, variable tariffs are optional for all electricity consumers. Compared with the constant tariffs (daylong constant prices) for office buildings, the cost of electricity is 50% higher for the peak period, and 49% and 7% lower for the off-peak and the normal periods, respectively according to the variable tariffs.

In this study, charge and discharge experiments were performed to investigate performance characteristics of the ice thermal energy storage system in the Laboratories of Mechanical Engineering Department of Çukurova University. Phase change of water (nucleation temperature, nucleation time and supercooling) inside the ice storage tank is investigated for different brine inlet temperatures. The effects of set temperature of the brine, brine inlet temperature, air temperatures at the inlet of the condenser and charging period on charging performance are investigated. However, two automatic control operating strategies (fan control and valve control) are investigated for discharge experiments.

The results of the experiments carried out with ice thermal energy storage system showed that mechanisms observed during the ice formation are very important parameters for system performance and they should be investigated in detail. Therefore, a parallel experimental system (Experimental Setup 2) was constructed to understand solid-liquid phase change heat transfer phenomena around a tube. Phase change phenomena around a horizontal tube are investigated both experimentally and analytically.

2. LITERATURE REVIEW

The literature search was divided into two sections: a) ice storage systems, and b) phase change of water around tube

2.1. Ice Storage System

Many cities throughout the world are faced with increasingly high energy costs. Often, these costs are not directly incurred due to the energy used, but rather due to the costs associated with the overall demand for electricity. Many electrical utility companies are having difficulties in maintaining sufficient capacity to serve the peak demand of their customers, while at the same time supplying reasonably priced electricity. One way to defer or void the construction of new and expensive power plants is to level the electrical load over time. One significant method for leveling the electrical demand in commercial buildings is to shift the electrical loads incurred by heating, ventilating, and air-conditioning equipment to periods of lower overall electrical usage. This load shifting can be accomplished by using thermal energy storage (TES) technologies. In many countries, utility companies and governments offer incentives to encourage such use of TES (Rosen, 2000).

An effective way to take advantage of the low electricity rates in effect during the night and other off-peak periods is through the use of cold storage, one type of which is ice storage. The basic principle behind ice thermal energy storage (ITES) is simple: in-expensive off-peak electricity is utilized during the night to create a large mass of ice, and during the day this ice store is melted by absorbing the heat from buildings needing cooling (Rosen, 2000).

In this section, a detailed literature review is carried out to assess ice thermal energy storage systems (ITES). Subcategories of literature review:

- General information about ITES systems and theoretical performance analysis for these systems
- Experimental studies
- Numerical studies

- Economical analysis studies

The basic types of thermal energy storage (TES) techniques and their individual advantages and disadvantages for space and water heating applications were reviewed by Hasnain (1998a). Typical data of some relevant properties of sensible and latent heat storage materials were given in tables. The inherent pros and cons of the ice storage and other cool storage technologies for off-peak air conditioning applications were described by Hasnain (1998b). Advantages of cool storage system over a conventional air conditioning system, primary features and operational strategies of cool storage systems are summarized in the paper. Case studies on cool thermal storage demonstrated not only savings in energy, and other operation and maintenance costs but also significant savings in initial capital costs for large applications without sacrificing comfort to the building occupants.

Rosen et al. (1999) also reported assessment of the thermodynamic performance of cold thermal storage systems using energy and exergy analyses. Analyses were performed for several cases of cold thermal storage systems, including storages that undergo sensible and/or latent heat changes. The results demonstrated that exergy analysis provided more realistic and accurate assessments of the efficiency and performance of cold thermal storage systems than those given by the more conventional energy analysis.

Thermodynamic performance of an encapsulated ice thermal energy storage system (ITES) for cooling capacity was assessed using energy and exergy analyses by Rosen et al. (2000). A full cycle, with charging, storing, and discharging stages, was considered. The results demonstrated how exergy analysis provided a more realistic and meaningful assessment than the more conventional energy analysis of the efficiency and performance of an ITES system. However, results were indicated that energy analysis leads to misleadingly optimistic statements of ice thermal energy storage system efficiency.

Dincer (2002) presented methods and applications of describing and assessing cool thermal energy storage systems in buildings. Various technical aspects and criteria for thermal energy storage systems and applications were explained and energy saving techniques and environmental impacts of these systems were

highlighted with illustrative examples. Then an energy and exergy analysis of thermal energy storage systems and their sub-processes was presented for system design and optimization. An illustrative example was also given to demonstrate how exergy analysis provides a more realistic and meaningful assessment than the conventional energy analysis of the efficiency and performance of a thermal energy storage system.

Although ice thermal energy storage systems for peak –load shifting are now in the market, very few performance testing and evaluation procedures have been developed. Some examples of previous work on ITES are cited here. The performance testing of commercial TES systems was first conducted at the Oak Ridge National Laboratory under the sponsorship of the Electric Power Research Institute. This testing served to provide uniform performance test results and to promote system improvements based on experimental results. Stovall (1991) conducted the performance testing of a Calmac ice storage system over a wide range of operating conditions. Storage tank equipped with coils designed for use with a secondary fluid system. The charge capacity decreased as ice built up around the coils within the storage tank due to the reduction in saturated suction temperature at the compressor. Water is free to flow into and out of the expansion volume, but the insulation prevents it from freezing. The average capacity, or charging time, appears to have only a moderate effect on the amount of derating and almost no effect on the capacity values. The effect of the brine concentration was investigated the analysis of the discharge data. Based on experimental comparisons, the increased concentration of brine was not likely to effect results.

Stovall and Tomlinson (1991) also investigated performance of a commercial 105.3 kW dynamic ice storage system. The system functioned by freezing water in thin layers and then periodically releasing these layers of ice from the ice making surface and dropping them into a storage tank. The ice storage system was tested over a wide range of operating conditions to characterize the ice-generating performance as a function of condensing conditions, ice building time, and defrosting time. The system capacity decreased with increasing periods of defrost and with

increasing condensing temperatures. In addition, the compressor power increased with defrosting times and with increasing condensing temperatures.

Sohn (1991) investigated design, construction, and performance of a small ice harvester system. The system consists of a 91.44 kW icemaker, a 1053 kWh above ground steel storage tank, and a building with a 245.7 kW cooling load at Fort Bliss, TX, USA. The system was designed to meet the building cooling demand from 12:00 noon through 16:00. During the 36-day monitoring period, the energy efficiency ratio of the existing chiller was 8, and that of the ice maker was 6.18. The system achieved its primary purpose of shifting electric power for space cooling from a peak to an off peak period to avoid the demand charge ($19.50/kW) and system consumed 29% more energy than the existing conventional cooling system.

Arnold (1991) investigated the performance of an encapsulated-ice store. The container was charged and discharged circulating the 36 % by mass mixture of ethylene glycol and water through the 0.66 m in diameter and 1.5 m high container filled with 750 capsules, each 77 mm in diameter and full of water. Results showed that variation in the rate of heat transfer during the charge and discharge of encapsulated ice stores varied significantly. The rate at the beginning was typically four times as great as the rate toward the end. Convection within capsules varied considerably over the range of bulk water temperatures used and was significant in affecting the rates of heat transfer during melting.

Lee and Jones (1996a) studied the laboratory performance of an ice-on-coil thermal energy storage system for residential and light commercial applications. A 153.73 kWh integrated thermal energy storage system was installed in the dual-air loop test facility at The University of Texas, Center for Energy Studies. The TES system was tested over a wide range of indoor and outdoor conditions to determine parameters such as ice building rate, compressor power, cooling rate, heating rate, desuperheater rate, energy efficiency ratio and power consumption factor. Results showed that the ice building rate increased with decreasing outdoor temperature. The energy efficiency ratio of the system increased with decreasing outdoor temperature. In addition, the discharge rate decreased as the bulk water temperature in the thermal

storage tank increased with time, reducing the energy available to meet the cooling load.

An internal melt ice-on-coil thermal storage tank was instrumented and tested over various inlet conditions of secondary fluid temperature and flow rate in a full-scale heating, ventilating, and air-conditioning laboratory by Neto and Krarti (1997). Different inlet conditions of temperature and flow rate were applied during each test. Typical loads were imposed on the system to establish the controlled inlet conditions. The measured data for one typical charging/discharging cycle were used to validate a numerical model developed for analyzing internal melt ice-on-coil ice storage tanks. The model predicted the average secondary fluid temperature leaving the tank during the charging and discharging periods within 1% of the measured secondary fluid temperature for all 10 tests performed. In addition, the numerical model predicted the total secondary fluid heat transfer within 5% of the values obtained from measurements for all 10 tests performed.

Choi et al. (2002) studied heat and performance characteristics during ice generation and discharge modes within a storage tank for a conventional and a new underwater ice-harvesting system. Before the first discharge of ice in the new type, the vertical temperature differences were very clear. However, in the conventional type, the temperature differences varied linearly. In the discharge mode, the temperature distributions in the new type kept the initial temperature to 90 min. The temperature difference in the conventional type is not large, and it varied linearly with the increase of time. The discharge capacity and temperature difference of fan-coil unit in the new type showed about 60% higher than these in the conventional type.

Yamada et al. (2002) constructed a liquid-ice cold thermal storage system, and the effect of the operation mode of the system such as the combination of the ice storage time and its release time on the system performance was investigated. The system performances were widely investigated analytically for the variety of operation conditions including the cycle performance of a refrigerator. The following conclusions were obtained: a) Simulation model was proven to be capable enough to describe the performance characteristics of ice thermal energy storage system. b) The

coefficient of performance COP was almost the same for all operation modes (different storage time, interval time and heat release time) in the study.

A number of analytical and numerical models have been developed to predict the performance of ice thermal energy storage systems. Jekel (1993) developed a mechanistic model for static ice-on-coil ice storage tanks for both charging and discharging. The effectiveness concept for both charging and discharging of ice storage tanks was developed. The effectiveness correlated the tank charge in terms of the maximum capacity based on inlet brine temperature. The effectiveness provided a simple model for predicting tank performance, and was useful for correlating experimental data. The performance from the model was compared favorably with manufacturer's data. The charging rates from the model were within 12 % of a manufacturer's average charging data and discharging rates from the model were within 10 % of the discharging data.

Analytical models for an ice-on-coil thermal energy storage system for charging and discharging modes were developed by Lee and Jones (1996b). The paper described the basic heat transfer analysis and presented the characteristics of the charging and discharging modes determined from the model. Experimental results (Lee and Jones, 1996a) were used to validate the models. The output results of the cooling charge model were the volume of ice in the thermal storage tank and cooling charge rate. The output of the cooling discharge model was the tank bulk water temperature. In general, the model predictions showed agreement with the experimental data.

Chaichana et al. (2001) developed a computer model in order to compare energy use in conventional systems and ice thermal storage systems. Energy consumption, energy cost saving and coefficient of performance (COP) of the compressor for each system were described. The results from the simulations showed that the low ambient temperature during nighttime reduced the total energy consumption by 5% using full storage as the cooling system for chosen building. The partial storage technique consumed 18% more energy than the conventional system and 24% more energy than the full storage system respectively due to the fact that the chiller used was operated inefficiently.

Henze et al. (2003) presented simulation-based results of an investigation of a commercial cooling plant with an ice storage system. Various ice storage systems, chiller compressors, and building types were analyzed under optimal control and three conventional controls (chiller-priority, constant-proportion, and storage-priority control). Independent of the non-cooling electrical load profile, it was found that good efficiency of the cooling plant in the ice making mode and rate structures with strong load-shifting incentives are prerequisites for making cool storage successful. On-peak demand reduction of storage-priority was near-optimal for many cases. Guidelines were presented to improve the load-shifting performance of chiller-priority and constant-proportion control.

Henze (2003) also investigated whether thermal storage systems could be controlled effectively in situations where cooling loads, non-cooling electrical loads, weather information, as well as the cost of electricity are uncertain. The analysis showed that the reduction in achievable utility cost-savings was small when relying on real-time pricing electricity rates that were made available by the utility only 1h ahead instead of an entire day-ahead. Real-time pricing rate data from two utilities were used in both a day-ahead and an hour-ahead fashion. Consequently, uncertain electrical utility rates do not imperil the superior cost-saving benefits of cool storage when governed by predictive optimal control.

Kousksou et al. (2005) studied dynamic modeling of the storage inside an encapsulated ice tank. The objective of the work was to the study an industrial process of energy storage, which consists in the use of a cylindrical tank filled with encapsulated phase change materials. A detailed analysis of the system permitted the development of the two dimensional porous medium model for cold storage with coolant flowing. First, the numerical model was compared with experimental results for the tank in vertical position. They found that the optimum running of the charge mode is obtained in the case of the vertical position where the motions due to the natural convection are in the same direction as the forced convection.

Numerous economic studies and cost analyses of ITES systems and their practical applications have been undertaken by many researches. Navon et al. (1997) discussed the economic aspects of the optimal design for HVAC with thermal energy

storage. Model for optimal design so determines the sizes of the main components of the system-namely the chiller and the storage tank-that the system's life cycle cost was minimal. Model was based on linear programming and was implemented in a computer program for HVAC systems with ice storage. The economic analysis indicated that for a wide range of typical loads, an HVAC system with storage of ice was economically feasible. Furthermore, the analysis showed that the cost-effectiveness of using HVAC systems with storage increased as the thermal load duration decreased and as the number of operating days per year increased.

Hasnain et al. (2000) investigated suitability of ice storage systems in large Saudi office buildings. Cool thermal storage economics were considered, and a cost analysis was presented to illustrate the savings that can be achieved by the use of cool thermal storage in Saudi Arabia, especially for peak electric load leveling purposes during the summer period. They found that incorporation of a partial ice storage system in Saudi office buildings reduced the peak time electrical power demand and the peak time cooling load in the range of 10-20% and 30-40%, respectively. In general, the savings resulting from the downsized cooling plant offset the cost of storage and the additional interface equipment.

The operating history of three ice thermal energy storage systems installed at university and includes operational performance, economic performance, maintenance record, and system reliability were investigated by Potter et al. (2006). All three systems utilized internal melt, ice-in-tank and total capacity of the systems was 17.585 kWh. Results were showed that with an annual savings of approximately $11.500, the payback period was approximately 16 years. Using the 65% discharge figure estimated by maintenance personnel, the initial costs could have been reduced and this downsizing would have reduced the payback period to slightly more than four years.

Habeebullah (2007a) investigated the economic feasibility of retrofitting an ice thermal storage system for the air conditioning plant of the Grand Holy Mosque of Makkah in Saudi Arabia. The capital recovery factor was calculated for 10% interest rate and payback period of 10 years. Full and partial load storage scenarios were considered. The results showed that with the current fixed electricity rate, there

was no gain in introducing ice storage systems for both storage schemes. Combined utilization of an incentive tariff model and storing technology showed reasonable daily savings for full load storing scheme. Savings out of partial load storing were not attractive even with the structured base tariff.

2.2. Phase Change of Water around Tube

The cool storage air-conditioning system is an important concept of many energy conservation programs in industry and in commercial applications. Water is widely used as the phase change material for cool storage because of the advantages of water, such as high value in latent heat, stable chemical property, low cost and easy acquisition, no environmental pollution concern. Akyurt and Zaki (2001) reviewed characteristics of solidification and melting. The properties of water and ice and the phase diagram of water have discussed with special emphasis on ice density. The four stages of freezing have identified, supercooling, nucleation and the formation of dendritic ice, the growth of concentric rings of solid ice at 0 °C and final cooling of the solid ice were treated in some detail.

The literatures on phase change problem are abundant including experimental studies and numerical methods. Simultaneous melting and solidification of a phase change material around two horizontal cylinders were studied by Sasaguchi and Viskanta (1987). Experiments carried out to examine the effects of the cylinder surface temperature difference and the spacing between the cylinders. Time wise variations of a temperature distribution midway between the two cylinders and area of melted region were measured. The results showed that the melt shape and the solid liquid interface motion were very sensitive to the surface temperature of the lower cylinder and the spacing between the cylinders.

Sasaguchi et al. (1994) also carried out experiments to examine the effects of initial temperature of water for the solidification and the effect of the surface temperature of the cylinders for the melting on the heat transfer using a single and two horizontal, vertically spaced cylinders in a rectangular enclosure. For solidification process in which the initial temperature of water was small (0.5 °C) so that natural convection was very weak, the value of the solidification fraction for the single cylinder case was larger than both values for the two cylinder cases with a large spacing. For the melting process, the change in the cylinder temperature largely affected the strength and the extent of the circulation due to the density inversion of water, and therefore largely affected the interface shape.

Supercooling phenomenon and the freezing probability of water inside horizontal cylinders during a cooling process of thermal storage were studied by Chen and Lee (1998). The effect of such factors as cooling rate, inside diameter of cylinders and mass of different nucleation agents was experimentally examined. The results showed that an increase of the cooling rate of water made the blockage extent of dendritic ice growth decreased under the same inside diameter. The addition of nucleation agents into water containers effectively improved the nucleation probability, and thus increased the coefficient of performance of cool storage air-conditioning system.

Liu et al. (1998) studied the performance of ice formation around an isothermal finned cylinder, horizontally located in rectangular enclosure. The effect of fin location on ice-layer formation was experimentally studied with two arrangements of the cylinder. The results show that the variation of ice layer around the finned cylinder was related with the initial temperature and fin arrangement. Amount of ice around an isothermal finned cylinder was found obviously larger than that of the bare cylinder of the same diameter under similar initial conditions. However, amount of ice with arrangement I of the finned cylinder (fins on downside of the cylinder) was better than that with arrangement II (fins on upside of the cylinder.

Chen et al. (2000) conducted experiments to investigate the thermal characteristics of an encapsulated thermal storage system using water added with nucleation agents as the PCM by varying the inlet coolant temperature and coolant flow rate. Experiments carried out with three different coolant flow rates and inlet coolant temperatures: 5, 10, 20 l/min, and -1 °C, -3°C, and -5°C. They found that if the inlet coolant temperature was lower than the temperature of 100% probability of crystallization, cool energy could be fully stored in the form of latent heat. When the inlet coolant temperature was set below the temperature of 0% probability of nucleation, the increase of the coolant flow rate did not have any effect on the crystallization of the PCM.

Milon and Braga (2003) studied the supercooling phenomenon of water inside cylindrical capsules used for cold storage process. It was verified that the

nucleation probability increases for smaller transfer fluid temperature values. For -2 °C and -4 °C, the probability of nucleation was 0%, independent of the material of the capsule. When supercooling appeared, dentric ice accompanied the solidification process, as well as the presence of a kind mushy region.

Mouse (2004) investigated the performance of ice storage system and stored thermal energy for solidification of phase change material around a vertical cylinder surface. Air bubbles were generated in the phase change material at various air flow rate as a gas holdup to enhance the heat transfer rate and accelerate the ice layer growth at the solid-liquid interface. The effect of air bubbles agitation was found to increase the ice layer growth rate and solidification front velocity by about of 20-45%. The stored thermal energy increased by about 55-115% as a consequence of using air bubbles flow.

Habeebullah (2007b) investigated experimentally the growth rate of ice on the outside of cooled copper tubes. The tubes, which were immersed in water in an insulated vessel, were internally cooled by circulating glycol through them. It was found that axial growth rate of ice is distinct at low values of the coolant Reynolds number and short freezing times. The slope of the ice thickness with axial distance showed moderate dependency on time but varied with coolant flow rate, and with Stanton and Biot numbers. The experiments performed demonstrate that during the early stages of the cooling process natural convection currents were created within the water bulk followed by the development of a stratified layer at nearly the freezing point floating on dense water at 4 °C. At this stage, the natural convection diminished and the rate of ice growth increased.

There have been many numerical studies as well as reports on experimental projects. Sasaguchi and Kusano (1997) studied a new numerical model to analyze solid-liquid phase change heat transfer in a complicated geometry. Solidification calculations of pure water around a single cylinder and two cylinders were performed to check the validity of the model. The interaction of two solidification layers were examined, and the effects of natural convection in the melt on the solidification process were also studied. Results showed that for the initial water temperature of 0 °C, the solidification progresses more rapidly for the single cylinder than that for

the two cylinders, but the reverse is true for initial water temperature greater than 4 °C.

Ismail and Goncalves (1997) developed a conduction-based model for solving the phase change heat transfer problem around a vertical cylinder submersed in the phase change medium. In the study, the problem evaluating the performance of a PCM cylindrical storage tank was formulated and solved. In the storage system, the PCM was contained in the cylindrical shell while the working fluid flowed into a set of tubes extending between the upper and lower distributing chambers. As a result, Biot number was found to be an influencing factor when its value is below 10, that the inlet working fluid temperature had very little effect and that the Stefan number was the dominant factor for values below 0.5.

Ismail and Melo (1998) also developed a convection based model for a PCM vertical storage unit. The paper presents a two dimensional axi-symetrical model for the formulation of the problem of fusion of PCM around a vertical cylinder in the presence of natural convection. Results show the effects of the geometrical and operational parameters on the solid-liquid interface, stream function, energy stored and melt mass fraction. The model was extended to produce charts and correlations for the mean heat transfer rate, total solidification (or fusion) time in terms of the geometrical parameter, the modified Rayleigh number and the Stefan number.

Shih and Chou (2005) investigated the solidification around a number of staggered cylinders in a fixed volume. Pure water was adopted as the working fluid and the non-Boussinesq model was used to calculate the variation in water density to account for the natural convection during solidification. When the initial temperature of water was fixed, the average growth rate of the ice layer for the case of four staggered cylinders was larger than for those of six and eight staggered cylinders. For the case of eight cylinders, the ice layer overlapped during solidification and occupied most of the region in the final stage. However, the growth rates of the ice layer decreased as water superheat increased and the natural convection was intensified when water superheat increased for all cylinder cases.

Latent heat thermal storage systems employing finned surfaces for increasing rate of energy storage were investigated by Erek et al. (2005). Numerical simulations

were performed to investigate the effect of several fin parameters (fin spacing and fin diameter) and flow parameter. The results were compared with experimental results. Three different inlet temperatures -10 °C, -15 °C and -20 °C and six different flow rates were studied. The flow rates were chosen so that Re number varies between 500 and 7000. As a result, the stored energy increases with increasing fin radius and decreasing fin space. In addition, the stored energy increases with increasing Reynolds number and Stefan number. After a certain value of Reynolds number, which is about 5000, the total amount of stored energy does not change too much.

From the literature given above, it is seen that investigation of performance characteristics, operating strategies and economic analysis of ice thermal energy storage systems and phase change of water is of great interest and further studies are needed. In this work, ice storage tank of an air-conditioning system based on ice storage is tested for charging and discharging periods. The effect of temperature of the brine at the inlet of the tank, temperature of the air at the inlet of the condenser and charging period on system performance are investigated for charging experiments. However focus is on the phase change of water inside the ice storage tank. Capabilities of the ice storage tank under two automatic control operating strategies (fan control and valve control) are investigated for discharge experiments.

Utilizing a second experimental system, phase change phenomena around a horizontal tube is investigated both experimentally and analytically. Experiments are carried at different brine inlet temperatures in order to study the dynamic behavior of ice layer formation on tube. A mathematical model is also written to calculate the heat transfer process for phase change phenomenon around a horizontal tube.

3. MATERIAL AND METHOD

Latent heat storage is a particularly attractive technique, since it provides a high energy storage density and has the capacity to store heat as latent heat of fusion at a constant temperature corresponding to the phase transition temperature of the phase change materials. Ice thermal storage systems use the latent heat of fusion of water. Thermal energy is stored in ice at freezing point of water 0 ºC. To store this energy, refrigeration equipment must provide charging fluid at temperatures of -9 ºC to -3 ºC (Dorgan and Elleson, 1993). This is below the normal operating range of conventional cooling equipment for air conditioning applications.

Depending on the ice storage technology, special ice making equipment is used, or standard production chillers are selected for low temperature service. The heat transfer fluid for ice making may be a refrigerant or a secondary coolant, such as glycol or some other antifreeze solutions. The low storage temperature of ice also provides the ability to produce lower temperature air for cooling.

3.1. Historical Background

Although ice storage and chilled-water storage systems increase currently in the air conditioning industry, the basic technologies were developed long ago. From a historical perspective, this section introduces the concept of comfort cooling using ice storage.

The use of natural ice or ice made without the aid of mechanical refrigeration goes back to far distant times; however, it began to be used extensively in the early years of the nineteenth century.

During the period from 1860 to 1900, mechanical refrigeration began to be applied to more than just ice making (Thevenot, 1979). In fact, the primary driving forces behind the development of mechanical refrigeration were:

a) the need for artificial ice,

b) the need for brewing and storing beer at low temperatures,

c) the need to preserve meat over extended periods of time by chilling or freezing,

d) the need to preserve milk and dairy product, fruits and vegetables, and other foodstuffs such as, ice cream, eggs, poultry, fish, chocolate, margarine and fats, wines, gassy drinks and fruit juices, and baked goods,

e) the need to satisfy the requirements of industrial process applications, such as those experienced in the slaughter and subsequent treatment of meat by packers, and those experienced in the immediate cooling of fresh milk after pasteurization by dairymen.

Although mechanical refrigeration was firmly established as a means to preserve goods, it was not until after 1890 that the first practical applications of industrial air conditioning emerged (Thevenot, 1979). This type of air conditioning was directed toward facilitating process applications or controlling the environment for certain materials or equipment. It was to these applications which mechanical refrigeration was primarily applied for the next thirty years. It was ice that would lead world into the age of comfort-cooling air conditioning.

Theaters were among the first applications to use air conditioning. In 1914, many theaters in the United States were cooled using ice. Figure 3.1 shows the means by which this was done (Cummings, 1989).

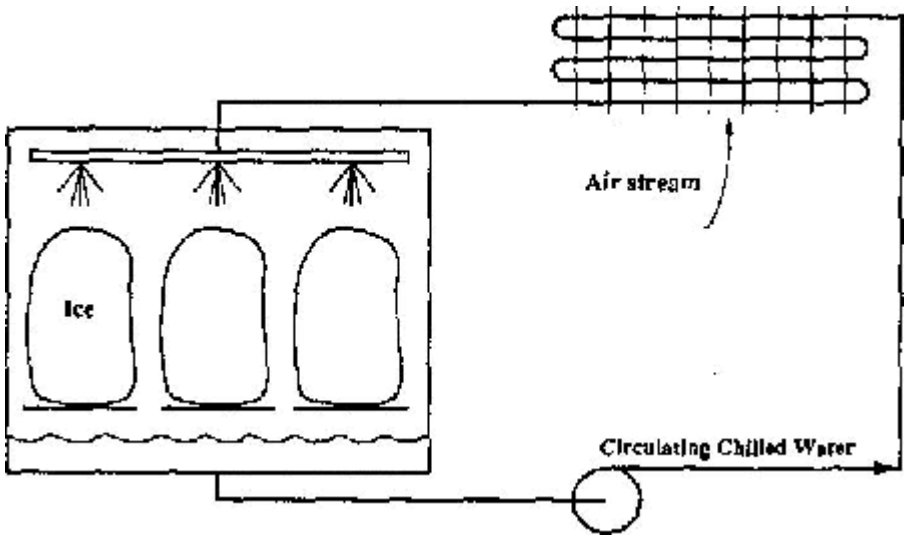


Figure 3.1. Air cooling by circulating ice-cooled water

Before the silent picture was to begin, ice was delivered by a horse-drawn ice wagon and then loaded into the vessel shown in schematic form in Figure 3.1. Water was then circulated through the coils, over which air was blown, and then sprayed uniformly over the blocks of ice from a header located above them. In this manner, sensible and latent heat from the air was transferred to the ice.

3.1.1. Cool Storage and the Electric Utility

The early applications of cool storage were limited to buildings with infrequent, short-term cooling loads, such as those experienced by theaters, churches, meeting halls, dairies, and breweries.

The goal of these applications was to significantly downsize the capacity of the air conditioning or refrigeration equipment and, thus, ultimately reduce the first cost of the system. This was possible since the extra capital required to purchase the storage equipment was outweighed by the savings obtained in selecting a relatively smaller chiller. Thus, the selection of a cool storage system was limited to special cases involving long periods between loads to allow for storage (Cummings, 1989).

Today, however, the selection of a cool storage system is not as stringently dependent on the length of time between loads; accordingly, other building load profiles have become amenable to cool storage. The new candidates for cool storage applications are office buildings, school and college buildings, laboratories, large retail stores, libraries, and museums. The reason for this increase in the number of application opportunities is not due to any inherent change in the technology itself; rather, it is driven by new electric rate structures.

The electric rate structures, as determined by the utility, are strongly dependent upon the utility's baseload (the minimum power demand on a utility's generation system over a specified period) capacity and its load factor (the quotient formed by dividing the utility's average load by its peak load, or more precisely, the integrated load over a period divided by the product of the maximum demand during that period and the length of time of the period). The load factor of American

utilities, on average, has been steadily declining since the 1960's where the average load factor was approximately 67 percent. Currently, the average load factor is approximately 62 percent (EPRI, 1987).

Ideally, the utilities would like a load factor of unity: a perfectly flat load profile where the average load is at all times equal to the peak load. This maximizes the effective use of generating capacity where the plant baseload capacity is, ideally, at all times greater than or equal to the instantaneous demand on the plant. Accordingly, the utility would have no need to invest in or operate peaking units, which are designed to meet demands that are in excess of the utility's baseload generating capacity. Typically, the operational cost per generated kilowatt for baseload electricity generation is only a small fraction of that for electricity generated by peaking units. Thus, utilities would like to avoid unnecessary use of the peaking units.

Cool storage offers a mechanism by which the utility can improve its load factor. Because of the large demand for commercial comfort cooling, the most severe seasonal demand occurs, for most utilities, during the hottest summer months. Of the total electrical demand by the commercial sector, approximately 44 percent is related to comfort cooling during a summer peak (EPRI, 1987). Accordingly, cool storage applications have the potential to enhance the utility's load profile by decreasing the demand for electricity during the peak period of the day and shifting it to the late evening and early morning hours.

3.2. Fundamentals of Cool Thermal Energy Storage

Cooling capacity can be stored either by chilling or freezing water (or such other materials as glycol and eutectic salts). Water is the storage material of choice for a variety of practical and thermodynamical reasons, including its ready availability, relative harmlessness, and its compatibility with a wide availability of equipment for its storage and handling. The choices between whether the water should be used in sensible or latent types, which equipment should be used, if eutectic salts should be applied to raise freezing temperatures, etc., are often not simple. Options are numerous, and answers are not clear cut. Ultimately, the cool

thermal energy storage system (CTES) selected must meet the particular needs and constrains of the specific facility in which it is installed.

CTES has many advantages. Lower night-time temperatures allow refrigeration equipment to operate more efficiently than during the day, reducing energy consumption. Lower chiller capacity is required, which leads to lower equipment costs. Also, using off-peak electricity to store energy for use during peak demand hours, daytime peaks of power demand are reduced, sometimes deferring the need to build new power plants.

CTES systems are presently operational in many commercial and industrial buildings in various countries. Many are not achieving expected design performance, often because TES design engineers and construction companies in the past lacked experience. Now, package-type TES systems are available and are commonly used, which involve more straightforward design and installation for conventional air conditioning systems. Therefore the economic and other benefits of thermal energy storage systems operating performance at design conditions for system owners is more likely.

There are principally three types of cool storage systems being considered today:

I. Chilled water
II. Ice
III. Eutectic salts

Of these, the first two are the most promising for general use at the present time. All systems have three basic components: a chiller, a storage tank and a means to deliver chilled water or air to the occupied space (Dincer, 2002).

3.2.1. Chilled Water Storage

Chilled water storage systems use the sensible heat capacity of water to store cooling. Water is cooled by chiller and stored in a tank for later in use in meeting

cooling needs. The amount of stored cooling energy depends on the temperature difference between the chilled water stored in the tank and the warm return water from the load. A well-designed chilled water storage system maximizes stored cooling capacity by maintaining a high chilled water temperature differential. This differential is maximized by maximizing the return water temperature, minimizing the storage temperature, and preventing the warm return water from mixing with the stored chilled water.

Chilled water storage systems are typically charged with water at temperatures between 4 ºC and 7 ºC. This temperature range is compatible with most nonstorage cooling systems and allows the use of conventional chillers, including absorption chillers operating at conventional temperatures. Storage volume for chilled water storage systems with temperature differentials of 6 ºC to 11 ºC is generally 0.048 and 0.091 m^3/kWh (Dorgan and Elleson, 1993). If a temperature differential of 17 ºC can be maintained, the required storage volume is reduced to about 0.056 m^3/kWh. This space requirement is three to seven times that of ice storage systems and two to three times that of eutectic salt phase-change systems. However, because chilled water storage tanks are relatively tall, plan area requirements are often comparable with other storage technologies. When space is available, chilled water storage can be an economical way of storing large amounts of cooling capacity.

Chilled water storage is most economical for applications with cooling loads requiring storage of more than 7000 kWh or about 760 m^3. The larger the tank, the lower the surface-to-volume ratio, and the lower the cost per ton-hour of stored cooling. Many large chilled water storage systems store over 3.800 m^3 of water; some storage over 19.000 m^3 (Dorgan and Elleson, 1993).

A chilled water system with multiple tanks or compartments can simultaneously store warm and chilled water. For example, one tank can store recovered heat to supplement the heating needs of a building during winter days, while another tank can store chilled water to meet simultaneous cooling needs in the core of building.

Chilled water storage is based on maintaining a state of thermal separation between cool charged water and warm return water. Storage systems achieve this separation by one of the following methods:

- Stratification
- Multiple tank
- Membrane or diaphragm
- Labyrinth and baffle

Stratified chilled water storage is generally acknowledged as the simplest, most efficient, and most cost-effective method of chilled water storage. Other systems have been used, however, and some may be appropriate in some applications.

Chilled water storage using stratified tanks with properly designed diffusers is a simple, low-maintenance cooling operation. Tanks for chilled water storage are often very large and may be very difficult to site due to space limitations and aesthetic considerations. Tanks may be installed partially or completely below grade, but this increases the first cost.

3.2.2. Ice Storage

Ice storage systems use smaller tanks and offer the potential for the use of low-temperature air systems, but require more complex chiller units. Ice CTES systems use the latent heat of fusion of water (335 kJ/kg) to store cooling capacity. To store energy at the temperature of ice requires refrigeration equipment that provides charging fluids at temperatures below the normal operating range of conventional air conditioning equipment.

Special ice-making equipment or standard chillers modified for low temperature service are used. The low chilled-water-supply temperatures available from ice storage allow the use of cool-air distribution, the benefits of which include the ability to use smaller fans and ducts and the introduction of less humid air into occupied spaces.

With ice as the storage medium, there are several technologies available for charging and discharging the store:

- Ice harvesting systems
- External melt ice-on-coil storage systems
- Internal melt ice-on-coil storage systems
- Encapsulated ice systems

3.2.2.1. Ice Harvesting Systems

The ice harvesting refrigeration plant generates and releases sheets or tubes of ice with a specially designed evaporator section. Water is pumped out of the storage tank at low pressure and is distributed over the evaporator surfaces, where it is chilled or frozen (Figure 3.2). The ice harvesting plant is technically called an ice harvester chiller, or ice harvester, since it operates as both an ice maker and as a water chiller (Dorgan and Elleson, 1993).

In the ice making mode, a portion of water flowing over the evaporator plates or tubes solidifies, forming a layer of ice that is periodically harvested or dropped into the storage below. In the water-chilled mode, warm return water flows over the same evaporator surfaces, is cooled, and falls into the tank as chilled water.

The selection of ice making or chiller mode is made automatically, depending on the temperature of the water as it enters the evaporator. If the water is at or near the freezing point, ice making mode is selected, and a defrost cycle is activated at intervals to release the ice from the evaporator.

In chiller mode, the defrost cycle is deactivated. The cooling capacity and efficiency increase with the temperature of the water entering the evaporator. During the discharge cycle, ice water is taken from the bottom of the tank and circulated to the building load. The discharge temperature remains relatively constant throughout the discharge cycle, rising only as the last ice has melted.

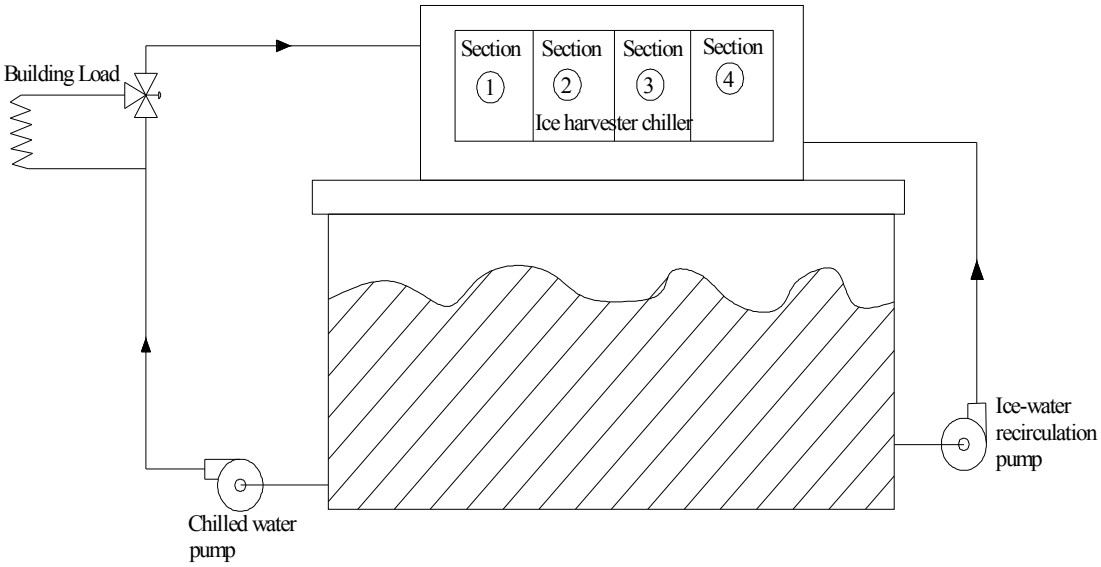


Figure 3.2. Ice harvesting system (Dorgan and Elleson, 1993)

Ice harvester thermal storage systems:

- Normally consist of a factory-assembled ice making plant mounted on top of a site-built storage tank which contains a mixture of ice and chilled water.
- Provide nearly instantaneous response to short-term cooling needs such as in batch processing of food products.
- Change mode automatically from ice generation to chilled water generation in accordance with load conditions.
- Produce high continuous discharge rates.
- Require sufficient overhead clearance to mount the evaporator package above the storage tank.

The refrigeration plant for an ice harvesting system is usually assembled and delivered as a package. Complete compressor, condenser, evaporator packages are available in sizes from about 35 to 530 kW nominal ice making capacity. Compressor-evaporator packages, with water-cooled condensers or for field connection to a remote condenser are available up to about 1300 kW ice making capacity (Dorgan and Elleson, 1993). Split systems and evaporator-only packages are also available. Packages typically include all required valves, accumulators, refrigeration controls, and associated pumps. An arrangement of automatically

controlled solenoid valves manages the flow of cold liquid refrigerant and hot refrigerant gas. Evaporators are available in flat-plate, tube, or double-wall tube configurations.

Ice harvesters typically produce evaporator temperatures in the range of -9 ºC to -3 ºC when in ice making mode and 1 ºC and higher when in chilling mode, depending on the return water temperature. Reciprocating and screw compressors using the refrigerant R-22 are most common for these systems because of the relatively wide range of evaporator temperatures. However, several built-up systems of 1400 kW ice making capacity or greater are used with multiple evaporator modules and ammonia refrigerant. The use of ammonia is well-suited to such applications, especially, where operating staff have the necessary refrigeration expertise, and can result in reductions in first cost.

Ice building and defrosting in the ice making mode is controlled by timers supplied with the ice harvester package. The machine builds ice for a predetermined amount of time, typically 10 to 30 min. During the defrost cycle, hot refrigerant gas is released into the evaporator for 20 to 60 s. to release the ice (Dorgan and Elleson, 1993). Refrigeration systems must be designed to accommodate the pressure fluctuations due to variations in condensing conditions during defrosting.

3.2.2.2. External Melt Ice-on-Coil Storage Systems

An external melt ice-on-coil storage system, sometimes referred to as an ice builder, builds and stores ice on the exterior surfaces of a heat exchange coil submerged in a non-pressurized water tank (Dorgan and Elleson, 1993).

To charge the storage system, liquid refrigerant or a secondary coolant, such as a glycol solution, is circulated inside the heat exchange tubes, causing ice to form on the outside of the tubes. To discharge storage cooling, the ice on the tubes is melted by warm return which circulates through the tank. The resulting chilled water is used to meet the building load. Air is bubbled through the water during the beginning of the charging cycle and during discharging; to equalize the water

temperature and promote even building and melting of the ice. Figure 3.3 illustrates the external melt charging and discharging process.

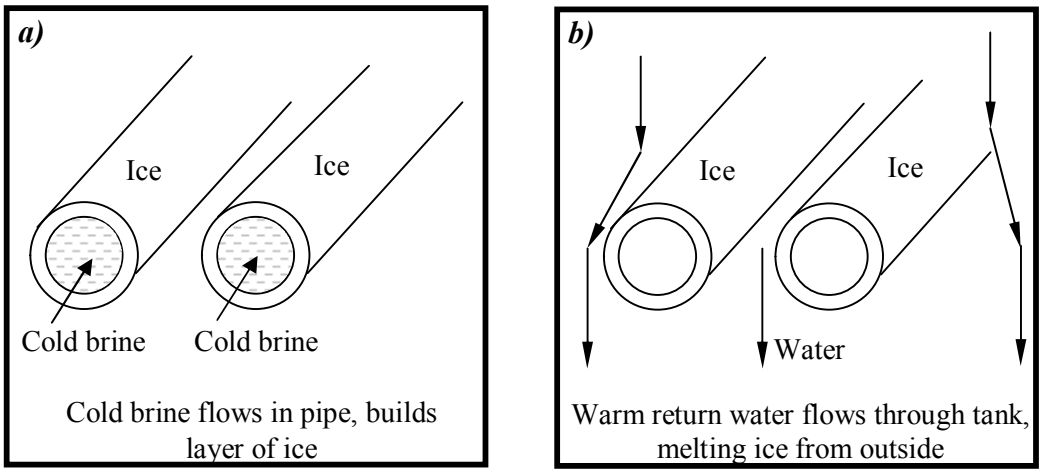


Figure 3.3. External melt ice storage ***a)*** Charge ***b)*** Discharge

Ice is normally built to a thickness of 40 to 65 mm on the pipes, depending on the application. The greater thickness requires lower charging temperatures and is generally applied where existing refrigeration is operating at -12 ºC to -9 ºC. Thinner ice is built in applications where higher charging temperatures and greater efficiency are desired.

If an external melt ice tank is overcharged, ice may freeze solid between adjacent tubes. While some bridging may not have serious consequences, extensive bridging can impede water flow and ice melting, resulting in increased discharge temperatures.

External melt ice-on-coil systems:

- require approximately 0.023 m^3 /kWh of storage tank volume per kWh of stored cooling.
- supply chilled water from an open ice-builder tank to the load.
- use liquid refrigerant or a secondary coolant as the charging fluid.
- provide discharge temperatures of 1 ºC to 2 ºC through most of the discharge cycle.

- ❖ are subjected to an efficiency penalty if all ice is not melted during each discharge cycle.

An external melt ice storage system building 40 mm thick ice requires a chiller capable of generating charging temperatures of -7 ºC to -3 ºC. For system building ice to 64 mm thick, charging temperatures of -12 ºC to -9 ºC are required (Dorgan and Elleson, 1993).

External melt systems can be divided into those that use refrigerant directly to build ice, with the ice-builder pipes acting as the evaporator, and those that build ice indirectly using a secondary coolant cooled by a chiller. The direct refrigerant system was used in early external melt systems, and is still widely applied in industrial applications such as dairies and food processing plants. Secondary coolant systems are mostly commonly used for HVAC applications, because the refrigeration plant is simpler to design, install, and maintain, and because the volume of refrigerant used is much less.

A direct refrigerant system is more efficient than a secondary coolant system, because there is one less step of heat transfer between the evaporating refrigerant and the ice building surface. However, designing, installing, and maintaining such a system requires refrigeration expertise not commonly available in the commercial HVAC industry. This approach is well-suited to applications where the necessary expertise is available, such as existing refrigeration plants.

3.2.2.3. Internal Melt Ice-on-Coil Storage Systems

In this study, an internal melt ice-on-coil storage system is considered. Therefore, this kind of systems is explained in detail in this section. Internal melt ice-on-coil storage systems use a secondary coolant as the charging and discharging heat transfer fluid, circulating it through tubes or coils submerged in water-filled tanks. To build ice, a chiller cools the coolant to -6 ºC to -3 ºC , and ice forms on the outside of the tubes. To discharge storage, warm coolant flows through the tubes, melting the ice from the inside out and reducing the coolant temperature for use in melting the cooling load.

Figure 3.4 illustrates the charging and discharging process in an internal melt system. Internal melt ice systems are typically configured with the storage tanks in series with the chiller, in either chiller upstream or chiller downstream arrangements.

Internal melt ice-on-coil systems:

- use a secondary coolant, typically ethylene glycol, as both the charging and discharging fluid in closed loop system.
- provide sustained discharge temperatures of 2 ºC to 3 ºC, which are depended on discharge rate and the amount of ice remaining.
- require chillers capable of producing charging temperatures of -6 ºC to -3 ºC.
- are available with modular tanks.

In the chiller upstream configuration using a partial storage operating strategy, warm return fluid from the building load is pre-cooled by the chiller before entering the storage tanks. This arrangement provides more efficient chiller operation because of the higher operating temperatures. However, the usable portion of the total nominal storage capacity is reduced because of the lower storage discharge temperature. In a chiller downstream configuration, warm return water first flows through the storage tanks, where it is cooled before entering the chiller.

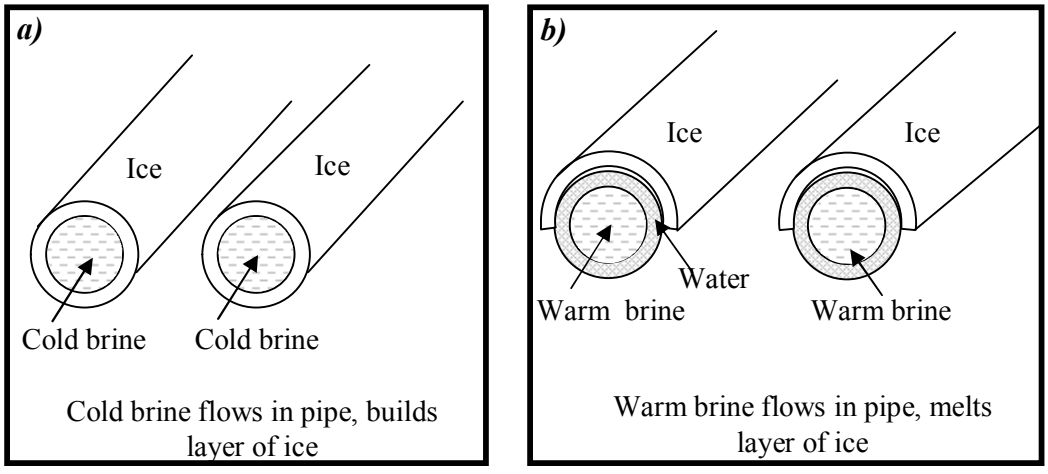


Figure 3.4. Internal melt ice storage ***a)*** Charge ***b)*** Discharge

This arrangement results in a higher usable storage capacity, as well as an assured constant discharge temperature. However, chillers operate at lower discharge

temperatures and less efficiently than in the chiller upstream arrangement. Figure 3.5a-b presents schematic diagrams of typical chiller upstream and chiller downstream configurations.

Internal melt thermal energy storage systems use standard chillers selected to provide coolant temperatures of -6 ºC to -3 ºC. Chillers that must also provide direct cooling will typically operate at 2 ºC to 6 ºC, depending on the specific application.

Positive displacement compressors, such as reciprocating or rotary screw types, are often used because of low charging temperatures and the relatively wide range of operating temperatures. Centrifugal compressors may be used provided they are properly selected for the intended range of evaporator temperatures.

Storage tanks for internal melt systems are available in several configurations. Modular tanks with 350 to 700 kWh nominal capacity are manufactured in cylindrical plastics or rectangular steel configurations, with plastic heat exchange tubing (Dorgan and Elleson, 1993).

Rectangular steel tanks are variable with galvanized steel heat exchange coils. Prefabricated steel pipe heat exchangers are also available for installation in site-built tanks, which are generally concrete.

Tanks can be located indoors or outdoors. Concrete tanks may be buried or located on-grade. Cylindrical tank modules can be stacked on a supporting framework. Modular tank manufacturers recommend an overhead clearance of 1 m to facilitate inspection and repair.

Modular internal melt tanks are designed to freeze all the water between the heat exchange tubes. If the tanks are overcharged, the water forced up into the expansion volume of the tanks during freezing will also be frozen. Since there is a little or no heat transfer surface in this area, it is difficult to melt ice once it forms here. The formation of such an ice cap reduces the storage capacity of the tank by reducing the volume of water available to cover the heat exchange tubes. However, this problem can be solved by installing a perforated, insulated partition between the active portion of the tank and the expansion volume. Water is free to flow into and out of the expansion volume, but the insulation prevents it from freezing.

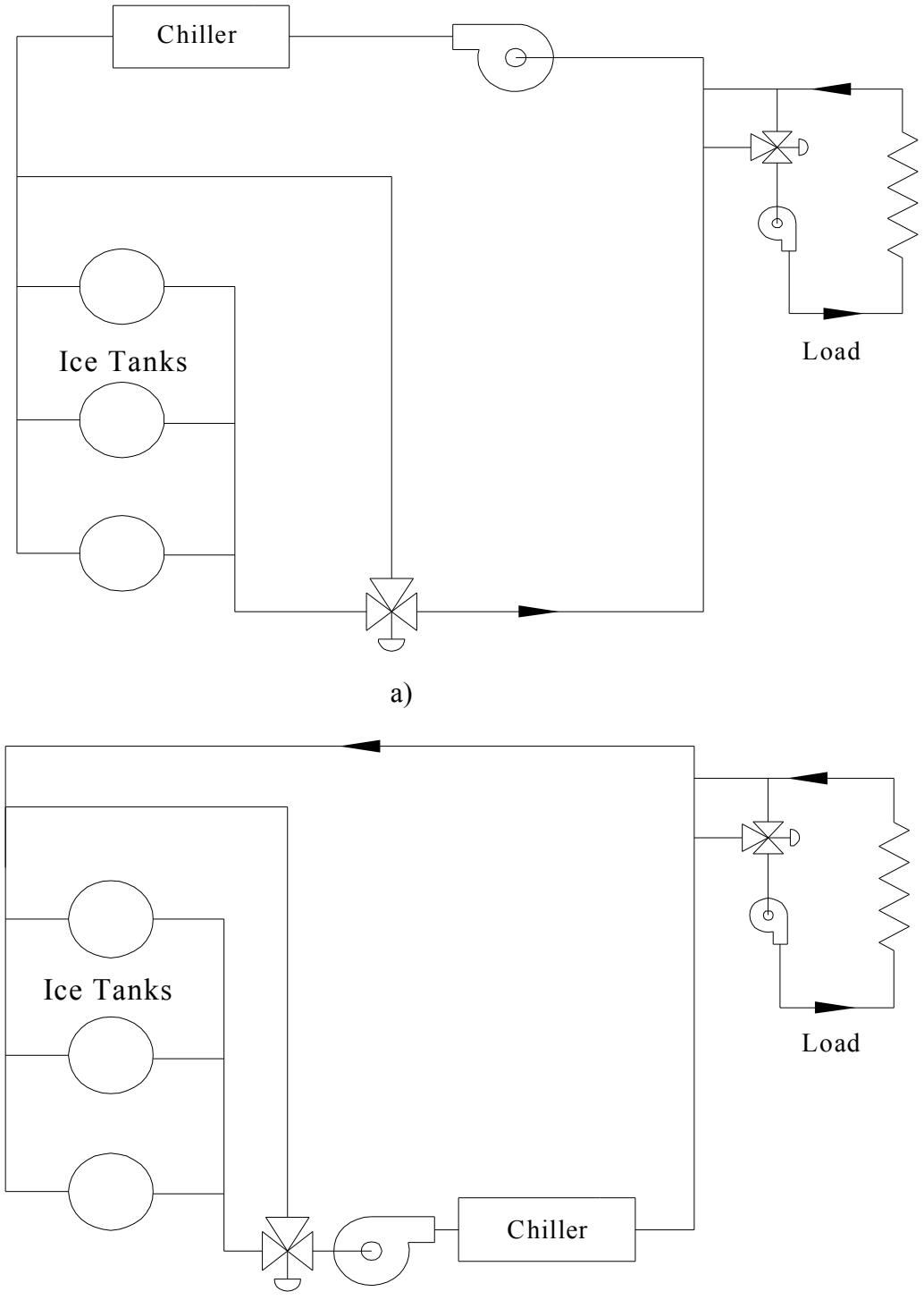


Figure 3.5. Typical internal melt storage configuration (Dorgan and Elleson, 1993) a) Chiller upstream b) Chiller downstream

An internal melt ice storage system is closed and pressurized. The storage loop can be directly connected to the building distribution loop or separated by a heat exchanger.

If a heat exchanger is used to separate the storage loop from the chilled water distribution loop, the distribution side must be protected from freezing during charging, when the coolant temperature may be as low as -6 ºC. Typically, a charging bypass is provided around the heat exchanger.

Flow should be diverted through the bypass using two linked two-way valves -rather than a three-way valve, since the three-way valve is more likely to allow some leakage to the heat exchanger. It is also advisable to provide heat exchanger freeze protection, such as starting secondary pumps if the primary side temperature falls below 2 ºC.

The low discharge temperature available from internal melt systems allow the use of chilled water temperature ranges of -4.4 ºC or higher, resulting in significant reductions in the cost of pumps, piping, and pump energy compared to typical non-storage systems. These discharge temperatures are also well-suited to the use of cold air distribution (Dorgan and Elleson, 1993).

3.2.2.4. Encapsulated Ice

As shown in Figure 3.6, an encapsulated ice thermal storage system consists of plastic containers of water immersed in a secondary coolant, such as an ethylene glycol. Freezing and thawing take place in the water held inside the containers (Dorgan and Elleson, 1993).

Encapsulated ice containers are made of high-density polyethylene and are designed to accommodate the expansion and resulting pressure of freezing ice. Spherical containers are factory-filled with deionized water and nucleating agent. Rectangular containers are generally filled on site with deionized water.

Encapsulated ice storage can use open, nonpressurized tanks, or pressurized tanks. Open tank systems generally require a restraining grate or barrier to keep the frozen containers submerged.

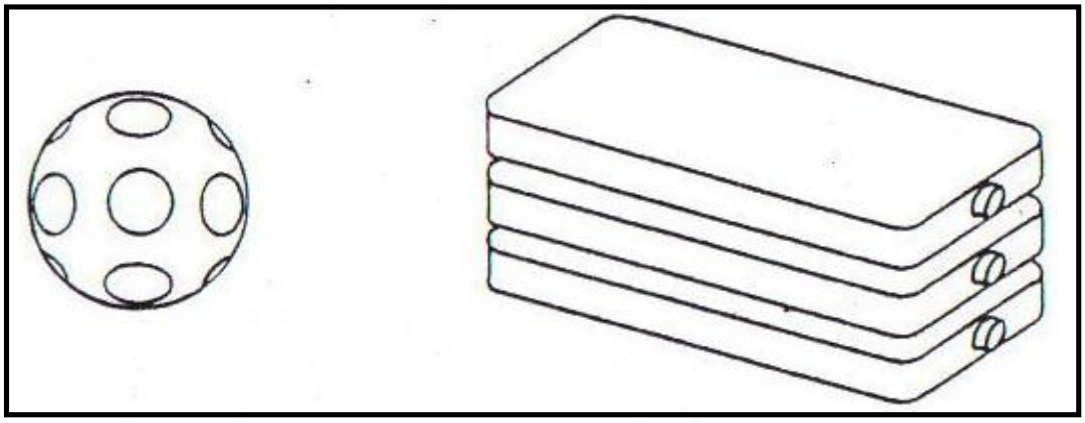


Figure 3.6. Encapsulated ice containers

To charge storage, coolant at -6 ºC to -3 ºC is circulated through the tank. The water inside the containers gives up its latent heat and freezes. To discharge storage, warm coolant carrying heat from the load is circulated through the tank, melting the encapsulated ice and lowering the coolant temperature. The chilled coolant is then used to meet the load either directly or through a heat exchanger. Figure 3.7 illustrates the formation of ice in spherical containers during charging and discharging.

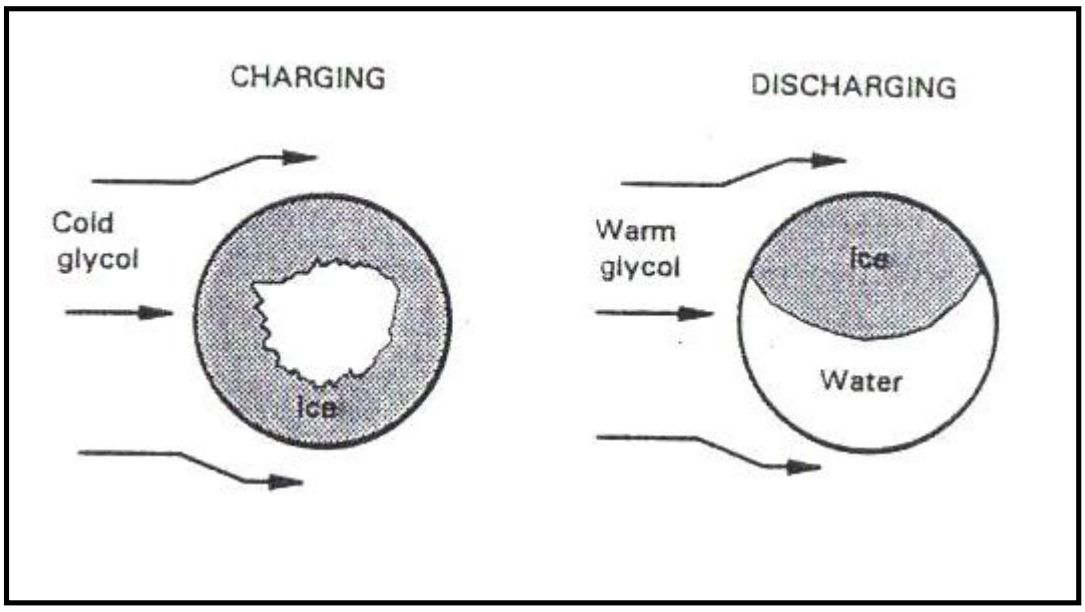


Figure 3.7. Charge and discharge of encapsulated ice storage

Spherical containers are simply funneled into a storage tank during installation. Due to their symmetrical shape, they settle into a packing arrangement that allows free circulation of the heat transfer fluid around each container.

The rectangular containers are manually stacked inside the tank. Molded feet on each container provide clearance for fluid circulation. These containers need to be stacked inside the tank in such a way that expansion and contraction movements and the force of circulating fluid does not open unwanted passages for fluid flow, which can lead to short-circulating and degradation in performance.

Encapsulated ice systems:

- use a secondary coolant, typically ethylene glycol, as a bath for plastic water containers.
- require approximately 0.019 to 0.023 m^3/kWh of available stored cooling.
- require chillers capable of producing charging temperatures of -6 ºC to -3 ºC.

Encapsulated ice systems are typically configured with the storage tanks in series with the chiller, in either chiller upstream or chiller downstream arrangements. Arrangements with the tanks in parallel with the chiller during discharge are also possible.

Encapsulated ice thermal energy storage systems use standard chillers selected to provide coolant temperatures of -6 ºC to -3 ºC. Chillers that also provide direct cooling typically operate at 2 ºC to 6 ºC, depending on the specific application. Positive displacement compressors, such as reciprocating or rotary screw types, are often used because of the low charging temperatures and the relatively wide range of operating temperatures. Centrifugal compressors may be used provided they are properly selected for the intended range of evaporator temperatures.

3.2.3. Eutectic Salt Phase-Change Materials

A eutectic salt is a chemical mixture which changes phase from liquid to solid at a specific temperature. Just as water stores a large amount of cooling at 0 ºC as it

changes from a liquid to solid ice, eutectic salts store cooling at their phase-change temperatures.

Eutectic salt phase-change materials have been used for various heat storage applications since the 1800 s, but only recently have they been used as a cool storage medium (Dorgan and Elleson, 1993). The most common formulation for cool storage applications is a mixture of inorganic salts, water, and nucleating and stabilizing agents, which melts and freezes at 8.3 ºC. This material is encapsulated in rectangular plastic containers, which are stacked within a storage tank. Figure 3.8 shows a stack of containers. Water serves as the heat transfer fluid; it circulates through the storage tank among the eutectic salt containers, carrying heat to or from the storage medium.

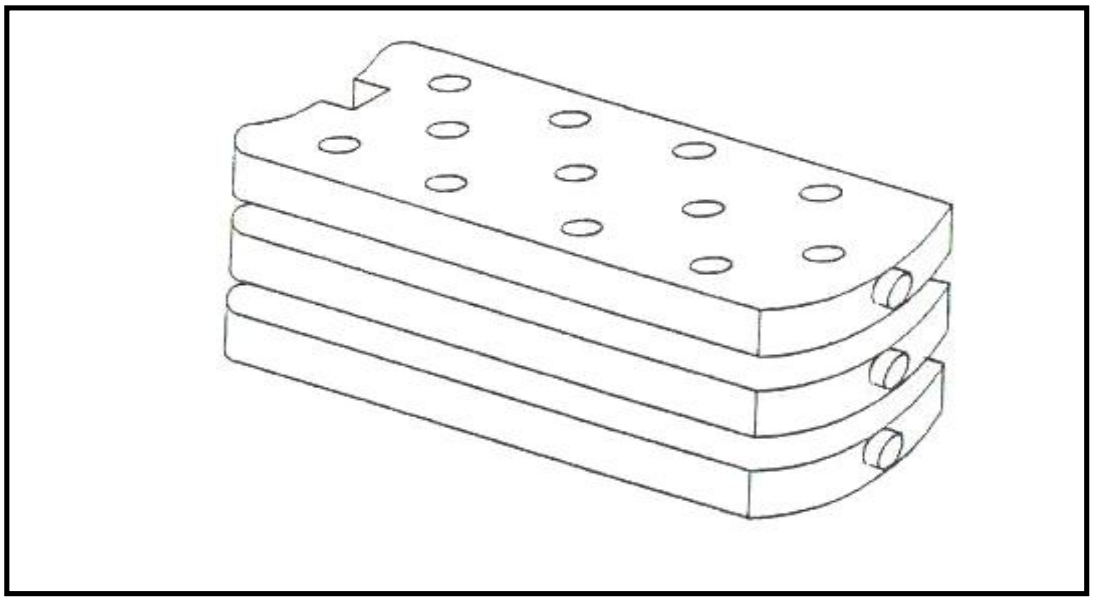


Figure 3.8. Stacked eutectic salt storage containers (Dorgan and Elleson, 1993)

The 8.3 ºC eutectic salt can be charged with typical conventional chilled water temperatures of 4 ºC to 6 ºC. This allows the addition of storage to existing systems with no modifications to existing chillers and few or no changes to existing distribution systems. Typical discharge temperatures of 9 ºC to 10 ºC are relatively high for most HVAC systems.

Eutectic salt mixtures are also available for lowering the storage temperatures of ice systems. Additives are available that produce freezing temperatures of -2 ºC to -11 ºC in ice storage tanks (Dorgan and Elleson, 1993).

Eutectic salt phase-change material systems:

- use conventional chilling equipment at standard temperatures, which makes this medium attractive for retrofits.
- have high storage discharge temperatures.
- require approximately 0,048 m^3/kWh of storage volume per kWh.

Eutectic salt storage systems use conventional chilling equipment to provide chilled water 4 ºC to 6 ºC to charge the storage tanks. Eutectic salt storage is generally used in applications having relatively high loads, which typically use centrifugal chillers.

However, there is no inherent reason other than size favoring one type of refrigeration equipment over another. Reciprocating or screw chillers can also be used. Absorption chillers could be used to charge eutectic salt systems. However, the efficiency of absorption chillers falls of significantly at leaving water temperatures below approximately 6 ºC.

Eutectic salt storage can often be added to an existing cooling plant, simply by adding a storage tank and associated piping. In most cases, existing chillers require no modification. Adding eutectic salt storage to a conventional system can also be easing the transition to non-CFC refrigerants. Eutectic salt storage enables a building owner to add capacity now, at relatively low expense, in anticipation of loss of capacity associated with the performance of the new refrigerants in the future. Because of their favorable charging temperature, phase-change materials are compatible with currently available refrigerants as well as any future replacements.

3.3. Operating and Control Strategies of CTES Systems

The cool storage operating mode desired determines the size of storage capacity required or, conversely, the amount of space available for storage influences

the operating mode selected. In either case, a number of variables must be considered, and these should be discussed comprehensively in feasibility analysis. Today, there are basically 4 control strategies available. They are full-storage, partial-storage, partial-storage load leveling type and partial-storage demand limiting type.

3.3.1. Full Storage

Full-storage, or load-shifting (Figure 3.9), shifts the entire on-peak cooling loads to off-peak hours and usually operates at full capacity to charge storage during all non-peak hours. On-peak times, all cooling loads are met from storage, and the chiller does not run. A full-storage system requires relatively large chiller and storage capacities and is most attractive where on-peak demand charges are high or the on-peak period is short.

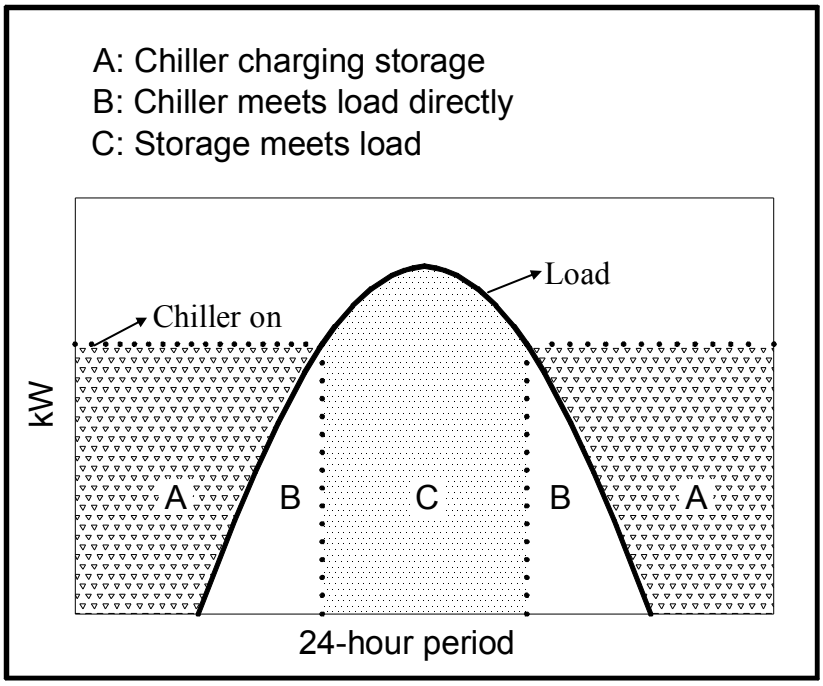


Figure 3.9. Full-storage operating strategy

3.3.2. Partial Storage

A partial-storage system meets a portion of the on-peak cooling load from storage, with the remainder of the load met by operation of the chilling equipment. With this strategy chiller capacity is less than design load. Partial-storage operating strategies can be further subdivided into load-leveling and demand-limiting operation.

Additional variations on the full- and partial-storage strategies are possible by scheduling the operation of multiple chillers.

Partial-storage systems use one of two control strategies to divide the load between chiller and storage. A chiller priority strategy uses the chiller to directly meet as much of the load as possible. Cooling is supplied from storage only when load exceeds chiller capacity. Storage-priority meets as much of the load as possible from stored cooling, using the chiller only when daily load exceeds total stored cooling capacity. Some systems use combinations of these strategies.

3.3.2.1. Partial-Storage Load Leveling Type

In a load-leveling system, the chiller typically runs at full capacity for 24 hours on the design day (Figure 3.10). When the load is less than the chiller output, the excess cooling is stored. When the load exceeds chiller capacity, the additional requirement is discharge from storage. This approach minimizes required chiller and storage capacities and is particularly attractive where peak cooling load is much higher than the average load. In many systems, cooling loads during off-design periods are small enough that partial-storage systems may be operated as full-storage systems. This can increase savings but care must be taken to not deplete storage before the on-peak period is over.

3.3.2.2. Partial-Storage Demand Limiting Type

A demand-limiting partial-storage system operates the chiller at reduced capacity at on-peak times (Figure 3.11).

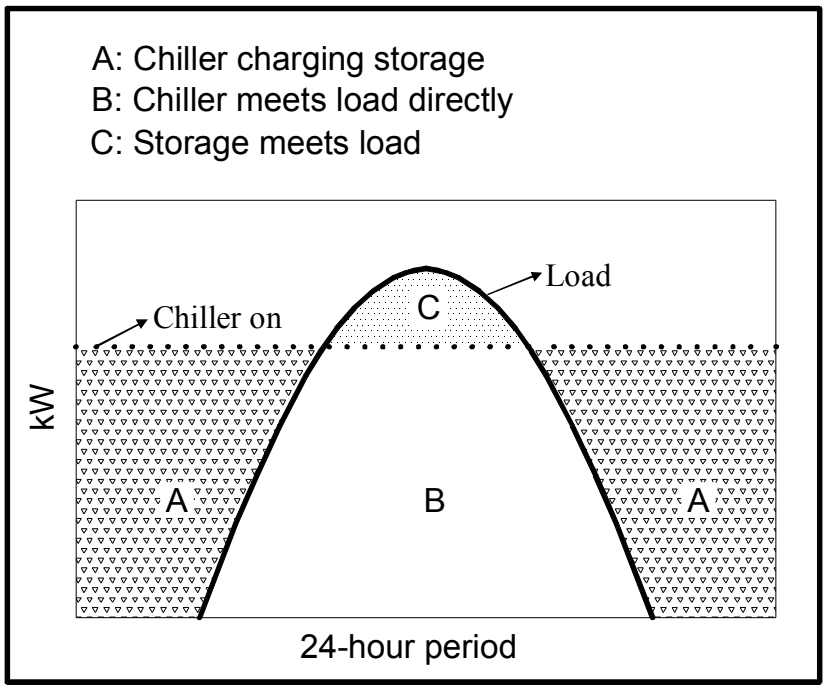


Figure 3.10. Partial-storage load leveling operating strategy

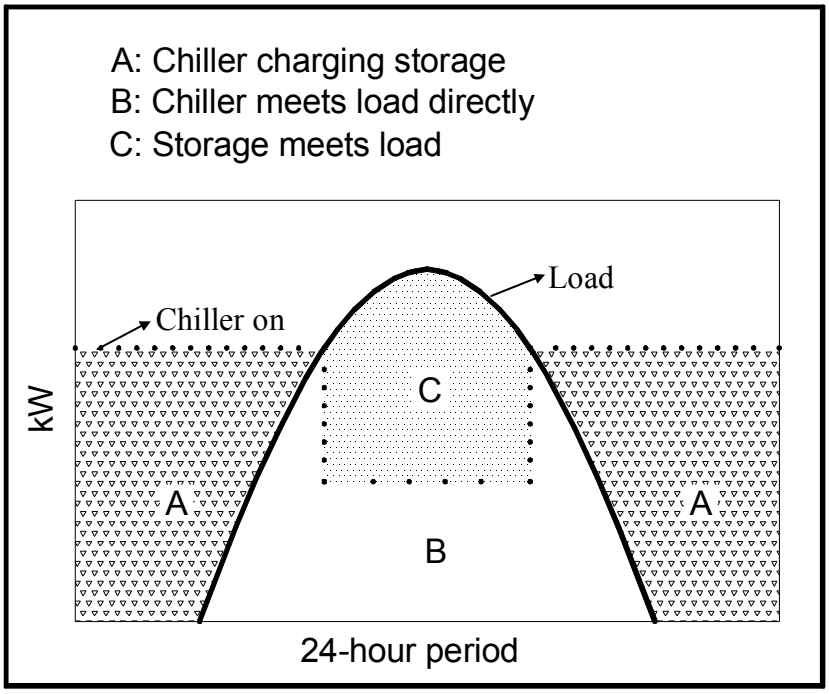


Figure 3.11. Partial-storage demand limiting operating strategy

The chiller may be controlled to limit facility demand at the billing meter. This strategy falls between load shifting and load leveling. Demand savings and equipment costs are higher than for load leveling, and lower than for load shifting. Here too care must be taken not to deplete storage before the end of the on-peak period.

3.4. Experimental Study

In the experimental part of the this study, a room that is located in the Laboratories of Mechanical Engineering Department of Çukurova University was air-conditioned using an internal melt ice-on-coil storage system. The system was designed and constructed originally by Güler (2002) and Serin (2002). In this study, after improving the existing experimental set up (Experimental Setup 1), several charge and discharge experiments were carried out to investigate performance characteristics of the ice storage system.

The results of the experiments carried out with Experimental Setup 1 showed that mechanisms observed during the ice formation (supercooling, nucleation, and dendritic ice formation) are very important parameters for system performance and they should be investigated in detail. Therefore, a parallel experimental system (Experimental Setup 2) was constructed to understand solid-liquid phase change heat transfer phenomena around a tube. Below details of both experimental setup are given.

3.4.1. Experimental Setup 1

General view of the ice storage based air-conditioning system (internal melt ice-on-coil) is shown in Figure 3.12 and also schematically in Figure 3.13. Although the system can be operated both under full-storage and partial-storage load leveling operating strategies, only full-storage was considered in this study. The experimental system included an air-cooled chiller, a circulation pump, an ice storage tank, interconnecting piping, controllers (two and three way valves), fan-coils, temperature controllers, measuring equipment and data collection system (Fertelli et al., 2006). The glycol-water solution (brine) of 30 % concentration by weight was used as the transport fluid.

During the charging cycle (Figure 3.13), the chilled brine issued from the chiller extracts heat from the storage tank, and is then returned to the chiller. As the charging process continues, the temperature of the storage medium decreases



Figure 3.12. Ice storage air-conditioning system

(and, correspondingly, so does the chiller's evaporator temperature which results in degradation of thermal performance) until it reaches its freezing point. At that time, ice begins to form on the surface of the tubes contained within the storage tank.

In this study, ice production (charging) was accomplished between 22:00 and 06:00 hours (off –peak period). According to the electric utility (TEDAS), the day is divided into three periods: 17:00 to 22:00 (peak period), 22:00 to 06:00 (off-peak period), and, 06:00 to 17:00 p.m. (normal period). At the present time, variable tariffs are optional for all electricity consumers in Turkey. Compared with the constant tariffs (daylong constant prices) for office buildings, the cost of electricity is 50% higher for the peak period, and 49% and 7% lower for the off-peak and the normal periods, respectively, according to the variable tariffs. During ice making period, temperature of brine was maintained between -4 ˚C and -8 ˚C at the exit of the evaporator.

During discharge operation, refrigeration equipment does not run during on peak hours, and all cooling loads are met from storage. Figure 3.14 illustrates discharging cycle of the experimental system. Brine is first chilled in the tank and then is circulated through the fan-coils to provide space cooling.

In this study, ice melting (discharging) was accomplished between 08:00 and 17:00 hours. During ice melting, temperature of brine at the inlet of the room to be air-conditioned was set to 7 $^{\circ}$C. A three-way valve (blending) provides a fixed temperature of brine temperature to the room.

Below details of the units used in Experimental Setup 1 are given.

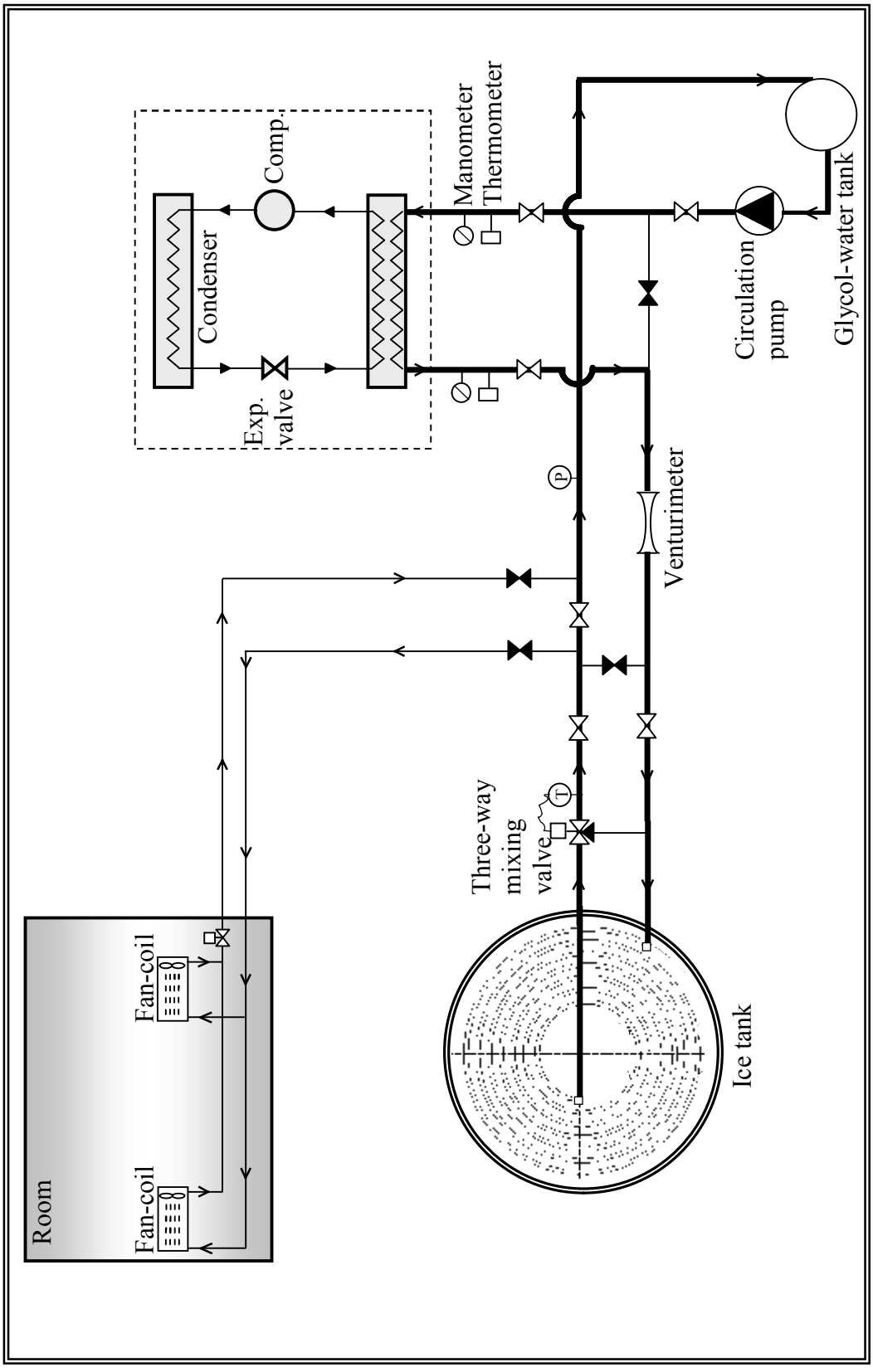


Figure 3.13. Schematic representation of the experimental setup 1 (Charging cycle)

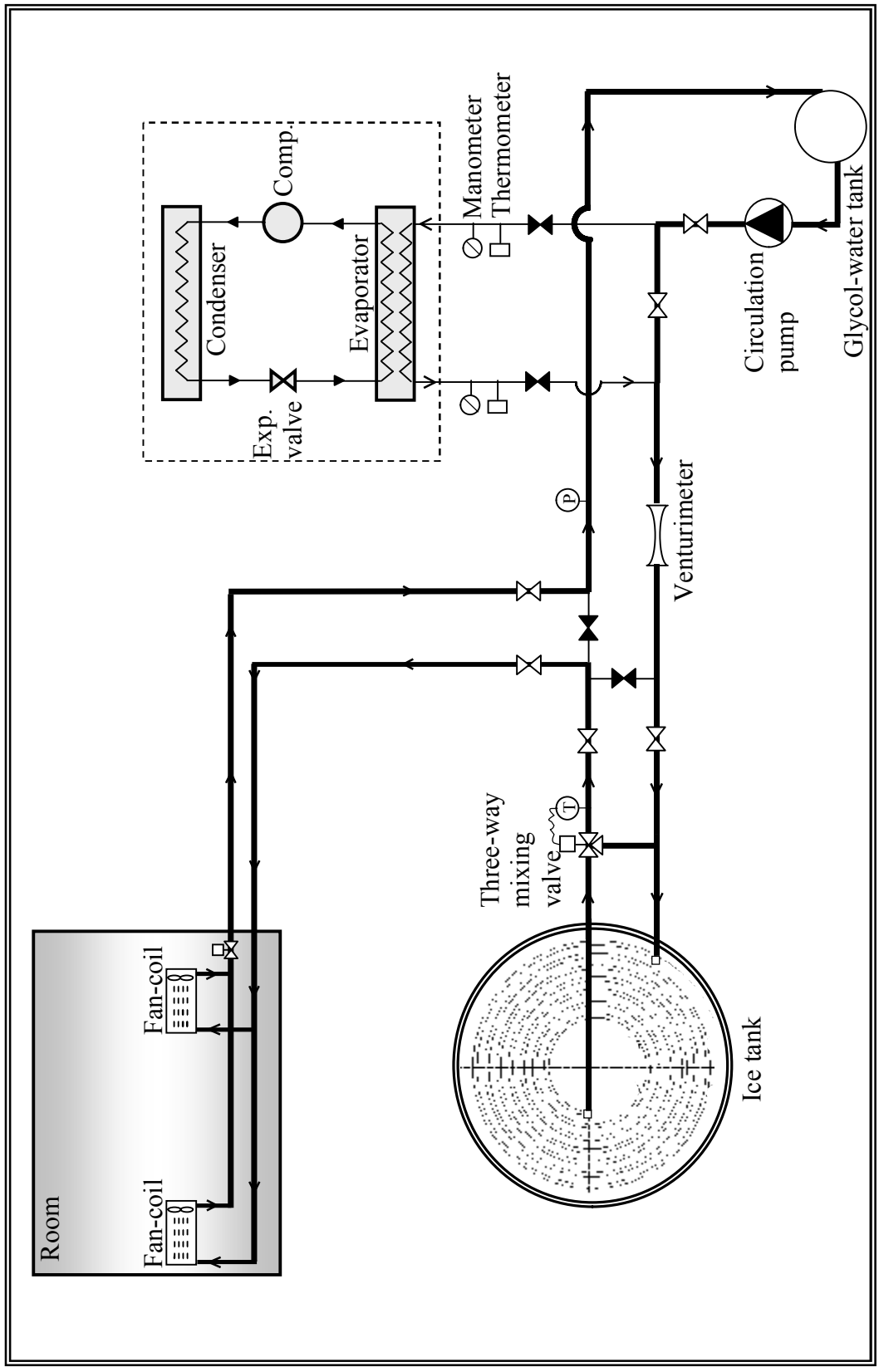


Figure 3.14. Schematic representation of the experimental setup 1 (Discharging cycle)

3.4.1.1. Air Cooled Chiller

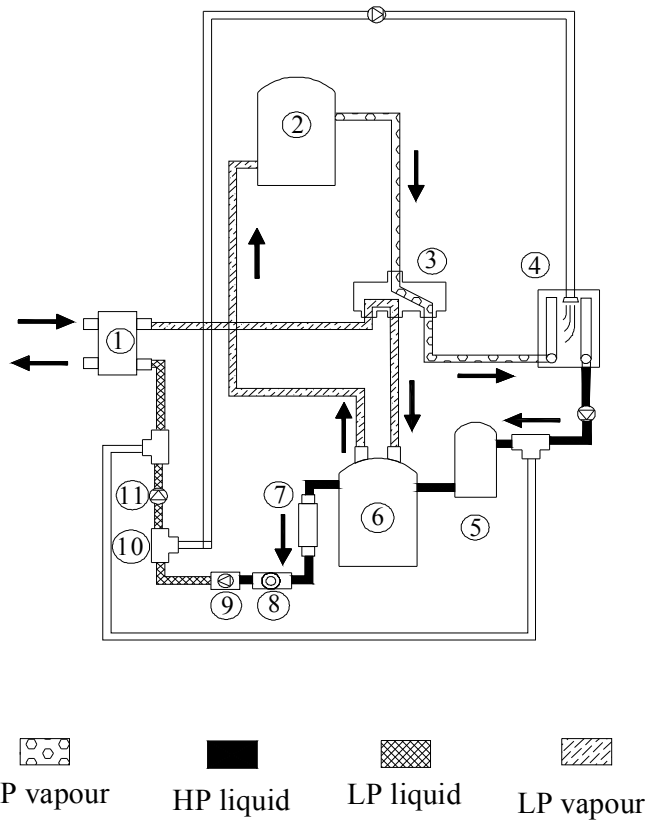
McQuay MHP 04P air-cooled water chiller with a nominal cooling capacity of 11.3 kW was used for the ice storage air conditioning. The chiller consists of a hermetic compressor, a refrigerant to water plate type evaporator, an air-cooled condenser, a direct drive propeller fan with hose proof motor and electrical control panel including all safety, control and operating devices and a water circuit kit.

The compressor motor, refrigerant gas cooled type, is equipped with automatic reset internal thermal protection (Mcquay, 2002). The evaporator is a direct expansion (DX), compact, high efficiency, brazed plate-to-plate type heat exchanger consisting of stainless steel plates. Design working pressure is 30 bar on both waterside and refrigerant side. The condenser coil consists of seamless copper tubes arranged in a staggered row pattern. The coil is mechanically expanded into aluminum fins with full fin collars. The condenser fan is propeller type and is directly driven by a motor with automatic reset internal thermal protection. Refrigerant circuit is equipped with a thermal expansion valve, filter-drier, sight glass, liquid receiver and low/high pressure switches. The chiller unit has, in addition, a reverse cycle 4-port valve, non-return valves and a suction accumulator. The 4-port valve and the set of non-return valves, tees and piping allow the unit to operate in either cooling mode or heating mode. The suction accumulator is used to eliminate any refrigerant liquid entering the compressor. All electrical equipment required for proper unit operation is located in a watertight panel with access on the side of the unit. Technical data for the MHP 04P unit is given in Table 3.1 (Mcquay, 2002). The refrigerant flow diagram of the chiller unit for cooling mode is shown in Figure 3.15.

The water circuit kit consists of a circulating pump, a 38-liter water storage tank, an expansion tank and a water flow switch. Technical data and principle diagram for water circuit kit are given in Table 3.2 and Figure 3.16.

Table 3.1. Technical data for MHP 04P air-cooled water chiller

MHP 04P	**Unit**	**Value**
Nominal cooling capacity /Nominal power input	kW/ kW	11,3 / 4
R22 charge	kg	4,1
Compressor		
Type/Number	-	Hermetic/1
Number of capacity step	-	1
Condenser fan and motor		
Number/fan diameter	mm	1/560
Fan rotational speed	rpm	500
Nominal power input	W	390
Nominal air volume	m^3/h	6400
Condenser coil		
Total face area	m^2	0,735
Fin spacing/number of rows	mm	2,1/2
Evaporator		
Nominal water flow (cooling mode)/ (heating mode)	l/s	0,54 / 0,62
Water pressure drop at nominal flow (cooling/heating)	kPa	14,4/20
Water connections		
Inlet/outlet	inch	1”
Dimensions and weight		
Width x Depth x Height	mm	1000x630x990
Operating weight	kg	188
Electrical data		
Supply voltage	(V/Ph/Hz)	400/3/50
Unit maximum current	A	8,1
Maximum starting current	A	62



1. : Evaporator
2. : Compressor
3. : Reverse cycle 4-way valve
4. : Condenser coil
5. : Liquid receiver
6. : Suction accumulator
7. : Filter- drier
8. : Sight glass and moisture indicator
9. : Thermal expansion valve
10. : Tee
11 : Non-return valve

Figure 3.15. Refrigerant flow diagram of the chiller for cooling mode (Mcquay, 2002)

Table 3.2. Technical data for water circuit kit

Water circuit kit	Unit	Value
Buffer tank capacity	l	38
Water pump flow rate	l/s	0.54
Pump external manometric head	mWG	15
Pump nominal power input	kW	0.46
Pump nominal operating current	A	1.1

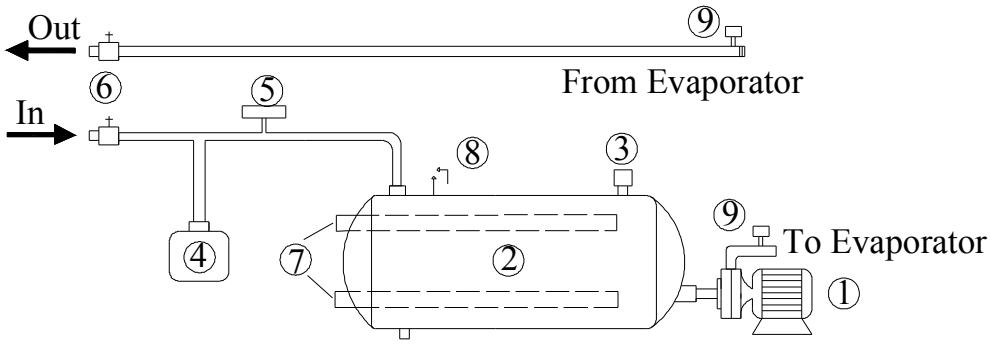


Figure 3.16. Schematic diagram of water circuit kit (Mcquay, 2002)

3.4.1.2. Ice Storage Tank

A circular polyethylene tank having a diameter of 1 m and an overall height of 1.5 m was used for the construction of ice storage tank. Ice storage tank contains approximately 900 kg of water. It is shown in Figure 3.17 and tank specifications are given in Table 3.3.



Figure 3.17. Ice storage tank

Table 3.3. Specifications of the ice storage tank constructed

Specifications	Unit	Value
Coil pipe surface area	m^2	16.7
Max. Operating pressure	bar	4.5
Outside diameter of the tank	mm	1000
Overall height of the tank	mm	1600
Volume of water	l	900
Outside and inner diameter of polyethylene collector pipe	mm	63/42
Outside and inner diameter of polyethylene coil pipe	mm	16/12

The tank was insulated using 9 mm thick expanded nitrile rubber. 338 m long polyethylene coil pipe was divided into 26 parts and each part (13 m long) was wounded to form a coil (Buyukalaca et al., 2003). The horizontal distance between two wounds was chosen to be 30 mm. The coils were replaced into the storage tank with a vertical distance of 30 mm between them. The horizontal and vertical spaces between the pipes were chosen for enough ice formation on each pipe (15 mm on each pipe).

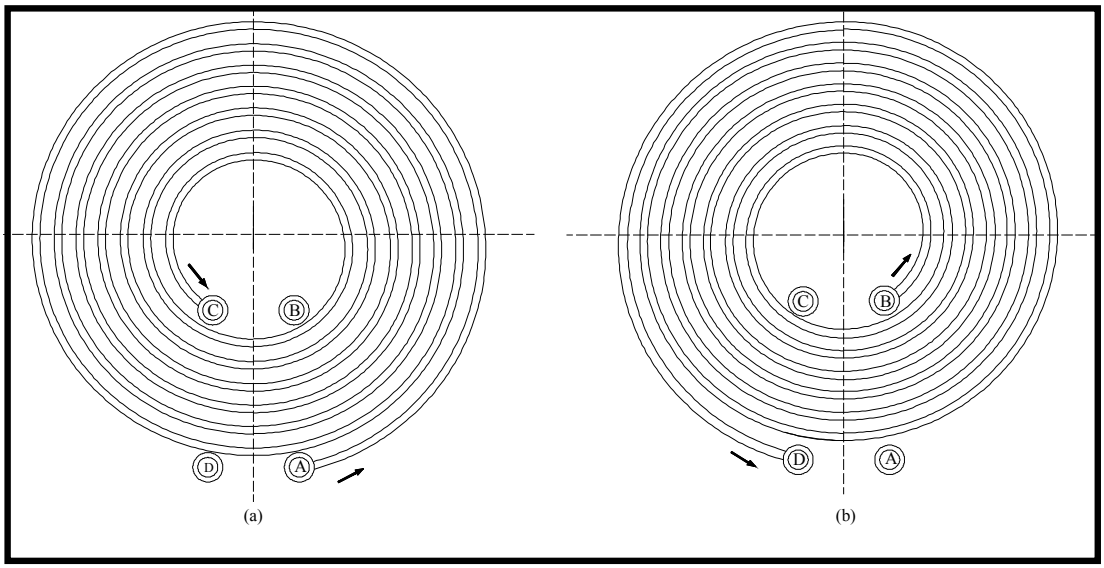


Figure 3.18. Coil distribution arrangement in the tank. (a) 1st, 3rd, 5th, … coils (b) 2nd, 4th, 6th … coils

The coils were connected from the both ends to polypropylene collector pipes having 42 mm inner diameter. Two of the collectors serve as supply and the other two as return collectors (Figure 3.18). For the 1st, 3rd, 5th, … coils, the transport fluid cooled in the chiller unit is supplied from the outer side of the coil (A) and the warm fluid is collected from the inner side (B). For the 2nd, 4th, 6th … coils, supply is from the inner side (B) and collection is from the outer side (D). This arrangement allows a uniform ice formation around the coils.

3.4.1.3. Air-Conditioned Room

Air-conditioned room (Figure 3.19) is an office room with the dimensions of 6 m × 5.8 m× 2.2 m. The walls of the room are not insulated and only the south and the north walls of the room face to outside. The room has two windows on the south wall and two on the north. The maximum daily total cooling load requirement between 8:00 a.m. to 5:00 p.m. was calculated to be 42 kWh (Serin et al., 2002).

Air-conditioning of the room was achieved using two fan-coil units located into the room. The brine cooled in the ice storage tank is circulated through the fan-coils. Teba TESA 2-GD fan-coils were used for air-conditioning of the room. Fan-coil specifications are given in Table 3.4.



Figure 3.19. Air-conditioned room

Table 3.4. Specifications of the fan-coils installed

Specifications	Unit	Value
Capacity	W	2800
Air flow(high speed)	m^3/h	510
Water inlet-outlet temperature	ºC	7/12
Dry – wet bulb air inlet temperature	ºC	27/19
Fan motor power	W	80

3.4.1.4. Automatic Control System

During the charge processes, temperature of the brine at the exit of the chiller is controlled by automatic control system in the chiller. The desired temperature of the brine was set on the control panel. The unit compares the actual brine and set temperatures, and produces a control signal for compressor. Depending upon the set temperature and the actual temperature, compressor is switched either on or off.

Automatic control system was used to control the temperature of the air-conditioned room and brine during the discharge process. The equipments that were used for the control of ice storage system during discharge:

- Three way valve (Blending)
- Control selection switch
- Temperature transmitter
- Two way valve
- Frequency controller
- Pressure transmitter

During the discharge processes, two options were considered in order to control the temperature of the air-conditioned room. One of them is fan control and the other one is valve control strategy. The desired temperature of the room and type of temperature control strategy (fan or valve control) were set on the control panel. The operation pressure of the system can also be set on the control panel.

A three-way valve (blending) provides a fixed brine temperature to the room to be air-conditioned. A temperature sensor measures the temperature of brine in the supply line just downstream of the three-way valve and this information is sent to a temperature controller. It is possible to set the desired supply temperature on the temperature controller. The three-way valve adjusts the temperature desired by arranging the volumetric flow rates of the brine coming from the storage tank and the brine coming from the room.

A temperature transmitter is used for the signals to control two-way valves or fans of the fan-coils. The transmitter measures the actual room temperature and sends the data to a temperature controller unit, which is located in the control panel.

The unit compares the actual room and set temperatures, and produces a control signal for the two-way valves or the fans depending upon the control strategy selected.

Figure 3.20 shows fan control strategy. For this control strategy, the flow rate of brine is constant during the experiment and the two-way valves are fully open. Depending upon the set temperature and the actual temperature inside the room, fans of the fan-coil units are switched either on or off.

For the valve control strategy (Figure 3.21), the two-way valve installed in the room is controlled by the temperature control unit that is fed by the temperature transmitters. If the temperature of the room differs (increases or decreases) from the set temperature, the valve changes the flow rate of the brine circulated in the fan-coils.

There are two fan-coil units in air-conditioned room. However, since they are in the same zone, they are not controlled separately. Only one two-way valve controls the flow rate of the brine returning from the fan-coils.

A frequency control unit was installed to reduce energy consumption of the circulating pump for the valve control strategy. The frequency controller adjusts the frequency of the circulation pump. That means the angular velocity and subsequently the volumetric flow rate of brine in the circulation pump change during operation.

A pressure transmitter was used to protect the system from overloads due to sudden pressure increase. If both of the two-way control valves are fully open, the frequency of the pump will be equal to that of the electric supply (around 50Hz), and the pump circulates the maximum amount of brine. When the thermal loads inside the room decrease, the two-way valves reduce the flow rate at brine circulating through the fan-coil units and consequently pressure increases in the line. This increase is captured by the pressure transmitter and a signal is sent to the frequency controller. The controller then reduces the frequency of the electricity feeding the circulating pump. As a result, the flow-rate and subsequently the pressure inside the line are reduced.

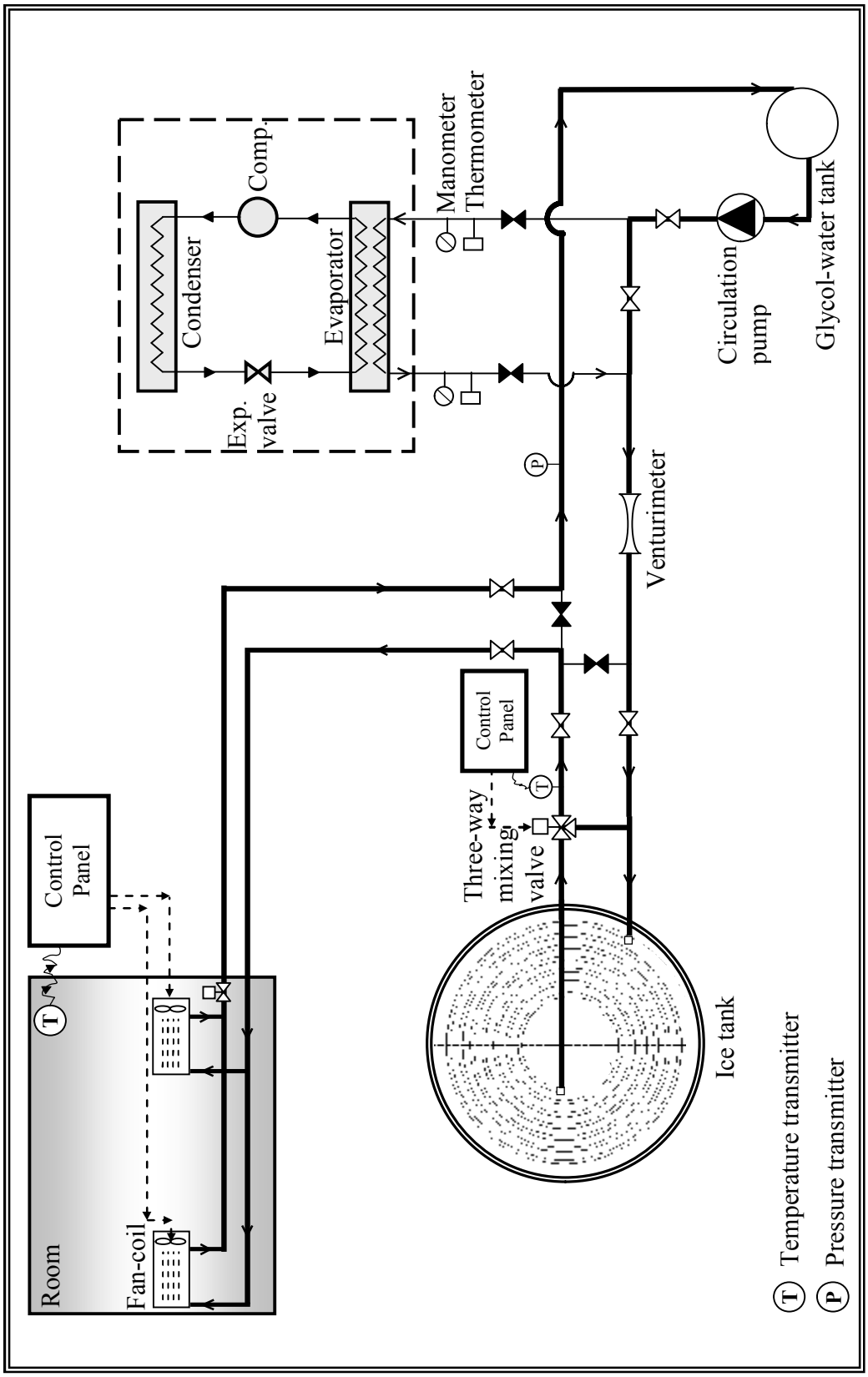


Figure 3.20. Schematic representation of the automatic control of the experimental system (Fan control)

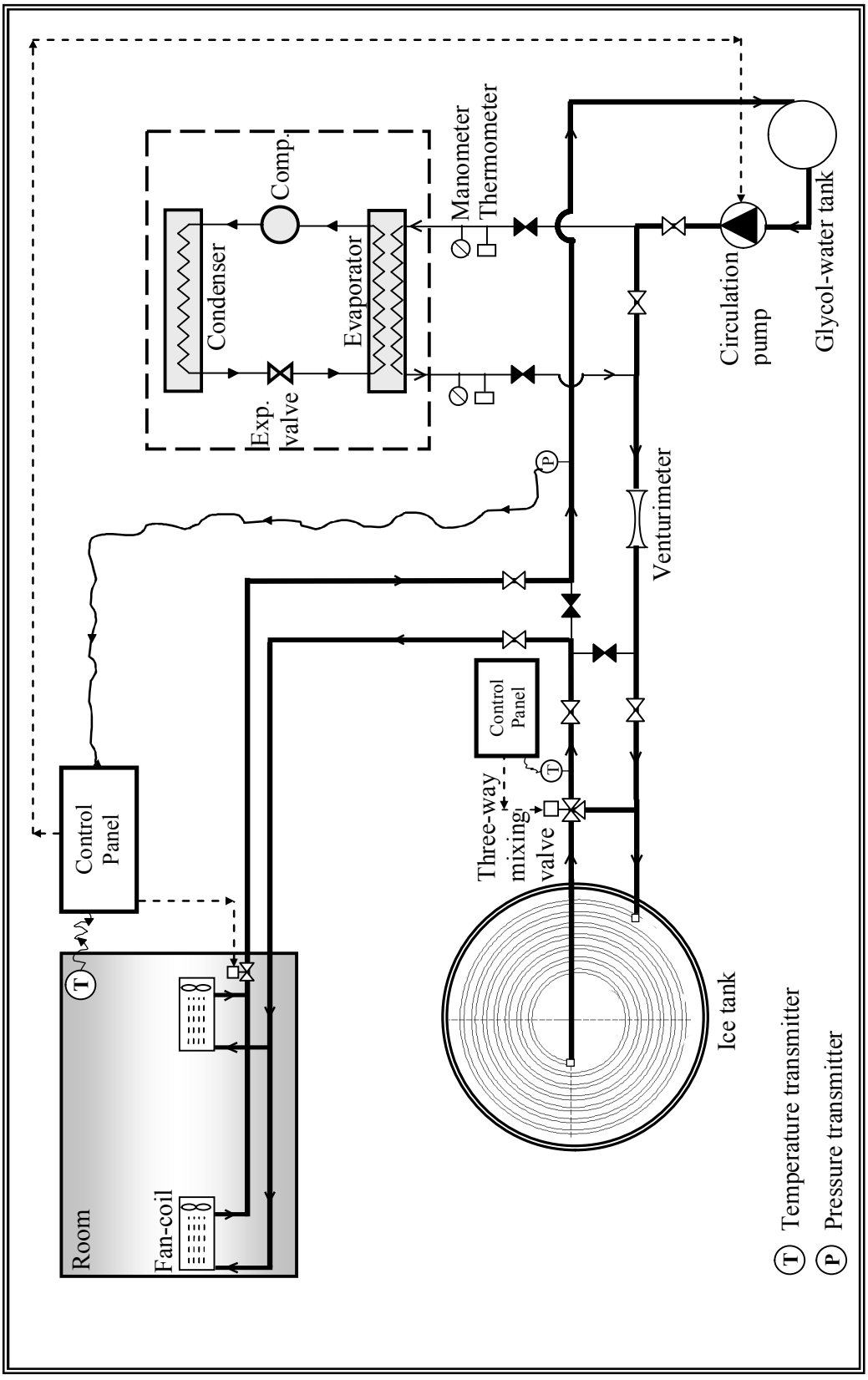


Figure 3.21. Schematic representation of the automatic control of the experimental system (Valve control)

3.4.1.5. Measurements Carried Out With Experimental Setup 1

The instrumentation was established so that the fluid energy flow could be determined at any location of the Experimental Setup 1. Temperature, pressure, and flow rate were known at the inlet and outlet of all the system components. The locations of the instruments are indicated in Figure 3.22 and are described in Table 3.5. Some of the instrumentation listed in Table 3.5 is not shown in the figure, including a thermocouple used to measure ambient air temperature. It can be seen from Figure 3.22 that flow rate of brine was measured using a venturimeter. Five thermocouples were used to measure temperature of brine at the inlet and exit of the chiller, circulation pump and ice storage tank. Air temperature at the inlet and exit of the condenser was also measured using two thermocouples. Totally 9 thermocouples were placed into water at three different axial and radial positions (Figure 3.23) for detecting variation of the water temperature in the ice storage tank.

All of the thermocouples and the humidity sensor are monitored continuously using a computer-controlled data acquisition system (Section 3.4.6) with a sampling rate of 30 readings/s. Other measurements were made via observations and records during tests. These observations include water height inside the tank, electrical energy consumption, flow rate of brine and pressure.

Table 3.5. Monitoring points for the Experimental System 1

Point Label	Unit
T1- T 9	Water temperatures in the ice tank
T 10	Brine temperature at the inlet of the tank
T 11	Brine temperature at the exit of the tank
T 12	Brine temperature at the exit of three-way mixing valve
T 13	Brine temperature at the inlet of the pump
T 14	Brine temperature at the exit of the pump
T 15	Air temperature at the inlet of the condenser
T 16	Air temperature at the exit of the condenser
T 17	Air temperature in the room
T 18	Ambient air temperature
H	Air relative humidity in the room

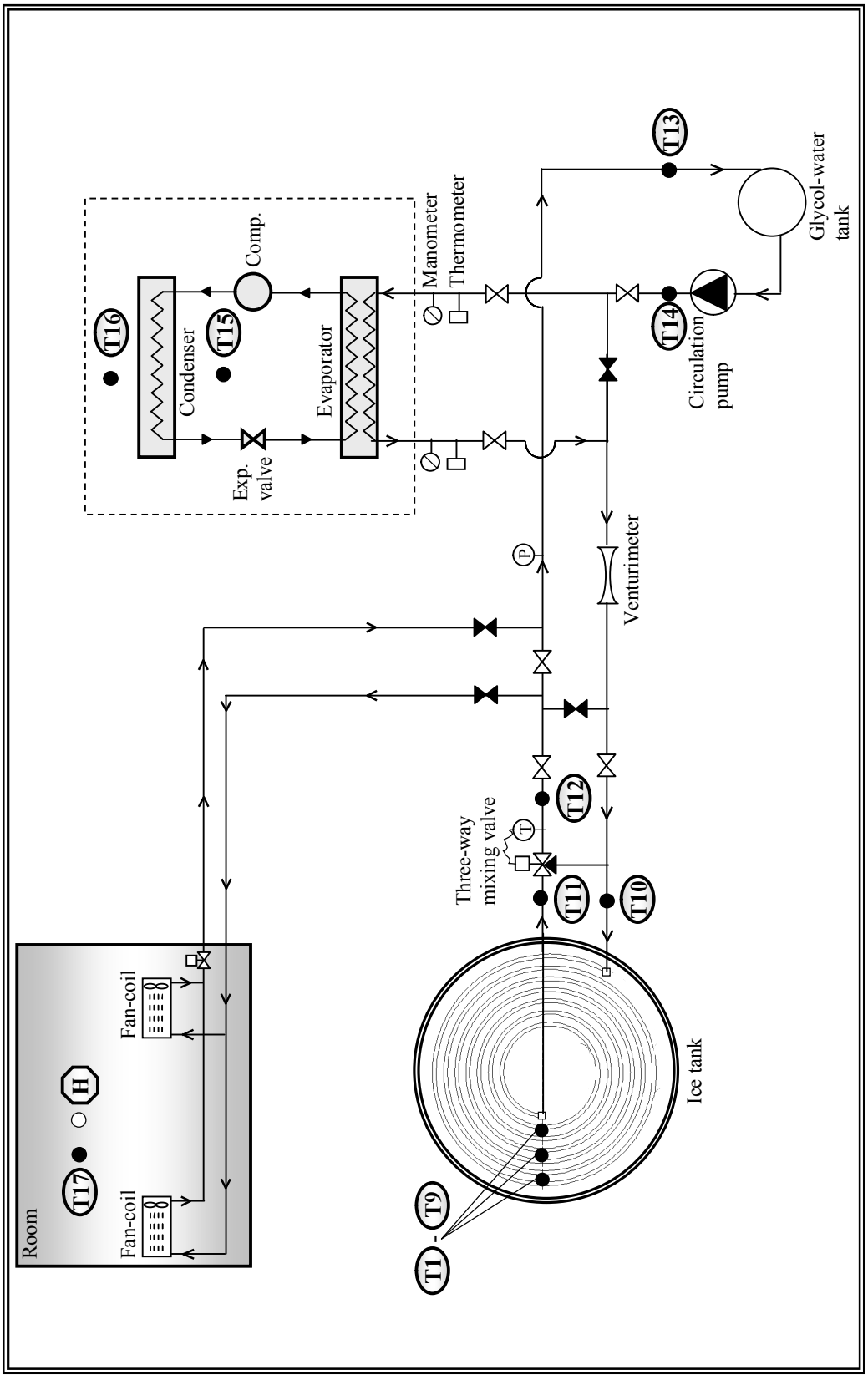


Figure 3.22. Measurement system on experimental setup 1

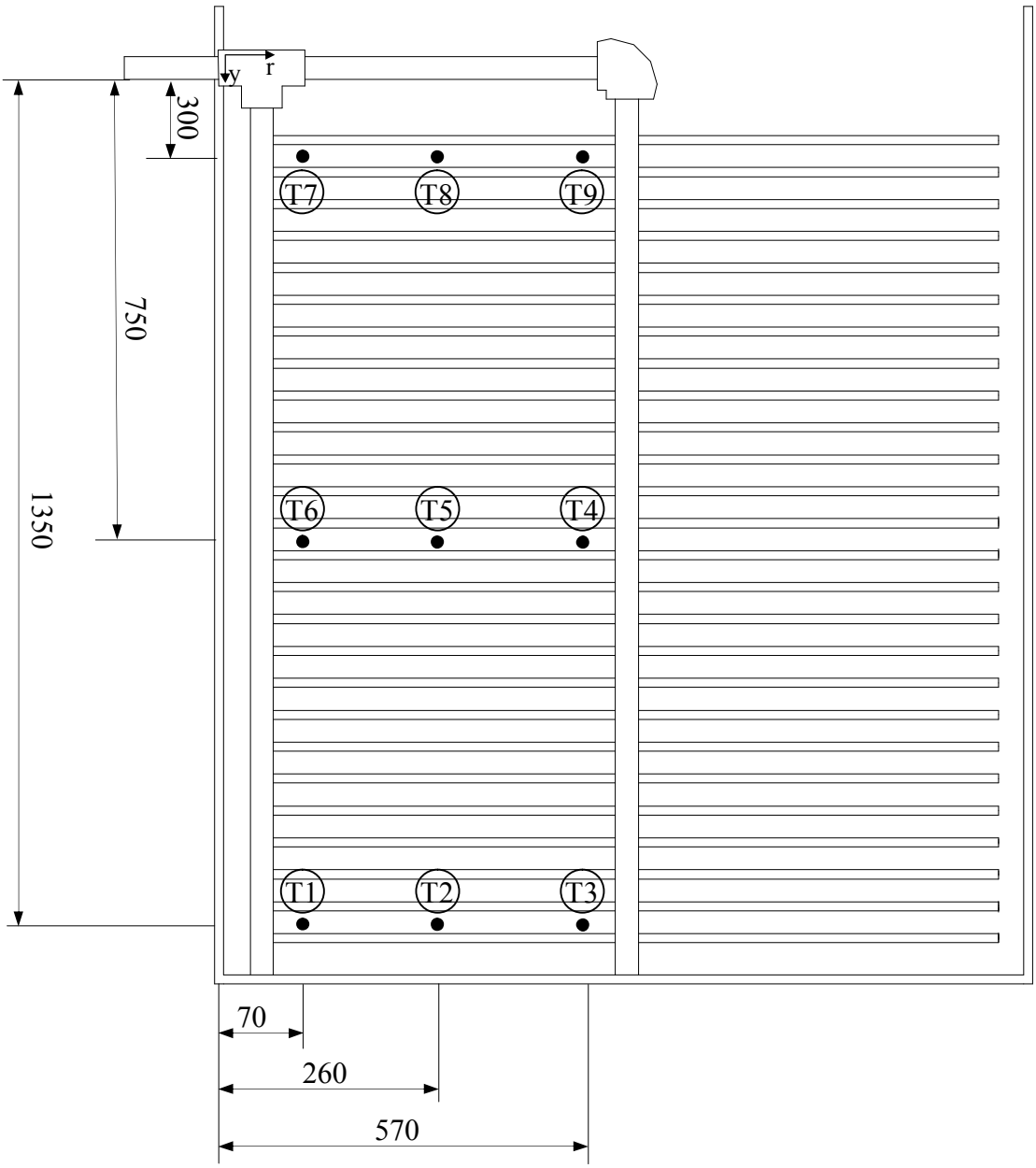


Figure 3.23. Water temperature measurement points in the ice storage tank

Two thermocouples were placed to measure average temperature of air in the room. Figure 3.24 shows connections of thermocouples to measure average temperatures.

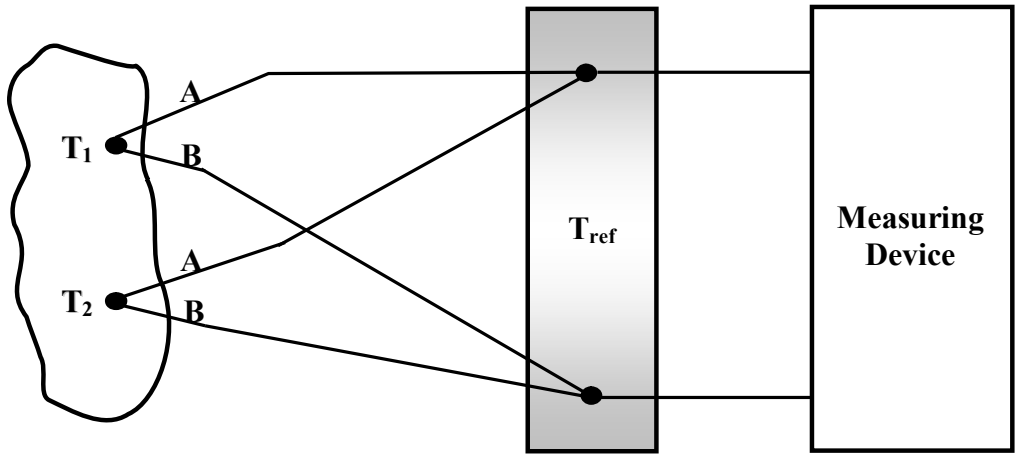


Figure 3.24. Connections of thermocouples to measure average temperatures

3.4.2. Experimental Setup 2

Using the experimental setup explained above, some charging and discharging tests were carried out to determine the performance of the ice storage air-conditioning system constructed and the results of these experiments showed that some mechanisms observed during the ice formation (supercooling, nucleation, and dendritic ice formation) are very important parameters for the system performance and they should be investigated in detail. Therefore, a new experimental system parallel to the Experimental System 1 was constructed to understand solid-liquid phase change heat transfer phenomena around a horizontal cylindrical tube. In this part, details of the second experimental setup are given.

General view of the second experimental system is shown in Figure 3.25 and Figure 3.26. As seen in the figure, the experimental unit consists of a test tube for ice formation, an air-cooled water chiller unit, a pump, piping, control valves and measurement system. The same test tube that was used in the Experimental System 1 for the ice coil construction was also used here. The test tube is made of polyethylene pipe with 16 mm outside diameter, 2 mm thickness and 4 m long. It was placed

inside a rectangular vessel of 64 mm wide, 75 mm high and 4000 mm long. The vessel was built from transparent acryclic plates of 4 mm thick, to be able to take photographs of solidification process around the tube. The vessel was filled with tap water to a depth of 50 mm and insulated from all sides including its cover, by 50 mm thick elastomeric rubber foam layer to reduce the heat transfer through the walls.



Figure 3.25. Experimental system 2

Brine (water-glycol solution with 30% glycol) was used as the heat transport fluid. It is cooled in the evaporator of the air-cooled water chiller unit and pumped to the test section passing through a valve, which is used for flow rate adjustment, and a rotameter. Temperature of the brine entering into the test section was kept constant at the desired level using a control system, which is constituted of motorized two and three way valves and temperature sensors.

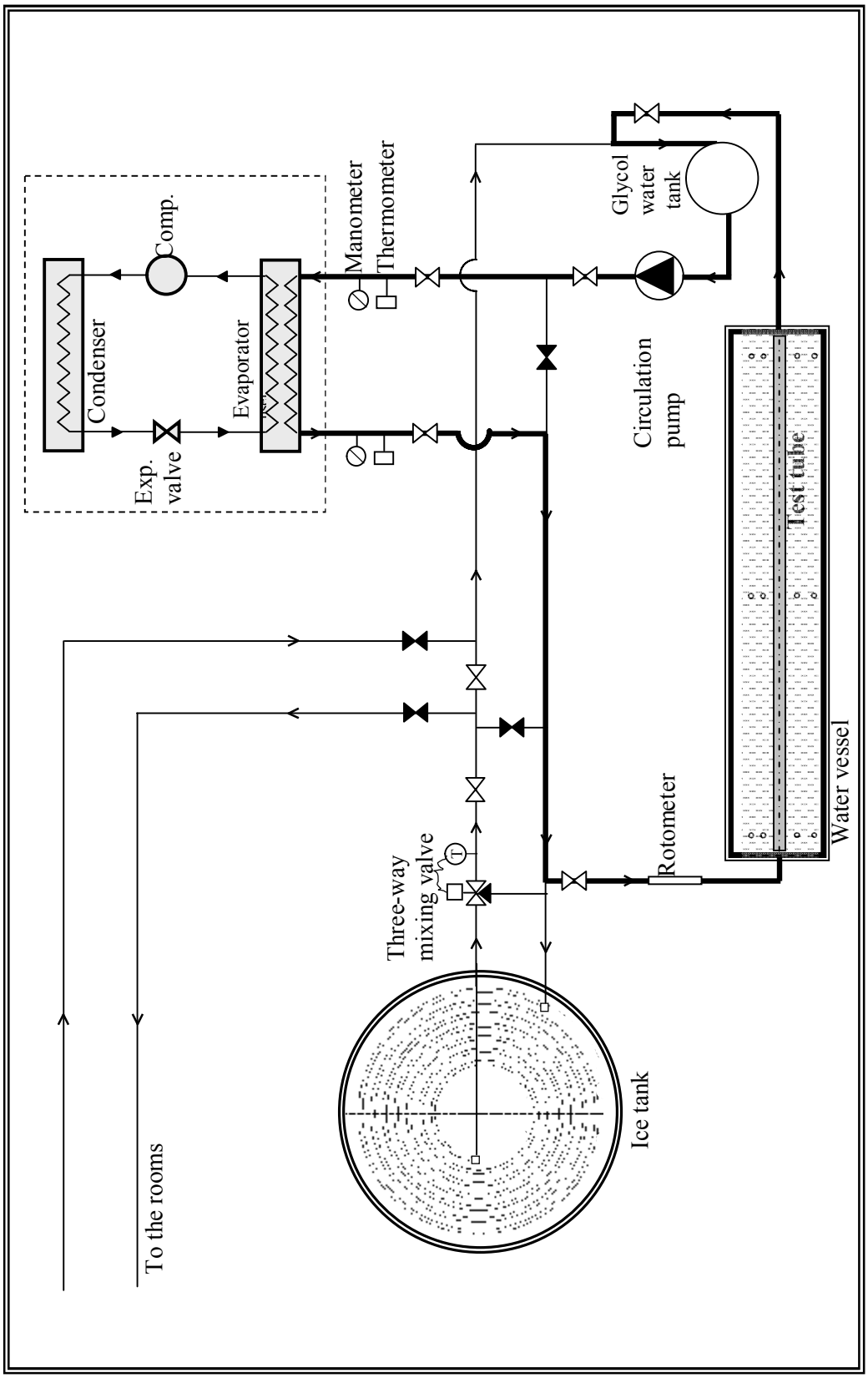


Figure 3.26. Schematic representation of the experimental setup 2

3.4.2.1. Measurements Carried Out With Experimental Setup 2

Two thermocouples were used to measure temperatures of the brine at the inlet and exit of the test tube. Totally 20 thermocouples were placed into water at 7 different axial positions (Figure 3.27) along the test tube for detecting variation of the water temperature in the vessel.

One thermocouple was utilized at each measuring station except the first (x/L=0.1), the middle (x/L=0.47) and the last (x/L=0.86) ones. Eight thermocouples were used at the first and the last stations, while four thermocouples were used at the middle one (Figure 3.28) to be able to detect the water temperature variation at these cross sections in detail.

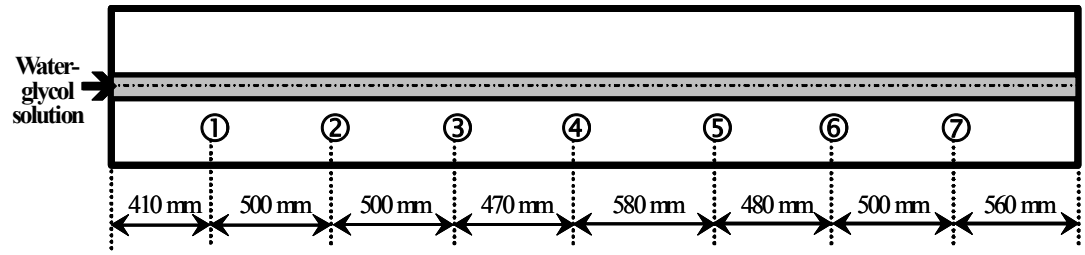


Figure 3.27. Measurement stations along test tube

Thickness of the ice formed around the tube was determined using a visual technique. Ice thickness was measured at the same stations where temperature measurements were made. Small observation windows are opened through the insulation material at the measuring stations to be able to make ice thickness measurements.

Photographs of the ice were taken with a digital camera (Nikon Coolpix 8700, 8MP, 10X optic zoom) from the front and the top of the vessel at each station to be able to detect circumferential changes in ice thickness. Different light sources and positions were tested during the prelimenary experimets to determine the best aperture arrangement. Figure 3.29 shows examples of the photographs taken during the experiments.

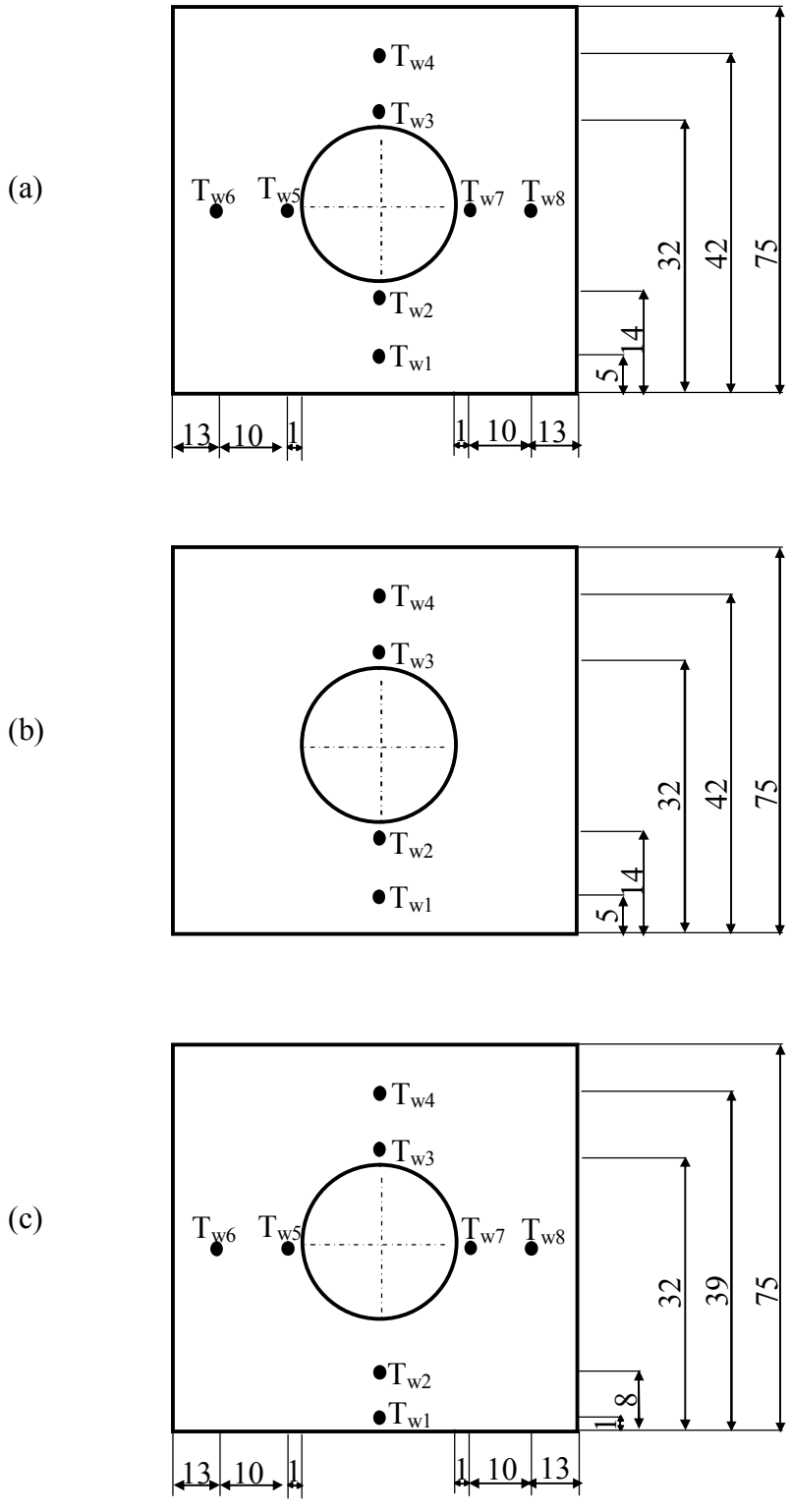
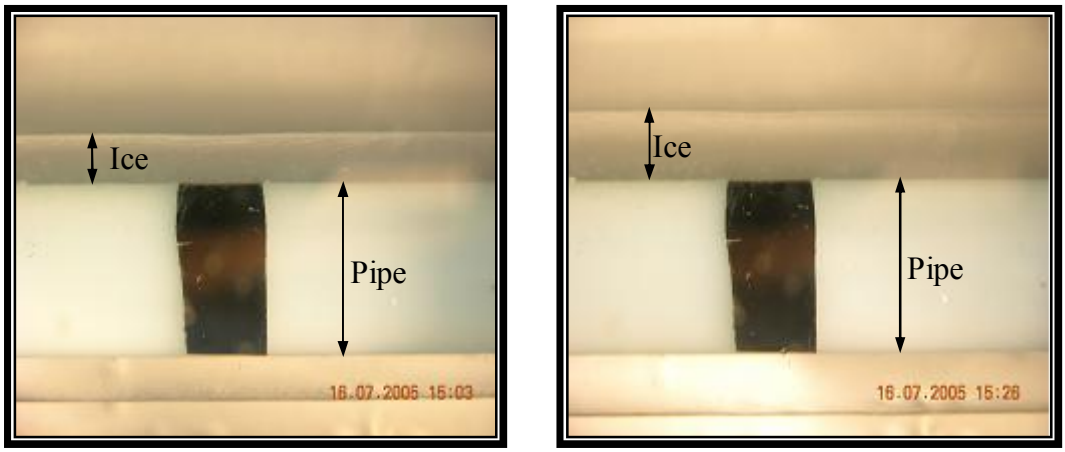


Figure 3.28. Temperature measurement locations within the water a) first (x/L= 0.1) b) middle (x/L= 0.47) c) last(x/L= 0.86)



(a) ***(b)***

Figure 3.29. Photographs of the ice formed around test tube at two different times

A traversing mechanism was designed to be able to detect the ice formation along the tube with a short period of time between the stations. The time period between any two measuring stations was 20 s at maximum. All photographs were taken in close-up mode with 5 MP resolution.

At the end of the experiments, the photographs taken were transferred to an image processing program (Image-ProPlus 4.5) for post processing. Using some of the techniques offerred by the program, bright images that clearly indicate the boundaries of the ice formed around the tube were obtained (Figure 3.30). From the images processed, thickness of the ice was determined for the top and bottom of the pipe separately (left and right sides of the pipe for the photographs taken from the top of the pipe) using the pipe diameter as a reference dimension.

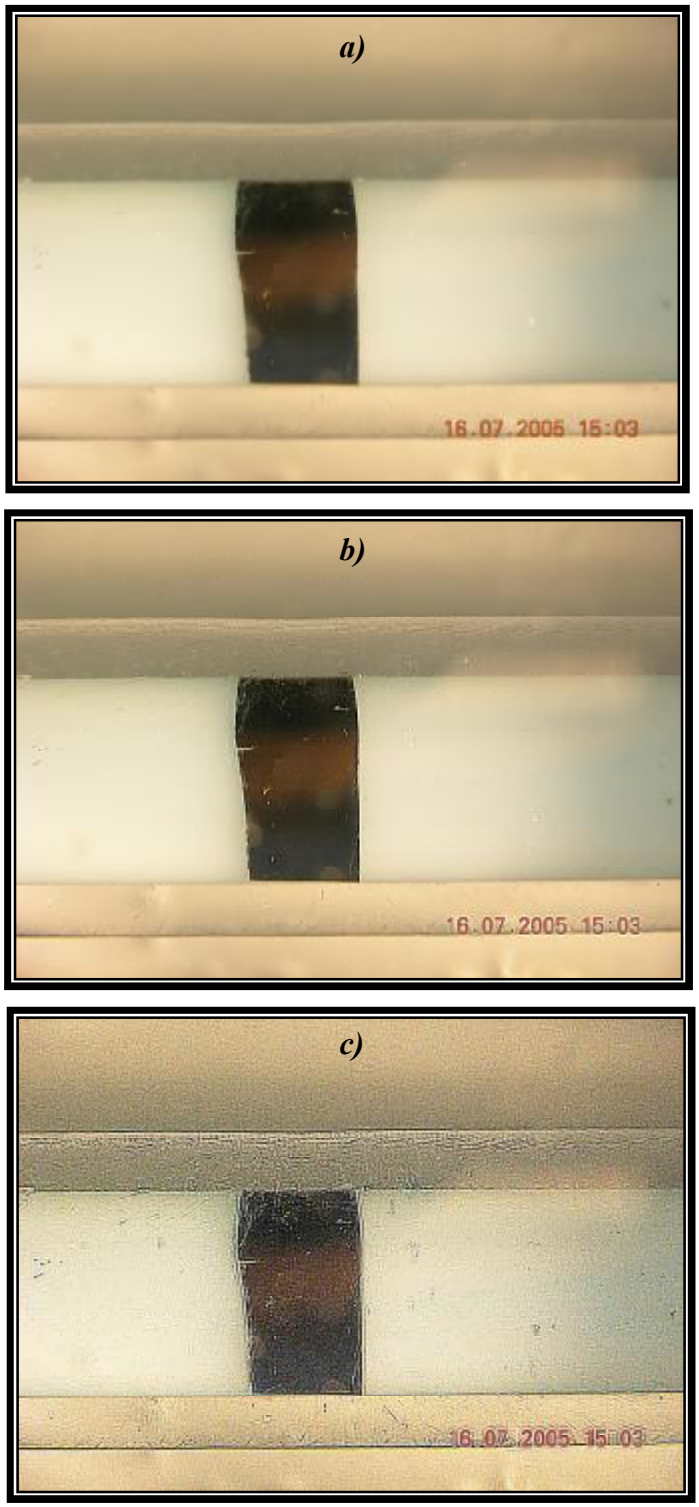


Figure 3.30. Post processing of photographs ***a)*** Original photograph ***b)*** First hipass filter ***c)*** Second hipass filter

3.4.3. Temperature Measurements

In the both experimental setups used in this study, K type thermocouples (T/C) were used to measure temperatures. Arrangement employed in the measurements is shown in Figure 3.31. Measuring junction (MJ) was placed into a measuring point to sense the temperature at that point. There are some desired properties from a measuring junction such as good electrical contact, low electrical resistance, and high mechanical strength. Welding, soldering, brazing, or twisting is some manufacturing processes for MJ. In this study, welding method was used.

The other end of the thermocouple is replaced into a small oil-filled tube, which is placed into ice-water mixture to supply 0 ºC reference junction (RJ). Copper wires were used to connect to measurement instrument.

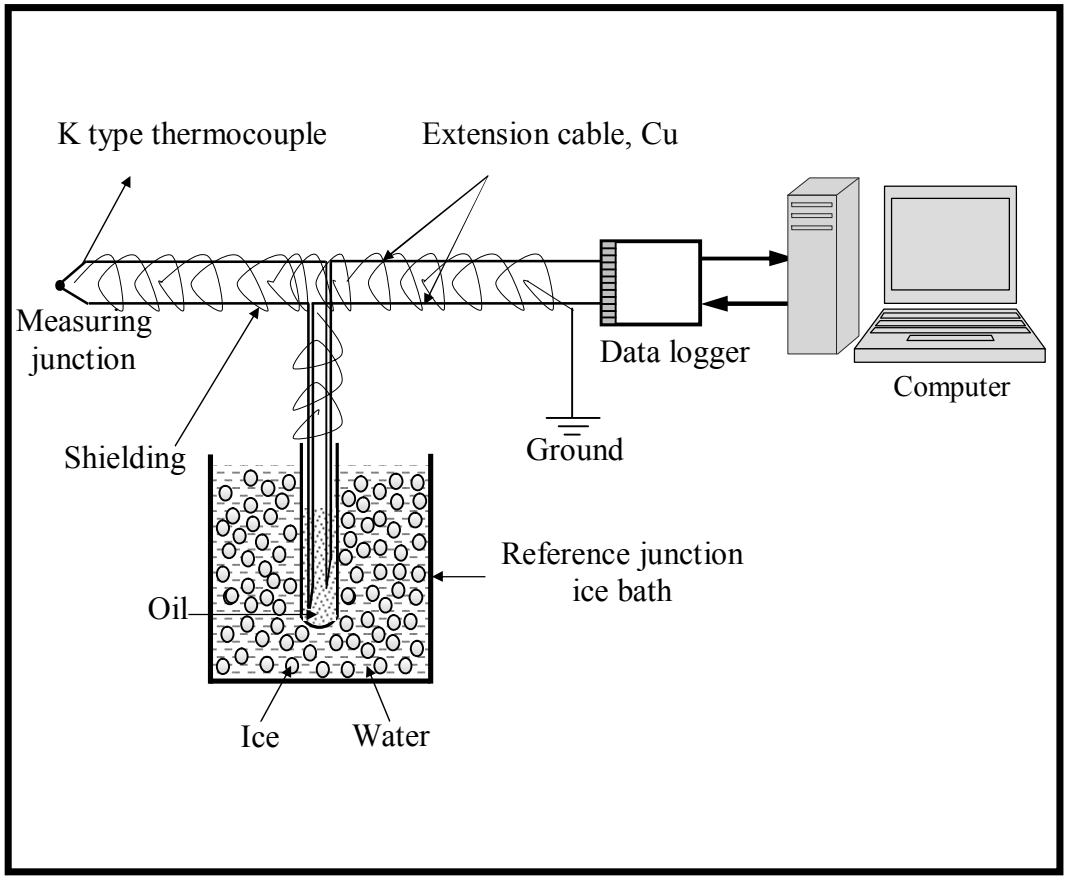


Figure 3.31. Schematic view of temperature measurement arrangement

The electromotor-force (emf) produced by the thermocouples is in the level of mV and measured by a data logger (Section 3.4.6). The data stored in the computer in the form of mV was later converted to degree Celsius using the calibration curve shown in Figure 3.32.

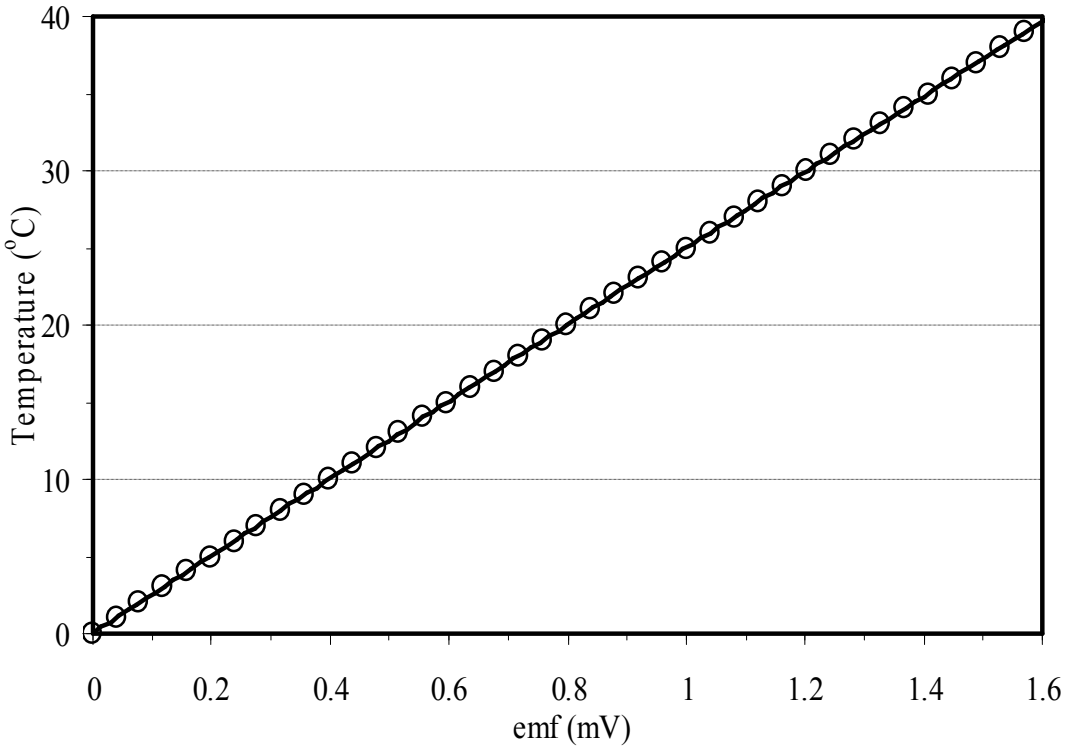


Figure 3.32. Calibration curve for T/C'used

3.4.4. Measurement of Brine Flow Rate

A venturimeter (Figure 3.33) was used to measure brine flow rate in the lines. Pressure difference between throat and tube of the venturimeter (ΔP) was measured using a monometer. Using the pressure difference (ΔP), the theoretical volumetric flow rate (ϑ_{teo}) can be obtained with the equation below:φ

$$\vartheta_{teo} = \frac{\pi . d^2}{4} . \sqrt{\frac{2.\Delta P}{\left(1-\beta^4\right)}} \qquad (3.1)$$

where d is diameter of throat and β is ratio of diameter of inlet to throat of venturimeter.

The actual volumetric flow rate (ϑ_{act}) can be calculated from the theoretical flow rate:

$$\vartheta_{act} = C_d . Q_{teo} \tag{3.2}$$

where C_d is flow coefficient and it was obtained by calibration.

The calibration results are shown in Figure 3.34. To perform a calibration of a venturimeter, water was pumped from a supply reservoir to a constant head reservoir. From there water flowed to a weighing tank through the measuring section with the venturimeter under test. In order to maintain constant flow rate, sufficient water was pumped to the constant head reservoir. Excess of water flowed back to the supply reservoir. The flow rate was adjusted with a control valve situated at the downstream end of the test section. The venturimeter was calibrated by measuring the volume of water that passes the venturimeter during a certain measuring time. Hereto the water was collected in the weighing tank, whereby the volume increment was measured and average flow rate was computed by dividing the volume by the time.

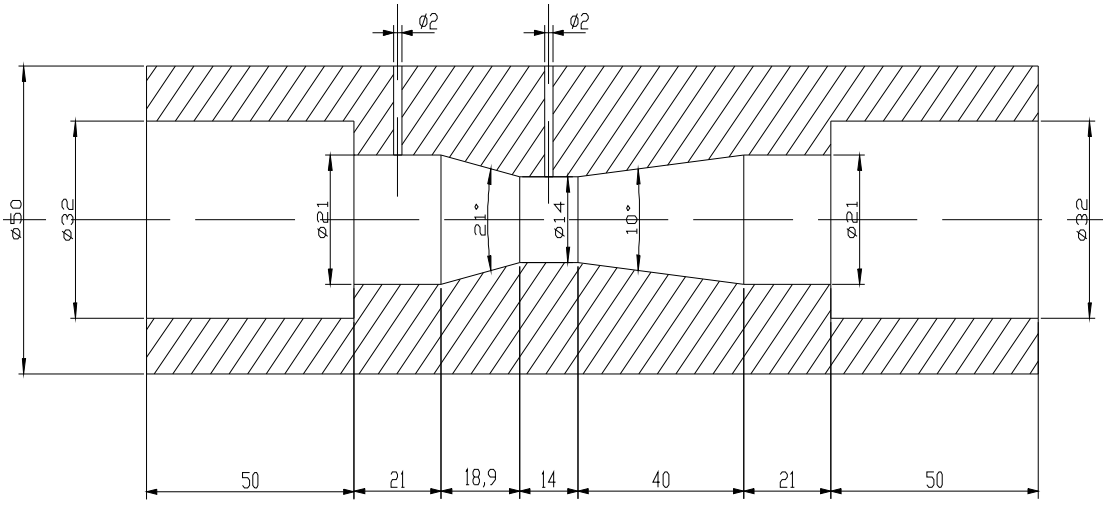


Figure 3.33. Venturimeter

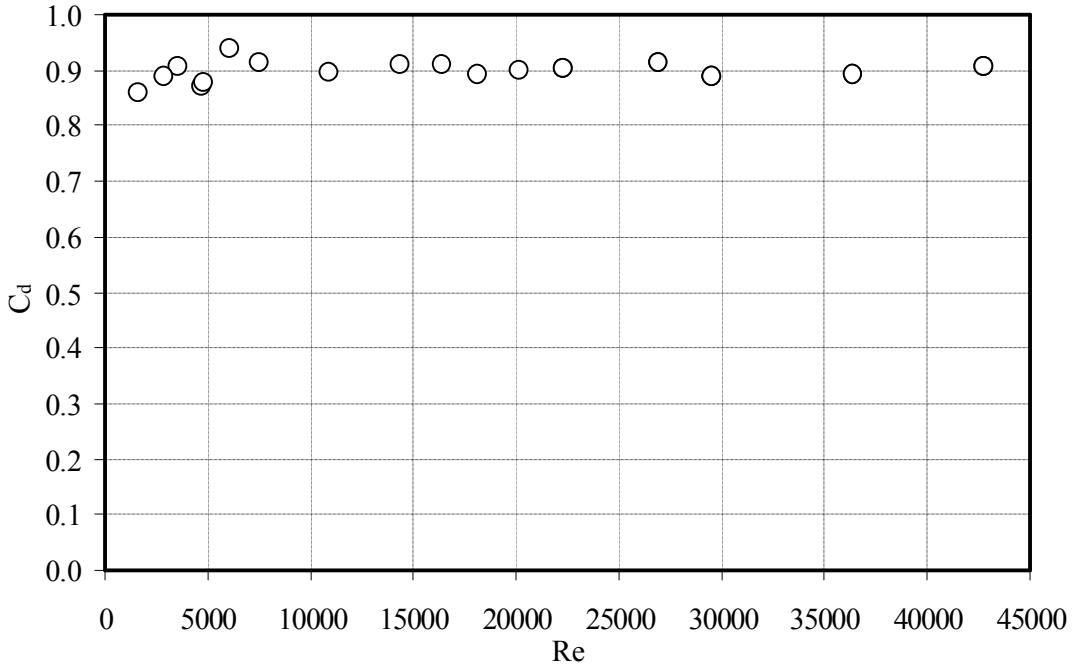


Figure 3.34. Calibration curve of the flow rate

3.4.5. Measurement of Relative Humidity

Humidity transmitter (produced by Vaisala) was used to measure relative humidity of air in the room. The accuracy of the transmitter is ±3%. Specifications of the relative humidity transmitter are tabulated in Table 3.6. The transmitter was powered by a power supply, which produces 12-24 VDC, and it has an output of 4-20 mA. Using a 250 Ω standard resistance, the current output was converted to voltage drop and fed to the data logger.

Before the experiments, relative humidity transmitters were also calibrated. The calibration of the humidity transmitters was performed using a small scale air conditioning unit used for student demonstrations.

The base unit comprises a centrifugal fan with speed control, steam humidifier (boiler), electrical pre-heaters, direct expansion cooling coil, electrical re-heaters and orifice plate for an air flow measurement. Air cooling is provided by vapor compression refrigeration system with pressure, temperature and refrigerant

flow measurement. Temperature of air is measured using precision wet and dry bulb thermometers.

The humidity transmitters were fitted into the discharge duct of the experimental unit. Amount of the steam, flow rate of the air and capacity of the pre and post heaters were adjusted to obtain required humidity at the discharge duct. Calibration process was carried out by reading output of the dry and wet bulb thermometers and the humidity transmitters. This process was repeated for various values of the relative humidity. The calibration curve obtained is given in Figure 3.35.

Table 3.6. Specifications of the humidity transmitter

Specifications	Value
Range	0 to 100 % RH
Accuracy	±3 % RH from 10 to 90 % RH
Sensor	Humicap capacitive thin-film
Output	4 to 20 mA
Temperature limits for RH readings	-10 to 60 ºC
Response time	15 seconds
Power supply	10 to 28 VDC

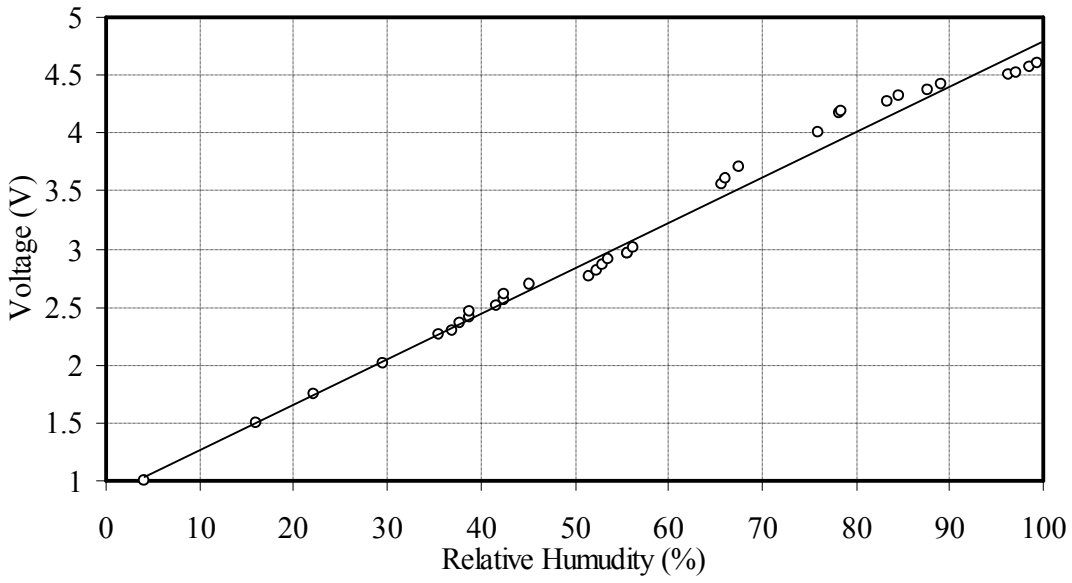


Figure 3.35. Calibration curve for the humidity transmitter

3.4.6. Data Logger System

The data acquisition system used in the present study consisted of a computer and P.A. Hilton Data Logger Model D101/42. The system has a 12 bit analogue-to-digital conversion unit (Figure 3.36). Command and data are transfer via 5 wires RS 232 serial link using ASCII character string sent and receive by the controlling computer. A data logger control software was configured to automate the test and measurement procedures. The program produced an output file with the raw voltage readings. Measured voltages are then converted into temperature or humidity. The measured parameters are outputs of the thermocouples and relative humidity transducer. All data were read and recorded by the computer through the data acquisition unit at intervals of 30 second or 2 minutes, depending on the mode of operation.

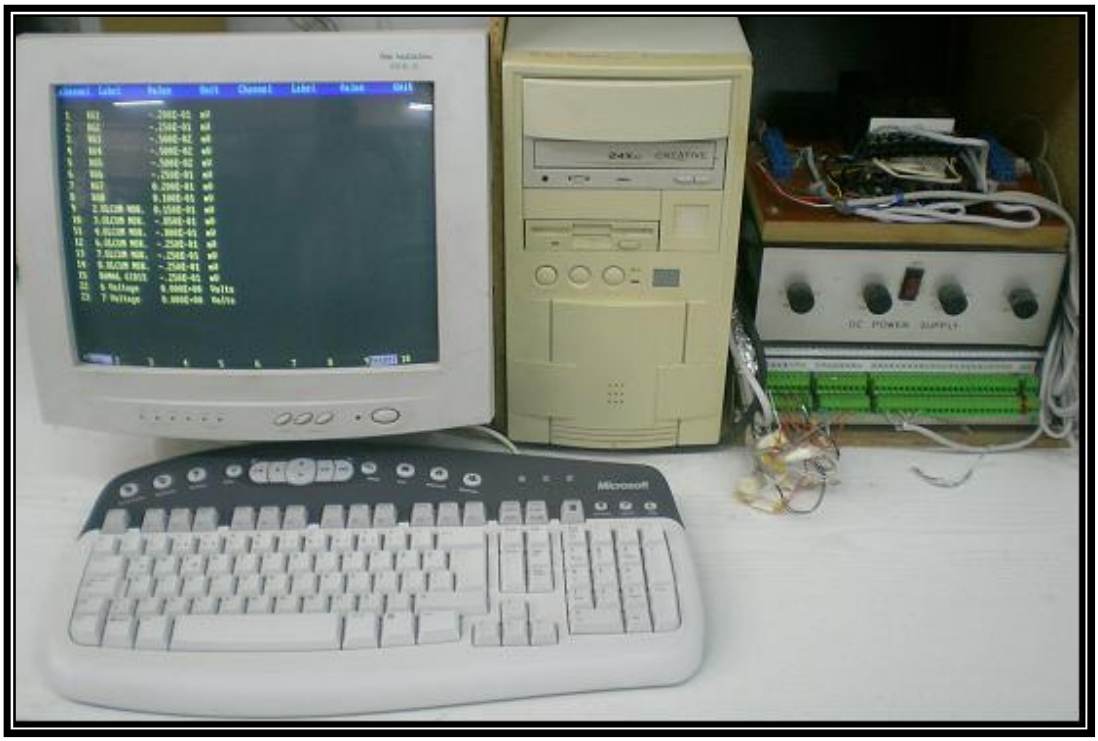


Figure 3.36. Data logger unit and the computer

3.5. Mathematical Model for Ice Formation around the Tube

A mathematical model was developed to calculate the heat transfer process for phase change phenomenon around a horizontal tube. Variation of ice thickness with time for different brine inlet temperatures was obtained from mathematical model. Experimental results obtained from the Experimental Setup 2 were used to validate the model.

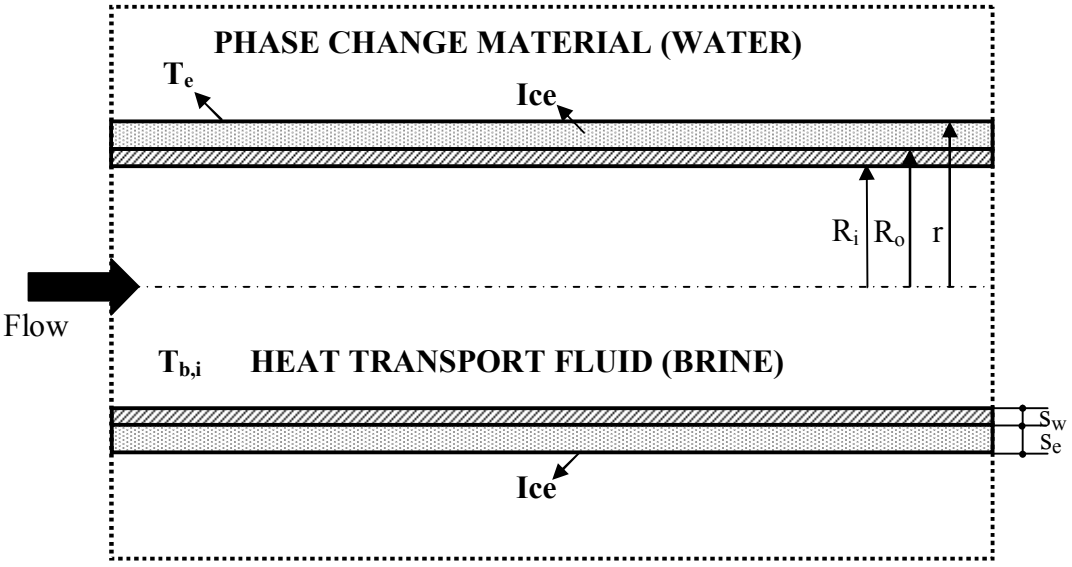


Figure 3.37. Schematic of ice formation process

The temperature of the brine ($T_{b,i}$) flowing through the tube in the vessel can be assumed constant (Figure 3.37). At an axial position of the tube, the amount of heat transferred per length of the tube ($\dot{Q}_x$) can be calculated from;

$$\dot{Q}_x = \frac{T_e - T_{b,i}}{R_p} \tag{3.3}$$

where T_e is the temperature of ice and R_p is the thermal resistance based on the peripheries, instead of the surface areas;

$$R_p = \frac{1}{h_i P_i} + \frac{s_w}{k_w P_{wm}} + \frac{s_e}{k_e P_{em}} \tag{3.4}$$

in which k_w and k_e are the thermal conductivity of the tube material and ice, respectively. h_i is the convective heat transfer coefficient inside the tube. The peripheries (P_i, P_{wm} and P_{em}) are obtained from the following equations:

$$P_i = 2\pi R_i \tag{3.5}$$

$$P_{wm} = \frac{2\pi(R_o - R_i)}{\ln \frac{R_o}{R_i}} \tag{3.6}$$

$$P_{em} = \frac{2\pi s_e}{\ln\left(\frac{R_o + s_e}{R_o}\right)} \tag{3.7}$$

Defining;

$$R_{po} = \frac{1}{h_i P_i} + \frac{s_w}{k_w P_{wm}} \tag{3.8}$$

and

$$R_p^* = R_p / R_{po} \tag{3.9}$$

the following equation is obtained from Eq. (3.4);

$$R_p^* = 1 + \frac{\ln(1 + s_e / R_o)}{2\pi k_e R_{po}} \tag{3.10}$$

The heat transferred from water to the brine flowing inside the tube causes ice formation on the outer surface of the tube. Therefore, Eq. (3.11) can be written;

$$\dot{Q}_x \, dt = \rho_e h_{ew} 2\pi r dr \tag{3.11}$$

where ρ_e is the density of the ice, h_{ew} is the latent heat of freezing water and t is the time. Using Eqs. (3.3) and (3.11) the following equation is obtained;

$$r\frac{dr}{dt} = \frac{T_e - T_{b,i}}{2\pi . h_{ew} . \rho_e . R_p} \tag{3.12}$$

Utilizing the following relations;

$$r = \left(R_o + s_e\right) \tag{3.13}$$

$$s_e^* = s_e / R_o \tag{3.14}$$

$$t^* = t\frac{T_e - T_{b,i}}{2\pi R_o^2 h_{ew} \rho_e R_{po}} \tag{3.15}$$

$$R_{po}^* = 2\pi R_{po} k_e \tag{3.16}$$

dimensionless differential equation (3.17) is obtained:

$$dt^* = (1 + s_e^*) \cdot \left(1 + \frac{\ln(1 + s_e^*)}{R_{p0}^*}\right) ds_e^* \tag{3.17}$$

Eq. (3.17) can be solved with the boundary condition:

$$t^* = 0 : \; s_e^* = 0 \tag{3.18}$$

as follows :

$$t^* = s_e^* + \left(1 + \frac{1}{R_{po}^*}\right)\frac{s_e^{*2}}{2} + \frac{1}{R_{po}^*}\sum_{i=3}^{\infty}\frac{s_e^{*i}}{i(i-1)(i-2)} \qquad (3.19)$$

Figure 3.38 shows variation of ice thickness obtained from the model with time for different brine inlet temperatures (-6 ºC, -7 ºC, -8 ºC and -9 ºC). As can be seen from the figure, with the increase of brine inlet temperature, ice thickness around the tube decreases.

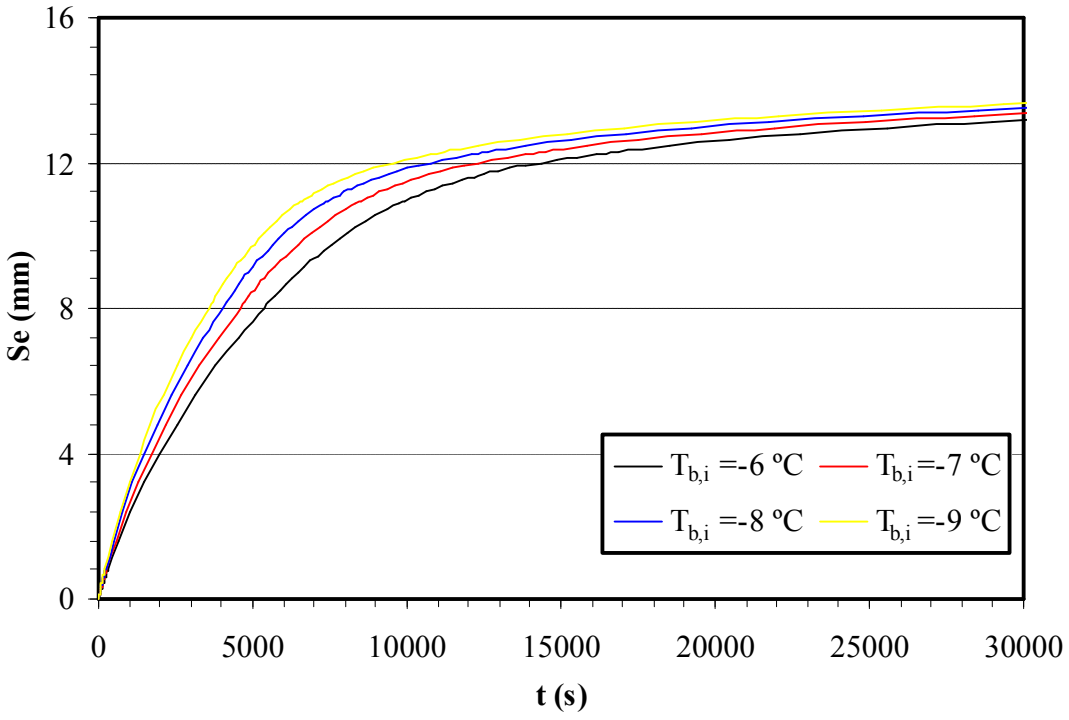


Figure 3.38. Variation of ice thickness obtained from model with time for different brine inlet temperatures

4. RESULT AND DISCUSSIONS

4.1. Results Obtained From Experimental Setup 1

Details of the Experimental Setup 1 are given in Chapter 3.4.1. Two series of experiments were carried out using Experimental Setup 1. In the first series, charging experiments were performed under a wide range of operating conditions. In the second series, discharging experiments were carried out for two automatic control operating strategies.

4.1.1. Charging Tests

The test plan was structured to test capabilities of the storage tank under a wide range of operating conditions. Temperature of the brine at the inlet of the tank, temperature of the air at the inlet of the condenser and charging period were primary variables during the charging tests. Table 4.1 shows test conditions for the charging experiments.

Experiments were carried out at a fixed flow rate between 0.75 kg/s and 0.80 kg/s, and different set temperatures of brine ($T_{b,s}$ = -4 ºC, -5 ºC, -6 ºC, -7 ºC and -8 ºC). Although brine temperature at the exit of the evaporator, which is approximately equal to brine temperature at the inlet of the tank ($T_{b,i}$), was set to a desired value in an experiment, actual instantaneous brine inlet temperature($T_{b,i}$) differs from the set value ($T_{b,s}$) and varies during the experiment. Therefore, average of the brine inlet temperature ($\overline{T}_{b,i}$) during each experiment was calculated and used to represent brine temperature.

An air-cooled chiller unit was used in this study and temperature of the air at the inlet of the condenser varies during an experiment parallel to variation in ambient temperature. Average air inlet temperature ($\overline{T}_{a,i}$) was used to represent temperature of the air at the inlet of the condenser.

Water temperature inside the ice storage tank was adjusted to approximately 7 ºC at the start of experiments. Air was injected into the water for a short period of

time from the bottom of the tank to obtain a homogeneous temperature distribution inside the tank just before the start of the experiment. The data were collected every 120 s for each monitoring point during the charging tests.

Results of the charging tests conducted were analyzed at two stages. First, effect of brine inlet temperature on ice formation inside the ice storage tank was investigated. After discussing the behavior of water during liquid-to-solid phase change process, spatial variation of nucleation temperature of the water inside the tank was examined for different experimental conditions. Effect of brine inlet temperature on ice formation was investigated in detail using the results of four experiments, each of which was carried out at a different brine inlet temperature.

In the second stage, performance characteristics of the ice storage system were studied. Effects of brine inlet temperature, air temperature at the inlet of the condenser and charging period were analyzed.

Table 4.1. Conditions of charging experiments

Test ID	**Charging period**	**Flow rate,** $\dot{m}_b$ **[kg/s]**	**Initial water temp.,** $T_{w,i}$ [ºC]	**Set temperature of brine at the inlet of the tank,** $T_{b,s}$ [ºC]	**Average brine temperature at the inlet of the tank,** $\overline{T}_{b,i}$ [ºC]	**Average air temperature at the inlet of the condenser,** $\overline{T}_{a,i}$ [ºC]
310106	7 h	0.79	7.8	-6.0	-5.0	15
010206	7 h 55′	0.79	11.2	-6.0	-4.6	16
070206	8 h	0.80	9.9	-6.0	-4.5	15
100206	7 h	0.79	7.0	-6.0	-4.6	16
120206	7 h	0.79	7.0	-6.0	-5.1	14
140206	7 h 19′	0.79	7.0	-7.0	-5.2	16
150206	7 h	0.79	7.0	-7.0	-5.3	17
200206	7 h	0.79	6.8	-7.0	-5.3	17
210206	7 h	0.80	7.0	-6.0	-5.0	18
220206	7 h	0.80	7.3	-5.0	-3.7	17
230206	6 h	0.80	7.0	-4.0	-2.1	18
23020G	7 h	0.80	7.0	-7.0	-5.2	18
010306	7 h	0.79	7.0	-6.0	-5.1	18
020306	7 h	0.79	7.0	-5.0	-3.7	18
030306	7 h	0.79	6.7	-6.0	-5.0	19
060306	7 h	0.79	7.1	-7.0	-5.1	18
080306	7 h	0.79	7.0	-7.0	-5.1	18
090306	7 h	0.79	6.9	-6.0	-5.0	16
150306	7 h	0.79	6.9	-6.0	-5.1	18
170306	7 h	0.80	7.1	-6.0	-5.0	18
220306	7 h	0.79	7.9	-7.0	-5.0	19
230306	7 h 13′	0.79	7.1	-6.0	-5.0	18
240306	6 h 57′	0.79	7.6	-5.0	-3.7	19
290306	7 h	0.79	7.0	-6.0	-5.0	18
300306	7 h	0.79	7.2	-7.0	-5.1	18
310306	7 h	0.79	7.2	-8.0	-5.1	18
030406	7 h 10′	0.79	7.1	-4.0	-2.1	19
040406	7 h	0.79	7.1	-4.0	-2.2	19
050406	7 h	0.79	6.7	-8.0	-5.3	17
170406	7 h	0.79	6.6	-8.0	-5.1	19
180406	7 h	0.79	7.0	-6.0	-5.1	20
190406	7 h	0.79	6.7	-7.0	-5.1	21
200406	7 h	0.79	7.2	-5.0	-3.8	21
240406	7 h	0.79	6.9	-7.0	-5.3	20
010506	7 h	0.79	6.9	-7.0	-5.2	21
020506	7 h	0.78	7.1	-5.0	-4.1	20

Test ID	Charging period [h]	Flow rate, $\dot{m}_b$ [kg/s]	Initial water temp., $T_{w,i}$ [ºC]	Set temperature of brine at the inlet of the tank, $T_{b,s}$ [ºC]	Average brine temperature at the inlet of the tank, $\overline{T}_{b,i}$ [ºC]	Average air temperature at the inlet of the condenser, $\overline{T}_{a,i}$ [ºC]
030506	7 h	0.78	7.0	-8.0	-5.1	21
040506	7 h 4′	0.79	7.0	-6.0	-4.9	21
050506	7 h	0.79	6.8	-5.0	-3.8	22
160506	7 h	0.80	6.5	-5.0	-4.0	24
180506	7 h	0.79	7.3	-7.0	-4.9	21
190506	7 h	0.79	7.0	-6.0	-4.8	23
210506	7 h	0.79	7.1	-5.0	-4.0	24
220506	7 h 5′	0.79	7.6	-6.0	-4.8	24
230506	7 h	0.78	6.6	-8.0	-5.1	25
240506	7 h	0.79	6.5	-5.0	-4.6	27
250506	7 h	0.78	7.0	-8.0	-4.9	28
260506	7 h	0.78	7.4	-7.0	-4.9	27
290506	7 h	0.77	6.9	-6.0	-4.8	28
300506	7 h	0.77	6.8	-8.0	-4.9	28
310506	7 h	0.77	7.0	-7.0	-5.0	27
030606	7 h	0.78	7.1	-8.0	-4.9	28
050606	7 h	0.76	6.9	-8.0	-4.8	28
060606	7 h	0.76	6.7	-6.0	-4.7	28
090606	7 h	0.78	6.8	-7.0	-5.1	23
09060G	7 h	0.79	6.8	-6.0	-5.0	25
100606	7 h	0.79	6.8	-8.0	-5.2	25
10060G	7 h	0.79	6.6	-8.0	-5.4	24
110606	7 h	0.79	7.1	-7.0	-5.2	25
120606	7 h	0.78	7.2	-8.0	-4.8	26
130606	7 h	0.79	6.8	-6.0	-4.9	25
13060G	7 h	0.79	7.2	-5.0	-4.0	25
140606	7 h	0.79	7.2	-8.0	-4.9	25
14060G	7 h	0.79	6.9	-7.0	-5.1	25
1506T0	3 h 52′	0.78	5.6	-8.0	-4.8	26
1606T1	2 h 39′	0.78	6.9	-8.0	-4.3	25
1606T2	3 h 15′	0.78	4.3	-8.0	-5.0	27
1706T1	1 h 49′	0.78	6.1	-8.0	-4.0	26
1706T2	5 h 54′	0.78	6.3	-8.0	-4.7	27
1906T1	4 h	0.78	9.6	-8.0	-4.5	29
1906T2	2 h 34′	0.78	5.5	-8.0	-3.8	28
2106T1	4 h 37′	0.78	8.2	-8.0	-4.3	28

Test ID	Charging period [h]	Flow rate, $\dot{m}_b$ [kg/s]	Initial water temp., $T_{w,i}$ [ºC]	Set temperature of brine at the inlet of the tank, $T_{b,s}$ [ºC]	Average brine temperature at the inlet of the tank, $\overline{T}_{b,i}$ [ºC]	Average air temperature at the inlet of the condenser, $\overline{T}_{a,i}$ [ºC]
2106T2	5 h 34′	0.78	8.3	-8.0	-4.5	27
2206T1	4 h 8′	0.78	6.5	-8.0	-4.5	27
2206T2	6 h 10′	0.78	7.1	-8.0	-4.7	27
260606	7 h	0.75	7.5	-7.0	-4.7	28
270606	7 h	0.77	7.0	-5.0	-3.9	29
280606	7 h	0.78	7.2	-5.0	-3.9	28
2906T1	1 h 45′	0.78	7.0	-8.0	-3.5	26
2906T2	2 h 20′	0.78	6.3	-8.0	-4.1	26
3006T1	1 h 43′	0.78	6.9	-8.0	-3.6	28
3006T2	2 h 9′	0.78	6.8	-8.0	-4.1	25
3006T3	2 h 18′	0.78	6.6	-8.0	-3.7	29
030706	7 h	0.76	7.3	-6.0	-4.6	28
040706	7 h	0.78	6.3	-7.0	-5.3	25
110706	7 h	0.78	7.2	-8.0	-5.2	26
11070G	7 h 38′	0.78	7.0	-8.0	-5.1	25
120706	8 h	0.78	7.0	-8.0	-5.1	26
190706	7 h	0.78	7.0	-8.0	-4.9	27
19070G	8 h	0.78	7.0	-8.0	-4.7	28
210706	8 h	0.79	7.2	-8.0	-5.0	27
22070G	8 h	0.78	7.5	-8.0	-4.9	27
250706	8 h	0.78	7.0	-8.0	-4.9	27
25070G	8 h	0.78	7.0	-8.0	-5.1	27
100806	8 h	0.77	7.5	-8.0	-5.1	27
140806	8 h	0.77	7.3	-8.0	-4.9	27
150806	8 h	0.78	7.3	-8.0	-4.8	27
160806	8 h	0.79	7.2	-8.0	-4.8	28
170806	8 h	0.78	6.9	-8.0	-5.0	28
210806	8 h	0.76	7.1	-8.0	-5.1	29
250806	8 h	0.79	7.0	-8.0	-4.9	28
020906	8 h	0.78	7.2	-8.0	-5.1	27
050906	8 h	0.79	7.2	-8.0	-4.8	27
120906	7 h	0.79	7.8	-8.0	-5.0	27
140906	7 h 20′	0.78	7.3	-8.0	-4.8	25
041006	7 h	0.79	7.3	-8.0	-4.9	24
051006	6 h 50′	0.80	7.0	-8.0	-5.0	23
061006	7 h	0.79	7.2	-8.0	-5.0	24
2811S1	2 h	0.79	7.0	-8.0	-	23
2811S2	2 h	0.79	7.0	-8.0	-	23

4.1.2. Phase Change of Water

Phase change of water is one of the main parameters affecting the performance of ice storage system. Evidence of phase change process was monitored by measuring of the temperature of water inside the storage tank during the charging tests. Totally 9 thermocouples were placed into water inside the ice storage tank for detecting variation of the water temperature (Figure 3.23). In this study, phase change of water was analyzed for a typical charging experiment (Experiment 050407) and variation of nucleation temperature with radial distance was investigated for three axial positions for all the charging experiments.

Typical curves for temperature changes with time during the charging process of water inside the ice storage tank are shown Figure 4.1 (Experiment 050407). The charging process can be divided into three regions: the region of sensible cooling, the region of dendritic ice formation, and latent heat storage region.

The first stage involves the process from the beginning of cooling from an initial temperature (7 °C) till the metastable state before nucleation occurs (approximately 5279 s), which is called the sensible heat storage processes (Figure 4.2). Natural convection is the dominant heat transfer mechanism in this region and temperature decreases steadily with time. Water remains in the liquid phase even the temperature drops below the freezing point at the end of this region. Cold water is collected at the lower and warmer water is at the upper part of the tank until density inversion of the water around 4 °C, which starts at 1440 s. With the start of density inversion, cold and warmer waters exchange positions: cold water shifts upper and warmer water shifts lower part of the tank (Figure 4.2). After this time, water temperature continues decreasing with an equal rate at each point.

Variation of the water temperature with radial distance for the first 1440 s of the experiment is very similar to that shown in Figure 4.3, which shows the distribution at 1000 s. Variation of temperature with radial distance is negligible. Stratification of the water can be seen clearly from the figure. At the end of the sensible cooling region, temperature of the water drops below the freezing temperature of water (supercooling) in entire tank and water is still in liquid phase.

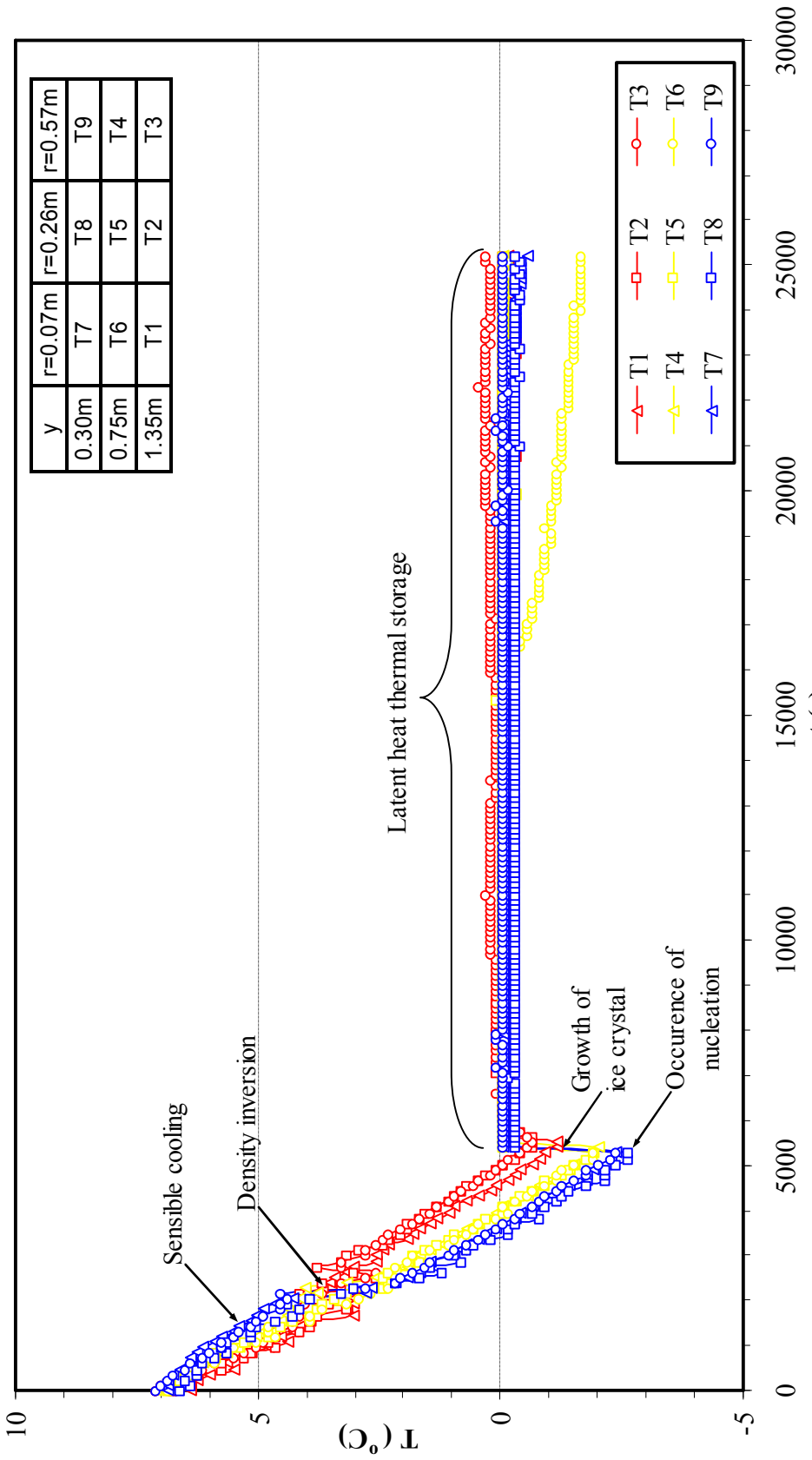


Figure 4.1. Phase change during cooling proceses of water inside the ice storage tank (Experiment 050407)

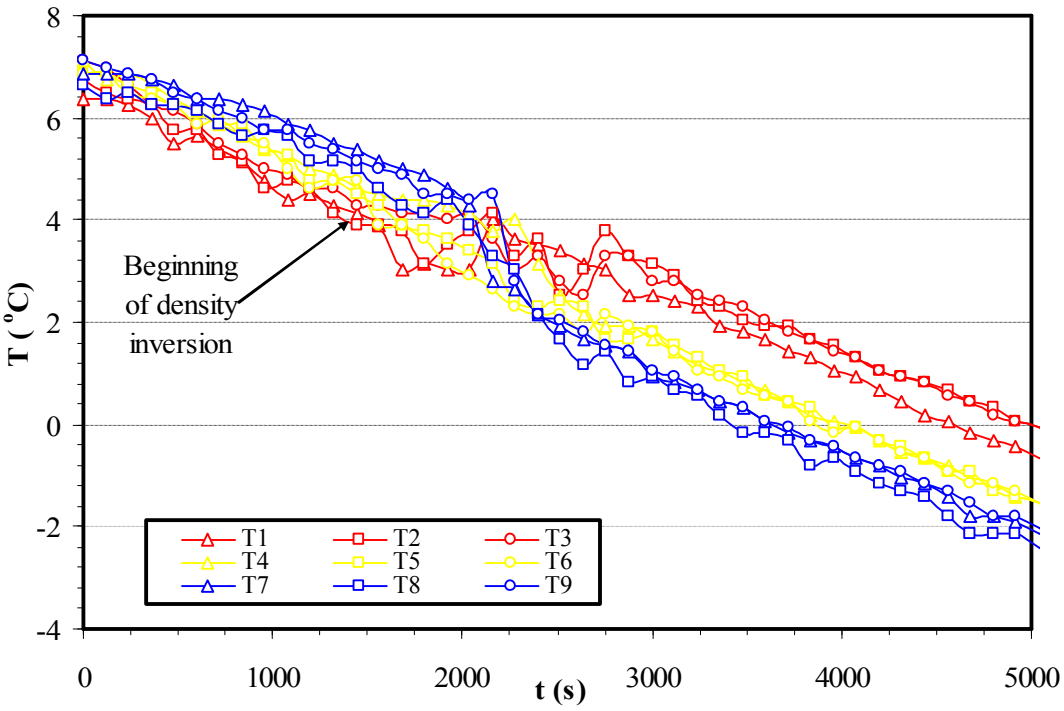


Figure 4.2. Variation of water temperature with time for sensible heat thermal storage processes around density inversion (Experiment 050407)

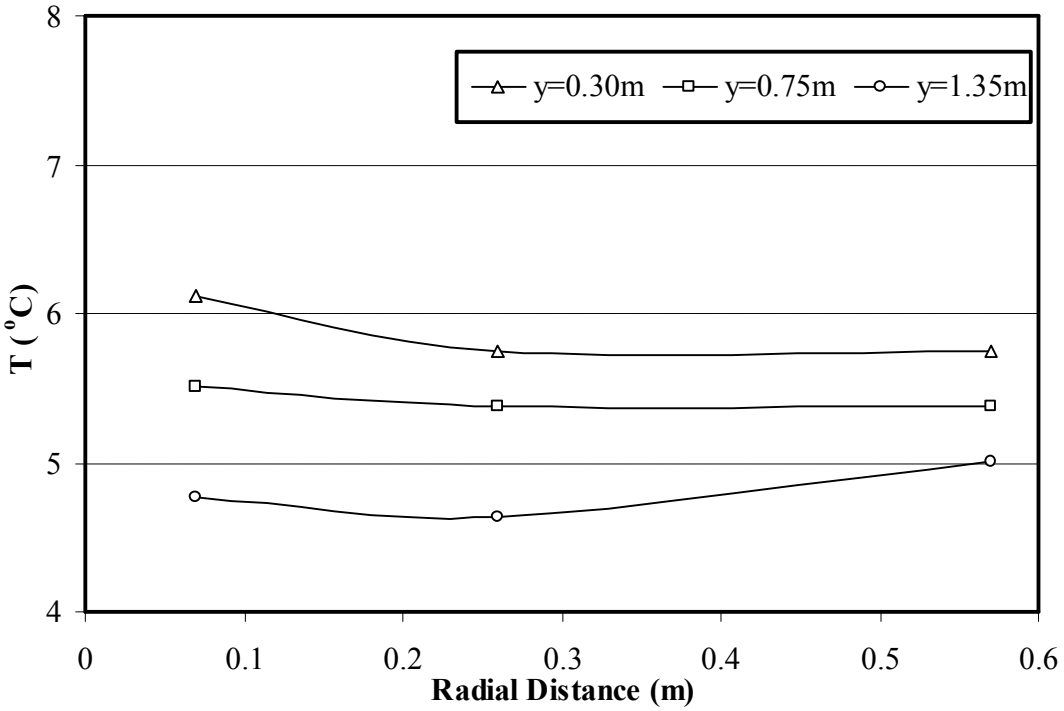


Figure 4.3. Variation of water temperature with radial distance at 1000. s during the experiment before density inversion (Experiment 050407)

The second stage is the process from the start of nucleation to the completion of dendritic ice formation, called the dendritic ice formation processes (Figure 4.4). This process begins with the occurrence of nucleation. The term nucleation implies a starting point, or a nucleus, for ice formation and the temperature at which ice begins to form is known as the nucleation temperature (T_n). As shown in the figure, when the coldest water at the upper part of the storage tank reaches - 2.7 °C (nucleation temperature) ice nucleation starts at this part of the tank. The dendritic ice spreads rapidly from the nucleation site down the center and bottom region of the tank. During dendritic ice growth, a large amount of latent heat is released into the supercooled water. This energy causes the temperature of supercooled water to rise suddenly from -2.7 °C to its freezing point, 0 °C. After water temperature returns to 0 °C, no more dendritic ice growth occurs.

Figure 4.5 shows variation of the water temperatures with radial distance at the beginning of nucleation. As can be seen from the figure, effect of radial distance is negligible and nucleation temperature increases from the upper to the lower part of the tank.

Figure 4.6 illustrates nucleation times at the temperature measurement points inside the ice storage tank (top, middle, and bottom). The time passes from the beginning of the experiment to the start of the nucleation is called nucleation time (t_n). Nucleation first starts at the upper part of the tank and propagates downward.

The third stage involves the phase-change process from the completion of dentritic ice formation till charging is finished, called the latent heat thermal storage processes. A very thin layer of dendritic ice formation starts at the outer surface of the pipe during the second stage. Thickness of the ice increases gradually during latent heat thermal storage processes. Variation of water temperature with time for this region is shown in Figure 4.7. During this period, temperature remains at freezing point temperature (0 ºC) for a certain period of time (Figure 4.8). However, when ice is formed on the tube surface, temperature of the ice begins to fall below 0 ºC, due to heat transfer from the water inside the tank to brine (cooling of ice). Temperature decrease can be clearly observed from thermocouple 6, which is covered by the ice after 15000 s.

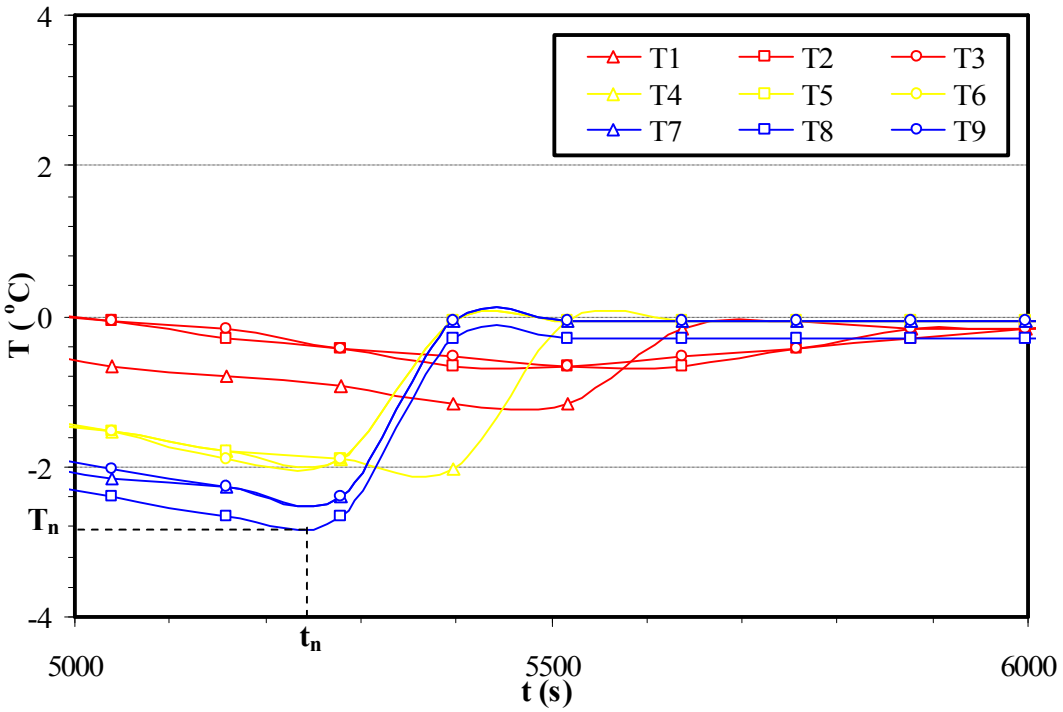


Figure 4.4. Variation of water temperature with time for dendritic ice formation processes after density inversion, (Experiment 050407)

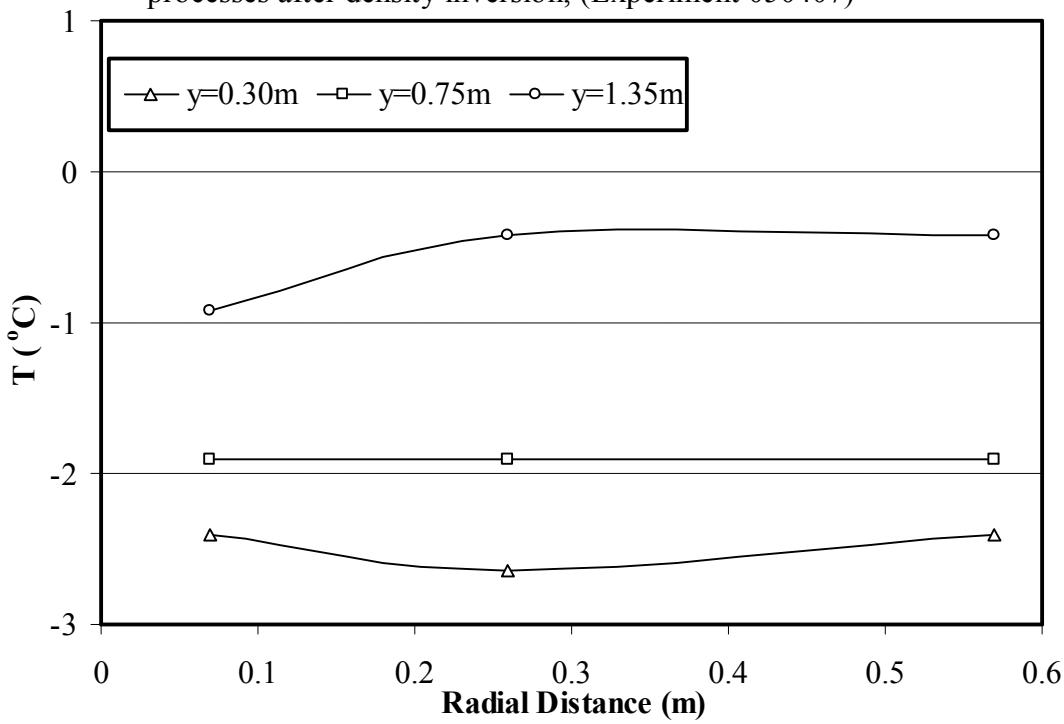


Figure 4.5. Variation of water temperature with radial distance at the beginning of nucleation, t_n =5279 s (Experiment 050407)

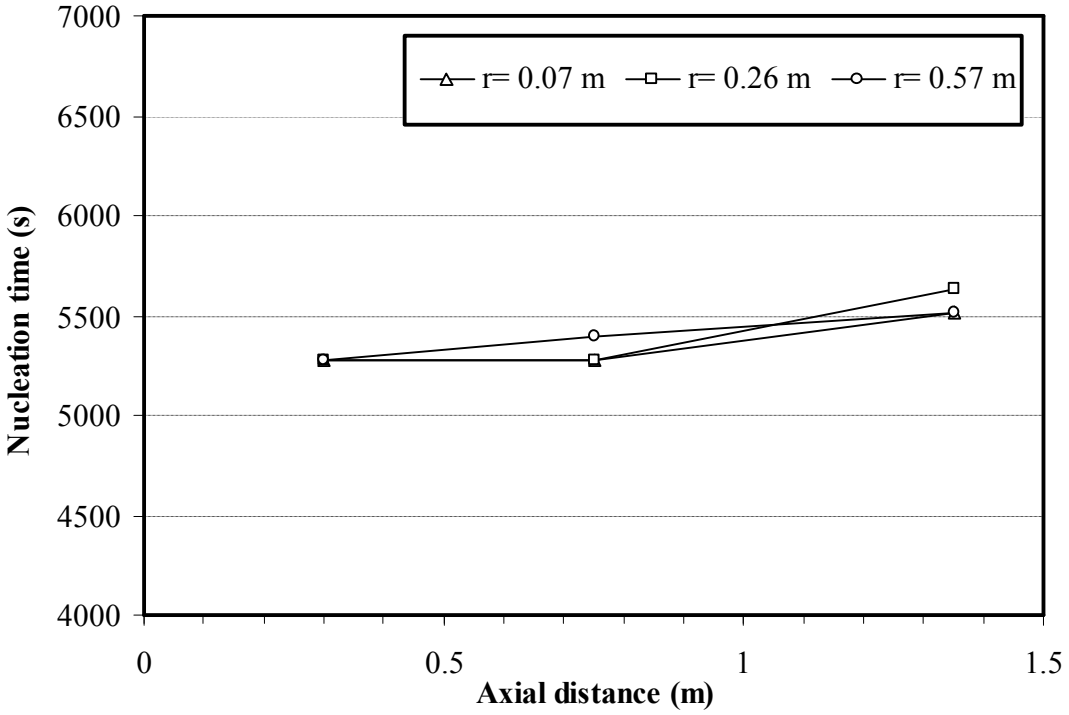


Figure 4.6. Nucleation times at the temperature measurement points inside the ice storage tank (Experiment 050407)

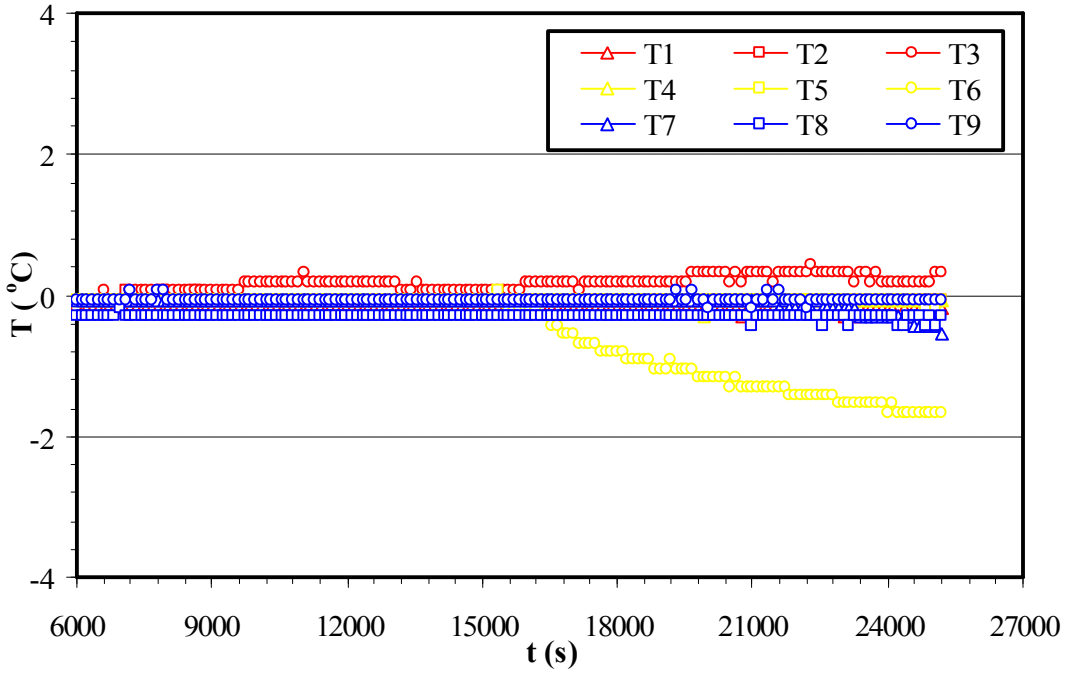


Figure 4.7. Variation of water temperature with time for latent heat thermal storage process (Experiment 050407)

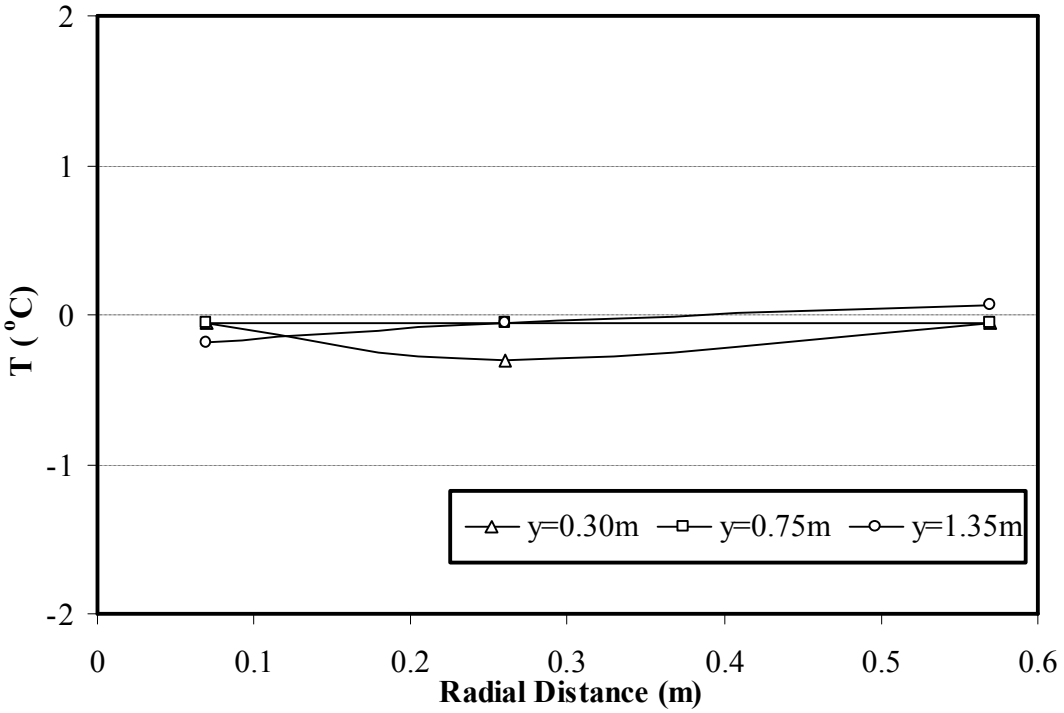


Figure 4.8. Variation of water temperature with radial distance for 13196. s during the experiment (Experiment 050407)

4.1.3. Nucleation Temperature and Nucleation Time

In this section, spatial variation of nucleation temperature inside the storage tank and effect of brine set temperature on nucleation temperature were investigated.

Figures 4.9 and 4.10 show variation of nucleation temperature with radial distance at three axial positions (y=0.3 m, y=0.75 m and y=1.35 m) inside the tank for 6 different brine inlet temperatures, $\overline{T}_{b,i}$ = -4.7 ºC, -4.8 ºC, -4.9 ºC, -5.0 ºC, -5.1 ºC, -5.3 ºC (Experiments 260606, 190506, 140606, 030306, 300306, 200206). As seen from the figures, nucleation temperature does not change considerably with radial distance at all the levels of the tank. Therefore, an average nucleation temperature was obtained at each axial position (y= 0.3m, y=0.75m and y=1.35m) by averaging the three nucleation temperatures at the level of interest.

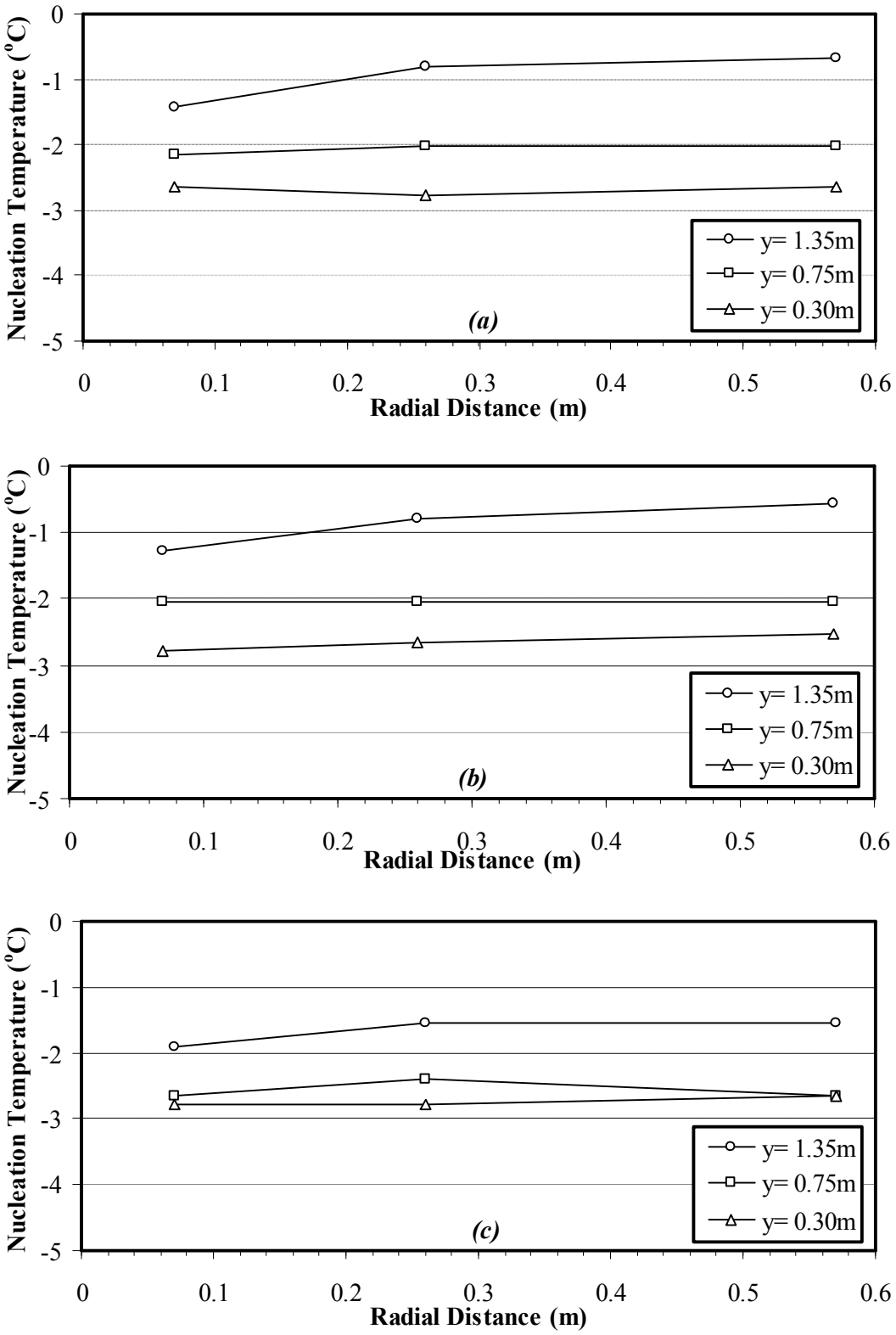


Figure 4.9. Variation of nucleation temperature with radial distance for ***a)*** $\overline{T}_{b,i}$ = -5.3 °C (200206) ***b)*** $\overline{T}_{b,i}$ = -5.1 °C (300306) ***c)*** $\overline{T}_{b,i}$ = -5 °C (030306)

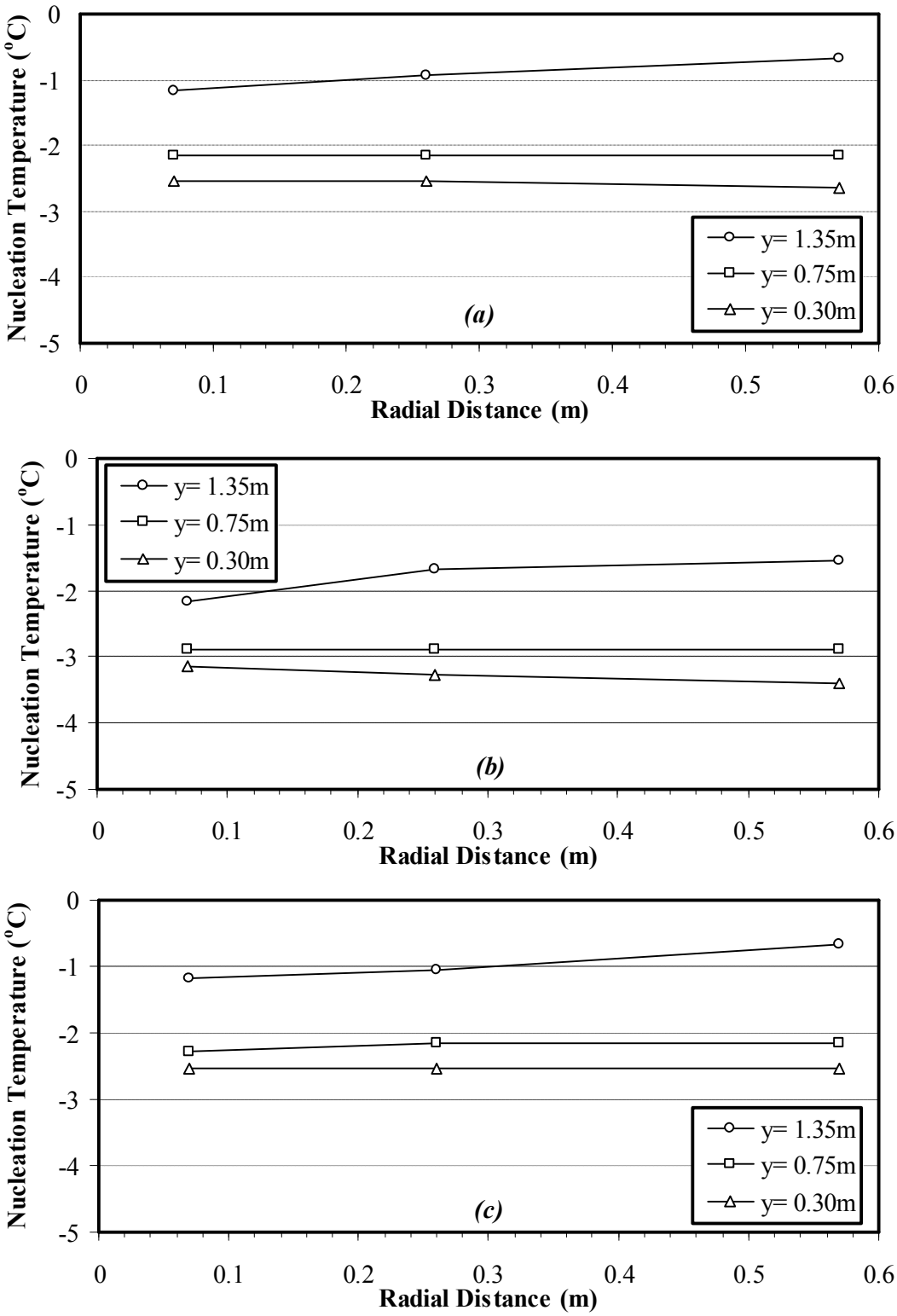


Figure 4.10. Variation of nucleation temperature with radial distance for ***a)*** $\overline{T}_{b,i}$ = -4.9 °C (140606) ***b)*** $\overline{T}_{b,i}$ = -4.8 °C (190506) ***c)*** $\overline{T}_{b,i}$ = -4.7 °C (260606)

Figures 4.11 and 4.12 show variation of nucleation temperature with axial distance for different brine inlet temperatures. Results of the all of the charging experiments are included in the figures. Nucleation temperature increases almost linearly with the axial distance for all brine temperatures. As can be seen from the figures, the minimum nucleation temperature is observed at the upper part of the tank (y=0.3m). This is due to both collection of the coldest water in this region and inlet of the brine into the cooling coil from the top of the tank. Nucleation temperature increases towards the bottom of the tank. A temperature difference between 1 to 2 ºC is evident between the top (y=0.3 m) and the bottom (y=1.35) for all cases. However, nucleation process starts at different temperatures (nucleation temperature) even under the same experimental conditions.

It was not possible to determine nucleation times accurately for the charging experiments carried out because dendritic ice formation is completed inside the whole tank in approximately 60 s and data collection rate was too low (1 reading in 120 s) in these experiments. Therefore, two additional experiments (2811S1 and 2811S2) were performed with higher data collection rate (1 reading in 3 s) to be able to detect start of nucleation. Similar to the other charging experiments, temperature of the water was adjusted to 7 ºC at the beginning of the experiments and brine temperature was set to -8 °C.

Figure 4.13 shows nucleation time at the temperature measurement points inside the ice storage tank. As can be seen from the figure, nucleation time is almost independent of radial position but varies with axial distance. It first starts at the top of the tank and propagates rapidly towards the bottom.

It was not possible to obtain variation of nucleation temperature with brine inlet temperature due to fact that nucleation does not start at a fixed temperature for a given brine inlet temperature. Instead, nucleation temperature varies within a band. For instance, nucleation temperature changes between -2.07 ºC and -3.10 ºC for $\overline{T}_{b,i}$=-5.3 ºC, between -2.03 ºC and -4.09 ºC for $\overline{T}_{b,i}$= -5.1 ºC, between -2.57 ºC and -3.60 ºC for $\overline{T}_{b,i}$= -4.9 ºC. Therefore, more experiments should be carried out to be able to link the nucleation temperature with brine inlet temperature.

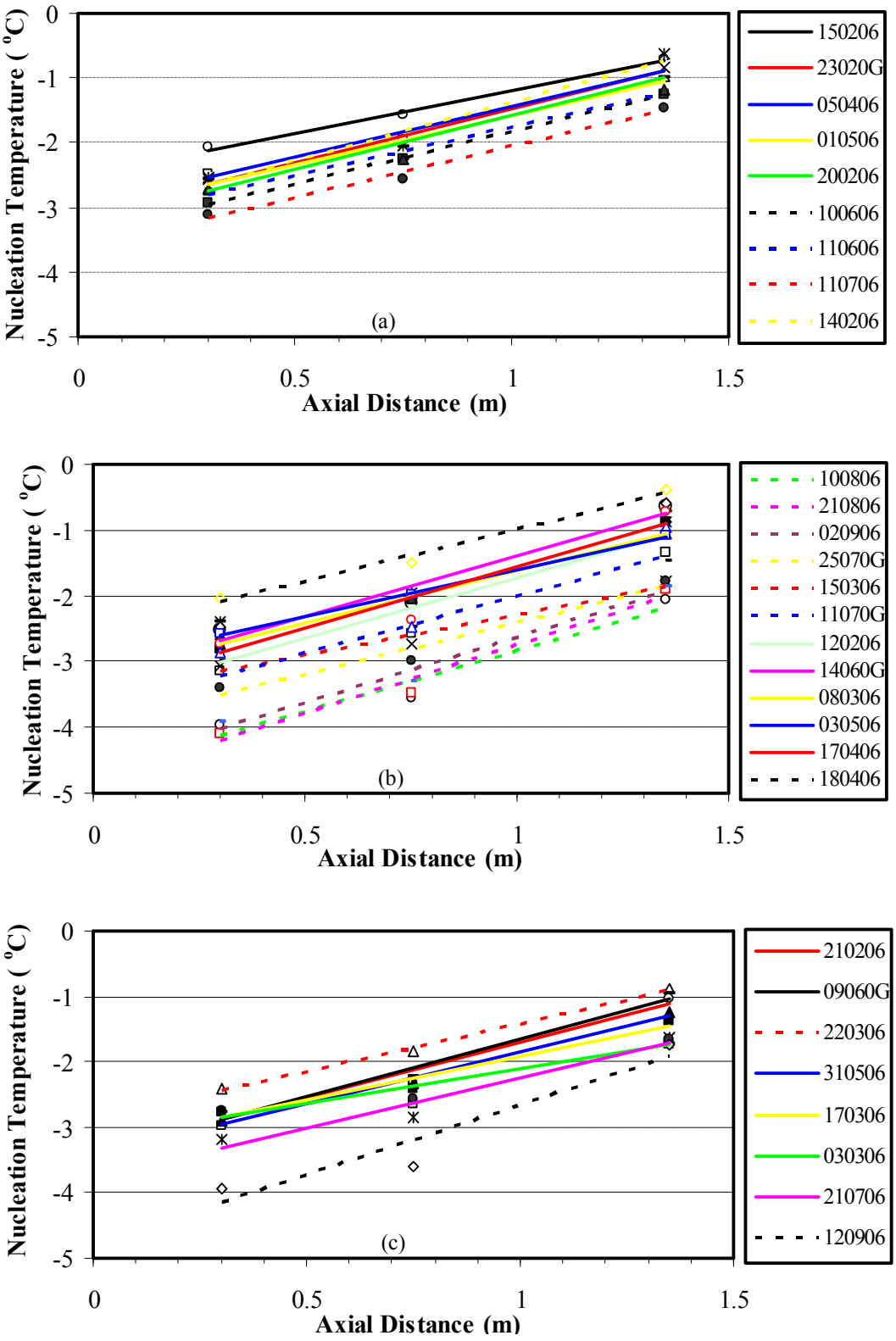


Figure 4.11. Variation of nucleation temperature with axial distance for ***a)*** $\overline{T}_{b,i}$ = -5.3 °C ***b)*** $\overline{T}_{b,i}$ = -5.1 °C ***c)*** $\overline{T}_{b,i}$ = -5 °C

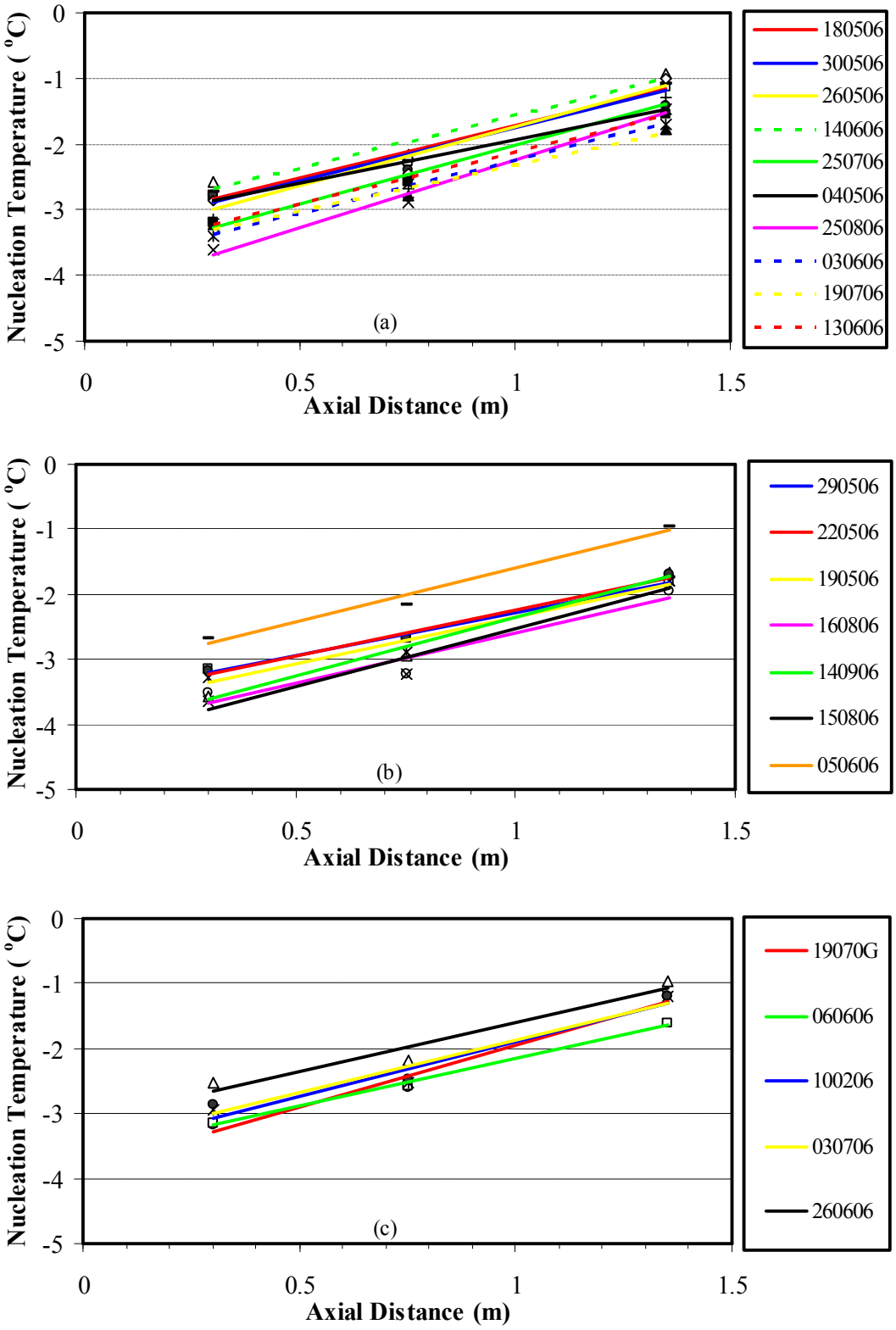


Figure 4.12. Variation of nucleation temperature with axial distance for ***a)*** $\overline{T}_{b,i}$ = -4.9 °C ***b)*** $\overline{T}_{b,i}$ = -4.8 °C ***c)*** $\overline{T}_{b,i}$ = -4.7 °C

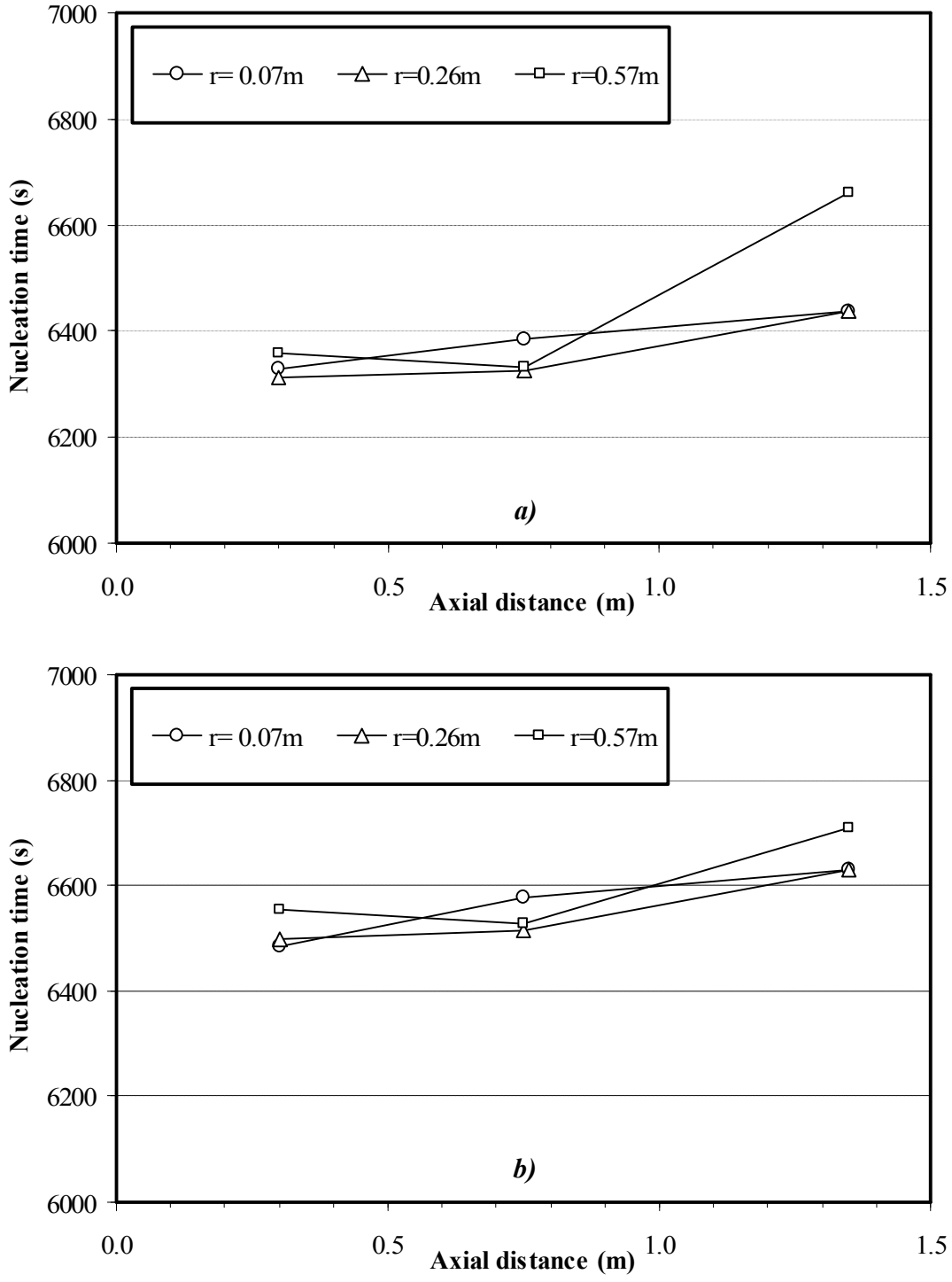


Figure 4.13. Nucleation time at the temperature measurement points inside the ice storage tank ***a)*** Experiment 2811S1 ***b)*** Experiment 2811S2

Even the number of experiments is increased to a certain number, which is enough for a statistical analysis; it will be difficult to predict start of nucleation. Only a probability distribution can be obtained. Such a study was carried out by Chen and Lee. They investigated the supercooling phenomenon and nucleation probability of water inside horizontal cylinders during a cooling process of thermal storage. They performed experiments for different inlet coolant temperatures (from -3 ºC to -10 ºC) and determined probability of freezing. The results indicated that the lower the coolant temperature, the greater the probability of nucleation. The probability of nucleation was zero for the coolant temperatures higher than -4 ºC and one for those lower than -9 ºC (Chen and Lee, 1998).

4.1.4. Effect of Brine Inlet Temperature on Phase Change of Water

Brine inlet temperature is one of the main parameters affecting the performance of ice storage. In this study, results of five of the charging experiments carried out (Table 4.1) representing different brine set temperatures ($T_{b,s}$ = -4 ºC, -5 ºC, -6 ºC, -7 ºC, -8 ºC) were considered (Table 4.2) to investigate effect of brine inlet temperature on supercooling phenomenon. Apart from the brine set temperature, all other conditions of these experiments are very close to each other. Experimental conditions for the experiments selected in this section are listed in Table 4.2.

Table 4.2. Conditions of charging experiments

Test ID	**Charging period** [h]	**Flow rate,** $\dot{m}_b$ [kg/s]	**Initial water temp.,** $T_{w,i}$ [°C]	**Set temperature of brine at the inlet of the tank,** $T_{b,s}$ [°C]	**Average brine temperature at the inlet of the tank,** $\overline{T}_{b,i}$ [°C]	**Average air temperature at the inlet of the condenser,** $\overline{T}_{a,i}$ [°C]
030406	7	0.256	7	-4	-2.13	18.5
020306	7	0.256	7	-5	-3.69	18
170306	7	0.256	7	-6	-4.98	18
060306	7	0.256	7	-7	-5.12	18
050406	7	0.256	7	-8	-5.29	18

Figures 4.14 - 4.16 show temperature histories of brine and air for different measurement points on the system for $T_{b,s}$= -4 ºC. Figure 4.14 shows variation of water temperature with time in the storage tank. For $T_{b,s}$= -4 ºC, temperature of the water inside the tank decreases smoothly from initial temperature of 7 ºC down to –1.9 ºC. Nucleation process does not start at all and water is in supercooled state at all the locations inside the tank. Therefore, water in the storage tank is maintained at a metastable state and the cold energy is stored only by sensible heat.

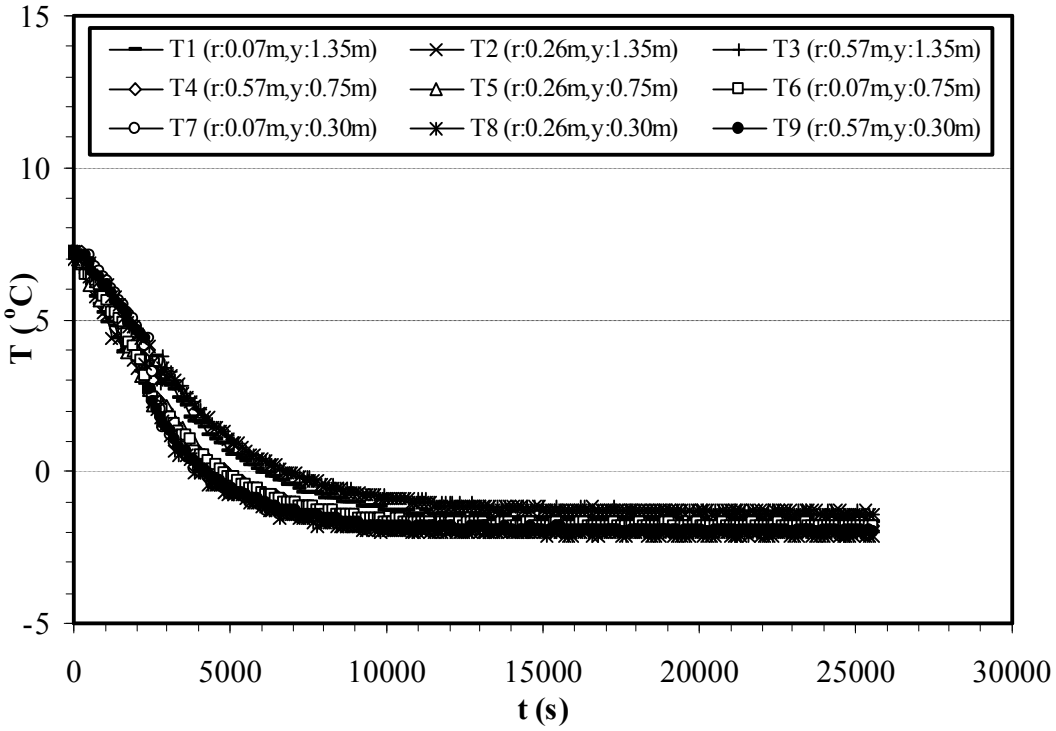


Figure 4.14. Variation of water temperature with time in the storage tank ($T_{b,s}$ = -4 ºC)

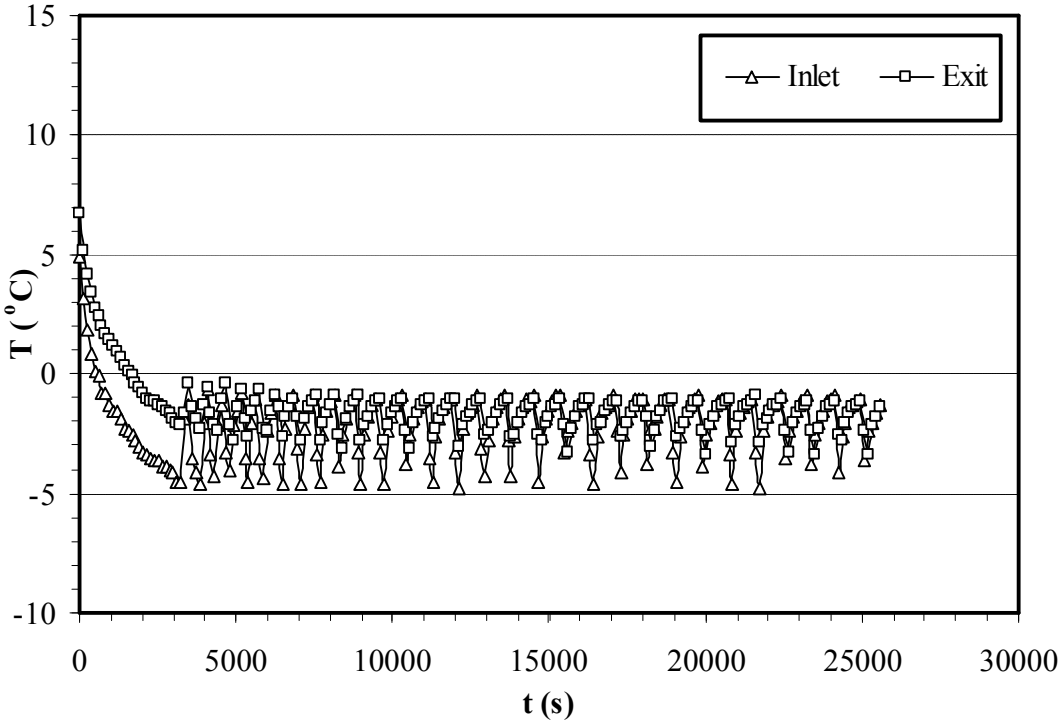


Figure 4.15. Variation of brine temperature with time at the inlet and exit of the tank ($T_{b,s}$ = -4 ºC)

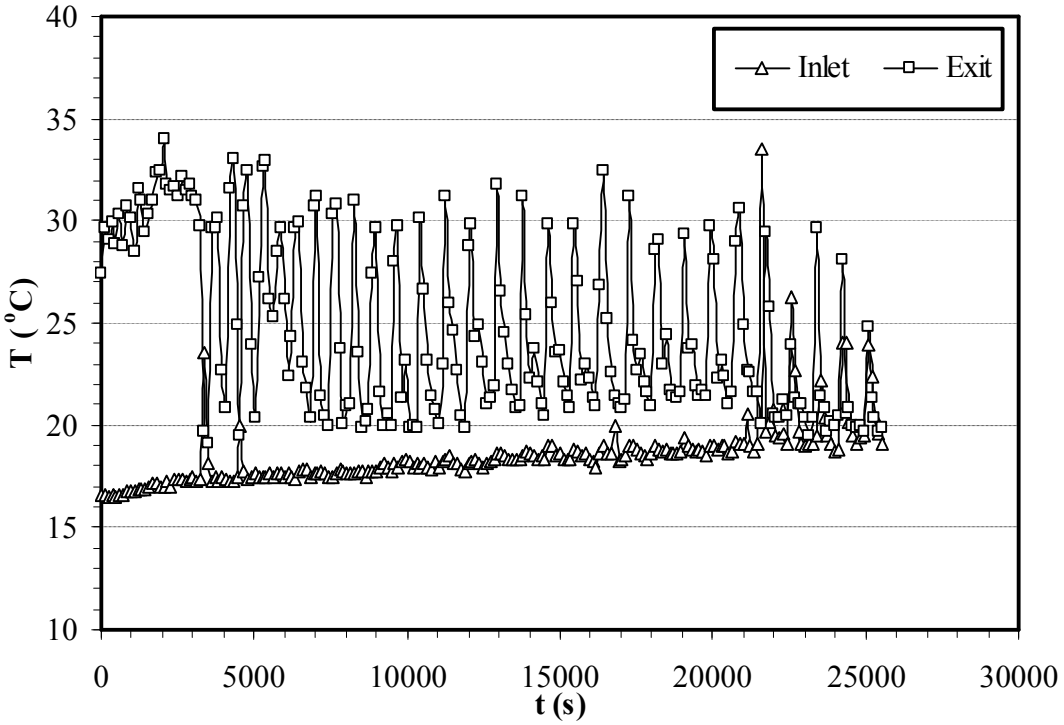


Figure 4.16. Variation of air temperature with time at the inlet and exit of the condenser ($T_{b,s}$ = -4 ºC)

Only a sensible cooling region can be observed in this case and there is no ice formation inside the tank. This indicates that nucleation of water will not start if the set temperature of the brine is equal or higher than -4 ºC even though water is below its freezing point.

Variation of brine temperature with time at the inlet and exit of the tank are shown in Figure 4.15. Fluctuations of temperatures can easily be seen from the figure. When the chiller reaches set temperature of brine (in this case, about -4 ºC), it stops (off mode) and with the increase of brine temperature, the chiller operates again (on mode). It can be seen from the figure that the chiller switches between on and off modes during the experiment. Therefore, water temperature in the ice storage tank is not decreased down to a temperature that is enough for the start of nucleation, and consequently ice formation cannot start. Intermittent working of the chiller unit can also be seen from the temperature of the air circulated through the condenser. Figure 4.16 shows the variation of air temperature with time at the inlet and exit of the condenser.

Figure 4.17 shows variation of water temperature with time in the storage tank for the case of $T_{b,s}$ = -5 ºC. Temperature of the water decreases down to -3.5 ºC and nucleation of water starts approximately 12000 s after the start of the experiment. Occurrence of nucleation is followed by latent heat thermal storage process, during which a relatively thick layer of ice starts to form around the tube outer surface. It is seen from Figure 4.18 that the reason for a long time requirement for the start of nucleation is on-off operation of the chiller during this period. However, the intermittent working of the chiller is not limited to this early period and it continues during the remaining part of the experiment. When the average water temperature in the ice storage tank decreases approximately 0 ºC, brine inlet temperature attains the set temperature and the chiller switches off. It switches on later when the brine temperature increases above the set temperature. Parallel to the mode of the compressor, temperature of the air passing through the condenser fluctuates (Figure 4.19).

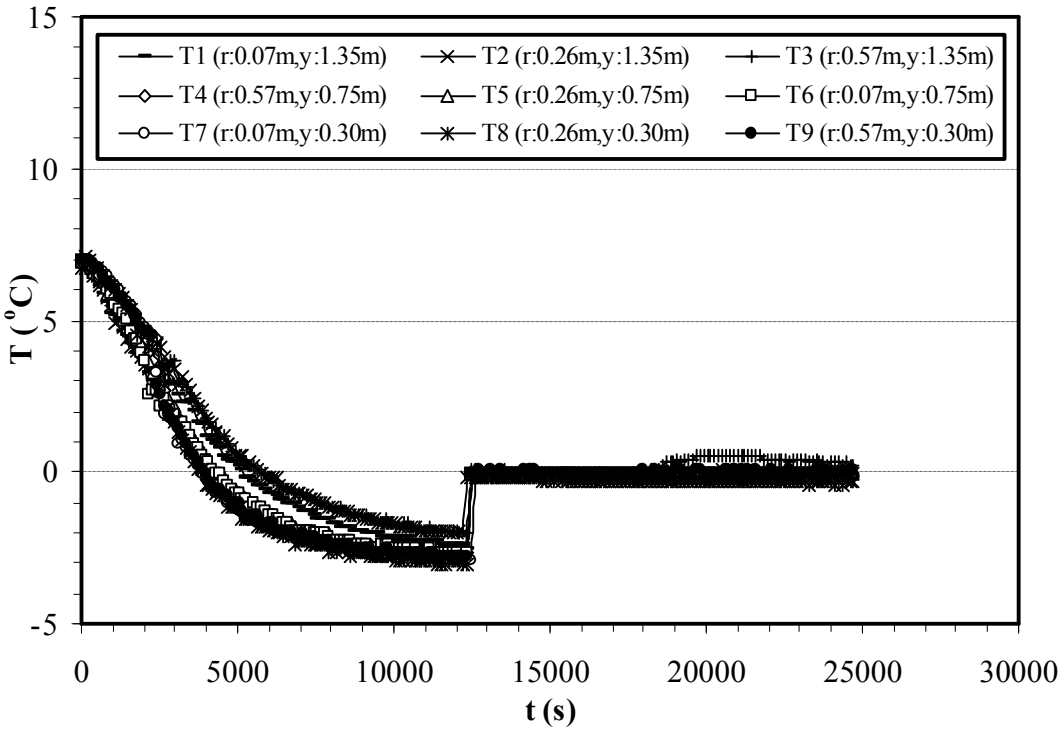


Figure 4.17. Variation of water temperature with time in the storage tank ($T_{b,s}$ = -5 ºC)

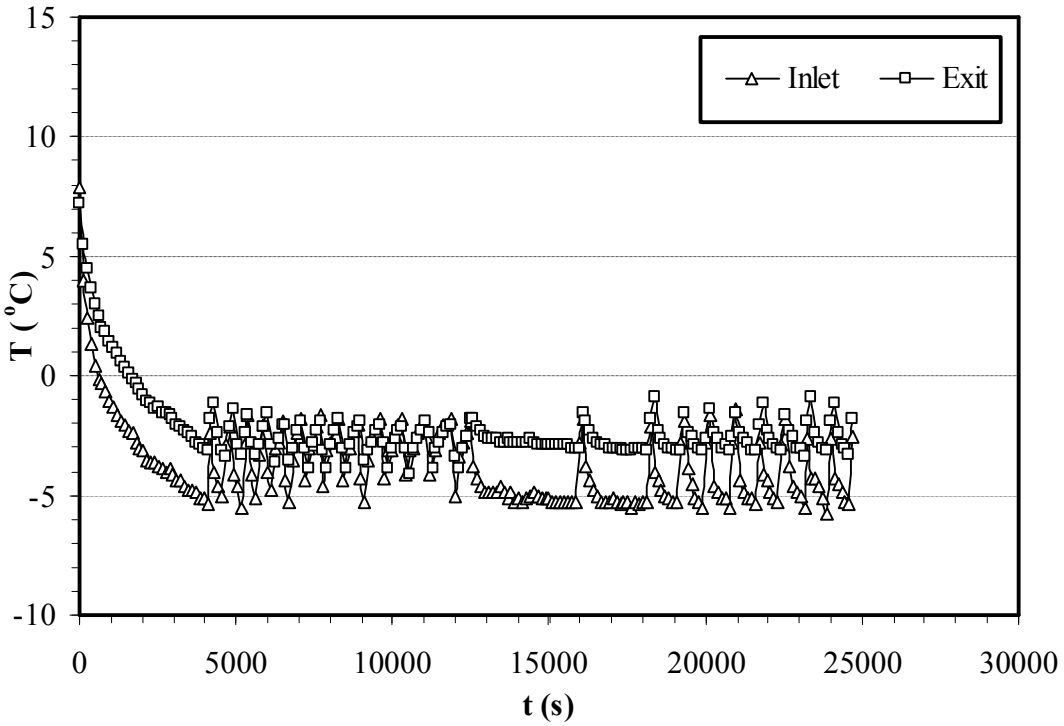


Figure 4.18. Variation of brine temperature with time at the inlet and exit of the tank ($T_{b,s}$ = -5 ºC)

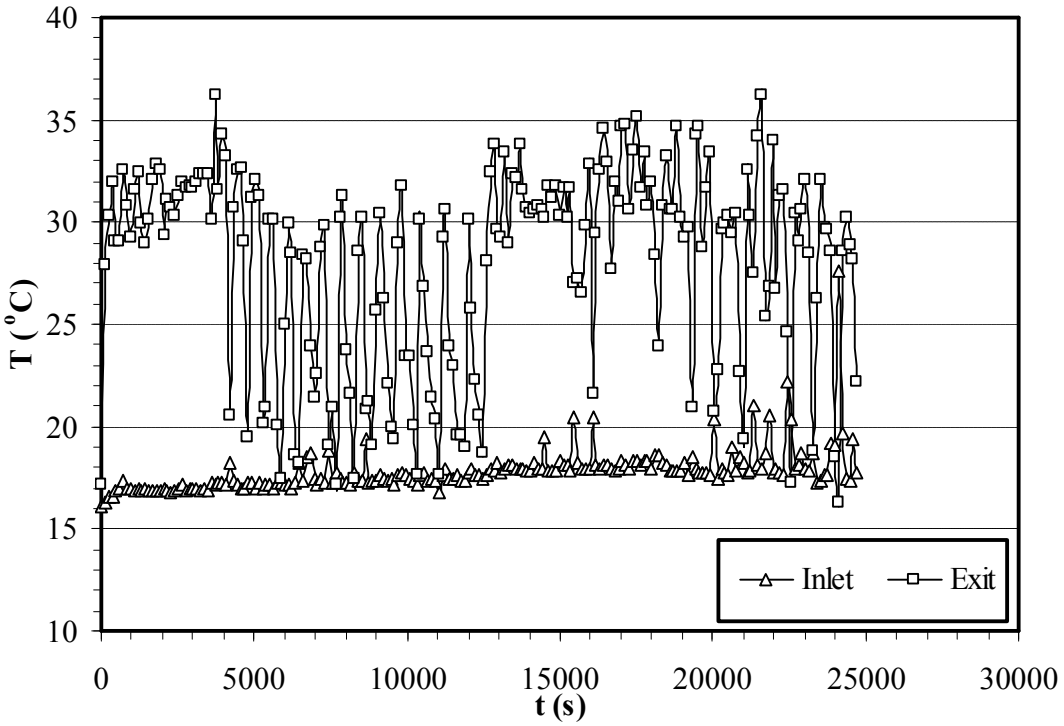


Figure 4.19. Variation of air temperature with time at the inlet and exit of the condenser ($T_{b,s}$ = -5 ºC)

The histories of the water temperatures in the ice storage tank under the condition of a moderate tank inlet brine temperature ($T_{b,s}$ = -6 ºC) are shown in Figure 4.20. In this case, the temperature of water needs a shorter time period (6500 s) to reach the nucleation temperature as compared with the case of $T_{b,s}$ = -5 ºC. It is observed from Figure 4.21 that with the decrease of brine inlet temperature, the number of off positions of the chiller decreases. When the water temperature reaches freezing temperature, the chiller stops a few times. However, after dentric ice formation is completed, the chiller operates continuously and never stops during the remaining part of the experiment. Figure 4.22 shows variation of air temperature with time at the inlet and exit of the condenser. Intermittent operation of the chiller can be seen clearly from the fluctuations of the air temperature at the exit of the chiller.

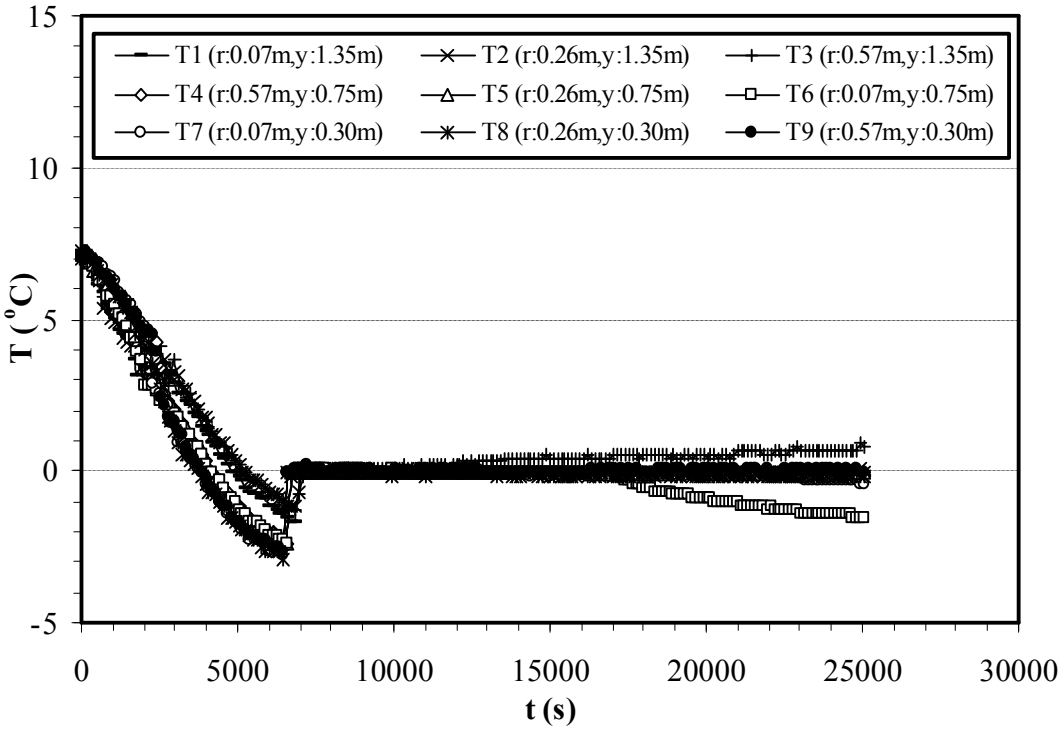


Figure 4.20. Variation of water temperature with time in the storage tank ($T_{b,s}$ = -6ºC)

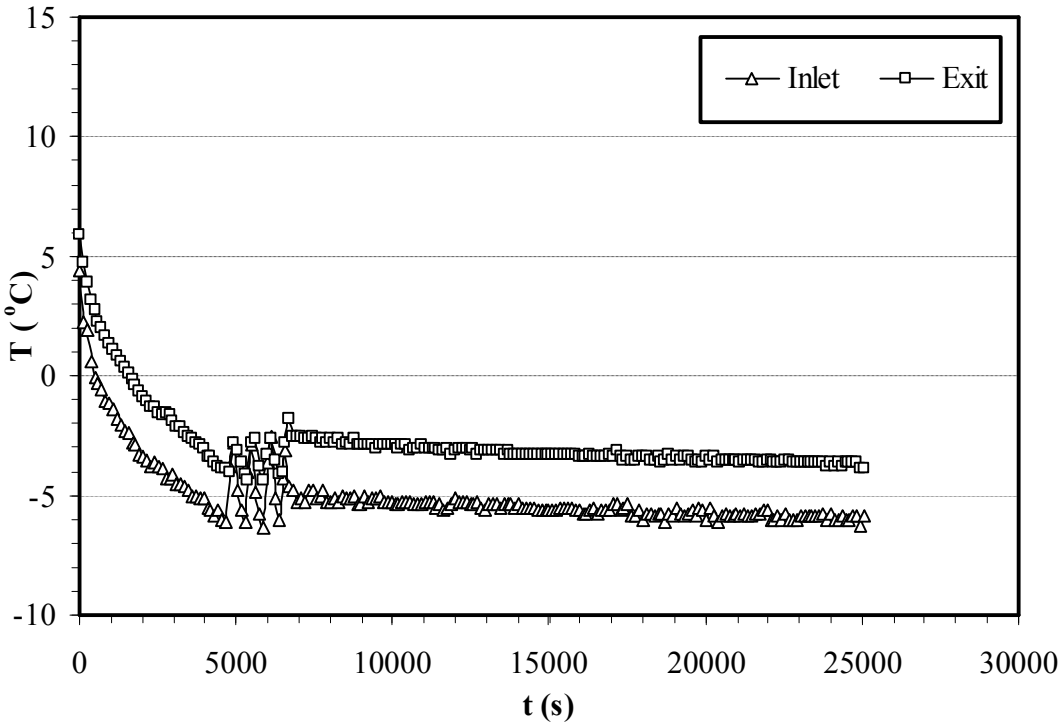


Figure 4.21. Variation of brine temperature with time at the inlet and exit of the tank ($T_{b,s}$ = -6 ºC)

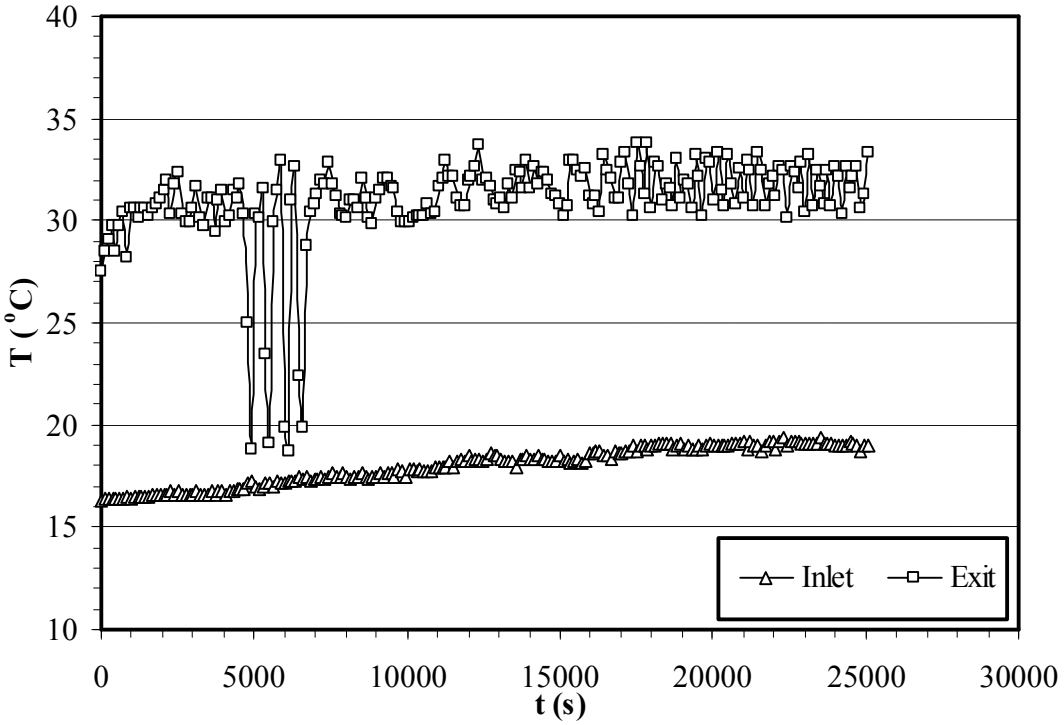


Figure 4.22. Variation of air temperature with time at the inlet and exit of the condenser ($T_{b,s}$ = -6 ºC)

In Figures 4.23 – 4.25, variation of water, brine and air temperatures with time for different measurement points are demonstrated for $T_{b,s}$ = -7 ºC. In this case, nucleation time is smaller than the other cases. As shown in Figure 4.23, time needed to cool water from initial temperature down to nucleation temperature is approximately 5500 s. Set temperature is never attained and the chiller operates continuously during the experiment (Figure 4.24).

The fluctuations in the air temperature passing through the condenser evident for the other set temperatures are not seen in this case since the chiller operates continuously (Figure 4.25).

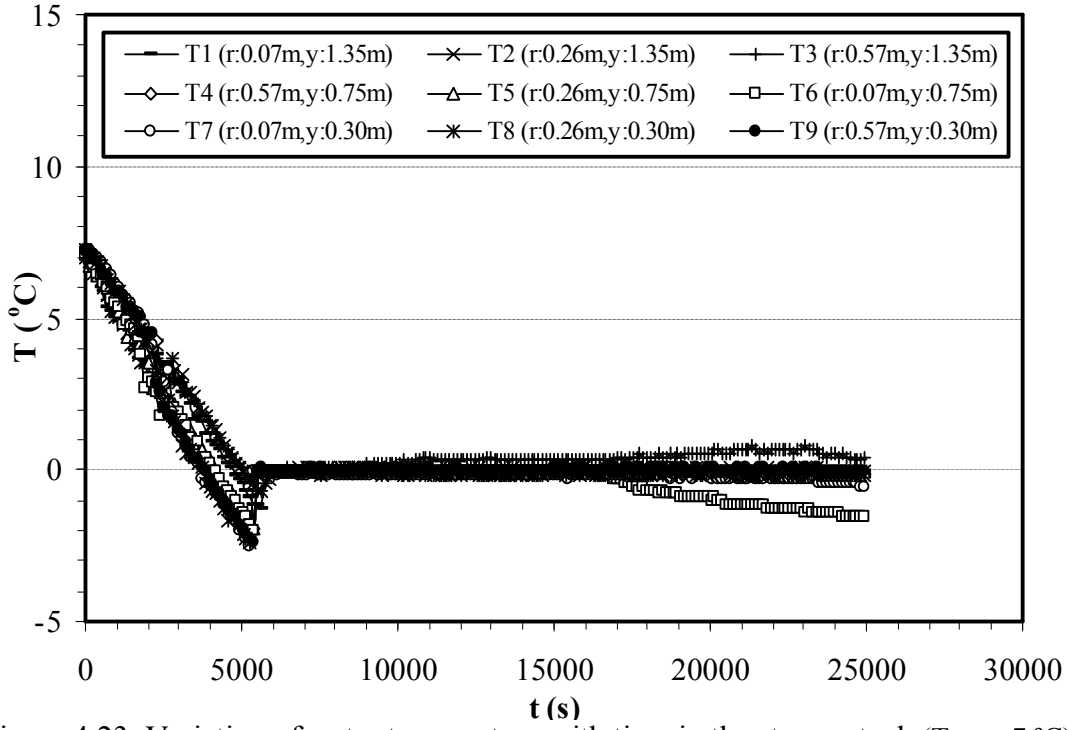


Figure 4.23. Variation of water temperature with time in the storage tank ($T_{b,s}$ = -7 ºC)

Nucleation time (approximately 5500 s) for $T_{b,s}$ = -8 ºC is the same as that for $T_{b,s}$= -7 ºC (Figure 4.26) and it is smaller than the previous cases. As can be seen from Figure 4.27, the chiller cannot lower the brine temperature down to set temperature (-8 ºC). The same results can also be seen from Figure 4.28 that shows variation of air temperature with time at the inlet and exit of the condenser.

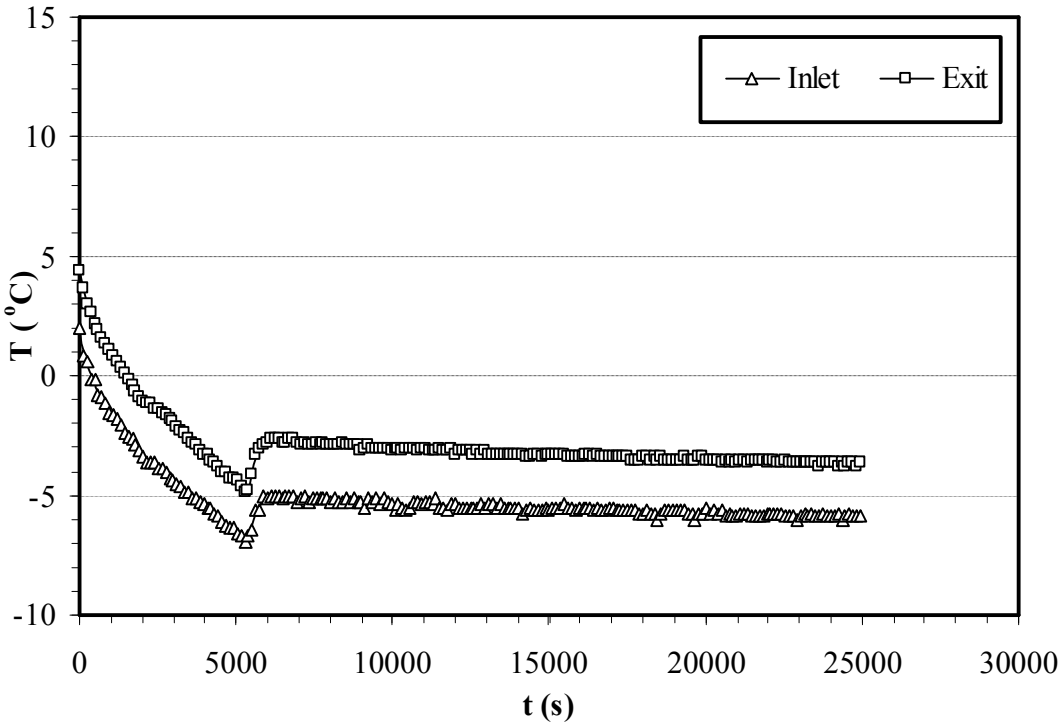


Figure 4.24. Variation of brine temperature with time at the inlet and exit of the tank ($T_{b,s}$ = -7 ºC)

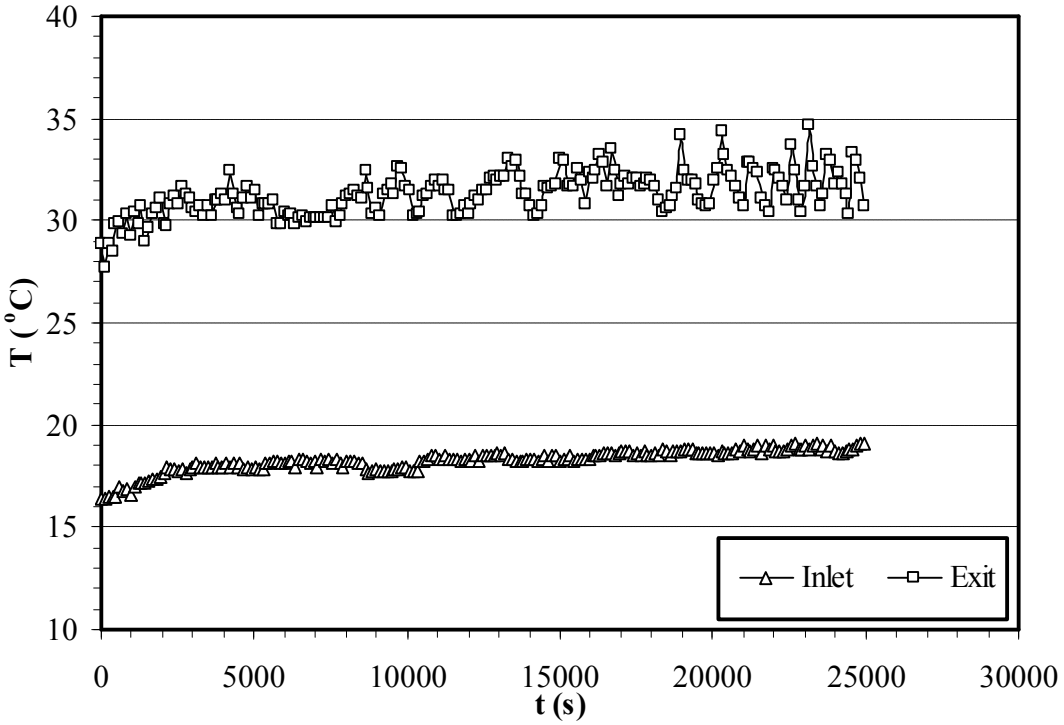


Figure 4.25. Variation of air temperature with time at the inlet and exit of the condenser ($T_{b,s}$ = -7 ºC)

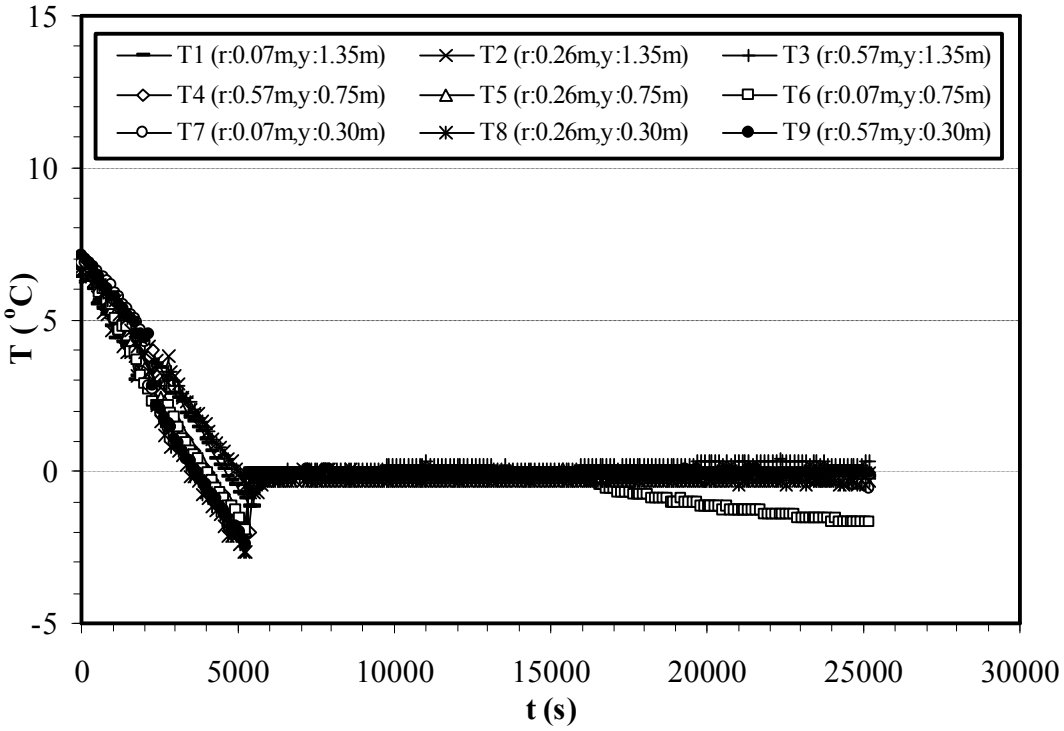


Figure 4.26. Variation of water temperature with time in the storage tank ($T_{b,s}$ = -8 ºC)

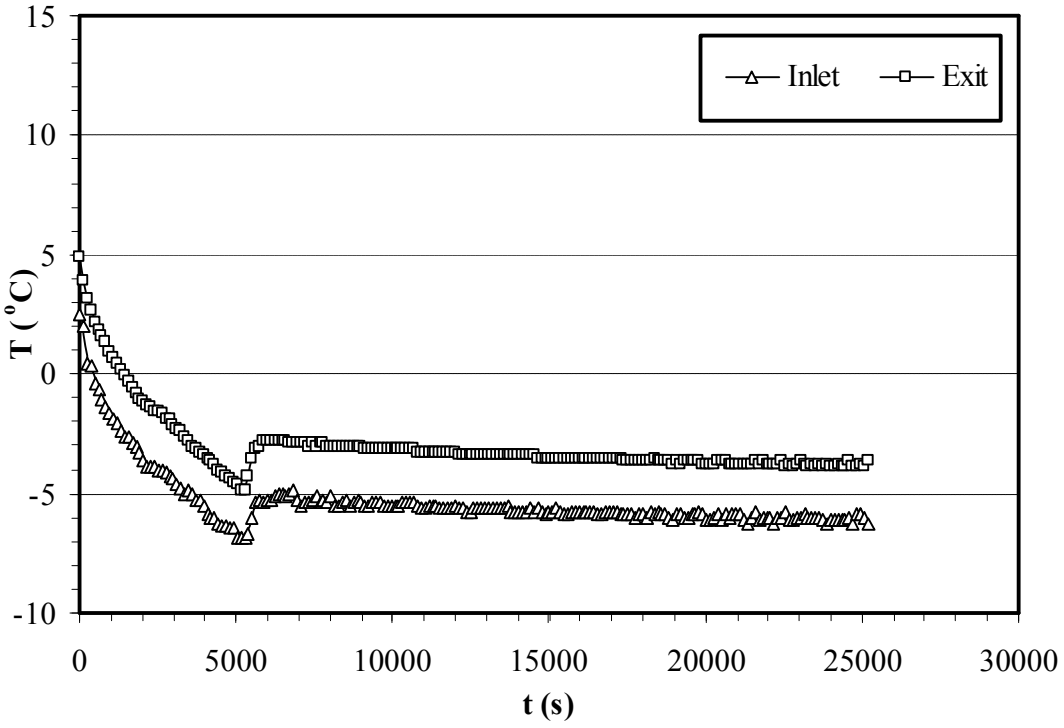


Figure 4.27. Variation of brine temperature with time at the inlet and exit of the tank ($T_{b,s}$ = -8 ºC)

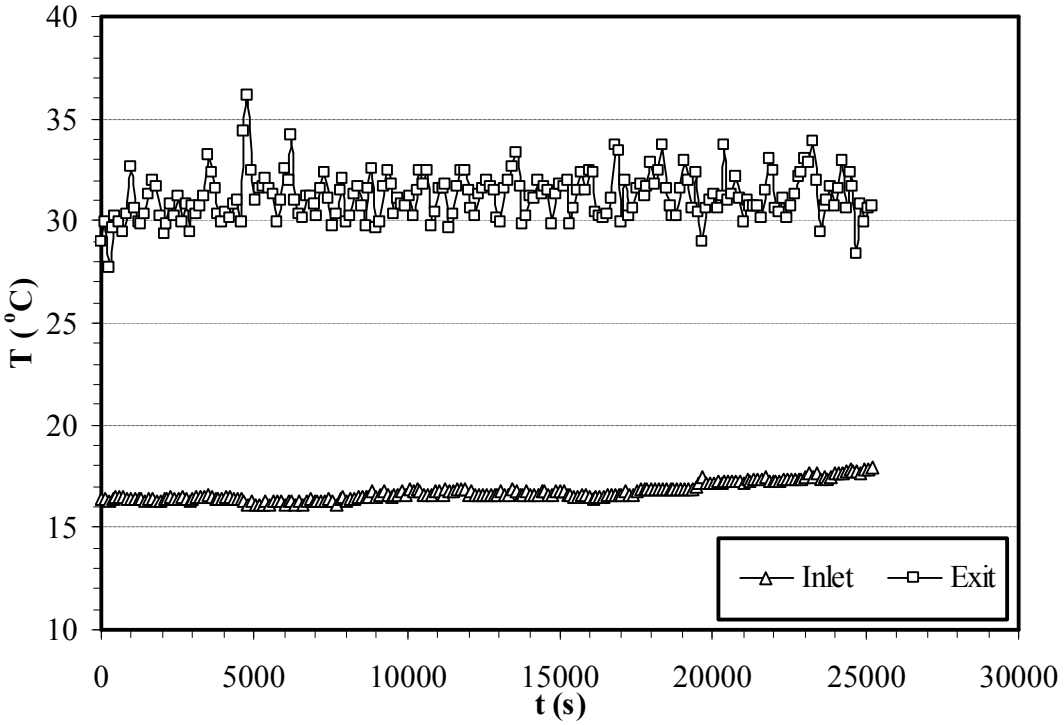


Figure 4.28. Variation of air temperature with time at the inlet and exit of the condenser ($T_{b,s}$ = -8 ºC)

The cumulative energy stored ($Q_{s,b}$) in the tank during the charging period can be calculated from the brine side using brine flow rate $\dot{m}_b$ and the temperature difference of brine between the inlet (T_{in}) and exit (T_{ex}) of the tank by summing the stored energy throughout the course of the charging test:

$$\mathbf{Q}_{s,b} = \int_{t=0}^{t=t_f} \dot{\mathbf{m}}_b \times \mathbf{C}_b \times \left[\mathbf{T}_{ex}(t) - \mathbf{T}_{in}(t)\right] dt \qquad (4.1)$$

where C_b is specific heat of brine, t_f is the charging period.

Figure 4.29 shows the energy stored for different brine inlet temperatures ($T_{b,s}$= -4 ºC, -5 ºC, -6 ºC, -8 ºC). For the case of $T_{b,s}$ = -4 ºC, no ice formation was observed because temperature of the water did not decrease down to a temperature at which nucleation can initiate. Therefore only sensible energy storage can be achieved

if the set temperature of the brine is equal or higher than approximately -4 ºC. In this case, the energy that can be stored in the tank will be minimum. For the case of $T_{b,s}$ = -5 ºC, thermal energy can be stored only in the form of sensible heat until 12000 s at which the first ice formation is observed. After ice formation starts, the gradient of the curve increases sharply. The amount of energy storage is in the form of latent heat in this region. Start of nucleation can also be seen for the set temperatures of $T_{b,s}$ = -6 ºC and $T_{b,s}$ = -8 ºC. However the change in the gradient of the curves is not so pronounced.

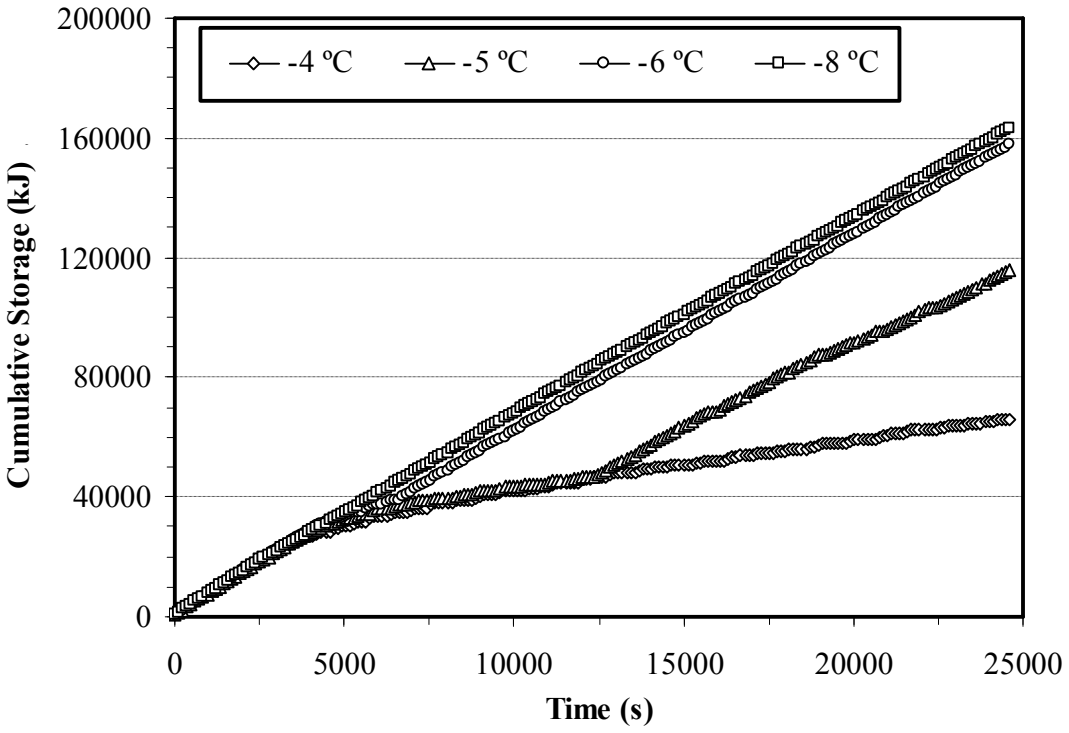


Figure 4.29. Variation of cumulative energy storage with time for $T_{b,s}$ = -4 ºC, -5 ºC, -6 ºC and -8 ºC

It is clear that the brine inlet temperature seriously affects the onset of the phase change of water and the nucleation time of water. The following conclusions can be drawn from the present results:

- The results indicate that if the set temperature of the brine is equal or higher than -4 ºC, water inside the ice storage tank will continue to exist in the metastable state without freezing and only the sensible heat storage is attained.

- If set temperature of the brine is chosen -5 ºC and -6 ºC, the thermal energy can be stored in the form of latent heat. However, ice formation will be delayed due to on-off operation of the chiller.
- With the decrease of brine set temperature, heat removal rate from the water inside the tank is increased and consequently the nucleation time decreases. According to the present experimental results, if set temperature of the brine is preferred -7 ºC and -8 ºC, the time needed to cool water from initial temperature down to a temperature at which nucleation can initiate will be reduced.

4.1.5. Charging Performance

Charging performance of the system η_{charge} was defined as (Dincer, 2002):

$$\eta_{charge} = \frac{Q_s}{W} \tag{4.2}$$

where, Q_s and W represent the total (sensible and latent) cold energy stored in the tank and the total energy consumed during charging process, respectively. The main energy consuming devices are the chiller and the circulation pump.

The data available for each operational test permit redundant calculations that increase our understanding and confidence in the test results. For example, the stored energy for the ice storage tank was determined from both water (tank) and brine sides. Brine properties as a function of concentration and temperature were taken from ASHRAE (ASHRAE Fundamentals, 2001).

The amount of cold energy stored in the tank can be calculated from the water side considering the latent and sensible portions. The former was calculated from the amount of ice produced inside the storage tank during the charging period, the latter was obtained based on measurements of temperature of water inside the storage tank. The total cold stored energy for the ice storage tank $Q_{s,w}$ can be expressed:

$$Q_{s,w} = M_e \times h_{fg} + M_w \times C_w \times (T_{w,i} - T_{w,f}) \tag{4.3}$$

The first term in this equation represents the latent heat and the second one is for sensible heat. In equation 4.3, M_e is mass of ice produced in the ice storage tank during the charging period, h_{fg} is latent heat fusion of water, M_w is mass of water in the ice storage tank, C_w is specific heat of water, $T_{w,i}$ and $T_{w,f}$ are initial and final temperature of water, respectively.

The amount of cold stored energy during charging period ($Q_{s,b}$) was also calculated from the brine side using Eq. 4.1.

The amount of cold energy stored in the tank was calculated both from the water and brine sides using the procedures given above for all the experiments carried out and it was found that the maximum difference between the two approaches is less than 8%.

Amount of cold energy stored (latent +sensible), energy consumption and charging performance for all charging experiments are illustrated in Table 4.3.

Table 4.3. Amount of cold energy stored and charge performance for all charging experiments

Test ID	Amount of ice [kg]	Latent energy stored [kJ]	Sensible energy stored [kJ]	Total energy stored [kJ]	Energy consumption [kJ]	Charging performance
310106	404	135324	29448	164772	106344	1.55
010206	446	149400	42012	191412	122508	1.56
070206	445	149040	37404	186444	124452	1.50
100206	417	139680	26496	166176	109044	1.52
120206	420	140688	26568	167256	109800	1.52
140206	436	146052	26604	172656	112752	1.53
150206	435	145692	26496	172188	112608	1.53
200206	446	149400	25416	174816	113760	1.54
210206	416	139320	26820	166140	111924	1.48
220206	256	85752	27396	113148	86724	1.30
230206	0	0	26208	26208	50760	0.52
23020G	533	178524	26460	204984	86328	1.84
010306	425	142344	26316	168660	113364	1.49
020306	255	85428	25992	111420	88740	1.26
030306	420	140688	25200	165888	110376	1.50
060306	425	142344	26928	169272	113040	1.50
080306	432	144684	26460	171144	112680	1.52
090306	415	138996	25848	164844	108324	1.52
150306	420	140688	26028	166716	109908	1.52
170306	418	140004	26604	166608	109836	1.52
220306	420	140688	29772	170460	112608	1.24

Test ID	Amount of ice [kg]	Latent energy stored [kJ]	Sensible energy stored [kJ]	Total energy stored [kJ]	Energy consumption [kJ]	Charging performance
230306	420	140688	26604	167292	112896	1.21
240306	265	88776	28512	117288	112320	1.04
290306	415	138996	26208	165204	110160	1.50
300306	425	142344	27036	169380	113436	1.49
310306	425	142344	27036	169380	112644	1.50
030406	0	0	26712	26712	56376	0.47
040406	0	0	26856	26856	56196	0.48
050406	435	145692	25308	171000	111852	1.53
170406	425	142344	24840	167184	112680	1.48
180406	410	137340	26424	163764	111456	1.47
190406	425	142344	25128	167472	113544	1.49
200406	275	92124	26964	119088	93096	1.28
240406	415	138996	25992	164988	112320	1.47
010506	420	140688	25848	166536	112752	1.48
020506	330	110520	26568	137088	98928	1.39
030506	420	140688	26244	166932	112284	1.49
040506	405	135648	26136	161784	110196	1.47
050506	276	92448	25524	117972	90576	1.30
160506	315	105516	24552	130068	95796	1.36
180506	424	142020	27504	169524	113328	1.50
190506	390	130644	26316	156960	109548	1.43
210506	295	98820	26784	125604	94392	1.33
220506	395	132300	28620	160920	109656	1.47
230506	422	141336	25020	166356	113436	1.47
240506	305	102168	24552	126720	100980	1.25
250506	405	135648	26316	161964	117324	1.38
260506	400	133992	28152	162144	116100	1.40
290506	387	129636	25776	155412	113796	1.37
300506	406	135972	25416	161388	117360	1.38

Test ID	Amount of ice [kg]	Latent energy stored [kJ]	Sensible energy stored [kJ]	Total energy stored [kJ]	Energy consumption [kJ]	Charging performance
310506	405	135648	26676	162324	116928	1.39
060606	375	125604	25272	150876	115308	1.31
090606	405	135648	25524	161172	110736	1.45
09060G	400	133992	25740	159732	110736	1.44
100606	425	142344	25596	167940	113220	1.48
10060G	420	140688	24804	165492	109008	1.52
110606	420	140688	26856	167544	114696	1.46
120606	373	124920	26964	151884	109548	1.39
130606	392	131292	25668	156960	110988	1.41
13060G	295	98820	27180	126000	96336	1.31
140606	410	137340	26928	164268	113688	1.44
14060G	415	138996	25956	164952	112968	1.46
260606	377	126288	28116	154404	118620	1.30
270606	260	87084	26604	113688	101556	1.12
280606	410	137340	27216	164556	104904	1.57
030706	370	123912	27288	151200	116964	1.29
040706	415	138996	23580	162576	117252	1.39
110706	390	130644	26928	157572	116676	1.35
11070G	437	146376	26136	172512	129708	1.33
120706	445	149040	26460	175500	134172	1.31
190706	365	122256	27396	149652	118980	1.26
19070G	430	144036	26136	170172	135936	1.25
210706	425	142344	27216	169560	135036	1.26
22070G	427	143028	28116	171144	135396	1.26
250706	430	144036	26568	170604	133380	1.28
25070G	435	145692	26316	172008	135684	1.27
100806	420	140688	28044	168732	135108	1.25
140806	425	142344	27648	169992	137052	1.24

Test ID	Amount of ice [kg]	Latent energy stored [kJ]	Sensible energy stored [kJ]	Total energy stored [kJ]	Energy consumption [kJ]	Charging performance
150806	430	144000	27396	171396	136260	1.26
160806	420	140688	27180	167868	137268	1.22
170806	425	142344	25992	168336	136152	1.24
210806	410	137340	26820	164160	136692	1.2
250806	420	140688	26352	167040	137232	1.22
020906	430	144036	28692	172728	132552	1.3
050906	445	149040	27288	176328	132228	1.33
120906	375	125604	29304	154908	117720	1.32
140906	415	138996	27648	166644	119880	1.39
041006	395	132300	27612	159912	114120	1.4
051006	385	128952	26460	155412	109800	1.42
061006	405	135648	27288	162936	116640	1.4

Figures 4.30 - 4.34 show variation of charging performance with average brine inlet temperature for different air temperatures at the inlet of the condenser. As the brine inlet temperature increases, the amount of the energy stored in the tank decreases, which in turn causes a decrease in the charging performance. This is due to intermittent operation of the chiller unit at higher brine inlet temperatures. Similar trends are observed for all the air temperatures at inlet of the condenser observed in the experiments. The figures also show a least square error linear fit to the experimental data.

Figure 4.35 shows variation of charging performance with brine inlet temperature for all air temperatures at the inlet of the condenser. It can be seen from the figure that charging performance decreases with the increase of brine inlet temperature, although the scatter in data is considerable. The gradients of the linear fits are not exactly the same.

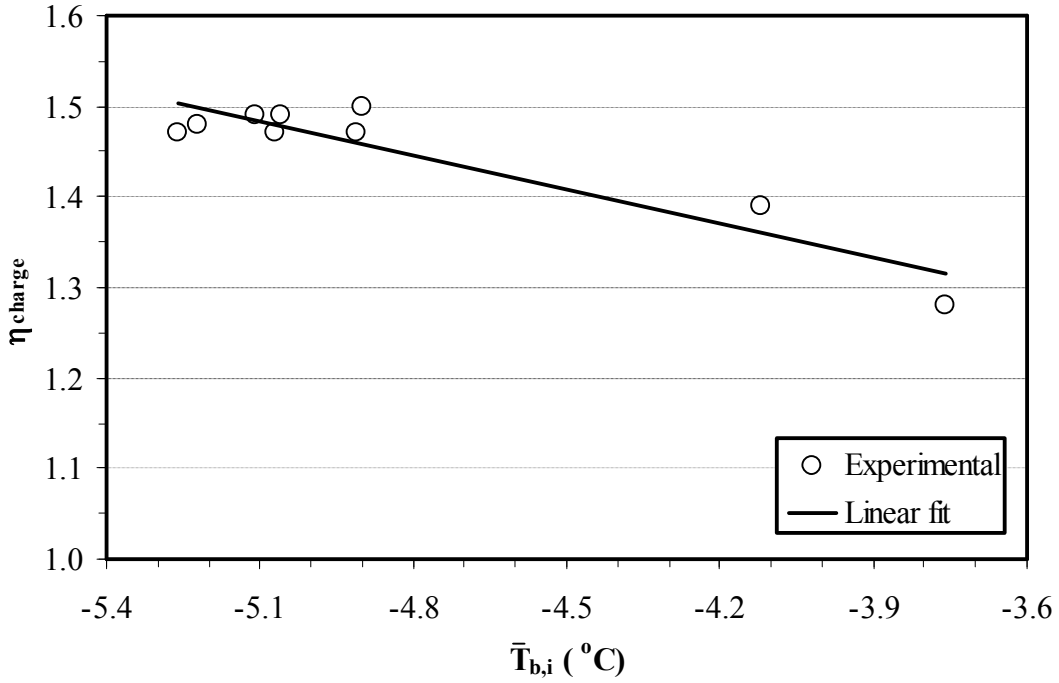


Figure 4.30. Variation of charging performance with brine inlet temperature for $\overline{T}_{a,i}$ = 20-21 ºC

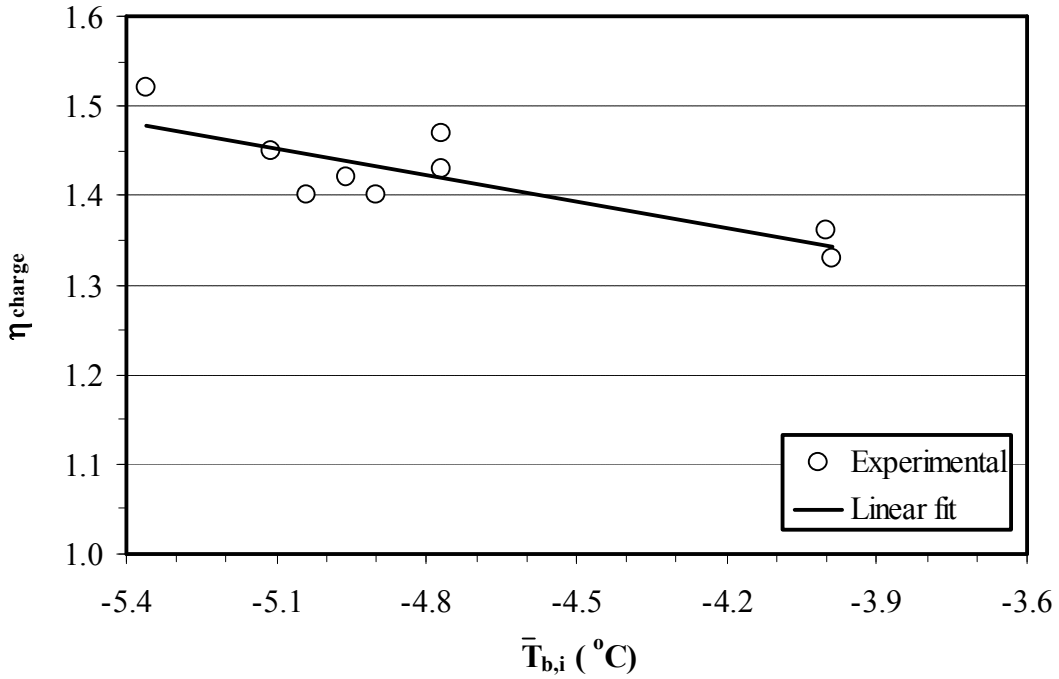


Figure 4.31. Variation of charging performance with brine inlet temperature for $\overline{T}_{a,i}$ = 23-24 ºC

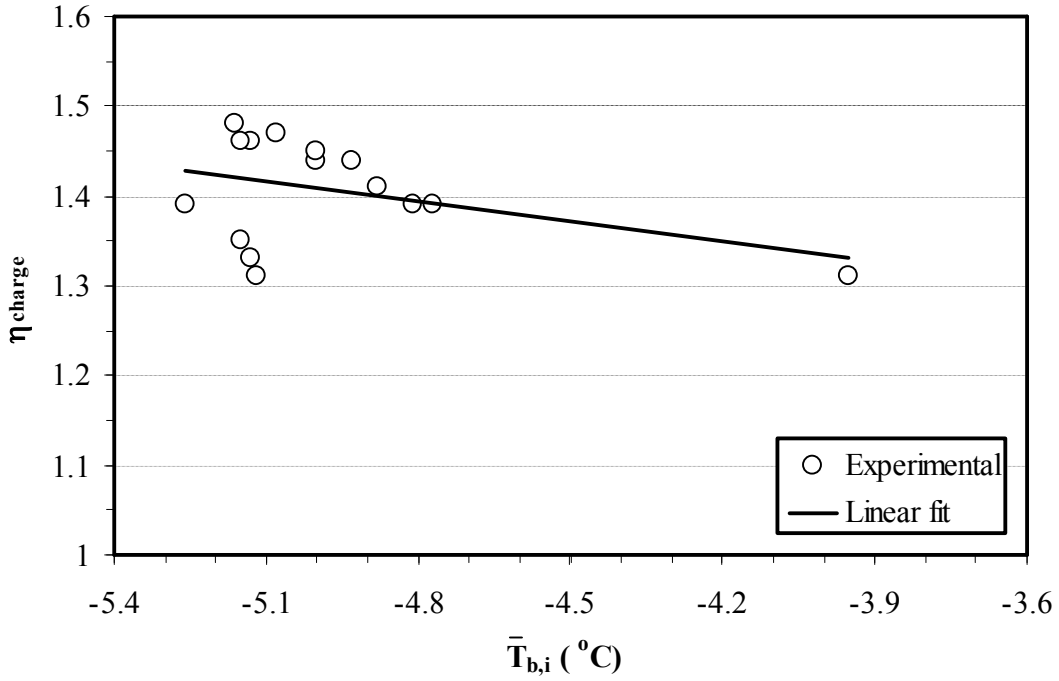


Figure 4.32. Variation of charging performance with brine inlet temperature for $\bar{T}_{a,i}$ = 25 ºC

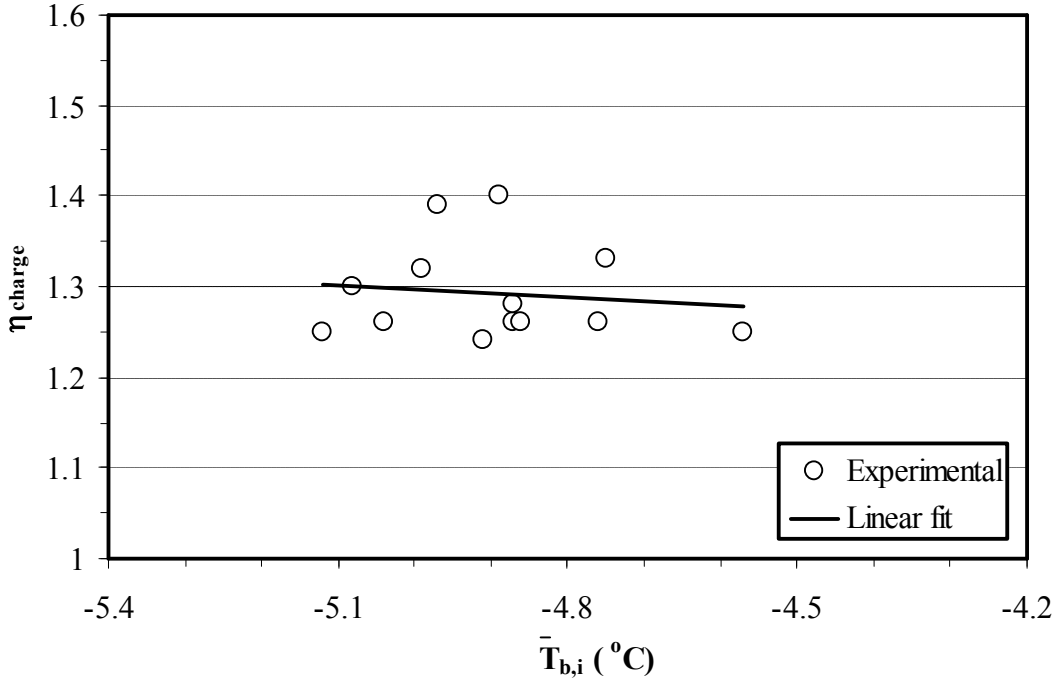


Figure 4.33. Variation of charging performance with brine inlet temperature for $\bar{T}_{a,i}$ = 27 ºC

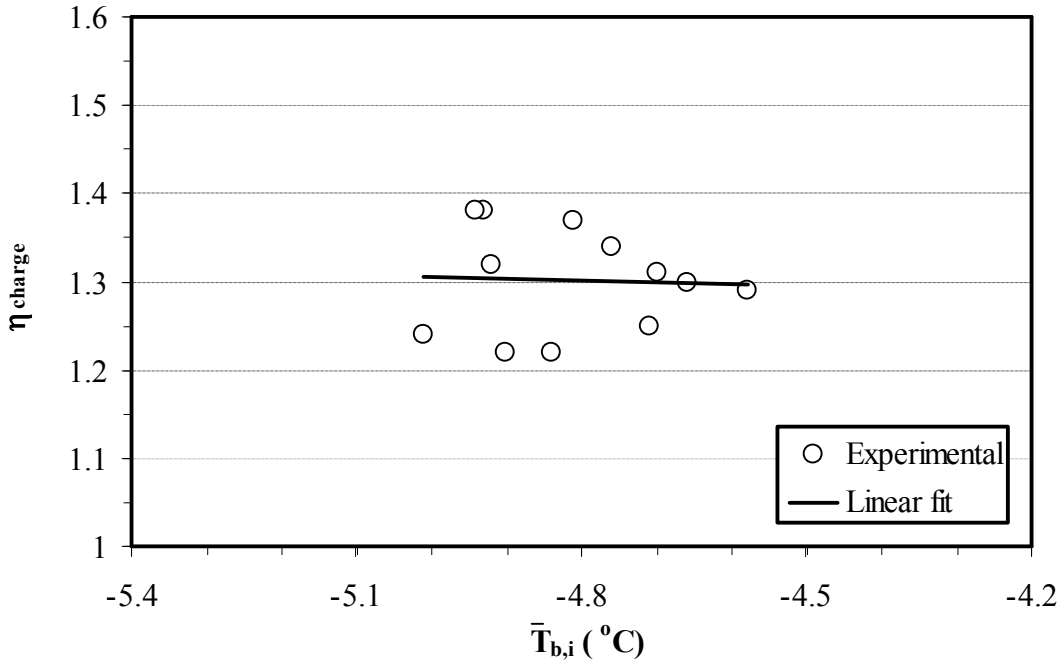


Figure 4.34. Variation of charging performance with brine inlet temperature for $\overline{T}_{a,i}$ = 28 ºC

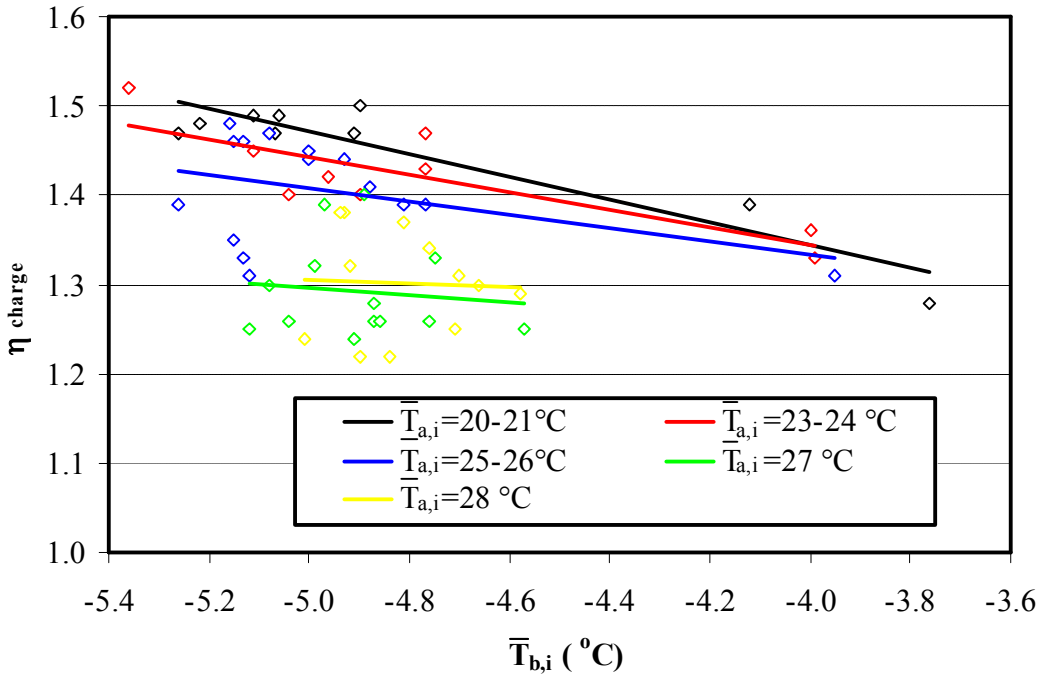


Figure 4.35. Variation of charging performance with brine inlet temperature for all air temperatures at the inlet of the condenser

Variation of charging performance with air inlet temperature for different brine inlet temperatures ($\overline{T}_{b,i}$ = -4.8 ºC, -4.9 ºC and -5.3 ºC) is shown in Figures 4.36-4.38, which also show a least square error linear fit to the experimental data. As can be seen from the figures, when air temperature at the inlet of the condenser increases, charging performance decreases. Variations of charging performance with the air inlet temperature are plotted together for all the brine inlet temperatures in Figure 4.39. It was not possible to control air temperature during an experiment and to change it systematically from one experiment to another one. Therefore, Figure 4.39 is not capable of offering a clear picture for the effect of air temperature on charging performance. However, a general trend can be read: charging performance decreases with the increase of air inlet temperature, as expected. Air inlet temperature directly controls the condenser temperature, which in turn affects the performance of the chiller unit.

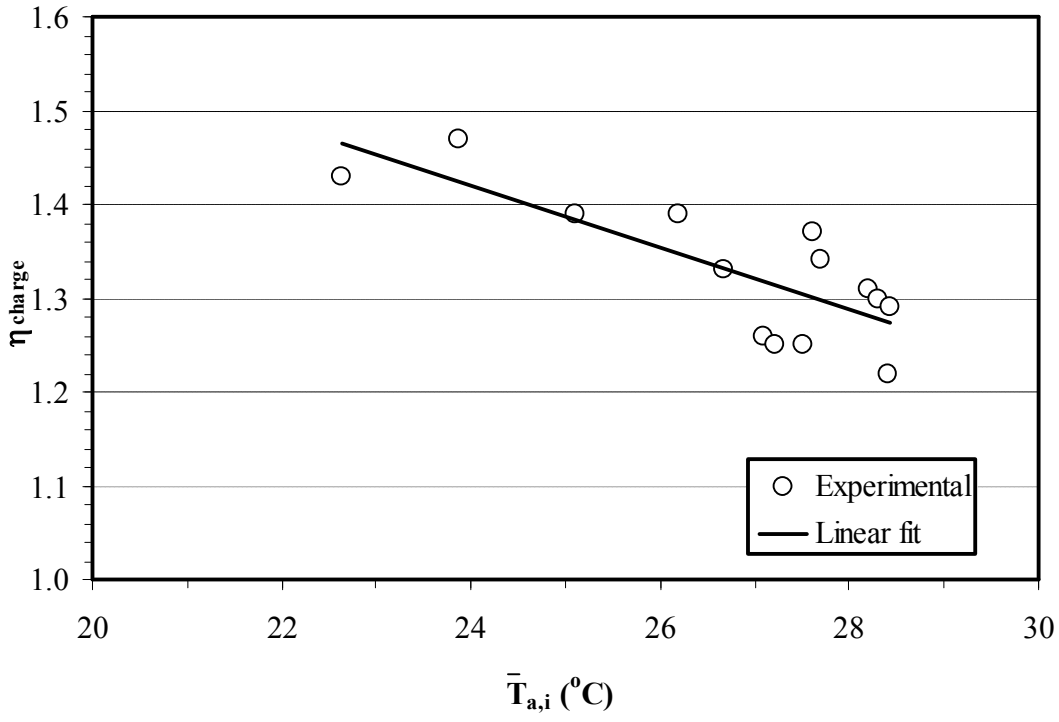


Figure 4.36. Variation of charging performance with air inlet temperature for $\overline{T}_{b,i}$ = -4.8 ºC

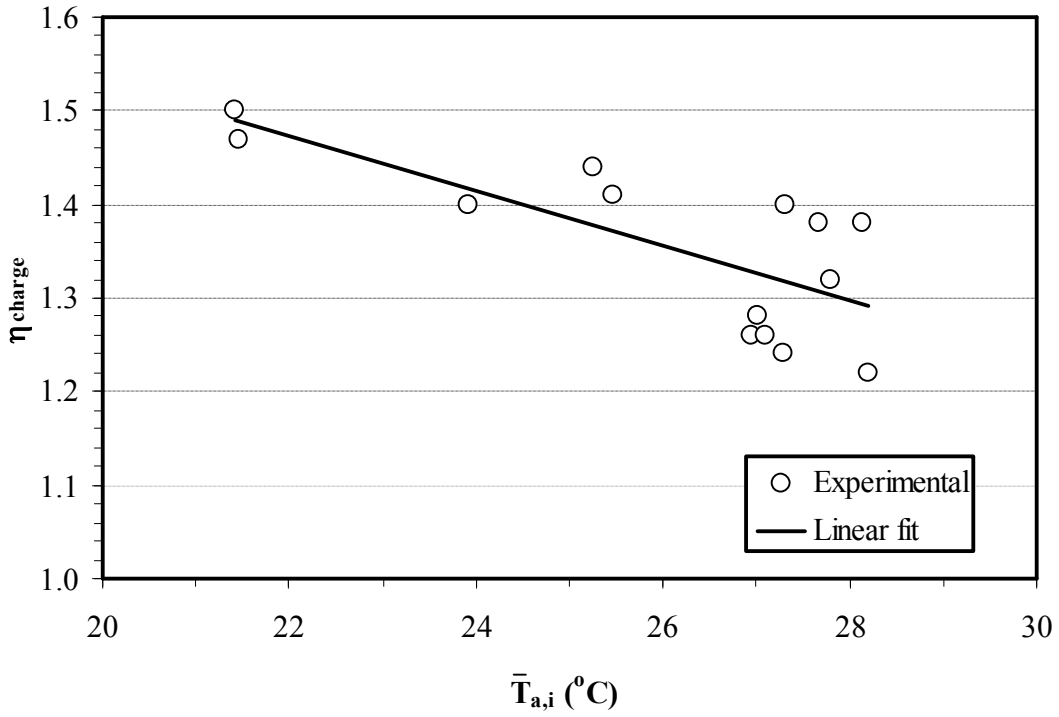


Figure 4.37. Variation of charging performance with air inlet temperature for $\bar{T}_{b,i}$ = -4.9 ºC

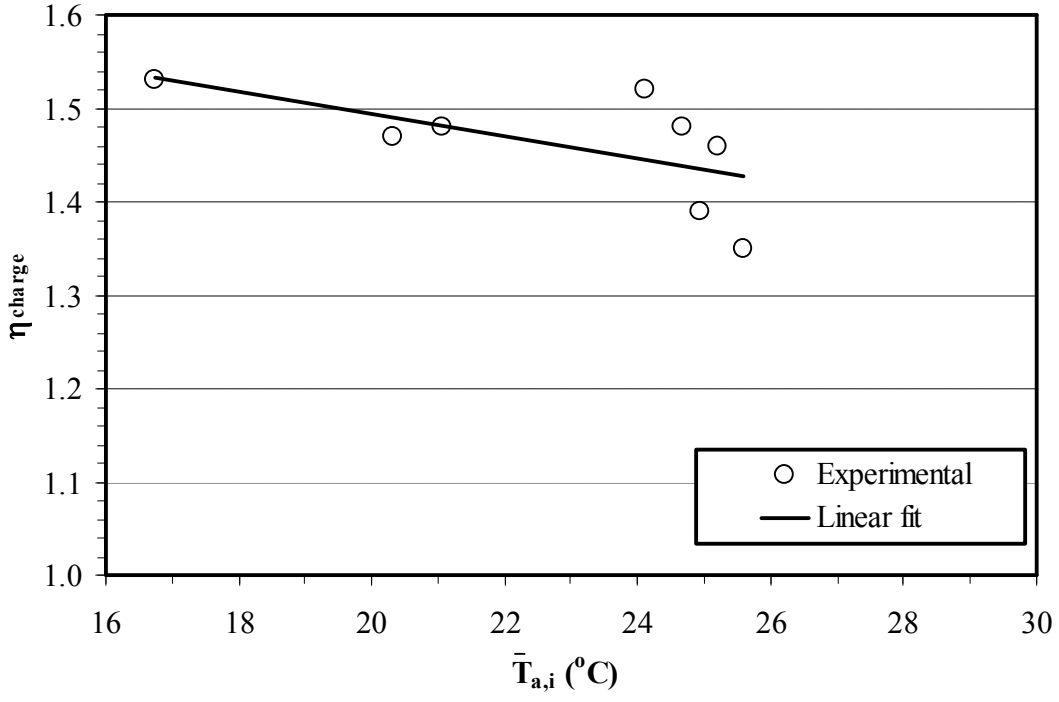


Figure 4.38. Variation of charging performance with air inlet temperature for $\bar{T}_{b,i}$ = -5.2 ºC and -5.3 ºC

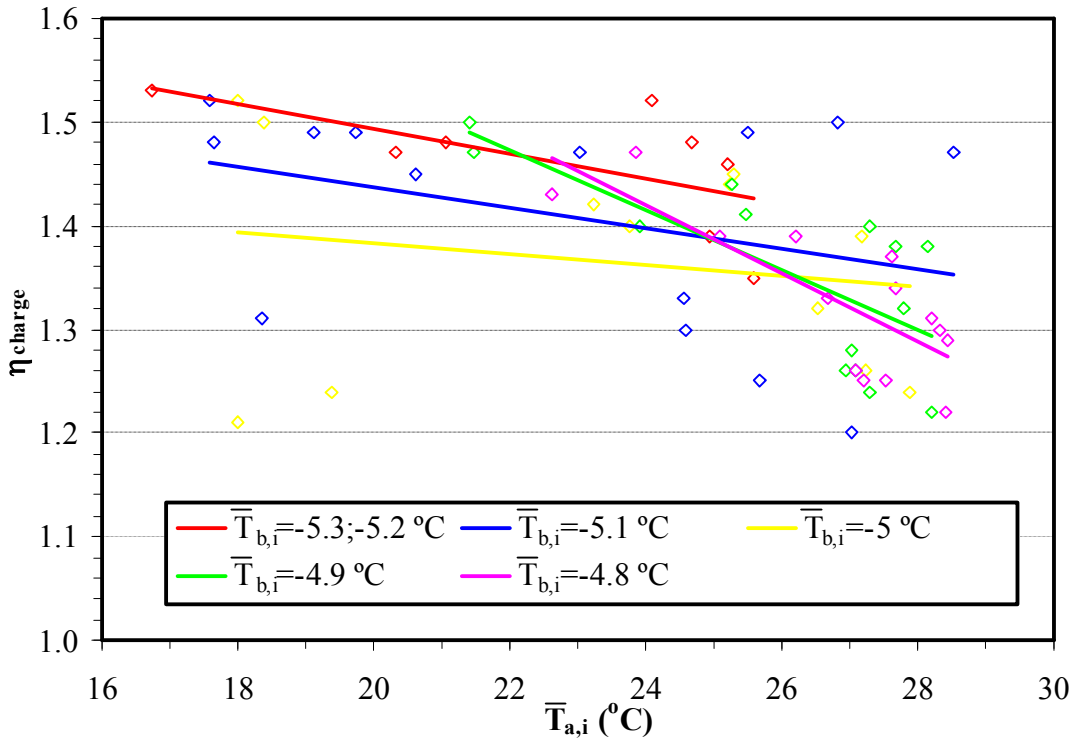


Figure 4.39. Variation of charging performance with air inlet temperature for all brine inlet temperatures

4.1.6. Charging Period

In this part of the study, effect of charging period on charging performance was investigated. A series of experiments were carried out with different charging periods between 1h 43′ and 8 h (Table 4.1). In these experiments, the flow rate of brine was adjusted to 0.78 kg/s, average air temperature at the inlet of the condenser was 27 °C and brine temperature was set to -8 °C. Some parameters of these 18 experiments are shown in Table 4.4.

Table 4.4. Conditions of experiments for effect of charging period

Test ID	Charging period	Initial water temperature inside the tank, $T_{w,i}$ [°C]
3006T1	1 h 43′	6.9
2906T1	1 h 45′	7.0
1706T1	1 h 49′	6.1
3006T2	2 h 9′	6.8
3006T3	2 h 18′	6.6
2906T2	2 h 20′	6.3
1906T2	2 h 34′	5.5
1606T1	2 h 39′	6.9
1606T2	3 h 15′	4.3
1506T0	3 h 52′	5.6
1906T1	4 h	9.6
2206T1	4 h 8′	6.5
2106T1	4 h 37′	8.2
2106T2	5 h 34′	8.3
1706T2	5 h 54′	6.3
2206T2	6 h 10′	7.1
250506	7 h	7.0
19070G	8 h	7.0

Similar to the other charging experiments, actual instantaneous temperature of the brine at the inlet of the tank is different from the set temperature. Although brine inlet temperature was set to -8 °C, average brine inlet temperature was

measured between -3.6 °C and -4.9 °C in all the experiments in this group. The amount of the energy stored and charging performance are shown in Table 4.5.

The amount of sensible energy stored varied between 16173 kJ and 36175 kJ in the experiments because of the differences in the initial water temperature in the tank. The amount of ice formed (the latent energy stored) and the total energy stored increase with the increase of charging period. While the amount of ice generated in the experiment with 1h 43′ charging period (3006T1) was only 50 kg, it rose to 430 kg in the experiment with 8 h charging period (19070G). Consequently, the total amount of energy stored increased from 42585 kJ to 170173 kJ (Table 4.5).

Table 4.5. Effect of charging period on amount of energy stored and charging performance

Test ID	Amount of ice [kg]	Latent energy stored [kJ]	Sensible energy stored [kJ]	Total energy stored [kJ]	Energy consumption [kJ]	Charging performance
3006T1	50	16747.2	25837.9	42585.1	28440	1.51
2906T1	50	16747.2	26251.3	42998.5	29520	1.45
1706T1	75	25120.8	22943.4	48064.2	29520	1.63
3006T2	90	30145.0	25476.1	55621.1	36000	1.54
3006T3	92	30814.8	24752.5	55567.3	39240	1.42
2906T2	95	31819.7	23718.7	55538.4	37440	1.48
1906T2	123	41198.1	20721.0	61919.1	42480	1.46
1606T1	125	41868.0	25992.9	67860.9	42120	1.62
1606T2	182	60959.8	16172.7	77132.5	52200	1.48
1506T0	220	73687.7	21134.5	94822.2	62640	1.51
1906T1	180	60289.9	36175.0	96464.9	69120	1.39
2206T1	215	72013.0	24339.0	96352.0	71640	1.34
2106T1	232	77707.0	31006.5	108713.5	77400	1.41
2106T2	295	98808.5	31058.1	129866.6	96120	1.39
1706T2	330	110531.0	23822.0	134353.0	97560	1.38
2206T2	335	112206.2	27078.0	139284.2	103320	1.38
250506	405	135652.3	26303.1	161955.4	117360	1.38
19070G	430	144025.9	26148.0	170173.9	136080	1.25

When the sensible, latent and total amount of energies stored for all the experiments in this group are analyzed (Figure 4.40), it can be seen that the amount of the latent and total energy stored increase proportionally with the charging period. Figure 4.40 also shows that the amount of sensible energy is almost constant and the fluctuations seen are thought to have been rooted from the differences in the water temperatures at the beginning of the experiments.

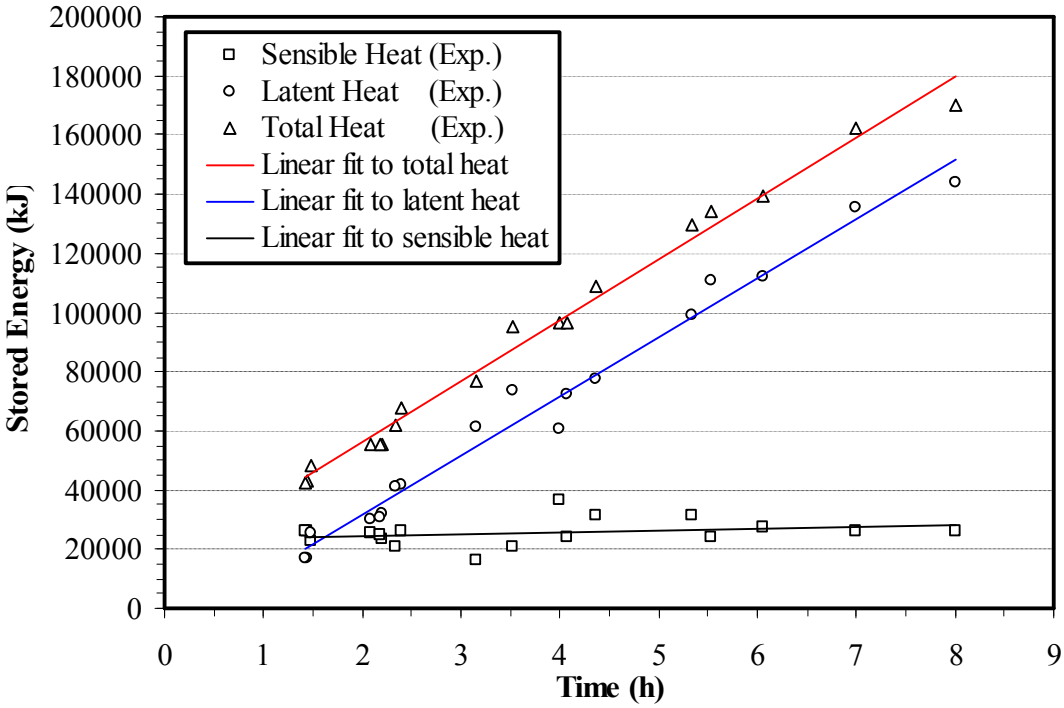


Figure 4.40. Variations of the energy stored with charging period for 18 charging experiments

When the volume of the water in the tank (900 l) is taken into consideration, it is seen that sensible portion of the stored energy becomes more important for the experiments with a charging period shorter than 3 hours. Least square error fits are also included in the figure.

Figure 4.41 shows variation of charging performance with charging period. Whilst the charging performance of the system varies between 1.50 and 1.60 for the experiments with a charging period between 1.5 and 2 hours, the performance decreases approximately 20 percent and falls down to 1.25 for the experiment with a

charging time of 8 hours. Since the thickness of the ice formed on the pipe increases when the charging period is lengthened, an additional resistance appears to the heat transfer between the brine and the water in the tank. The figure expressly shows the negative effect of the resistance increasing with ice thickness on the system performance.

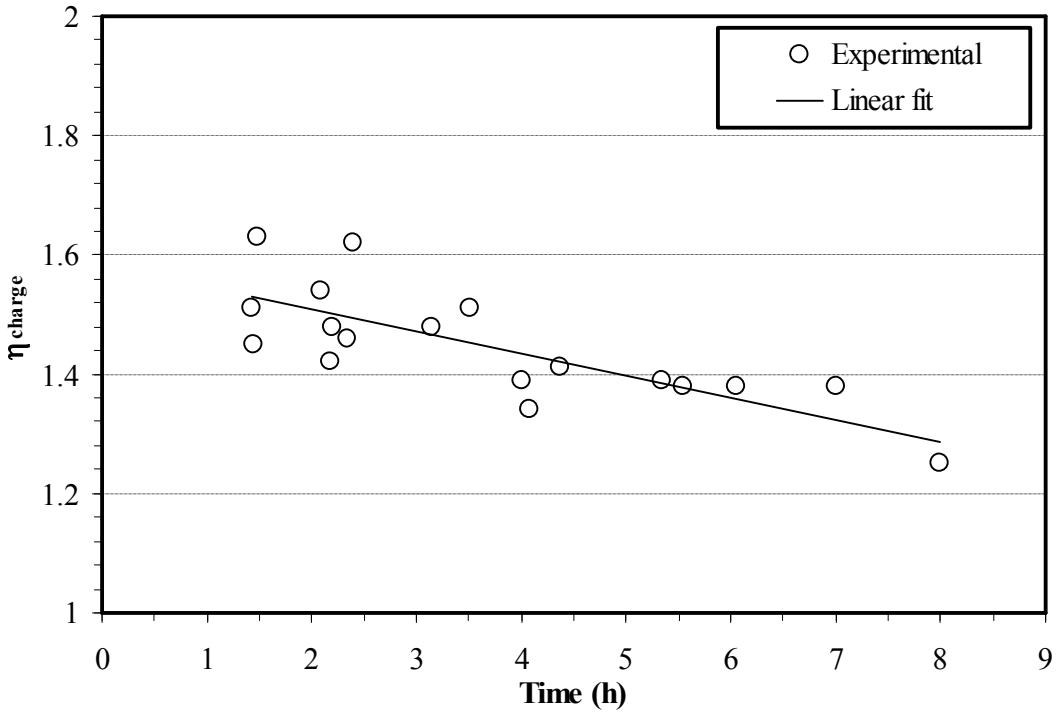


Figure 4.41. Variations of charging performance with charging period for 18 charging experiments

4.1.7. Discharging Tests

The test plan was structured to test capabilities of the storage tank under two automatic control operating strategies (fan control and valve control) for discharge experiments. 35 charging and discharging experiments were carried out between 6th July 2006 and 10th October 2006. All charging experiments were realized for a period of 8 hours and the ice formed during charging (night time) was used for performing the cooling during daytime (discharging). In the discharging experiments, cooling process was continued even after the ice was completely melted, in order to benefit from the sensible heat of the water stored in the tank. As Table 4.6 displays, valve control was used in 15 of the experiments and fan control was used for the remaining 20 experiments. Room thermostat was adjusted to a temperature varying between 23 ºC and 25 ºC in the experiments. The temperature of the water delivered to the room cooled was set to 7 °C using a three-way mixing valve in all experiments. This is the typical value for fan-coil applications.

In ice-storage systems, the thermal energy needed for cooling a space during discharging process is obtained by melting the ice and by benefiting from the sensible heat of the water in the tank. In this case, the cold water remaining in the tank after the ice is fully melted can be still used for cooling for a period until the water temperature reaches to a certain value. In this study, as the temperature of the water delivered to the room was set to 7 °C, discharging process was stopped when the temperature of the water in the tank reached to 7 °C.

The instantaneous cooling energy recovered from the tank during discharging which is approximately equal to the energy extracted from the room, was computed from the brine side using brine mass flow rate ($\dot{m}$) and temperature difference between the inlet and the exit of the ice storage tank. Cooling energy recovered (Q_d) from the tank during discharging can be expressed:

$$\mathbf{Q}_d = \int_{t=0}^{t=t_f} \dot{\mathbf{m}}_b \times \mathbf{C}_b \times \left[\mathbf{T}_{ex}(t) - \mathbf{T}_{in}(t)\right] dt \qquad (4.4)$$

where, $\dot{m}_b$ is flow rate of brine, C_b is specific heat of brine, T_{in} (t) and T_{ex} (t) are temperature of brine at inlet and exit of the tank, respectively.

Table 4.6. Conditions of discharge experiments

Test ID	Automatic control	$T_{room,set}$ [^oC]	$T_{valve,set}$ [^oC]	Total energy stored, Q_s [kJ]	Energy recovered from tank, Q_d [kJ]	$\eta_{discharge}$
060706	Fan	23.0	7.0	141084	116100	0.82
080706	Fan	21.0	7.0	136080	105012	0.77
090706	Fan	23.0	7.0	150084	123156	0.82
120706	Fan	23.0	7.0	159912	132552	0.83
130706	Fan	25.0	7.0	162720	130788	0.80
190706	Fan	25.0	7.0	136224	112140	0.82
200706	Fan	25.0	7.4	158652	135324	0.85
210706	Fan	25.0	7.4	157824	128556	0.81
220706	Fan	25.0	7.4	159372	130608	0.82
250706	Fan	25.0	7.4	158760	129816	0.82
110806	Fan	25.0	7.5	154656	129672	0.84
150806	Fan	25.0	7.4	156168	129456	0.83
160806	Fan	25.0	7.4	156816	127044	0.81
170806	Fan	25.0	7.4	156204	127404	0.82
180806	Fan	25.0	7.4	155880	126828	0.81
190806	Fan	25.0	7.4	155232	126828	0.82
220806	Fan	25.0	7.2	152028	148860	0.98
260806	Fan	25.0	7.2	153576	142632	0.93
270806	Fan	25.0	7.4	158760	129888	0.82
120906	Fan	26.0	7.9	141732	127332	0.90
290806	Valve	26.0	7.6	149184	-	-
300806	Valve	26.0	8.0	159768	-	-
030906	Valve	26.0	7.8	166644	-	-
040906	Valve	26.0	7.8	162108	-	-
060906	Valve	26.0	7.8	170964	-	-
150906	Valve	26.0	7.8	153504	-	-
160906	Valve	26.0	7.8	157824	-	-
180906	Valve	25.5	7.8	152748	-	-
190906	Valve	25.5	7.8	152172	-	-
280906	Valve	24.5	7.8	140760	-	-
031006	Valve	22.0	7.8	137988	-	-
041006	Valve	24.5	7.8	145620	-	-
051006	Valve	22.5	7.	144972	-	-
061006	Valve	23.0	7.2	150084	-	-
101006	Valve	23.0	7.2	147816	-	-

Discharging performance of the system ($\eta_{discharge}$) can be expressed (Dincer, 2002) as:

$$\eta_{discharge} = \frac{Q_{s,w}}{Q_d} \tag{4.5}$$

where, $Q_{s,w}$ is amount of total cold energy stored in the tank (Eq. 4.3).

Of the 35 discharge experiments, 20 experiments were carried out with fan control and 15 with valve control. As an example to results of the fan-controlled experiments, various parameters of Experiment 120706 are given in Figures 4.42-4.46.

When the temperature of the water inside the tank is considered (Figure 4.42), stratification is evident at the beginning of the discharge experiment. Warmer water is collected at the lower region of the tank, while cold water is at the top. As the discharge process proceeds, temperature increases rapidly at the bottom, whilst it does not change for a long period of time because of existence of ice at the middle and top parts of the tank.

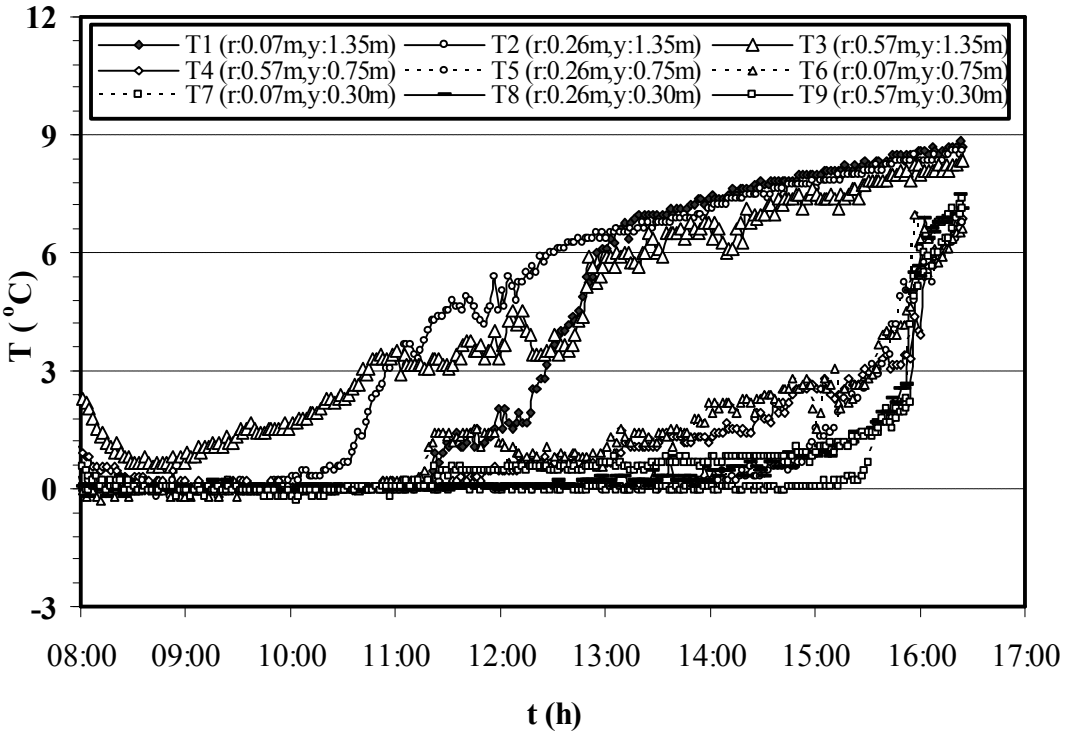


Figure 4.42. Variation of water temperature with time in the storage tank (Experiment 120706)

The delivery temperature for the brine pumped to the room was adjusted to be 7 °C in this experiment. Figure 4.43 displays that the three-way valve was successful to deliver the fluid to the room at the adjusted temperature until 15:40. After this point, the temperature of the brine was started to increase, because the ice in the tank completely melted, and the sensible heat of the water was begun to be used instead of the latent heat of the ice. A temperature difference of approximately 4 °C is attained between the supply and return temperatures of the brine during major part of the experiment. The return temperature was steady at a temperature of approximately 11°C.

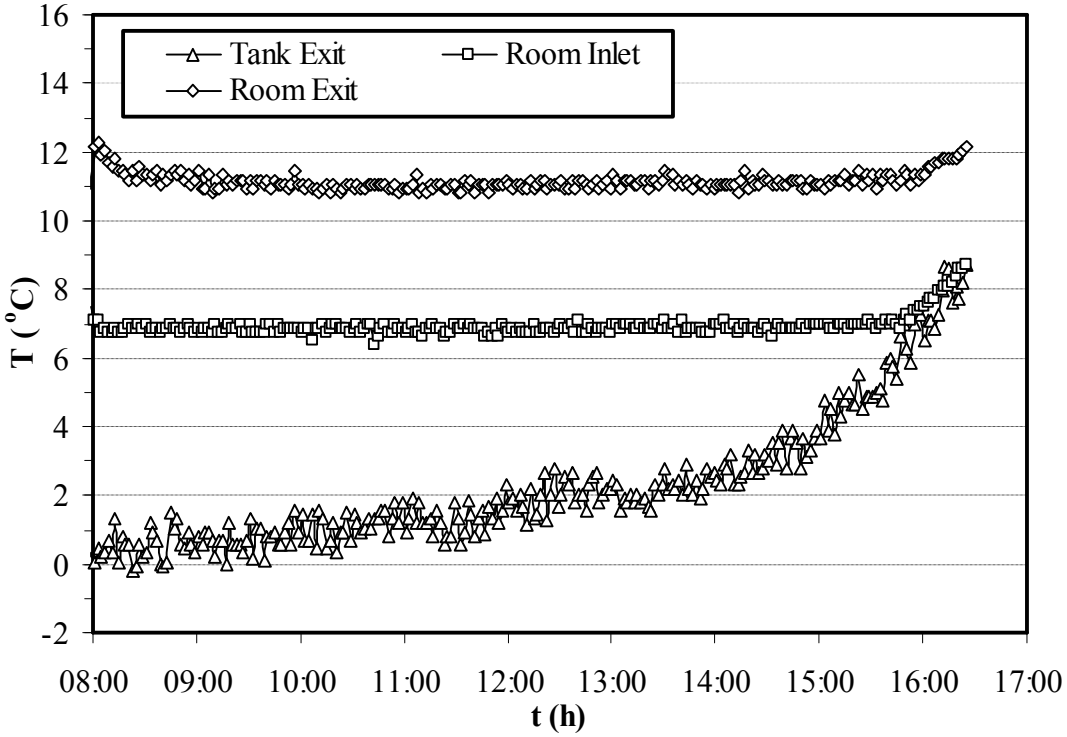


Figure 4.43. Variation of brine temperature with time at different measurement points (Experiment 120706)

Temperatures of the room cooled and ambient are shown in Figure 4.44. Ambient temperature increased steadily during the first part of the day, reaching to a maximum around 14:00. It then starts decreasing after 15:00. It is seen from the figure that the cooling system was able to lower the room temperature down to set value in the first hour of experiment and keep it at that level rest of the day until 16:30. Average ambient and the room temperature was 31.7 °C and 23.8 °C, respectively. Since the

cooling load of the room was high in this experiment, the load control system did not stop the fans of the fan coils located inside the room. The fans ran continuously during the experiment.

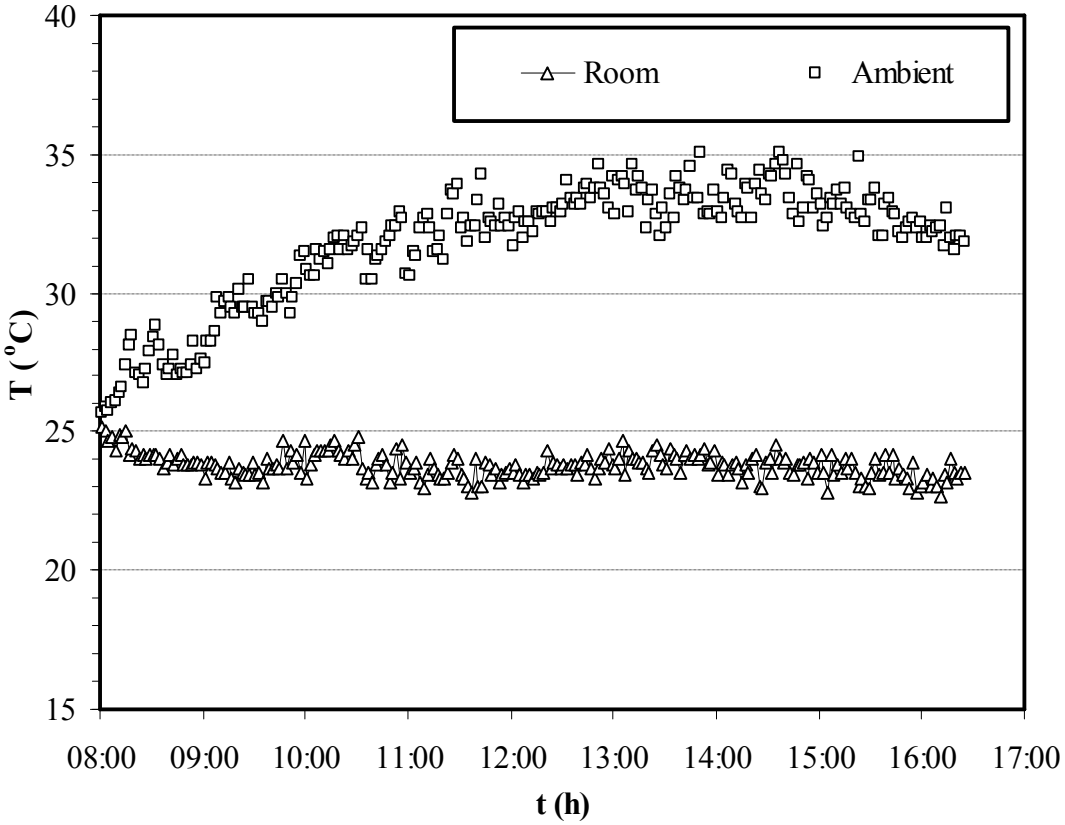


Figure 4.44. Variation of air temperature with time for room and ambient (Experiment 120706)

Figure 4.45 shows the variation of relative humidity of the room and ambient during the day. Relative humidity of the ambient was around 80% early in the morning and it decreased almost linearly until 13:00 and stayed constant later. Although relative humidity of the room increased slightly, it remained at an acceptable level of 50%.

The room conditions during the day are shown on a psychometric chart in Figure 4.46. The thermal comfort zone specified by the ASHRAE was also shown in the figure for comparison (ASHRAE Fundamentals, 2001). As can be seen from the figure, the room conditions were always inside ASHRAE comfort zone.

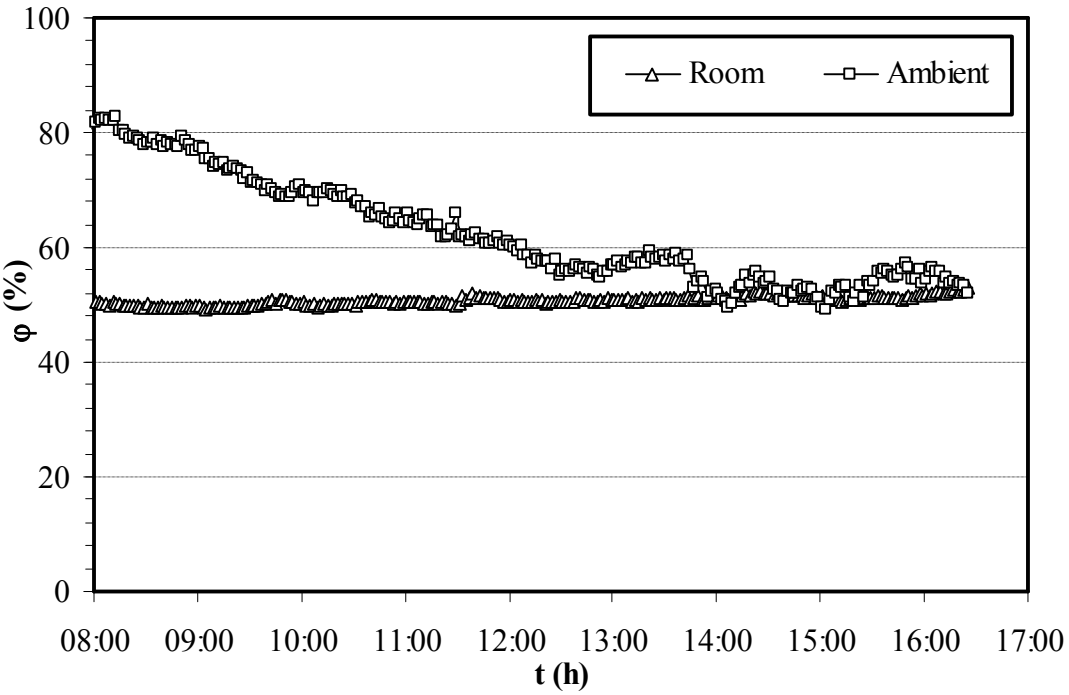


Figure 4.45. Variation of relative humidity with time for room and ambient (Experiment 120706)

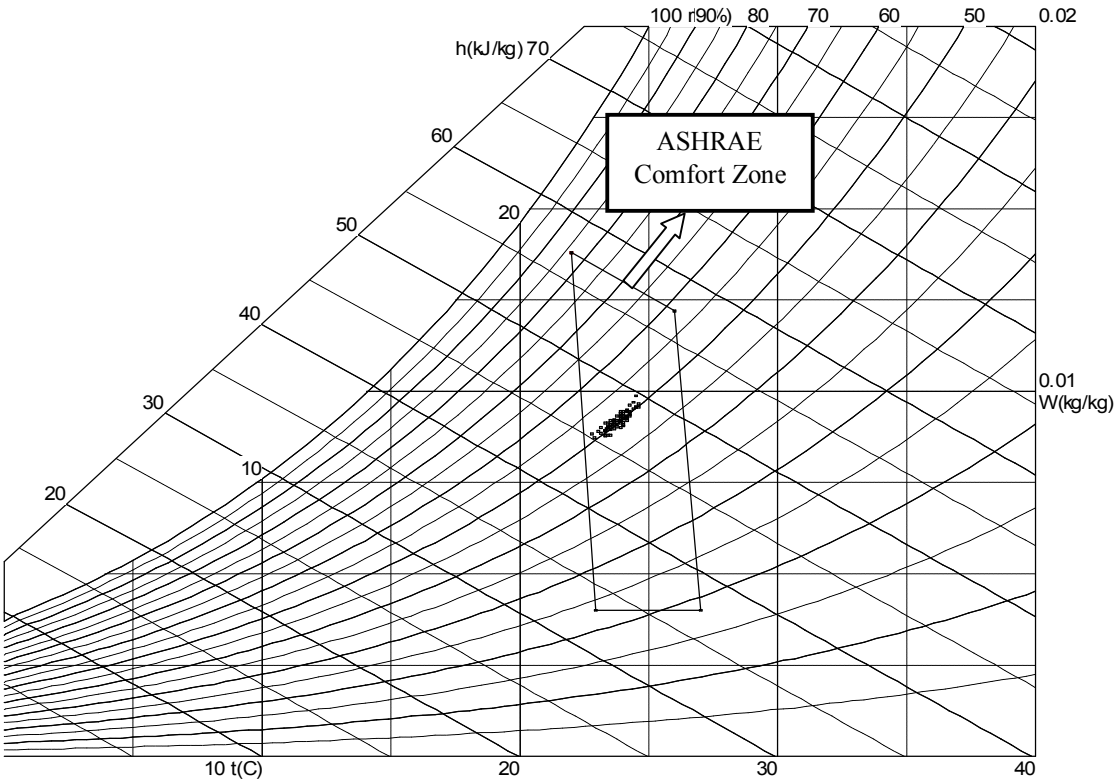


Figure 4.46. Comparison of air conditions obtained during experiment with ASHRAE comfort zone (Experiment 120706)

As a second example to the fan-controlled experiments performed, results of experiment 090706 are shown in Figures 4.47 - 4.50.

Temperature distribution of the water inside the tank (Figure 4.47) expresses a pattern similar to that for Experiment 120706 (Figure 4.42). Compared with experiment 120706, the same temperature stratifications are seen during discharging period.

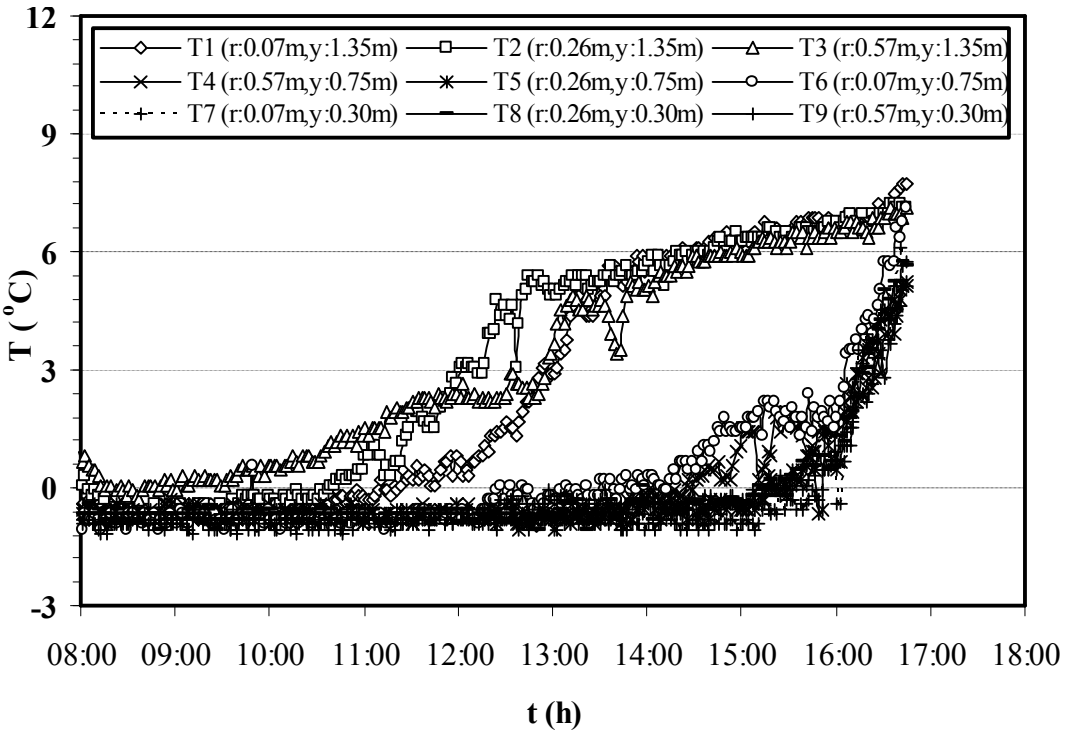


Figure 4.47. Variation of water temperature with time (Experiment 090706)

However, fluctuations in the temperature of the brine at the exit of the ice storage tank, and at the inlet and exit of the room were observed, during this experiment (Figure 4.48). The fluctuations are due to the operating strategy of the load control mechanism. When the room temperature reaches to the value set at the room thermostat (23 °C), the fans stops automatically and starts working later when the temperature exceeds the set value.

The brine leaves the room at around 9 °C when the fans are running. However, when the fans are at off position, heat removal from the room air is

reduced significantly because the heat transfer mechanism prevailing outside of the fan-coils is natural convection only. Therefore, brine temperature reduces down to 6.5 °C in these cases. Similar to the Experiment 120706, cooling is finished when the brine temperature is higher than 7 °C.

The fluctuations evident in the brine temperature leaving the room cause similar fluctuations in the tank exit and supply temperatures. However, amplitude of the fluctuations is damped significantly, especially at the tank exit (Figure 4.48).

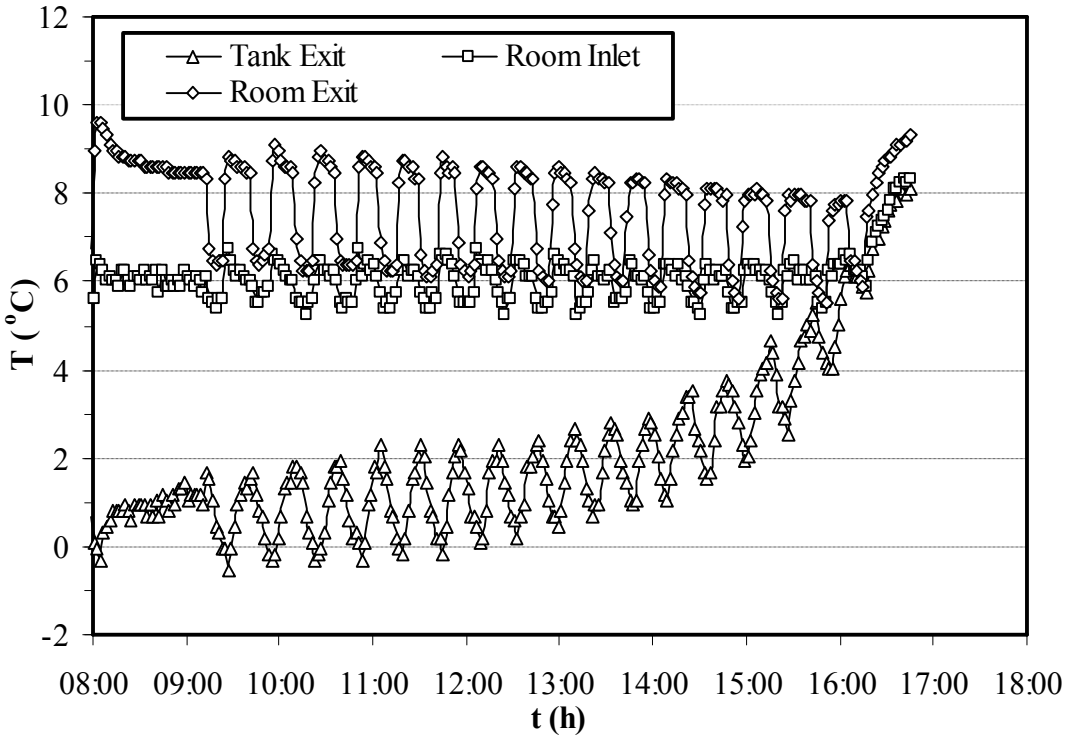


Figure 4.48. Variation of brine temperature with time at different measurement points (Experiment 090706)

Temperatures of the room and ambient are illustrated in Figure 4.49. Average ambient temperature was 30.2 ºC and room temperature decreased down to set value in the first hour of the experiment. It can be seen from the figure that the fans stops automatically when the room temperature reaches to the value set at the room thermostat (23 °C) and when the temperature exceeds the set value, they start working.

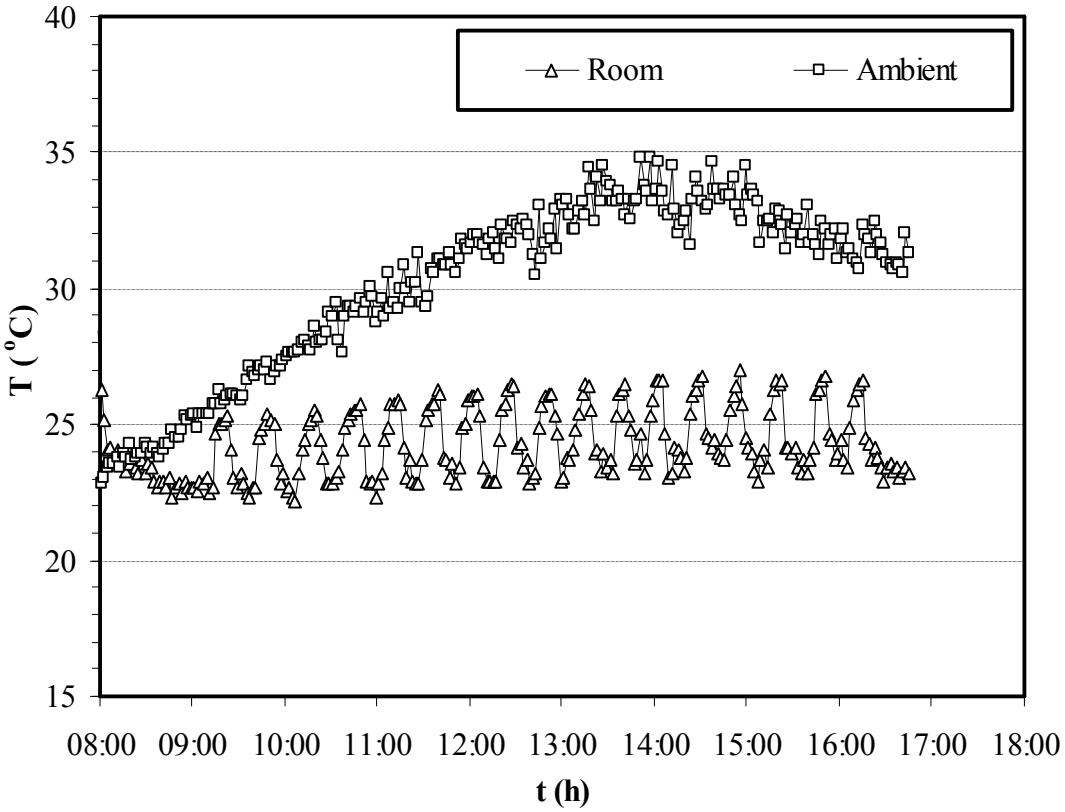


Figure 4.49. Variation of air temperature with time for room and ambient (Experiment 090706)

Figure 4.50 shows the variation of relative humidity of the room and ambient during the day. Relative humidity of the ambient was around 80% until 10:00 and it decreased almost linearly until 14:00. Although the room relative humidity exhibited fluctuations due to changes in the room dry bulb temperature (on-off operation of the fan), it was around 48% during the day.

The thermal environments (temperature and relative humidity) measured in the air-conditioned room were plotted on a psychometric chart together with ASHRAE comfort zone in Figure 4.51. Almost all the points were located inside the comfort zone. This shows that the automatic control system designed fulfills its requirements properly.

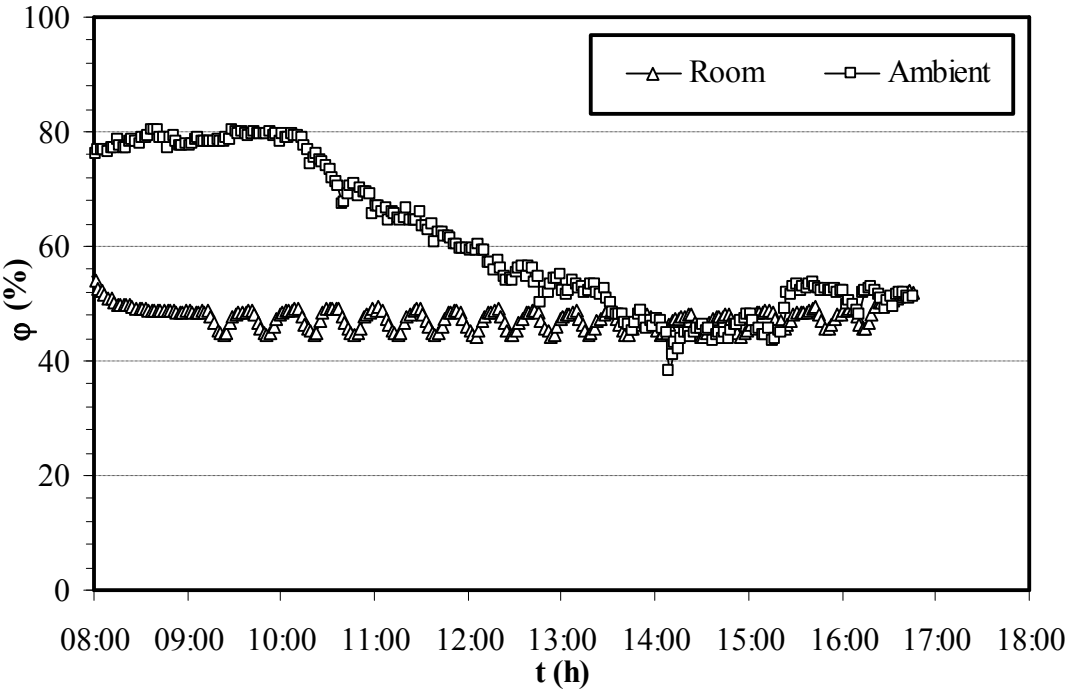


Figure 4.50. Variation of relative humidity with time for room and ambient (Experiment 090706)

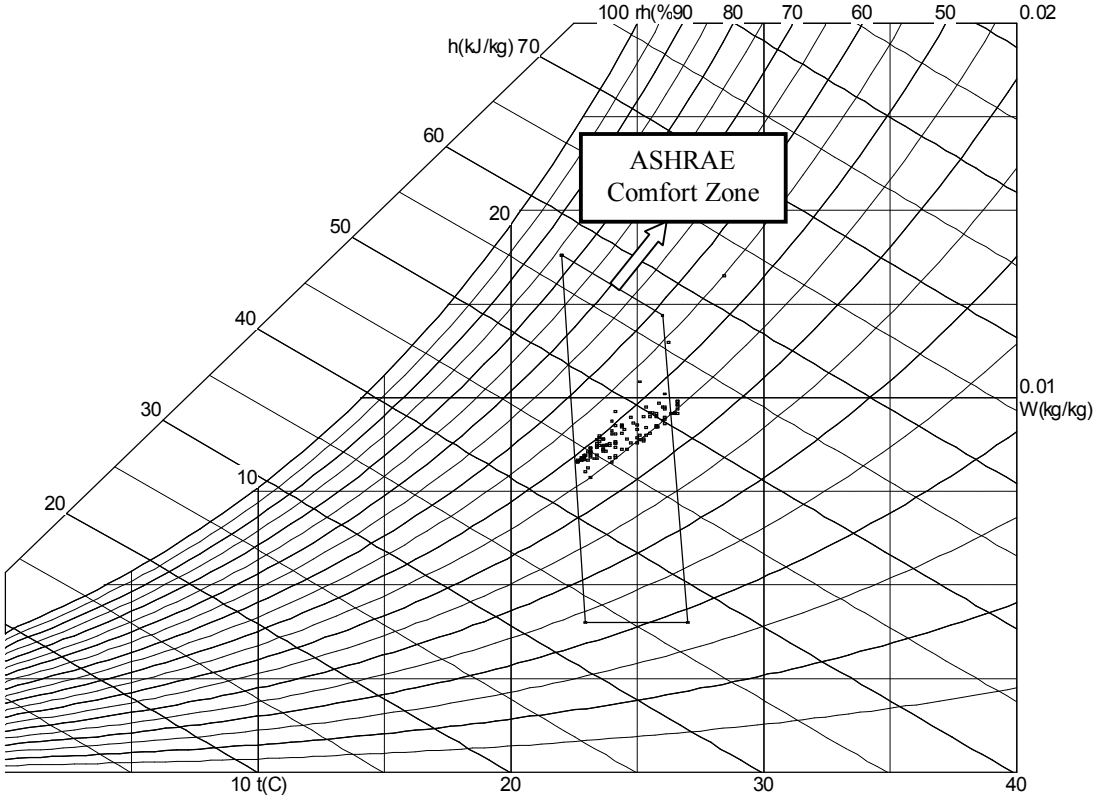


Figure 4.51. Comparison of air conditions obtained during experiment with ASHRAE comfort zone (Experiment 090706)

Figure 4.52 shows cumulative variation of the energy extracted from the room for two fan-controlled experiments (120706 and 090706). The cumulative energy during discharging period (Q_d) was also calculated from the brine side using Eq. 4.4.

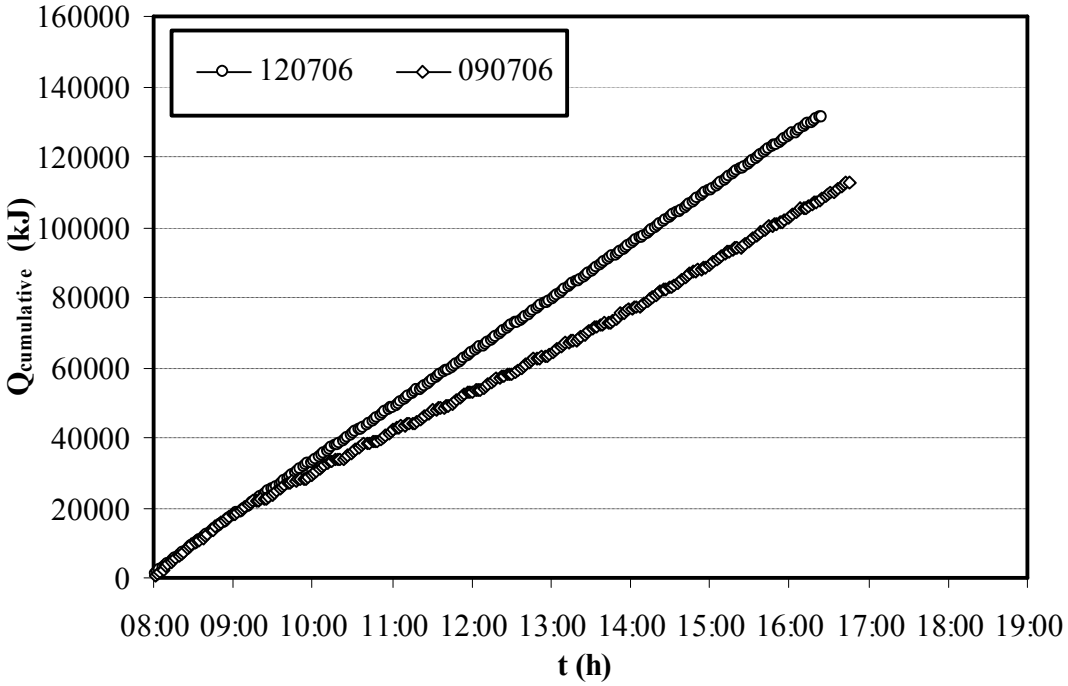


Figure 4.52. Variation with time of cumulative energy extracted from room for two fan-controlled experiments

The fans run continuously in Experiment 120706, since the room set temperature is not attained due to high room cooling load. In the second experiment (090706) the fans run intermittently, since the set value was achieved. In these experiments carried out with the same control strategy (fan control), the total discharging period was approximately equal. However, the rate of energy extraction is slower in Experiment 090706 (lower room cooling load) than in Experiment 120706. Although the amount of cooling energy stored at the beginning of discharging period for Experiment 090706 (150084 kJ) is lower than that for Experiment 120706 (159912 kJ), it was possible to cool the room until 16:30 h in both cases.

Figures 4.53-4.56 show the results of Experiment 030906, which is a typical example to the valve control experiments.

When the temperature of the water inside the tank is considered (Figure 4.53), stratification is evident at the beginning of the discharge experiment. Warmer water is collected at the lower region of the tank, while cold water is at the top. As the discharge process proceeds, temperature increases rapidly at the bottom, whilst it does not change for a long period of time at the mid and top parts of the tank because of existence of ice.

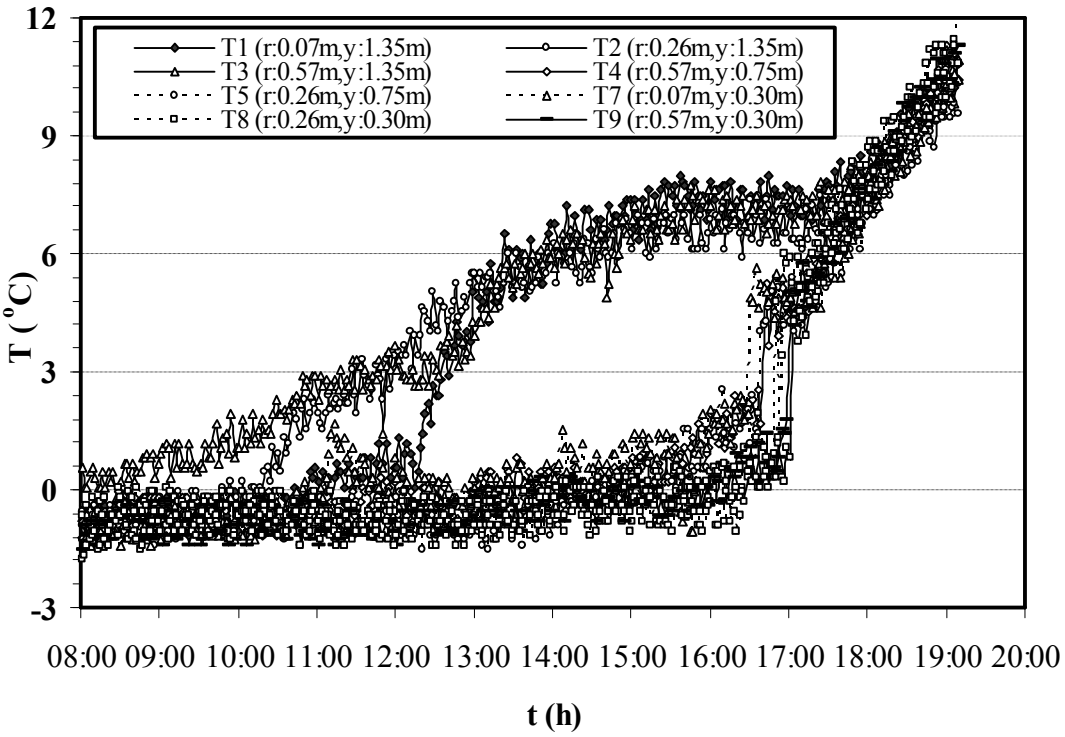


Figure 4.53. Variation of water temperature with time in the storage tank (Experiment 030906)

It is seen from Figure 4.54 that, the delivery temperature (7 °C) for the brine pumped to the room achieved during the day until 17:00 h. An almost constant temperature difference of about 5 ºC is observed between the supply and return brine temperatures.

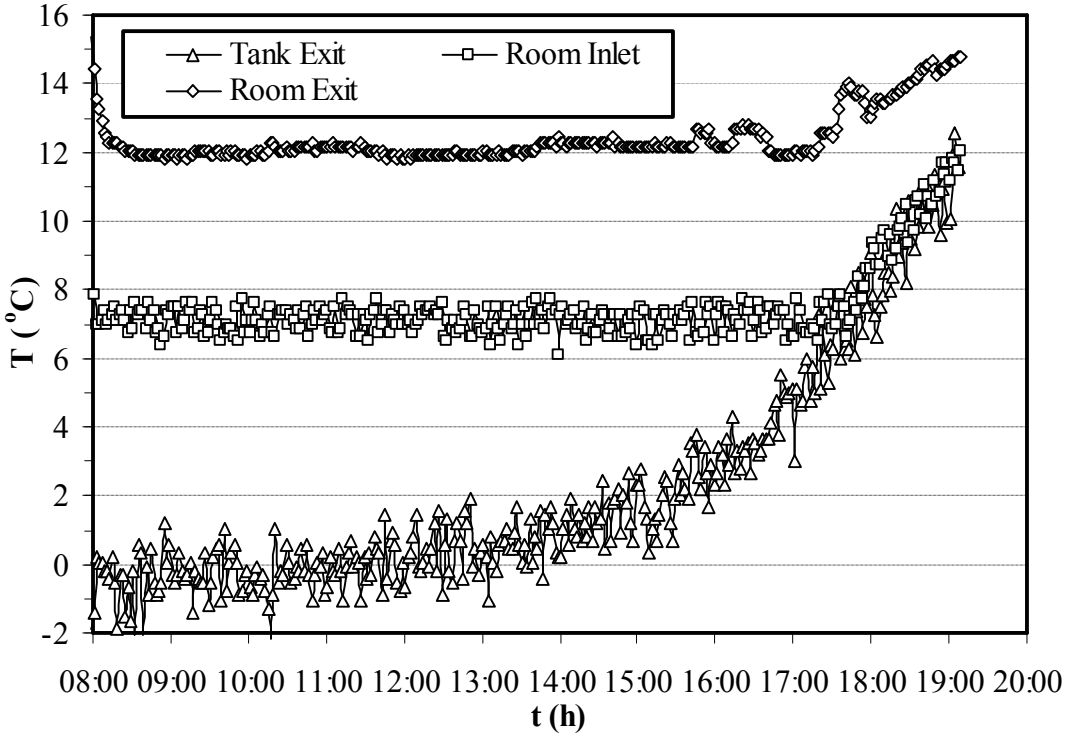


Figure 4.54. Variation of brine temperature with time at different measurement points (Experiment 030906)

Temperatures of the room cooled and ambient are shown in Figure 4.55. It is seen from the figure that the room temperature is approximately equal to the set value (25 ºC) during the experiment. Average ambient and the room temperature are 29.34 ºC and 25.2 ºC, respectively.

Figure 4.56 shows the variation of relative humidity of the room and ambient temperature during the day. Although relative humidity of the room increased slightly, it remained at an acceptable level of 50%.

The room conditions during the day are shown on a psychometric chart in Figure 4.57. As can be seen from the figure, the room conditions were always inside ASHRAE comfort zone.

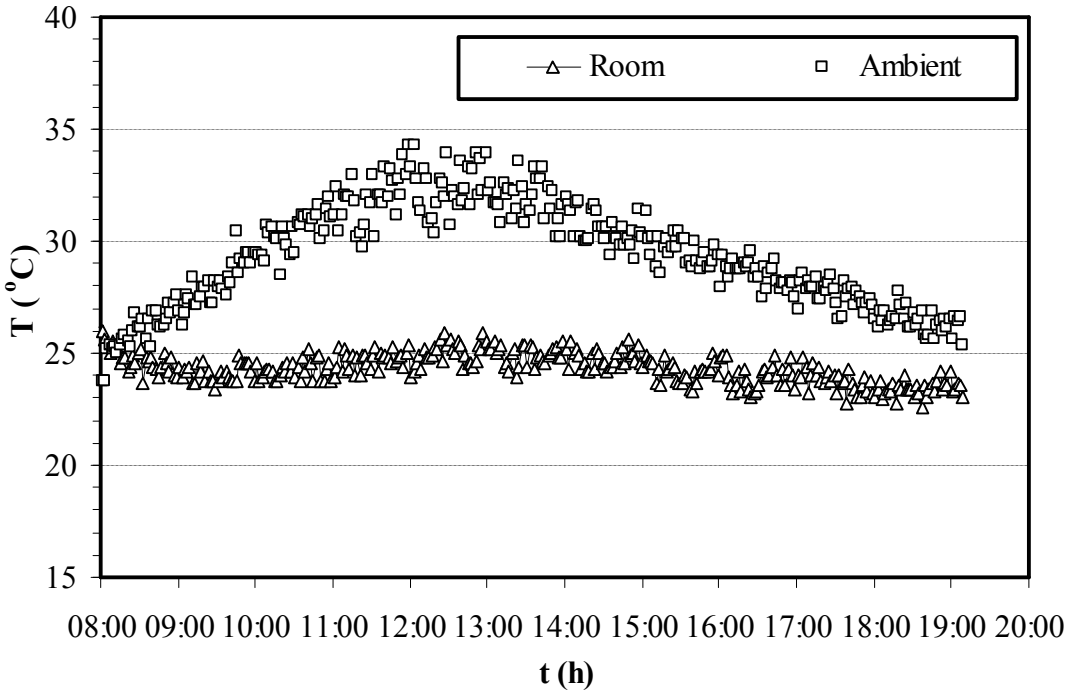


Figure 4.55. Variation of air temperature with time for room and ambient (Experiment 030906)

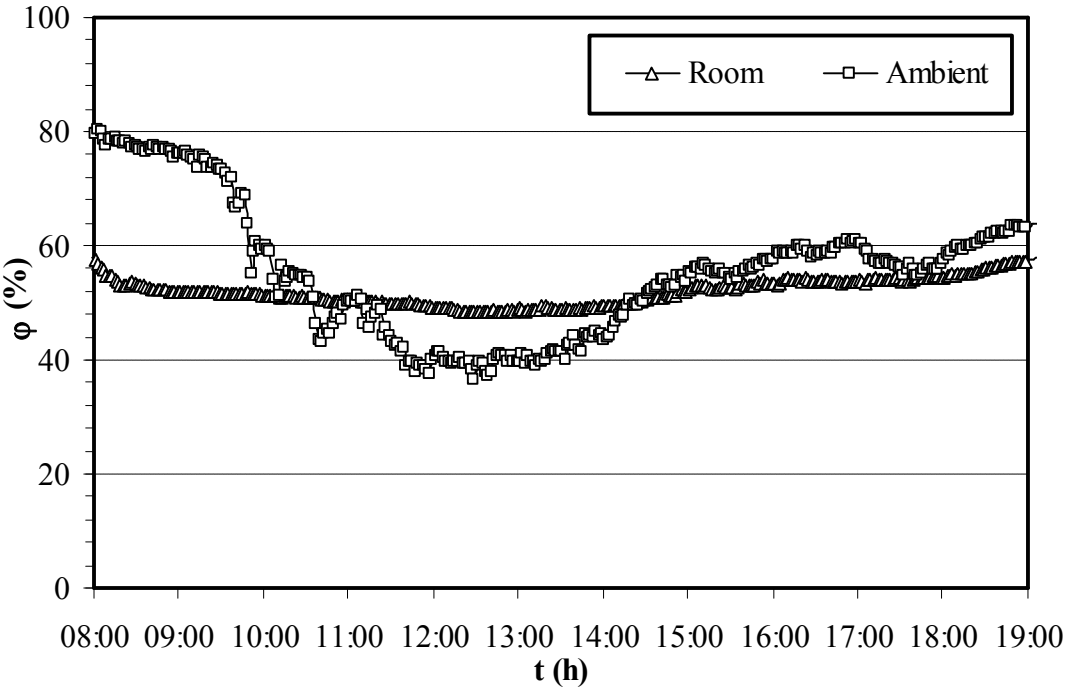


Figure 4.56. Variation of relative humidity with time for room and ambient (Experiment 030906)

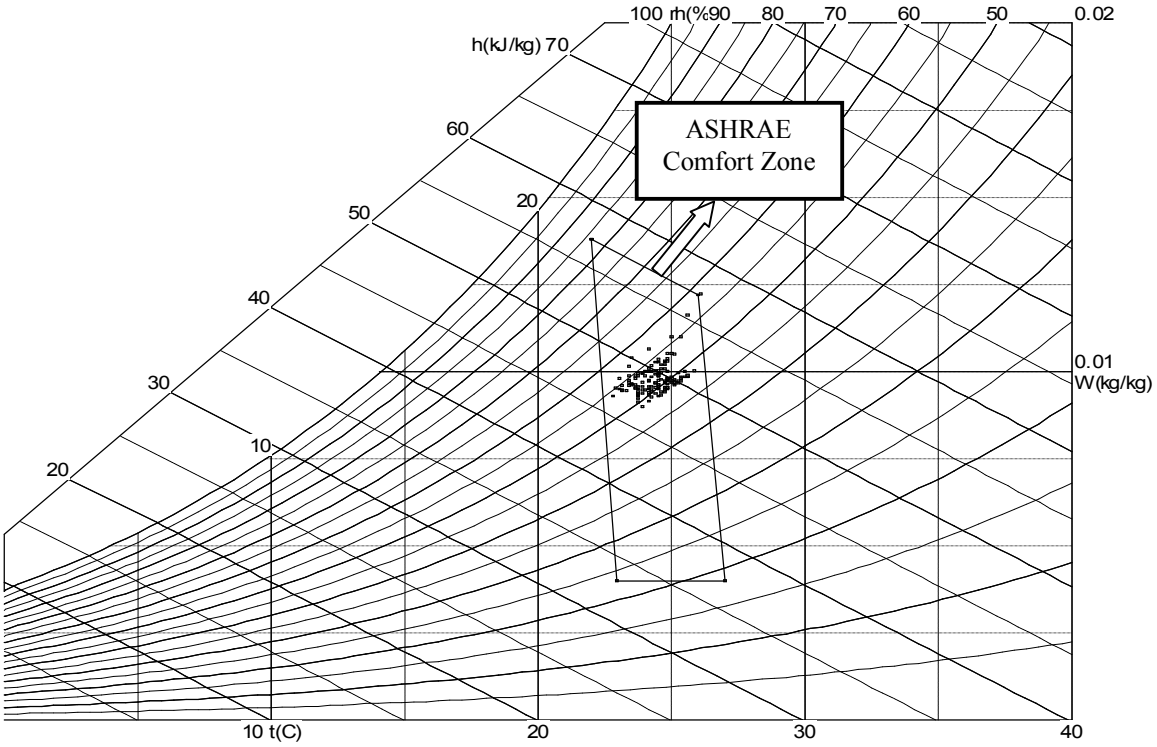


Figure 4.57. Comparison of air conditions obtained during experiment with ASHRAE comfort zone (Experiment 030906)

4.2. Results Obtained From Experimental Setup 2

Details of the Experimental Setup 2 are given in Chapter 3.4.2. In this study, phase change phenomena around a horizontal tube were investigated both experimentally and analytically. An experimental investigation was carried at three different brine inlet temperatures in order to study the dynamic behavior of ice layer formation on tube. A mathematical model was also written to calculate the heat transfer process for phase change phenomenon around a horizontal tube.

Experiments were carried out at a fixed transport medium flow rate of 900 l/h (corresponds to a Reynolds number of 5318 at the tube inlet) and three different inlet temperatures (-4.3 ºC, -4.9 ºC and -5.8 ºC). The temperature of the water inside the vessel was kept between 0 ºC and 1 ºC at the beginning of the experiments to minimize the natural convection effects.

Table 4.7. Conditions of phase change experiments

Experiment no	**Flow rate** [l/h]	**Average brine inlet temperature** [^{o}C]	**Average ambient air temperature** [^{o}C]	**Initial average water temperature for x/L=0.1** [^{o}C]	**Initial average water temperature for x/L=0.86** [^{o}C]
1	900	-4.3	23	0.39	0.19
2	900	-4.9	22	0.06	0.25
3	900	-5.8	23	0.66	0.27

Figure 4.58 shows time wise variations of the water temperatures at the measurement points inside the vessel for a brine inlet temperature of -5.8 ºC.

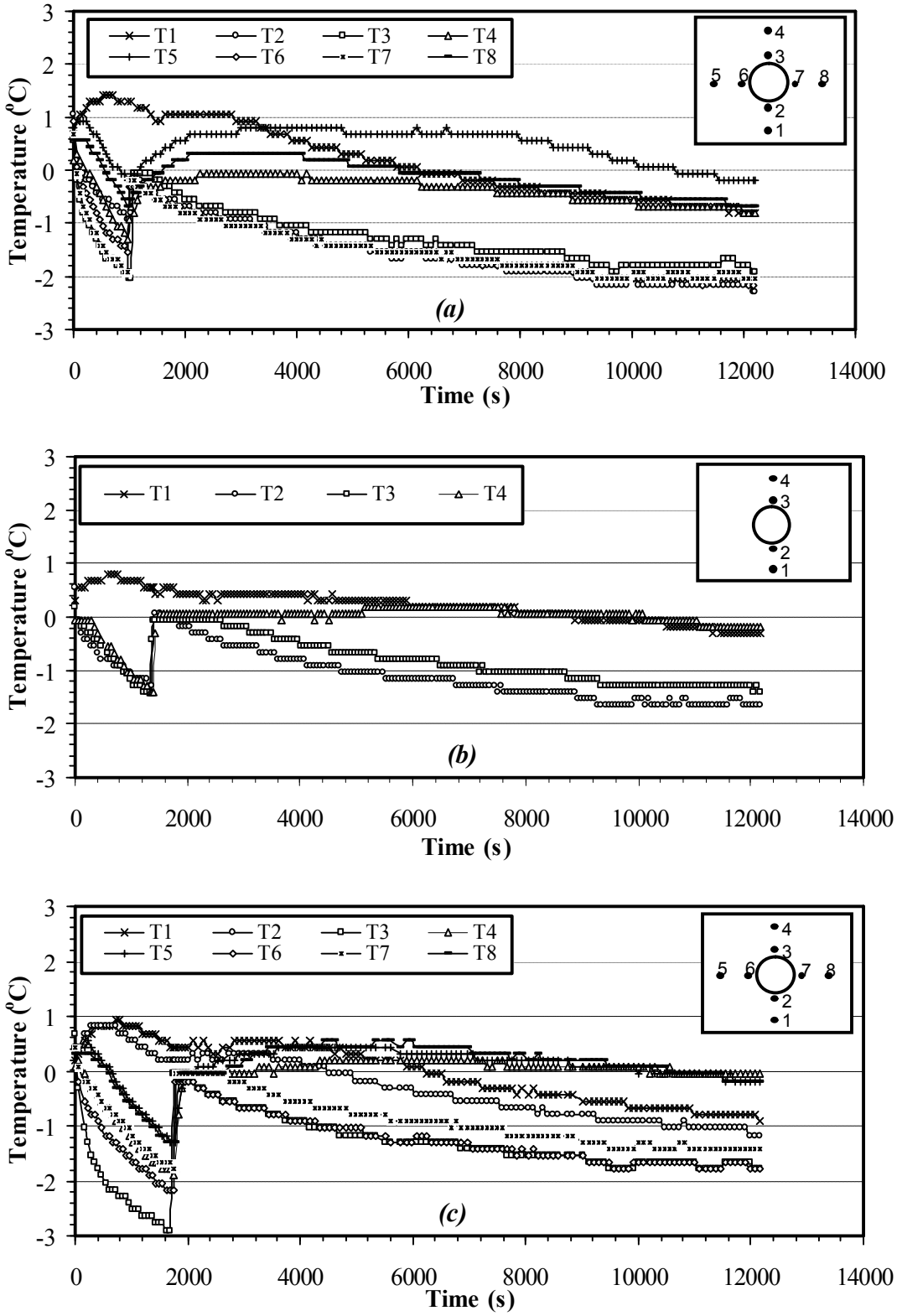


Figure 4.58. Variation of water temperature with time at three measurement stations for $\overline{T}_{b,i}$ = -5.8 ºC (***a:*** x/L = 0.1, ***b:*** x/L = 0.47, ***c:*** x/L = 0.86)

Sensible heat is extracted from the water inside the vessel and transferred to the transport medium. As a result, temperature of the water decreases steadily at all measurement points except at the bottom of the tube.

As can be seen from Figure 4.58, supercooling occurs at all measurement points except the bottom of the tube and the degree of it is between -1.4 ºC and -3 ºC. Once nucleation occurs, a very thin layer of dendritic ice formation starts at the outer surface of the tube in the entrance region (x/L=0.1), and propagates in the axial direction. When the dendritic ice first forms, the temperature rises rapidly to the freezing temperature as a result of the latent heat of fusion of water. Compared with the supercooling process, duration of this process is very short, lasting only 1 to 3 s, depending on the degree of supercooling and the position.

Dendritic ice formation is followed by latent heat thermal storage process, during which a relatively thick layer of ice starts to form around the tube outer surface. During this period, temperature remains at freezing point temperature (0 ºC) for a certain period of time. However, when the ice is formed, temperature of the ice begins to fall below 0 ºC, due to heat transfer from the water inside the vessel to brine (cooling of ice). Temperature decrease can be clearly observed when the measuring point (thermocouple) is covered by the ice (thermocouples 2, 3, 6 and 7 in Figure 4.58a).

The same processes can also be seen from Figure 4.59 that shows the variation of water temperature with time near the tube wall (thermocouple 3) at different axial positions. Since the thermocouple 3 is located very close to the tube, it is covered by the ice as soon as ice formation starts. Therefore, temperature stays constant at 0 ºC only for a very short period of time.

Variation of the time from the beginning of the experiment to the start of nucleation (nucleation time) along the pipe length is given in Figure 4.60 for $\overline{T}_{b,i}$ = -5.8 ºC. As can be seen from the figure, nucleation first starts at the entrance region, which is the coldest region, and propagates along the tube. Nucleation time increases almost linearly with the axial distance.

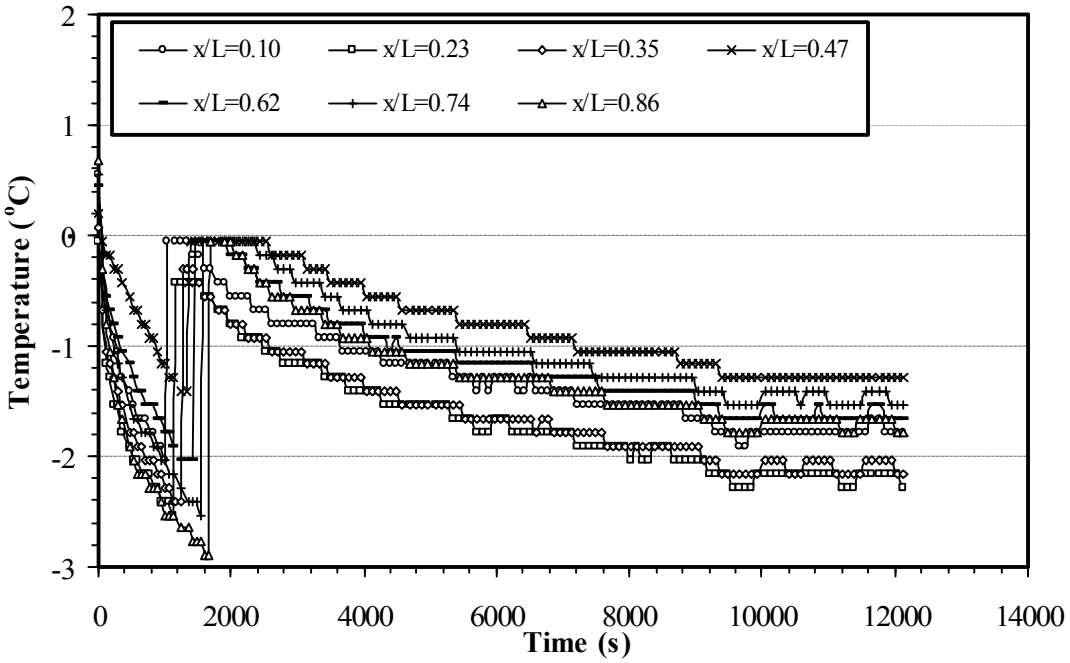


Figure 4.59. Variation of water temperature with time at positions just above the test tube (thermocouple 3) for different axial measurement stations ($\overline{T}_{b,i}$ = -5.8 ºC)

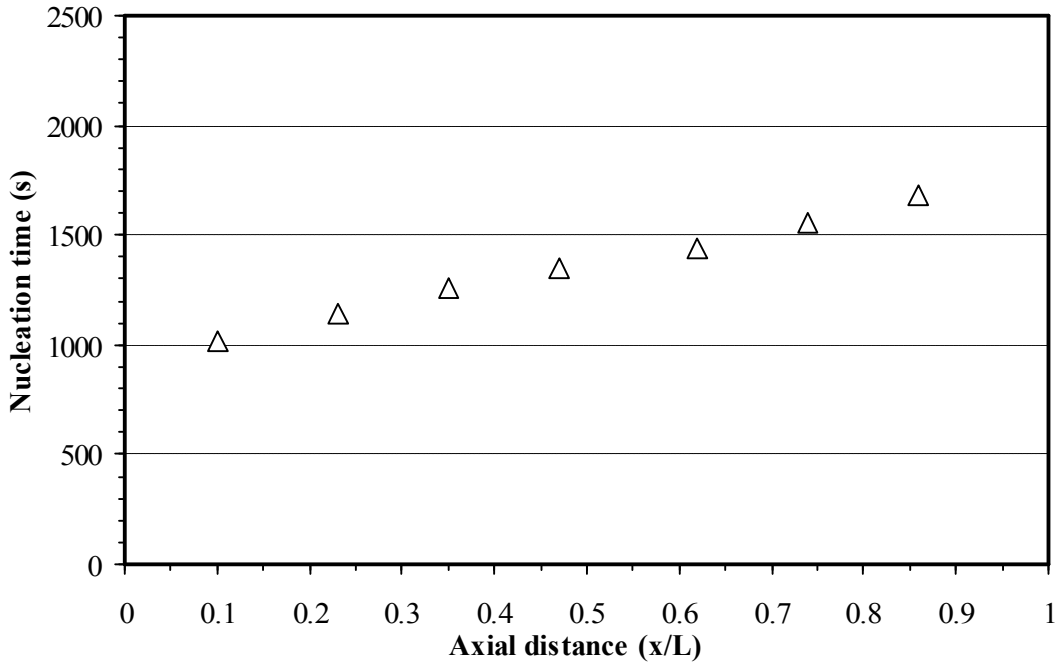


Figure 4.60. Variation of nucleation time along tube for $\overline{T}_{b,i}$ = -5.8 ºC

The thickness of the ice formed at the bottom, top, right and left sides of the tube was determined at different axial positions during the experiments. Figure 4.61 - 4.63 shows time wise variations of the ice thickness at seven axial positions (x/L= 0.1, x/L= 0.23, x/L= 0.35, x/L= 0.47, x/L= 0.62, x/L= 0.74, x/L= 0.86) for a brine inlet temperature of -5.8 ºC. Photographs of the ice formation from the top of the tube were not suitable for the post processing because of dense dendritic ice formation at the beginning of the experiments at the top of the tube.

At the beginning of the ice formation, thickness of the ice is almost equal around the tube. Ice formation is then better at the upper part of the tube than the lower due to collection of cold water at the upper and warmer water at the lower part of the vessel. The difference between the top and the bottom of the tube in terms of the ice thickness is approximately constant (0.6 mm) after 3000 s. at all measuring stations along the tube. The thickness of the ice at the right and left sides of the tube is close to each other.

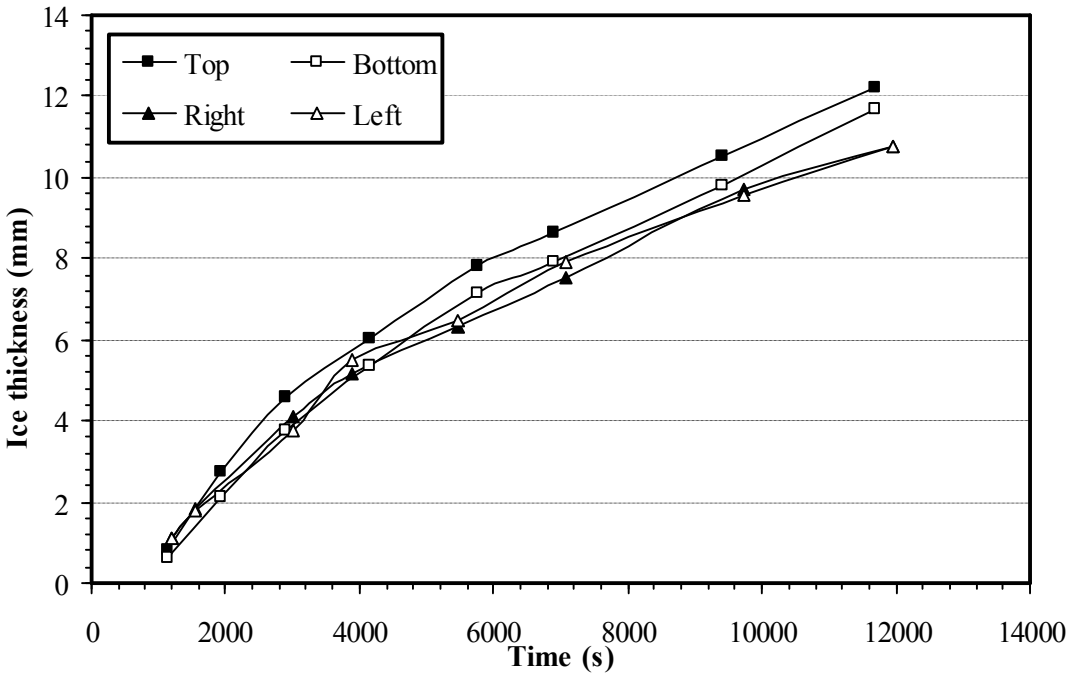


Figure 4.61. Variation of ice thickness with time for top, bottom and sides of tube for $\overline{T}_{b,i}$ = -5.8 ºC (x/L= 0.1)

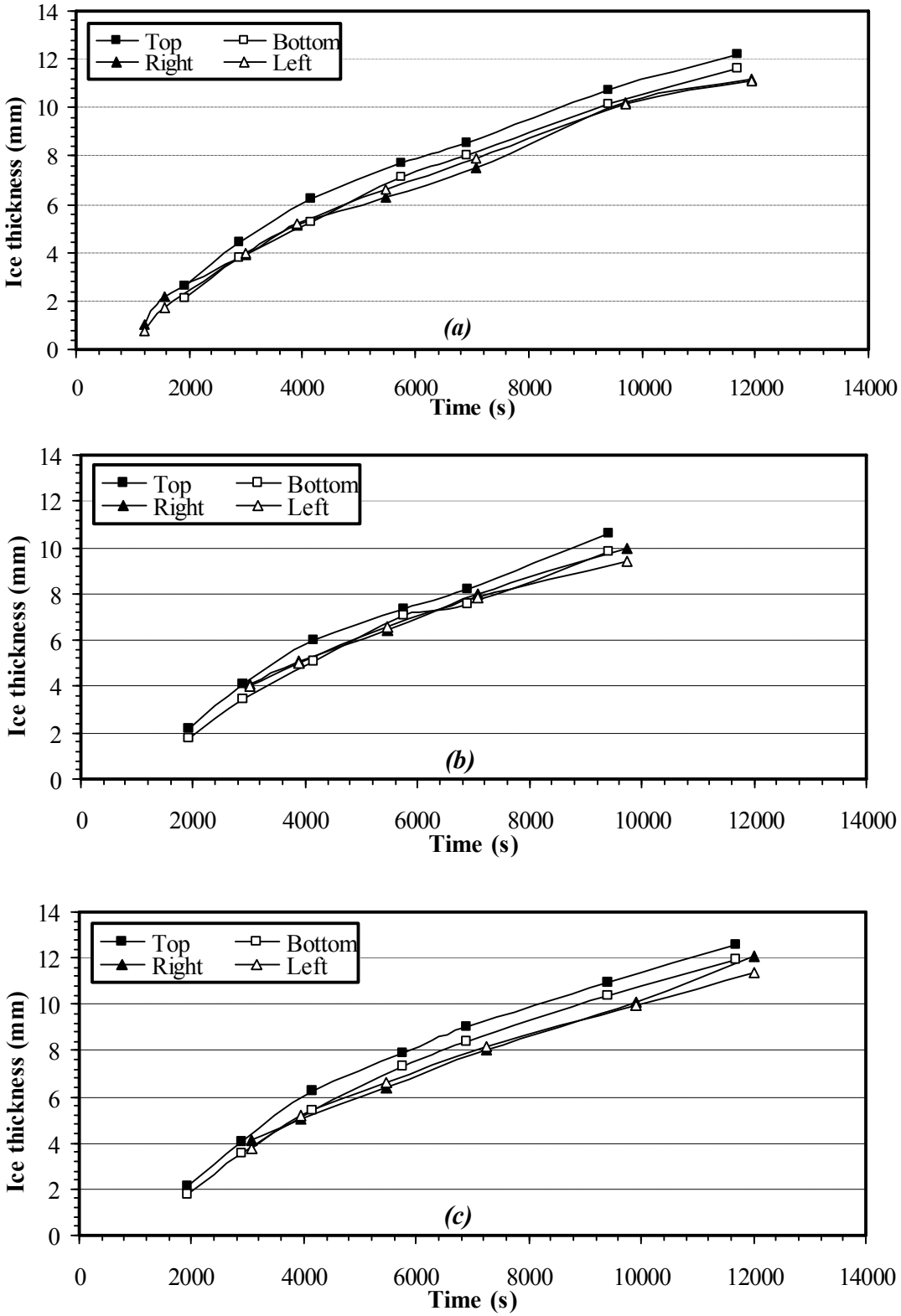


Figure 4.62. Variation of ice thickness with time for top, bottom and sides of tube for $\overline{T}_{b,i}$ = -5.8 ºC (***a:*** x/L= 0.23, ***b:*** x/L= 0.35, ***c:*** x/L= 0.47)

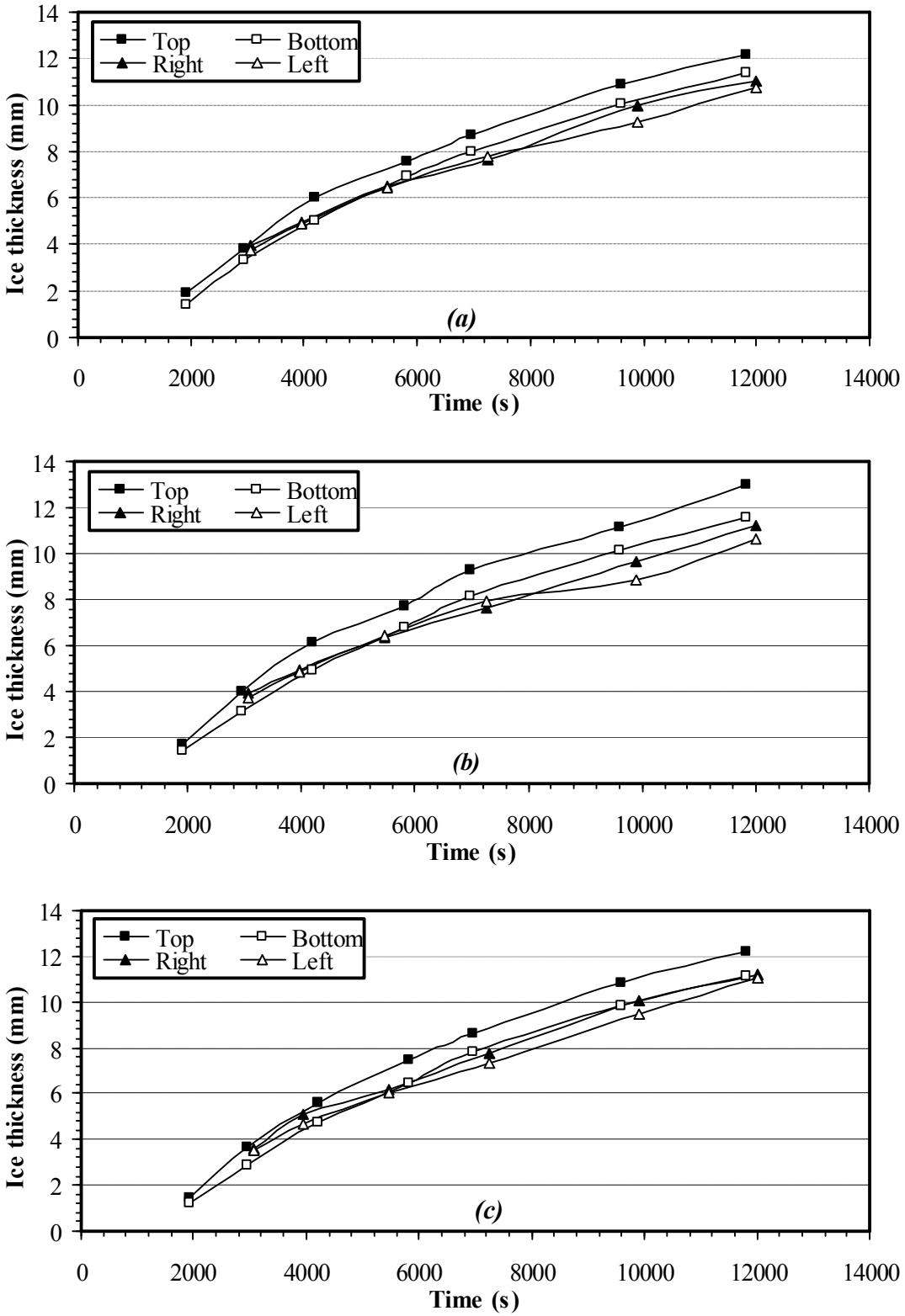


Figure 4.63. Variation of ice thickness with time for top, bottom and sides of tube for $\overline{T}_{b,i}$ = -5.8 ºC (***a:*** x/L= 0.62, ***b:*** x/L= 0.74, ***c:*** x/L= 0.86)

For second experiment, time wise variations of the water temperatures at the measurement points inside the vessel shows the Figure 4.64. It is evident from this figure that temperature of the water decreases steadily at all measurement points. Due to the density inversion effect of water, the temperature at the top of the tank becomes the cold spot in the vessel. As further cooling occurs, some extent of water at the top of the cylinder was supercooled.

Temperature of the water never decreases down to freezing temperature (0 ºC) at the bottom of the vessel (thermocouples 1 and 2) during ice formation. The slight temperature increase at the beginning of the experiment is due to collection of warm water at the bottom of the vessel.

In Figure 4.65, the variation of water temperature with time near the tube wall (thermocouple 3) at all axial positions is illustrated for $\overline{T}_{b,i}$ = -4.9 ºC. As can be seen from, supercooling occurs at all measurement points except the bottom of the tube and the degree of it is between -1.53 ºC and -2.65 ºC.

Figure 4.66 presents variation of the time from the beginning of the experiment to the nucleation time along the pipe length for a brine inlet temperature of -4.9 ºC. As expected, it is clearly evident from this figure that nucleation time increases with the axial distance. In this case, the temperature of water needs longer time (1500 s for first measurement point) to reach the nucleation temperature as compared with the case of $\overline{T}_{b,i}$ = -5.8 ºC.

The thickness of the ice formed at the bottom, top, right and left sides of the tube was determined at different axial positions during the experiments. Figures 4.67 - 4.69 show time wise variations of the ice thickness at seven axial positions (x/L= 0.1, x/L= 0.23, x/L= 0.35, x/L= 0.47, x/L= 0.62, x/L= 0.74, x/L= 0.86) for a brine inlet temperature of -4.9 ºC. It can be seen from figures that all the ice thicknesses around the tube increase with time.

However, the thickness of the ice formed at the top is maximum, and it is follwed by the ice formed at the bottom. The thickness of the ice formed at the right and left sides is close to each other and they are lower than that of top and bottom sides. Ice thickness around tube is substantially influenced by natural convection that occurs within the water.

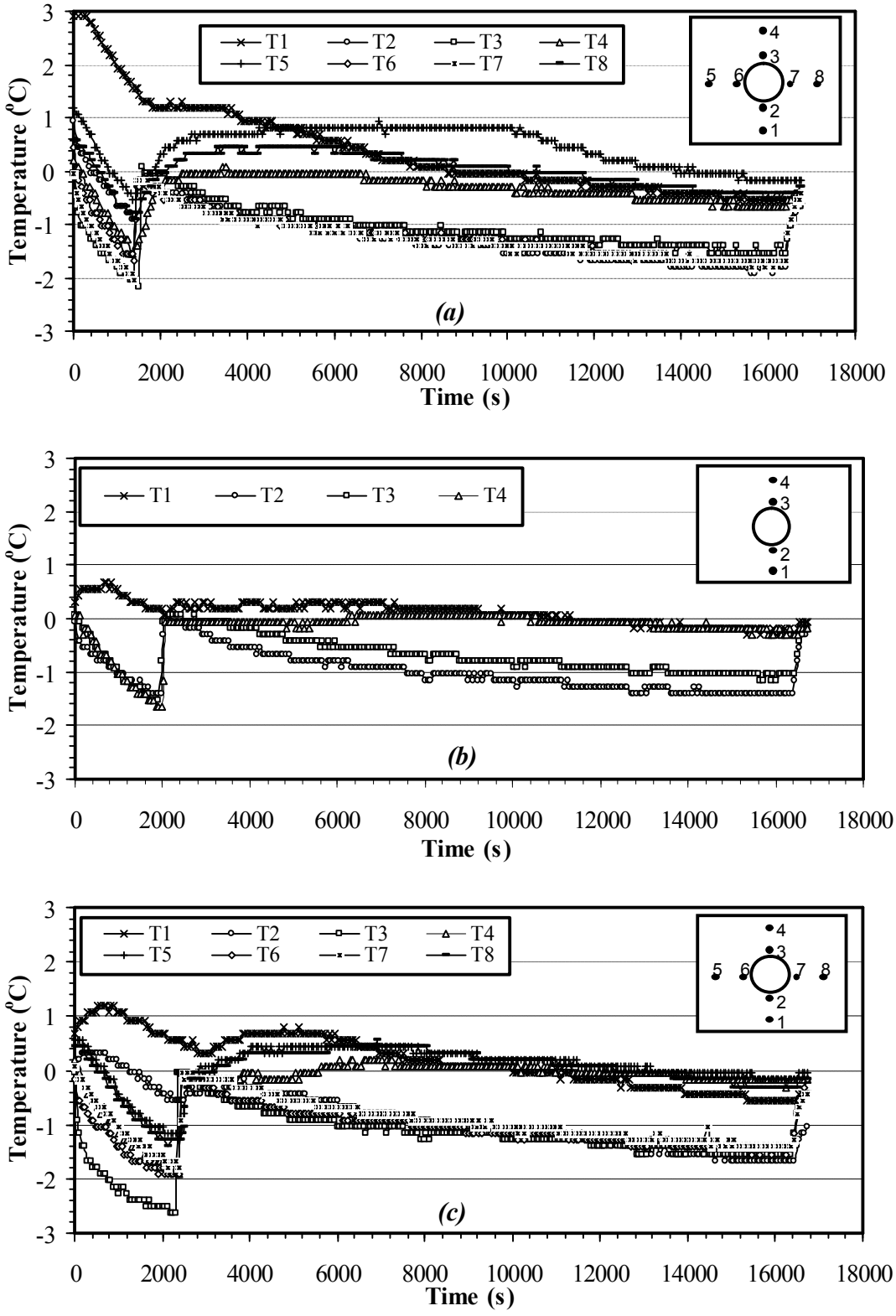


Figure 4.64. Variation of water temperature with time at three measurement stations for $\overline{T}_{b,i}$ = -4.9 ºC (***a:*** x/L = 0.1, ***b:*** x/L = 0.47, ***c:*** x/L = 0.86)

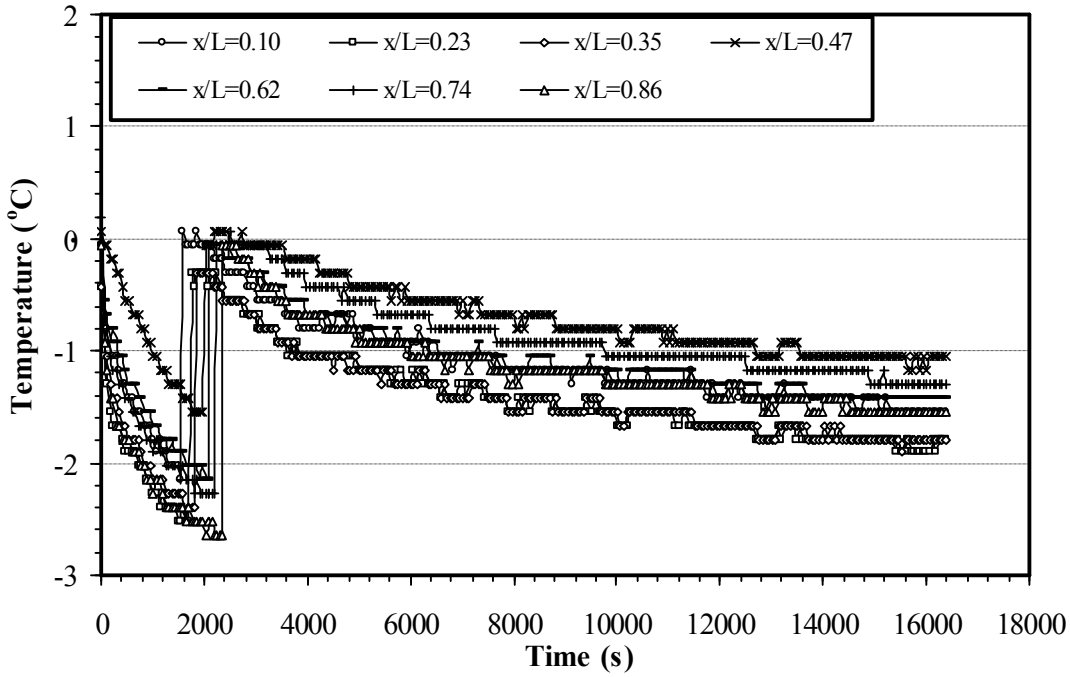


Figure 4.65. Variation of water temperature with time at positions just above the test tube (thermocouple 3) for different axial measurement stations ($\overline{T}_{b,i}$ = -4.9 ºC)

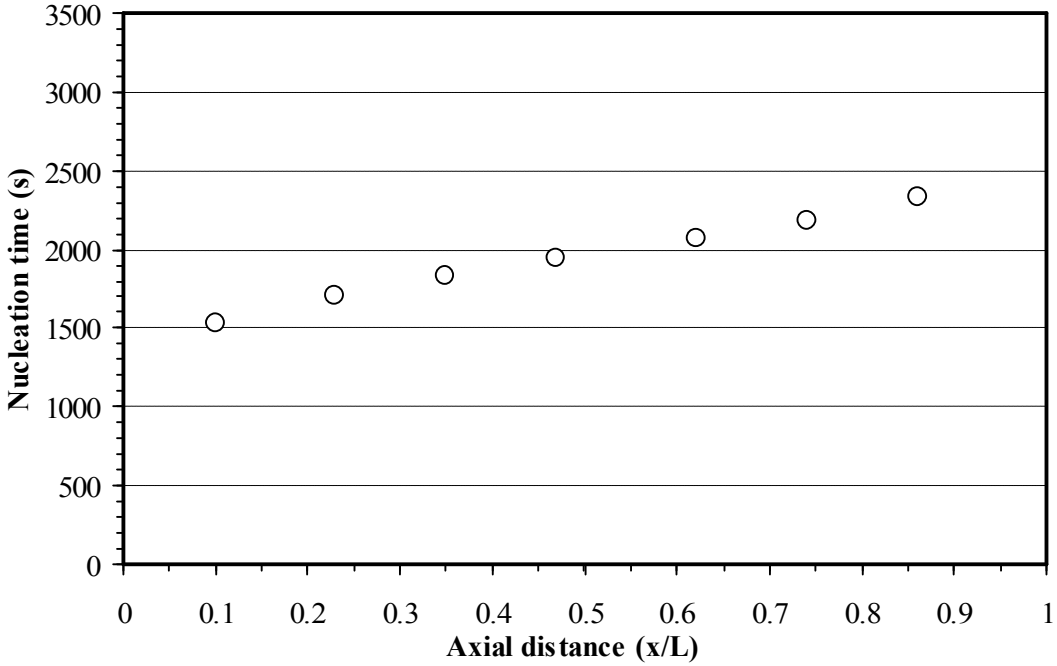


Figure 4.66. Variation of nucleation time along tube for $\overline{T}_{b,i}$ = -4.9 ºC

Figure 4.70 shows time wise variations of the water temperatures at the measurement points inside the vessel for a brine inlet temperature of -4.3 ºC. As shown in the figure, when the cold spot reaches the nucleation temperature of water, ice nucleation occurs at the upper part of the tube. The dendritic ice spreads rapidly from the nucleation site down toward the center and bottom region of the tube. The total time required for the whole dendritic ice growth to be completed is between 1s and 3s.

Figure 4.71 is plotted to show the variation of water temperature with time near the tube wall (thermocouple 3) at different axial positions. It is clearly seen from the figure that, supercooling occurs at all measurement points and except the bottom of the tube and the degree of it is between -1.53 ºC and -2.89 ºC.

Variation of the time from the beginning of the experiment to the start of nucleation (nucleation time) along the pipe length is given in Figure 4.72 for $\overline{T}_{b,i}$ = -4.3 ºC. As can be seen from the figure, nucleation first starts at the entrance region, which is the coldest region, and propagates along the tube.

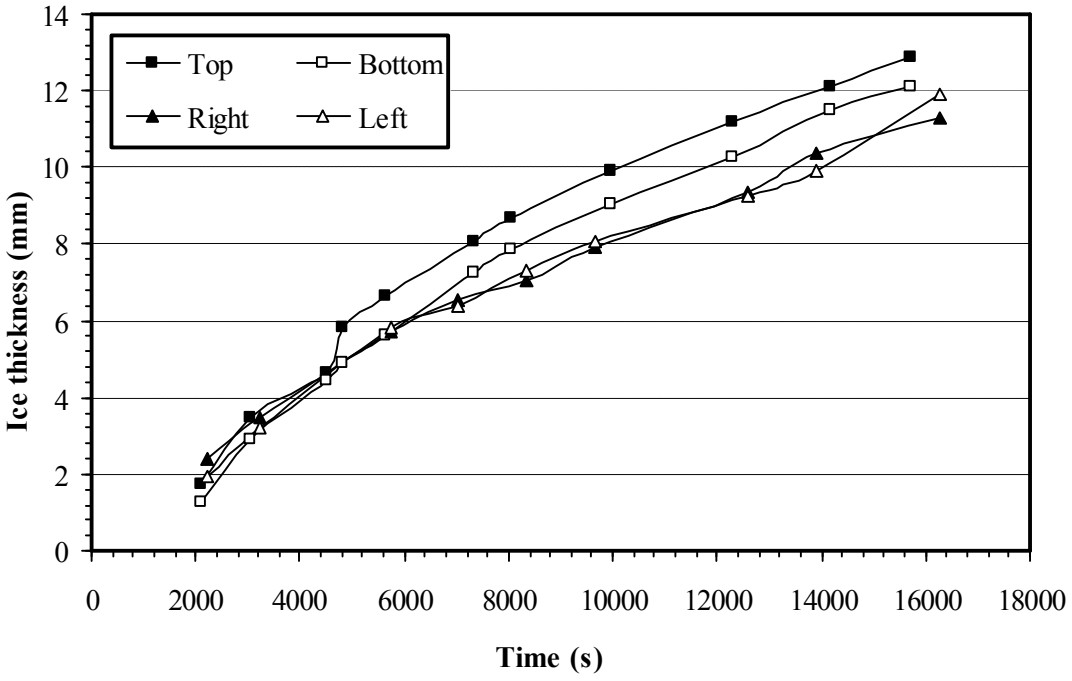


Figure 4.67. Variation of ice thickness with time for top, bottom and sides of tube for $\overline{T}_{b,i}$ = -4.9 ºC (x/L= 0.1)

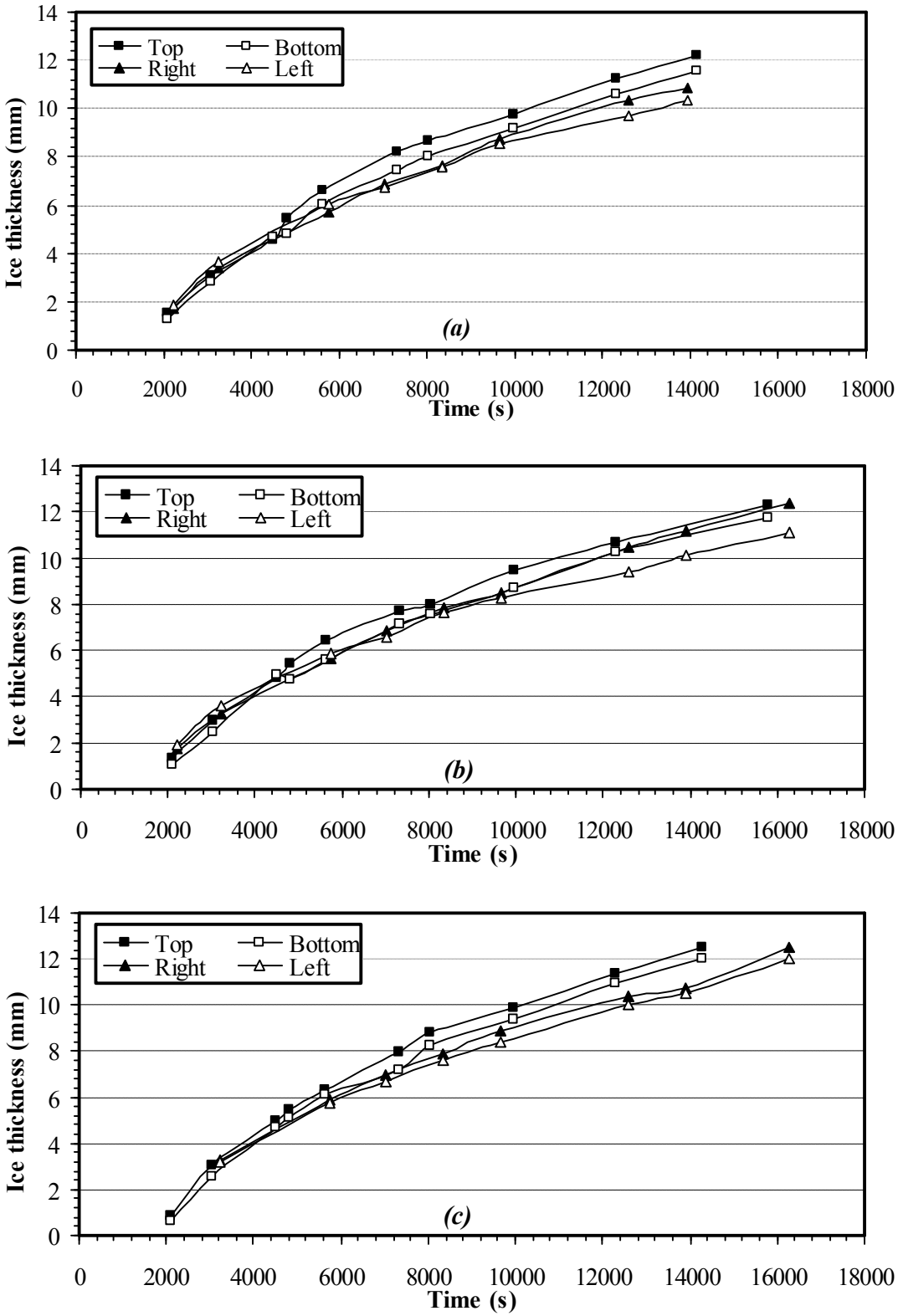


Figure 4.68. Variation of ice thickness with time for top, bottom and sides of tube for $\overline{T}_{b,i}$ = -4.9 ºC (***a:*** x/L= 0.23, ***b:*** x/L= 0.35, ***c:*** x/L= 0.47)

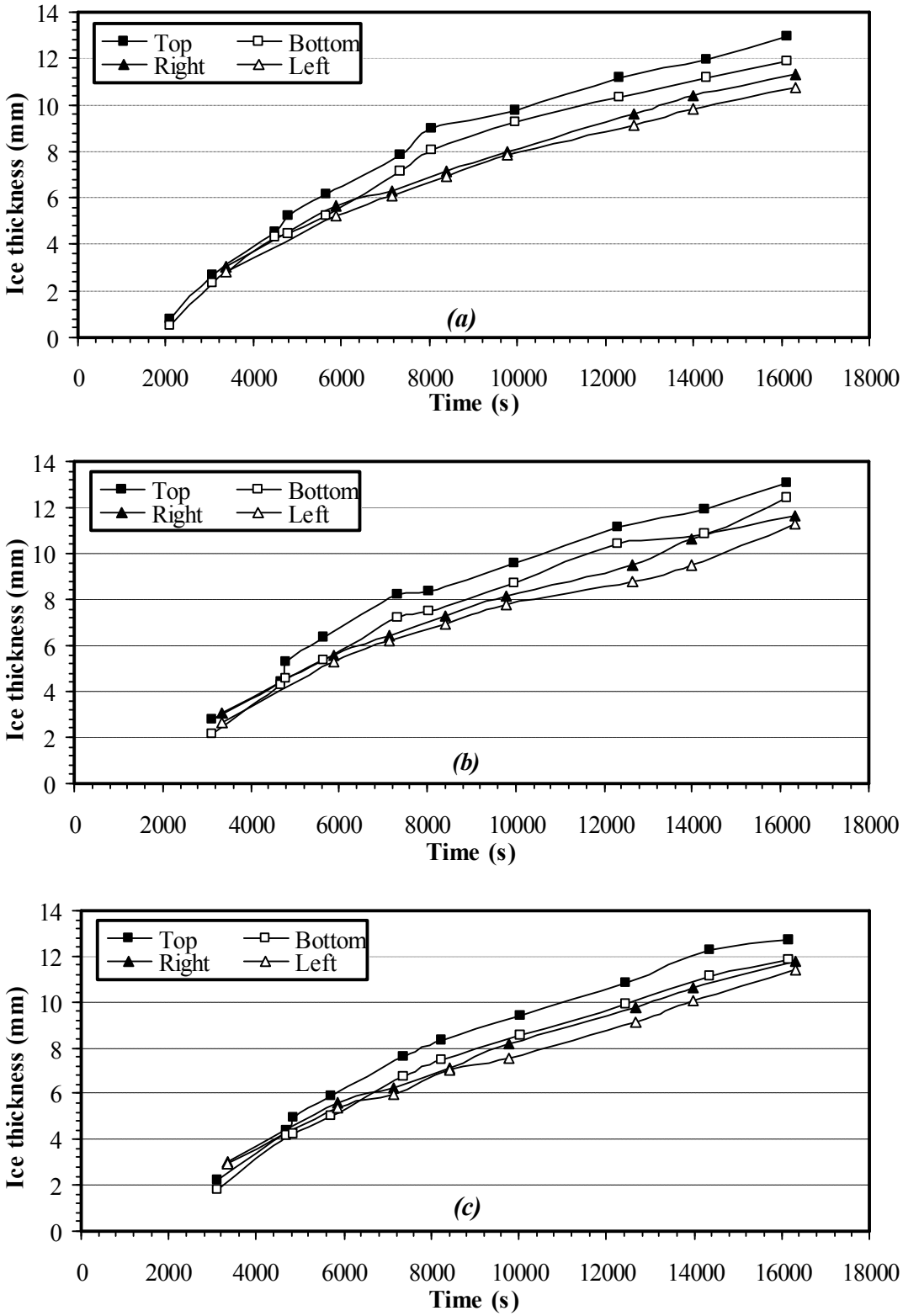


Figure 4.69. Variation of ice thickness with time for top, bottom and sides of tube for $\overline{T}_{b,i}$ = -4.9 ºC (***a:*** x/L= 0.62, ***b:*** x/L= 0.74, ***c:*** x/L= 0.86)

Figure 4.73-4.75 shows time wise variations of the ice thickness at seven axial positions for a brine inlet temperature of -4.3 ºC. In these figures, it is generally observed that there are differences between the thickness of the ice formed at the bottom and top sides of the tube due to collection of cold water at the upper and warmer water at the lower part of the vessel. Another point observed in figures is that the thickness of the ice at the right and left sides of the tube is close to each other.

The shape of the ice formation during the experiments at three axial positions (x/L=0.1, 0.47 and 0.86) is depicted in Figure 4.76 for three different brine inlet temperatures (-4.3 ºC, -4.9 ºC and -5.8 ºC). When the ice forms first, it has almost a circular shape. However, the shape is distorted in later stages of ice formation. Ice thickness at the top becomes higher than the bottom, right and left, and therefore, the shape takes an oval form.

Influence of brine inlet temperature on ice thickness is shown in Figure 4.77 for 3 different times during the experiments (2880 s, 6900 s and 11700 s) at an axial position of x/L=0.47. With the increase of brine inlet temperature, ice thickness decreases at all points around the tube. The same trend is also observed at other axial positions. As discussed above, ice formation is almost uniform around the tube at the initial stages of ice formation (2880 s). However later the uniformity is distorted and a clear difference between the top and bottom are observed at 11700 s.

It is obvious that brine inlet temperature seriously affects the onset of the phase change of water and nucleation time. Nucleation time increases with the increase of brine inlet temperature (Figure 4.78).

Increase of inlet temperature from -5.8 ºC to -4.3 ºC almost doubles the nucleation time at all axial positions along the tube. Due to high fluid inlet temperature, the temperature of water needs more time to reach the nucleation temperature. Similar results were also reported by (Chen et al., 2000) who conducted a series of experiments to investigate the supercooling phenomenon and the effect of inlet coolant temperature on the nucleation of water inside cylinder

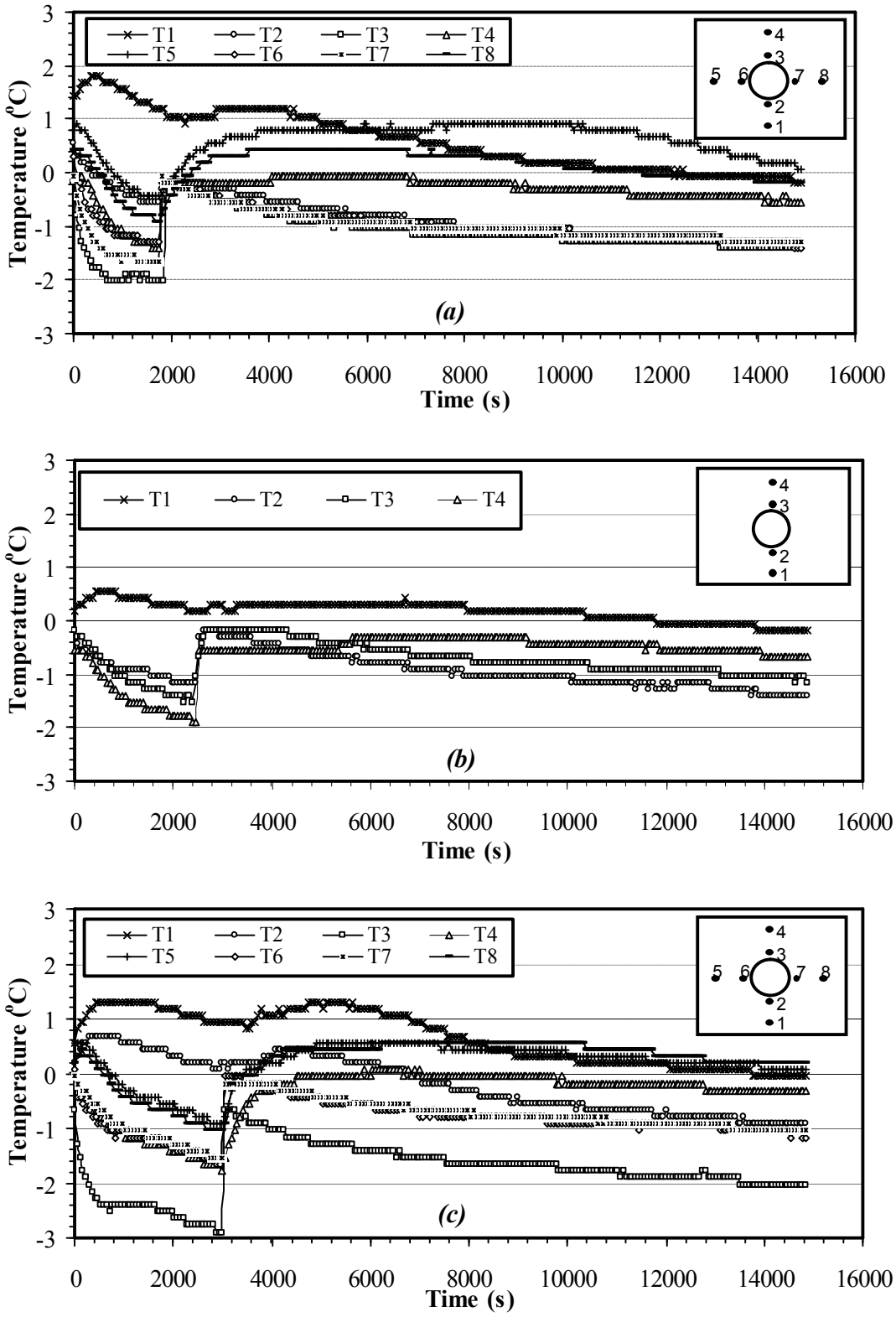


Figure 4.70. Variation of water temperature with time at three measurement stations for $\overline{T}_{b,i}$ = -4.3 ºC (***a:*** x/L = 0.1, ***b:*** x/L = 0.47, ***c:*** x/L = 0.86)

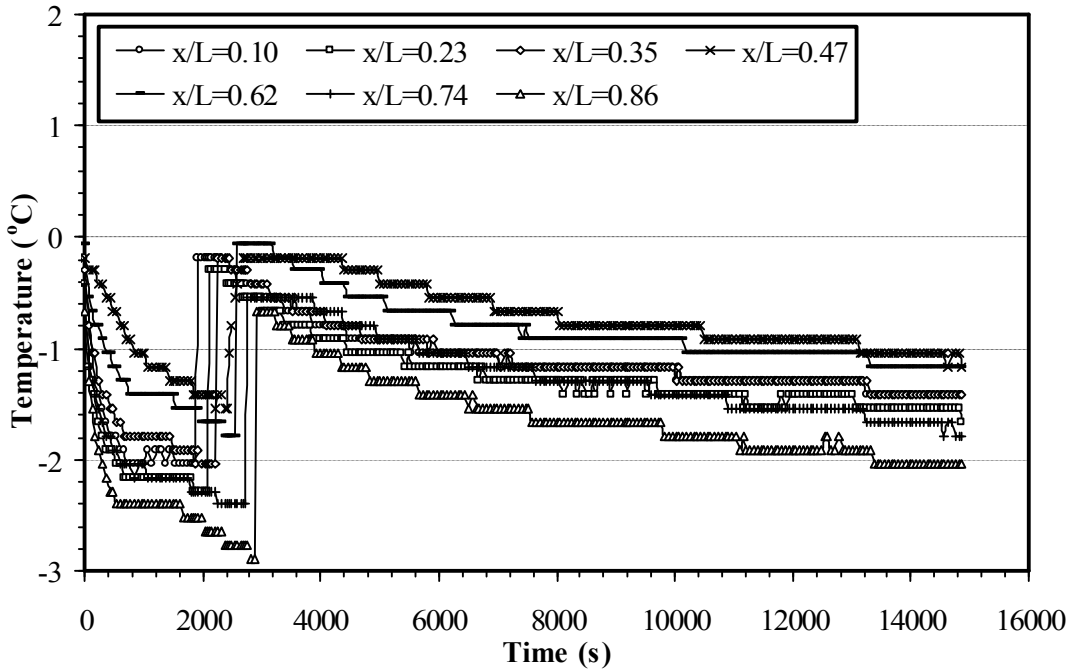


Figure 4.71. Variation of water temperature with time at positions just above the test tube (thermocouple 3) for different axial measurement stations ($\overline{T}_{b,i}$ = -4.3 ºC)

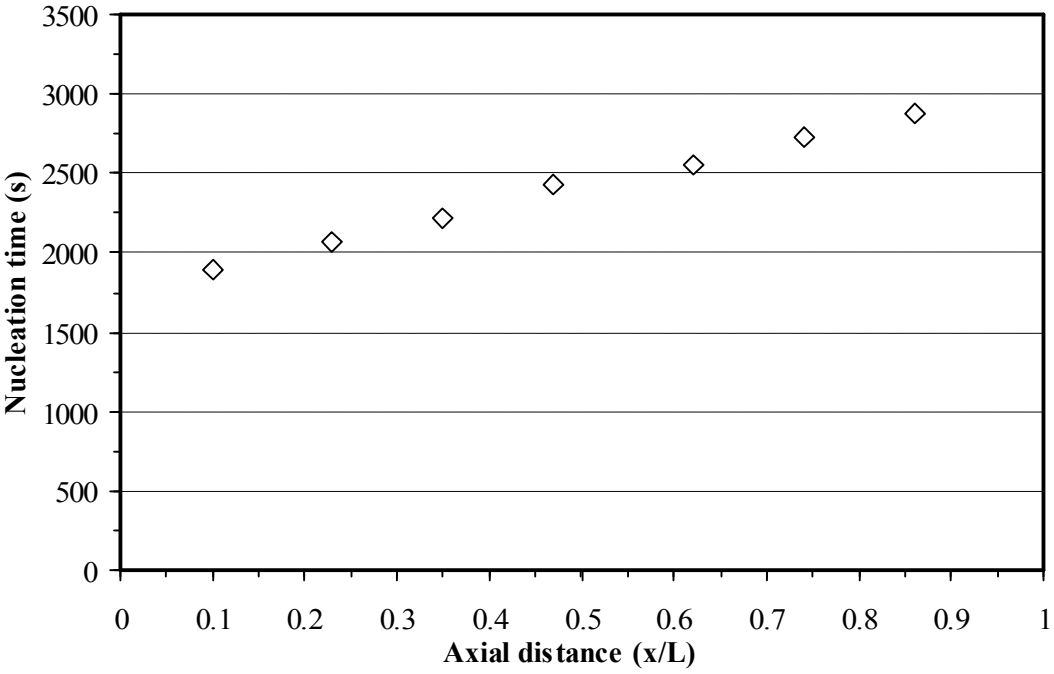


Figure 4.72. Variation of nucleation time along tube for $\overline{T}_{b,i}$ = -4.3 ºC

.

A simple model for the formation of ice around a cylindrical tube is given above. Comparison of the model and results is given in Figure 4.79 for three different brine inlet temperatures (-4.3 ºC, -4.9 ºC and -5.8 ºC). The experimental values shown in this figure were obtained by averaging ice thickness values determined at top, bottom, right and left of the tube at each axial position. Since the time scale starts from the formation of ice in the model, the experimentally obtained values at different axial positions were shifted according to time at which ice formation starts at the axial position of interest. Therefore, time scale in Figure 4.79 is not the absolute time scale, rather represents the time passed from the start of ice formation. The figure shows the experimental ice thicknesses at all axial positions with shifted time scales.

As can be seen from Figure 4.79, the agreement between the model and the experimental values is good during the ice formation process for all brine inlet temperatures. The model under predicts slightly ice thickness at the beginning of the process and over predicts at the end.

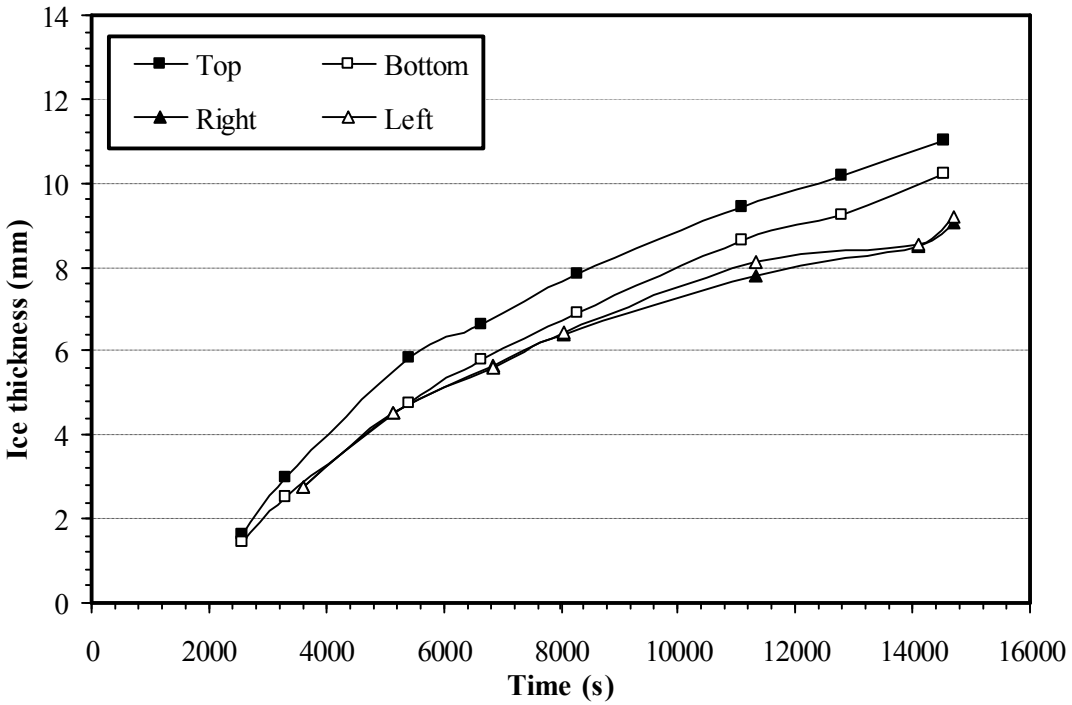


Figure 4.73. Variation of ice thickness with time for top, bottom and sides of tube for $\overline{T}_{b,i}$ = -4.3 ºC (x/L= 0.1)

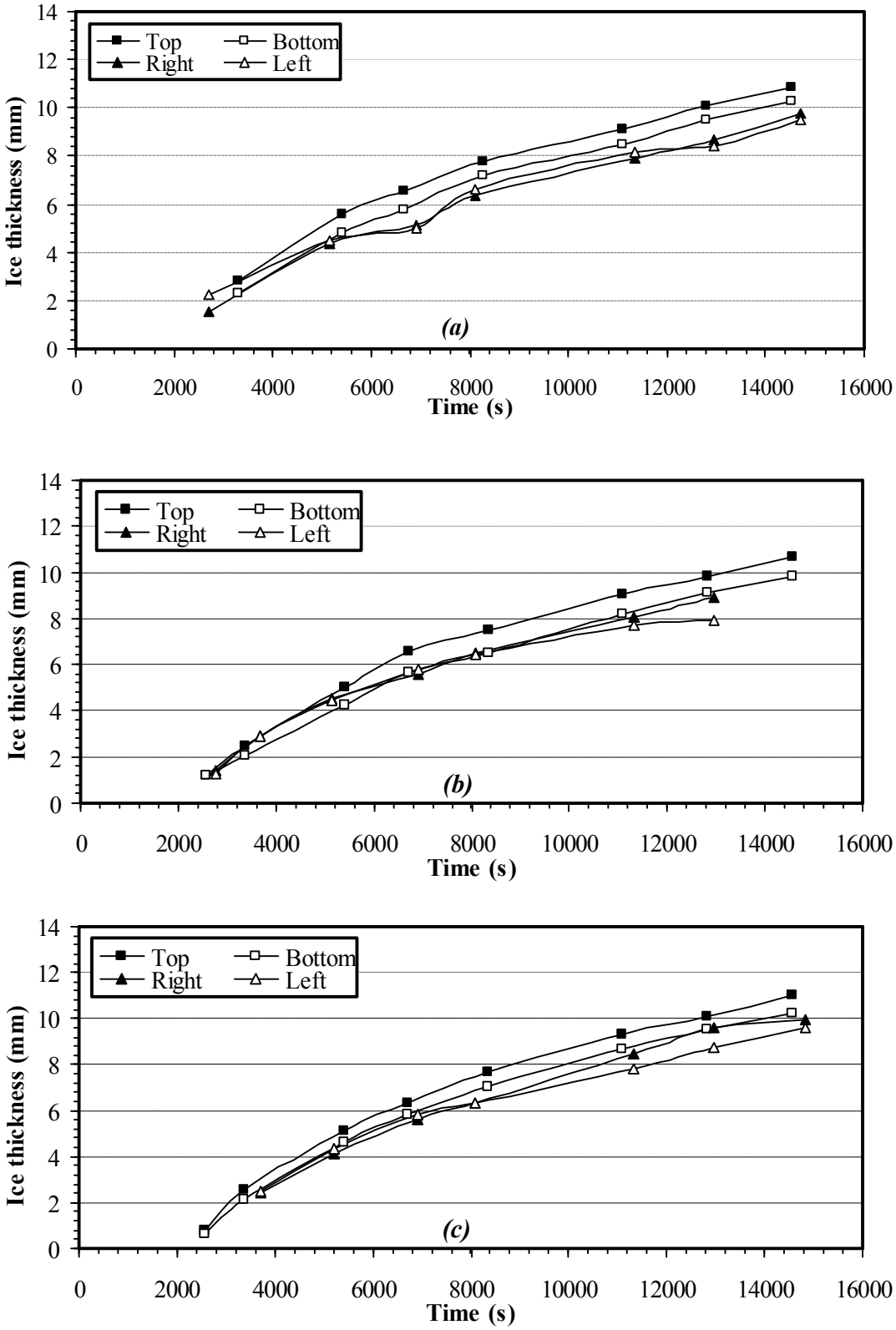


Figure 4.74. Variation of ice thickness with time for top, bottom and sides of tube for $\overline{T}_{b,i}$ = -4.3 ºC (***a:*** x/L= 0.23, ***b:*** x/L= 0.35, ***c:*** x/L= 0.47)

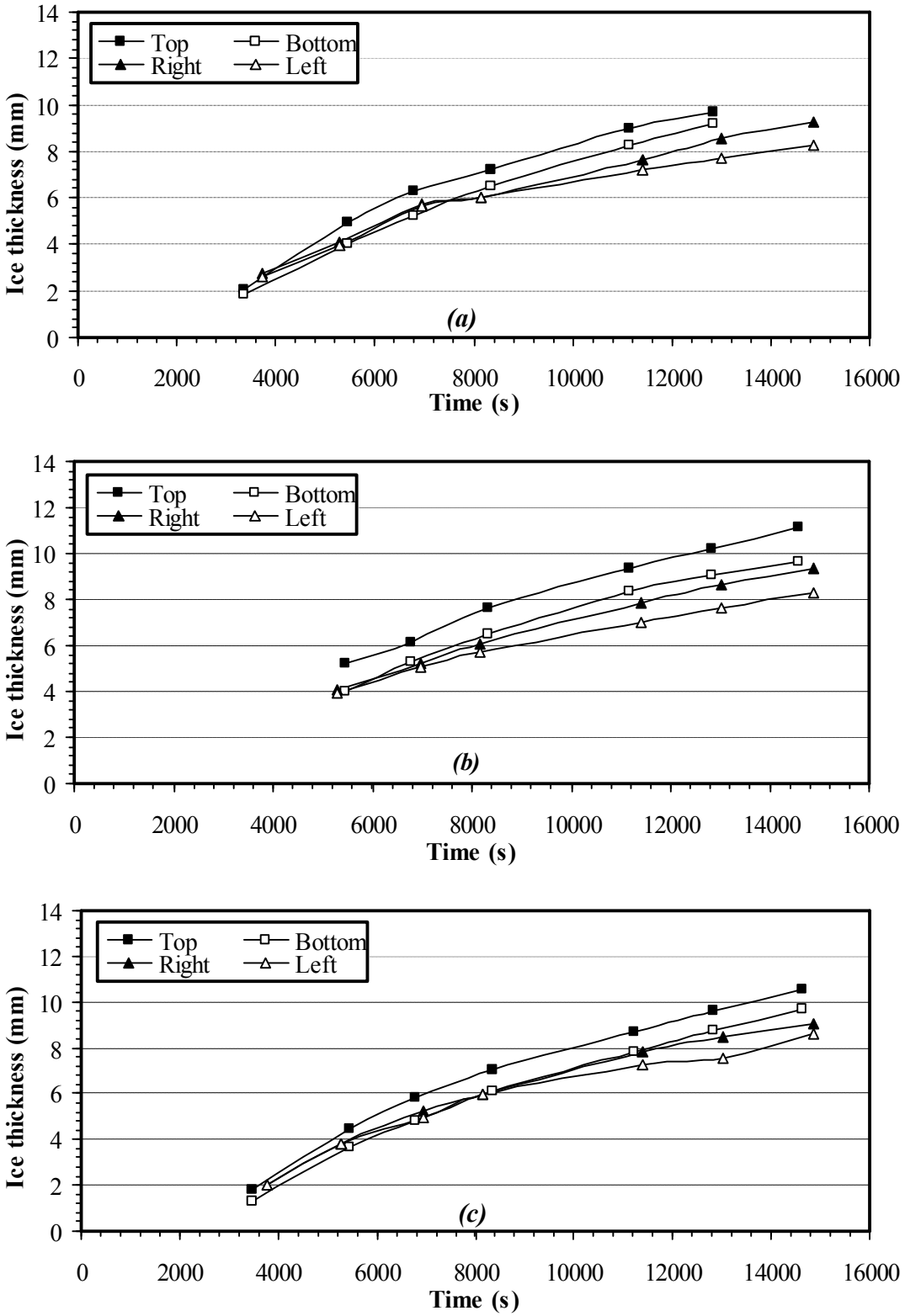


Figure 4.75. Variation of ice thickness with time for top, bottom and sides of tube for $\overline{T}_{b,i}$ = -4.3 ºC (***a:*** x/L= 0.62, ***b:*** x/L= 0.74, ***c:*** x/L= 0.86)

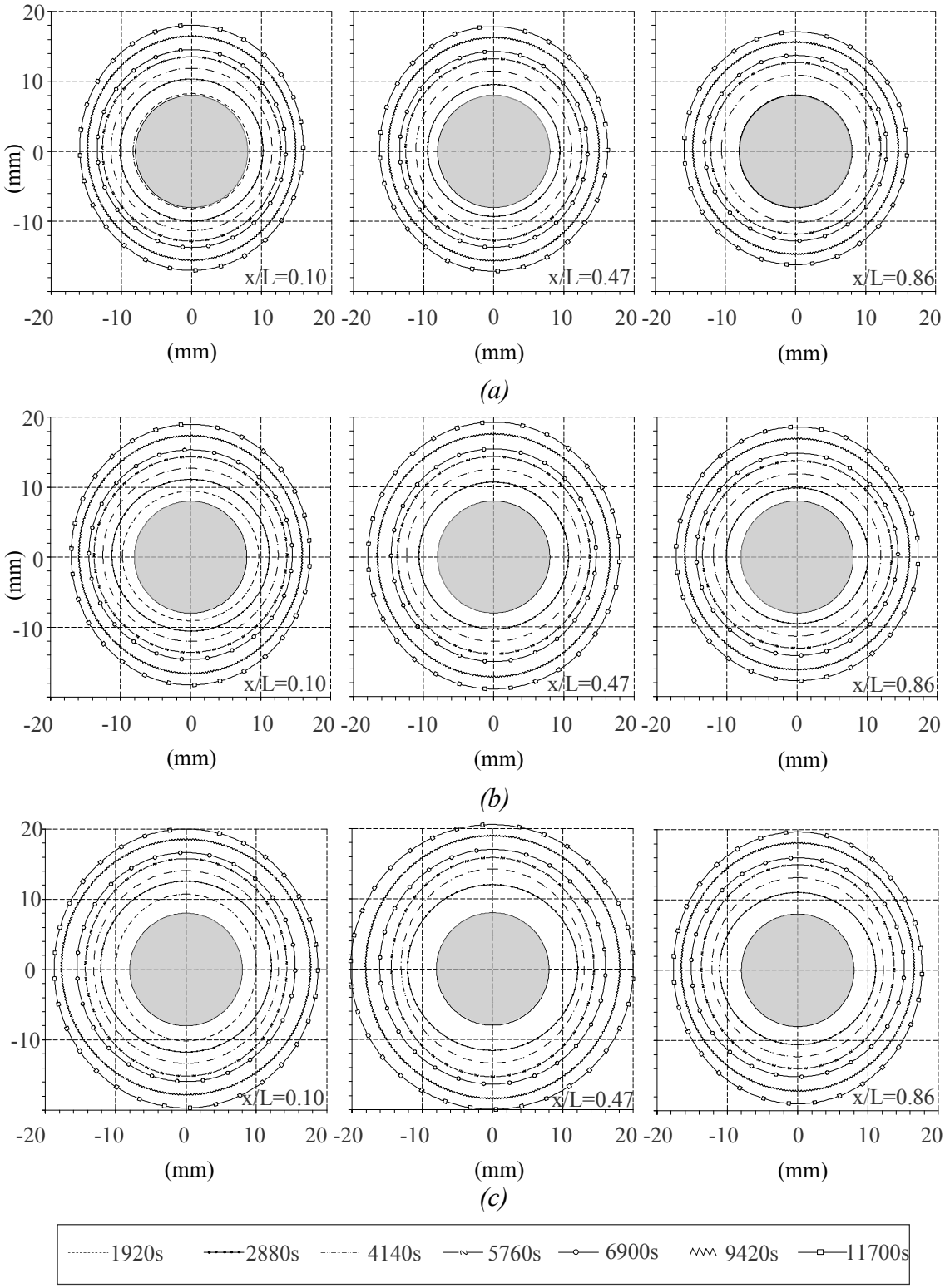


Figure 4.76. Evolution of ice-water interface with time for different brine inlet temperatures (*a:* $\overline{T}_{b,i}$ = -4.3 °C, *b:* $\overline{T}_{b,i}$ = -4.9 °C, *c:* $\overline{T}_{b,i}$ = -5.8 °C)

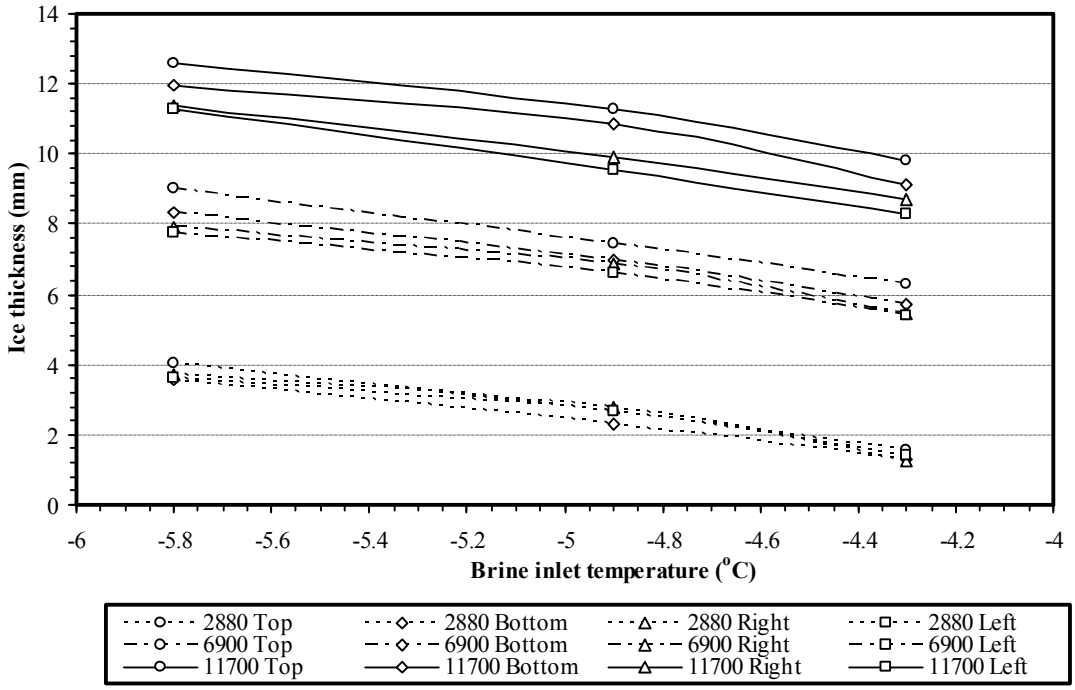


Figure 4.77. Influence of brine inlet temperature on ice thickness at x/L= 0.47

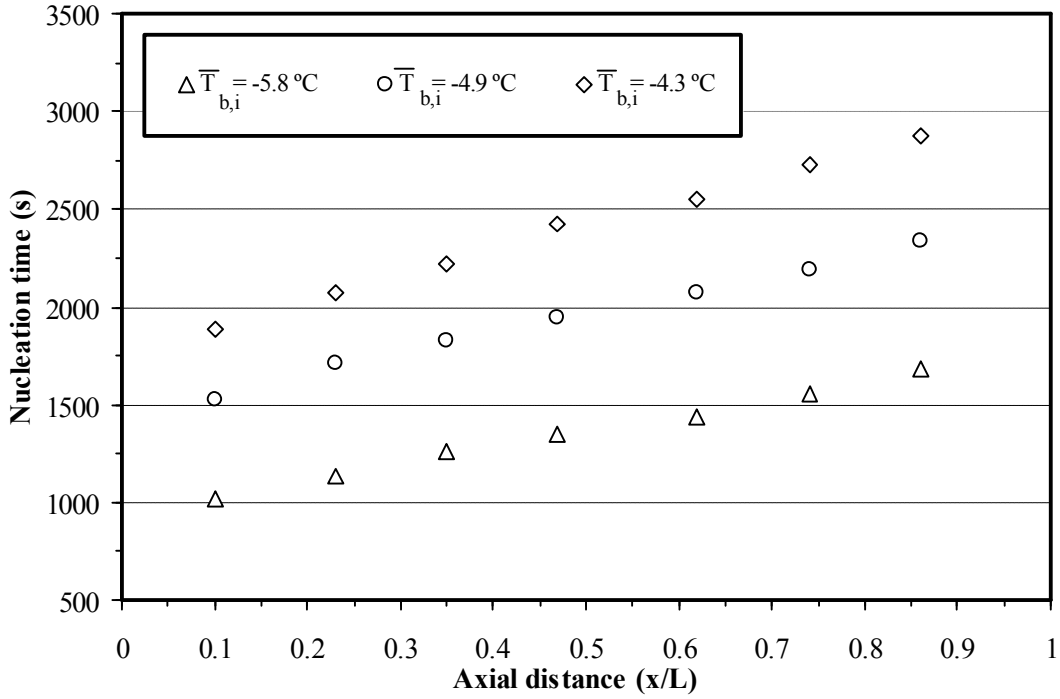


Figure 4.78. Variation of nucleation time along tube for different brine inlet temperatures

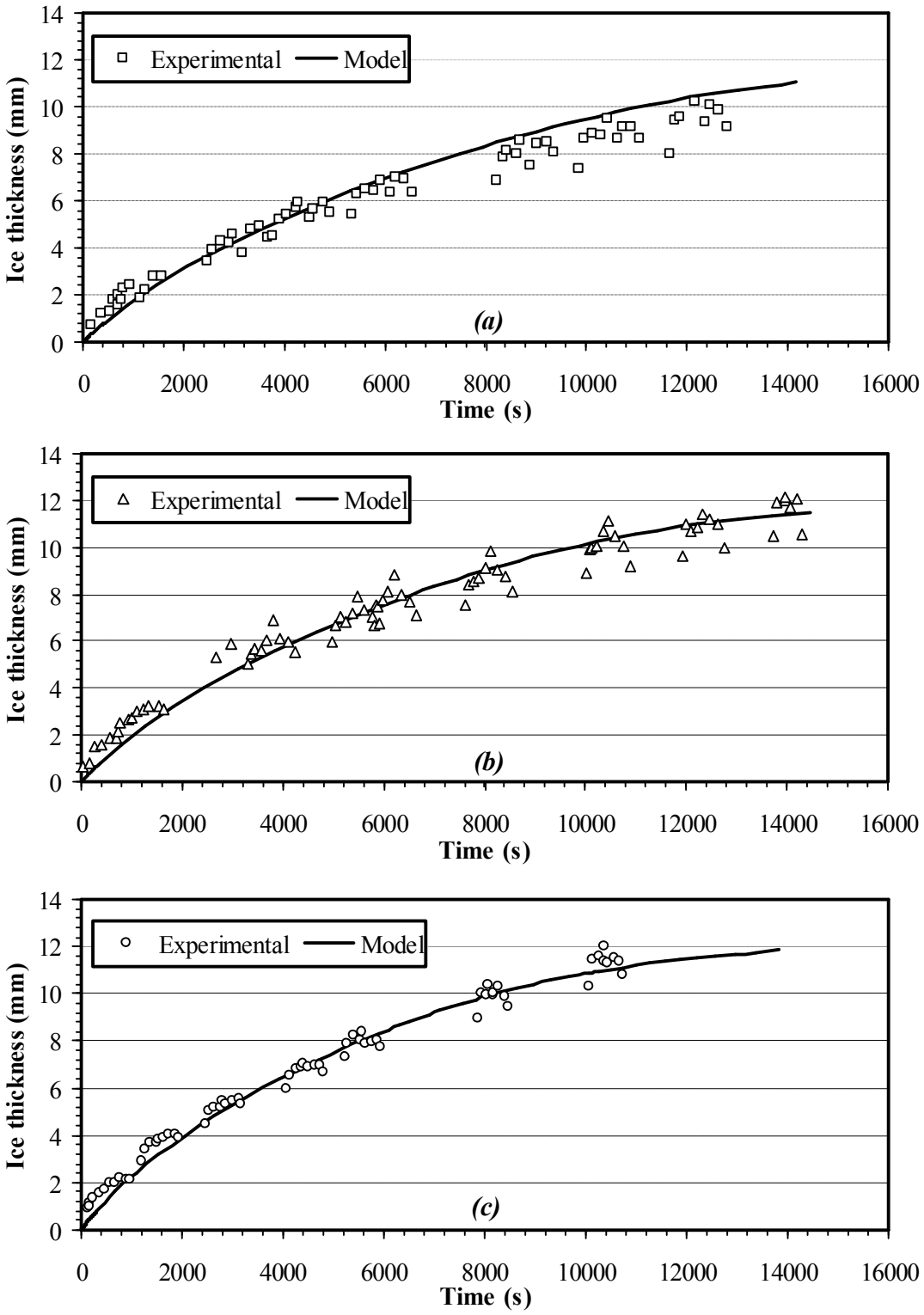


Figure 4.79. Comparison of ice thickness obtained from measurements and model for different brine inlet temperatures (***a:*** $\overline{T}_{b,i}$ = -4.3 °C, ***b:*** $\overline{T}_{b,i}$ = -4.9 °C, ***c:*** $\overline{T}_{b,i}$ = -5.8 °C)

5. CONCLUSIONS AND RECOMMENDATIONS

5.1. Conclusions

In the first section of this study, charge and discharge experiments were performed utilizing Experimental Setup 1 to investigate performance characteristics of the ice storage system. Based on the obtained results, our conclusions are summarized as follows:

1. Nucleation temperature does not change considerably with radial distance at all the levels of the tank. However, it increases almost linearly with the axial distance for all brine temperatures.
2. Nucleation temperature varies within a band for all brine inlet temperatures. Therefore, more experiments should be performed to be able to link the nucleation temperature with brine inlet temperature.
3. Experimental results show that set temperature of the brine affects the onset of the phase change of water.
    a. For $T_{b,s}$ = - 4 ºC, the water inside the ice storage tank exists in the metastable state without freezing and only the sensible heat storage is attained.
    b. For $T_{b,s}$ = - 5 ºC and - 6 ºC, the thermal energy can be stored in the form of latent heat. However, ice formation is delayed due to on-off operation of the chiller.
    c. For $T_{b,s}$ = - 7 ºC and - 8 ºC, heat removal rate from the water inside the tank is increased and consequently the nucleation time decreases. Set temperature is never attained and the chiller operates continuously for these brine set temperatures.
4. When brine inlet temperature increases, charging performance decreases for different air temperatures at the inlet of the condenser. However, charging performance decreases with the increase of air inlet temperature.

5. Charging performance of the ice storage system decreases with increasing charging period.
6. Discharge experiments were carried out for two automatic control operating strategies (fan control and valve control). The thermal environments (temperature and relative humidity) measured in the air-conditioned room were plotted on a psychometric chart together with ASHRAE comfort zone. Almost all the points were located inside the comfort zone. This shows that the automatic control system designed fulfills its requirements properly.

In the second section of this study, phase change phenomena and the effect of brine inlet temperature on ice formation around a horizontal tube in a rectangular vessel were investigated both experimentally (Experimental Setup 2) and analytically. The main findins are summarized below:

1. Experimental results show that supercooling occurs at all axial measuring stations along the tube and nucleation first starts at the entrance region and propagates along the tube. Nucleation temperatures are between -1.4 ºC and -3 ºC for all measurement points.
2. It is obvious that the brine inlet temperature seriously affects the onset of the phase change of water and nucleation time. With the decrease of brine inlet temperature, nucleation time decreases. Furthermore nucleation time increases with the axial distance for all brine inlet temperatures.
3. The thickness of the ice formed at the top and bottom sides of tube is different from each other, although the thickness of the ice formed at the right and left sides is close to each other. Ice thickness around tube is substantially influenced by natural convection that occurs within the water. With the increase of brine inlet temperature, ice thickness decreases at all points around the tube.
4. Ice thickness evaluated by mathematical model agrees reasonably with the experimental data for all brine inlet temperatures.

5.2. Recommendations for Future Works

The significant recommendations for future work are:

For experimental Set up 1:

- Effects on characteristics of ice storage system of adding various nucleation agents, which influences nucleation behavior of water inside the ice storage tank, can be studied.
- Influence of flow rate of glycol-water mixture (brine) on the system characteristics can be investigated.
- Influence of initial water temperature on the system characteristics can be investigated.
- Various methods (such as using finned coil and agitating water in the tank) for enhancing heat transfer between the water inside the tank and the coils can be examined. This may accelerate the ice layer growth at the solid-liquid interface.
- In this study, only full storage strategy was studied. Partial storage strategy should also be investigated

For experimental Set up 2:

- Effects of brine flow rate, initial water temperature and nucleation agents on the solidification around the tube can be studied in detail.
- Effect of different tube arrangements on the ice interaction and system performance can be investigated.

REFERENCES

AKYURT, M. and ZAKI, G., 2001. Freezing phenomena in ice-water systems. Energy Conversion & Management, 43, 1773-1789.

ARNOLD, D., 1991. Laboratory performance of an encapsulated ice store. ASHRAE Transactions 97, 2, 1170- 1178.

ASHRAE, 2001. ASHRAE Handbook-2001 Fundamentals, American Society of Heating Refrigerating, and Air-conditioning Engineers, Atlanta.

BUYUKALACA, O., YILMAZ, T., and FERTELLI, A. 2003. Ice storage air-conditioning system. Proceedings of the Eastern Mediterranean and Southeastern Anatolia Region Machine and System Design-Production Congress (in Turkish), Turkey 95-101.

CALMAC, 1991. An introduction to off-peak air conditioning OPAC for commercial applications, Product Brochure of Calmac, 1-8.

CHAICHANA, C., CHARTERS, W.W.S, AYE, L., 2001. An ice thermal storage computer model. Applied Thermal Engineering, 21, 1769-1778.

CHEN, S.L., LEE, T.S., 1998. A study of supercooling phenomenon and freezing probability of water inside horizontal cylinders. Int. J. Heat Mass Transfer, 41, 4-5, 769-783.

CHEN, S.L., CHEN, C.L., THIN, C.C., LEE, T.S. and KE, M.C., 2000. An experimental investigation of cold storage in an encapsulated thermal storage tank. Experimental Thermal and Fluid Science, 23, 133-144.

CHOI, S., KIM, J. D., KIM,E., and YOON, J. I., 2002. Experimental characteristics of a storage tank on a harvest-type ice storage system. Int. J. Heat Mass Transfer, 45, 7, 1407-1412.

CUMMINGS M.S., 1989. Modeling, design and control of partial ice storage air-conditioning systems., MSc. Thesis, University of Wisconsin-Madison.

DINCER, I., 2002. On thermal energy storage systems and applications in buildings. Energy and Buildings, 34, 377-388.

DINCER, I., ROSEN, M.A, 2002. Thermal energy storage systems and applications. John Wiley& Sons,England.

DORGAN C.E., ELLESON J.S., 1993. Design Guide for Cool Thermal Storage. American Society of Heating Refrigeration and Air-Conditioning Engineering, Atlanta.

EPRI, 1987. Commercial Cool Storage Design Guide. Hemisphere Publishing Corporation, Washington.

EREK, A., İLKEN, Z. and ACAR, M.A., 2005. Experimental and numerical investigation of thermal energy storage with a finned tube. International Journal of Energy Research, 29, 283-301.

FERTELLI, A., BÜYÜKALACA, O. and YILMAZ, T., 2006. Performance of an ice storage air-conditioning system. Proceedings of the Fifth GAP Engineering Congress (in Turkish), Turkey 273-280.

GULER R., 2002. Air-Conditioning System with Ice Storage. Operating Under Partial Storage Strategy, MSc. Thesis, University of Çukurova, Adana.

HABEEBULLAH, B.A., 2007a. Economic feasibility of thermal energy storage systems. Energy and Buildings, 39, 355-363.

HABEEBULLAH, B.A., 2007b. An experimental study on ice formation around horizontal long tubes. International Journal of Refrigeration, 30, 5, 789-797.

HASNAIN, S.M., 1998a. Review on sustainable thermal energy storage techologies, part:I Heat storage materials and techniques. Energy Conversion &Management, 39, 11, 1127-1138.

HASNAIN, S.M., 1998b. Review on sustainable thermal energy storage techologies, part:II Cool thermal storage. Energy Conversion &Management, 39, 11, 1139-1153.

HASNAIN, S.M., ALAWAJI, S.H., AL-IBRAHIM A.M., SMIAI M.S., 2000. Prospects of cool thermal storage utilization in Saudi Arabia. Energy Conversion &Management, 41, 1829-1839.

HENZE, P.G., 2003. Impact of real-time pricing rate uncertainity on the annual performance of cool storage systems. Energy and Buildings, 35, 313-325.

HENZE, P.G., KRARTI, M. and BRANDEMUEHL, M.J., 2003. Guidelines for improved performance of ice storage systems. Energy and Buildings, 35, 111-127.

ISMAIL ,K.A.R. and GONCALVES M.M., 1997. Analysis of a latent heat cold storage unit. International Journal of Energy Research, 21, 1223-1239.

ISMAIL, K.A.R. and MELO, C.A., 1998. Convection based model for a PCM vertical storage unit. International Journal of Energy Research, 22, 1249-1265.

JEKEL, T.B, MITCHELL, J.W. and KLEIN, S.A., 1993. Modeling of ice-storage tanks. ASHRAE Transactions, 99, Part 1, 1016-1024.

KAHWAJI G.Y., MOHAMMED S.A., 2006. Modeling and design of an ice-storage module. University of Sharjah Journal of Pure & Applied Sciences, 3, 3, 113-132.

KOUSKSOU, T., BEDECARRATS, J.P., DUMAS, J.P. and MIMET, A., 2005. Dynamic modeling of the storage of an encapsulated ice tank. Applied Thermal Engineering, 25, 1534-1548.

LEE, A. H. W. and JONES, J. W., 1996a. Laboratory performance of an ice on coil thermal energy storage system for residential and light commercial applications. Energy, 21, 2, 115-130.

LEE, A. H. W. and JONES, J. W., 1996b. Modeling of an ice-on-coil thermal energy storage system. Energy Convers. Mgmt, 37, 10, 1493-1507.

LIU D., WENZHU Z. and ZHIHANG C., 1998. Experimental investigation on ice formation around an isothermal three-parallel-fin cylinder horizontally located in a rectangular enclosure. Proceedings of heat and mass transfer conference of China Engineering Thermalphysics Society, 1, 132-139.

MACCRACKEN, C.D., 1990. OPAC-All new for the 1990s, ASHRAE Journal, 32, 4, 44-46.

MCQUAY, 2002. Technical Brochure. Teba.

MILON, J.J., BRAGA, S.L., 2003. Supercooling water in cylindirical capsules. Fifteenth Symposium on Thermophysical Properties, June 22-27, Colorado, USA.

MOUSE, M., 2004. Solidification of phase change material around a vertical cylinder surface in holdup air bubbles. International Journal of Refrigeration, 28, 403-411.

NAVON, R., ARKIN, H., and BURG, I., 1997. Economic evaluation of HVAC systems with ice storage designed using an optimization technique. Construction Management and Economics, 15, 429-439.

NETO, J.H.M. and KRARTI, M., 1997. Deterministic model for an internal melt ice-on-coil thermal storage tank. ASHRAE Transactions, Part 1, 103, 125-138.

POTTER, R.A., GEURTSEN, A., DOUGLASS S., 2006. Thermal energy storage: Aging gracefully in the Ocean State. ASHRAE Transactions, 112, 683-687.

ROSEN, M.A., PEDINELLI, N. and DINCER, I., 1999. Energy and exergy analyses of cold thermal storage systems. International Journal of Energy Research, 23, 1029-1038.

ROSEN, M.A., DINCER, I. and PEDINELLI, N., 2000. Thermodynamic performance of ice thermal energy storage systems. Journal of Energy Resources Technology, 122, 205-211.

SASAGUCHI, K. and VISKANTA, R., 1987. An experimental study of simulteneous melting and solidification around two horizontal vertically spaced cylinders. Experimental Heat Transfer, 1, 223-236.

SASAGUCHI, K., KUSANO, K. and KITAGAWA H., 1994. Solid/liquid phase change heat transfer around two horizomtal, vertically spaced cylinders- an experimental study on the effect of density inversion of water. Heat Transfer-Japanese Research, 23, 7, 645-657.

SASAGUCHI, K., KUSANO, K. and VISKANTA, R., 1997. A numerical analysis of solid liquid phase change heat transfer around a single and two horizontal, vertically spaced cylinders in a rectangular cavity. Int. J. Heat Mass Transfer, 40, 6, 1343-1354.

SERIN, H., 2002. Design of an air-conditioning system with ice storage. MSc. Thesis, University of Çukurova, Adana.

SERIN, H., GÜLER, R., BÜYÜKALACA, O. and YILMAZ, T., 2002. Design of an ice storage air-conditioning system. Proceedings of the Fourth GAP Engineering Congress (in Turkish), Turkey pp. 192-197.

SHIH, Y.C. and CHOU, H., 2005. Numerical study of solidification around staggered cylinders in a fixed space. Numerical Heat Transfer, Part A, 48, 239-260.

SOHN, C.W., 1991. Field performance of an ice harvester storage cooling system. ASHRAE Transactions, 97, 2, 1187-1193.

STOVALL, T.K., 1991. Calmac ice storage test report. ORNL/TM-11582, Oak Ridge National Laboratory.

STOVALL, T.K. and TOMLINSON, J.J., 1994. Laboratory performance of a dynamic ice storage system. ASHRAE Transactions, Symposia, 1179-1186.

THEVENOT, R., 1979. A history of refrigeration throughout the world. International Institute of Refrigeration, France.

TEDAS, 2008. 2008 yılı için elektrik kWh birim fiyatları. (http://www.tedas.gov.tr/253,2008_Yili_Tarifeleri.html)

WENDLAND R.D., 1990. Cool storage status update. ASHRAE Journal, 32, 4, 26-29.

YAMADA, M., FUKUSAKO, S. and KAWANAMI, T., 2002. Performance analysis on the liquid-ice thermal storage system for optimum operation. International Journal of Refrigeration, 25, 267-277.

YILMAZ, T., 1999, Theoretical and Applied Heat transfer, 1st ed., Papatya Book Publishing.

CURRICULUM VITAE

Ahmet FERTELLI was born on September 03, 1975 in Sivas. After completing his education in primary and high school, he enrolled in Çukurova University Mechanical Engineering Department in 1993. He had graduated from the Mechanical Engineer Department of Çukurova University with a Bachelor of Science degree in 1998. He had obtained Master of Science degree from the Mechanical Engineering Department of Cumhuriyet University in 2001. He had commenced the studies leading to the degree of Doctor of Philosophy in 2002 at the Department of Mechanical Engineering, Çukurova University. He has been working as a Research Assistant at the Mechanical Engineering Department of Çukurova University since 2002. He is married and has a son.

APPENDIX

Physical properties of parameters which is used in calculations :

Properties of polyethylene pipe (Serin, 2002) :

Inner diameter	: 12 mm
Outer diameter	: 16 mm
Thickness	: 2 mm
Thermal conductivity	: 0.36 W/mK

Properties of ice for 0 °C (Yılmaz, 1999) :

Density	: 917 kg/m^3
Thermal conductivity	: 0.36 W/mK

Properties of glycol-water mixture (ASHRAE, 2001) :

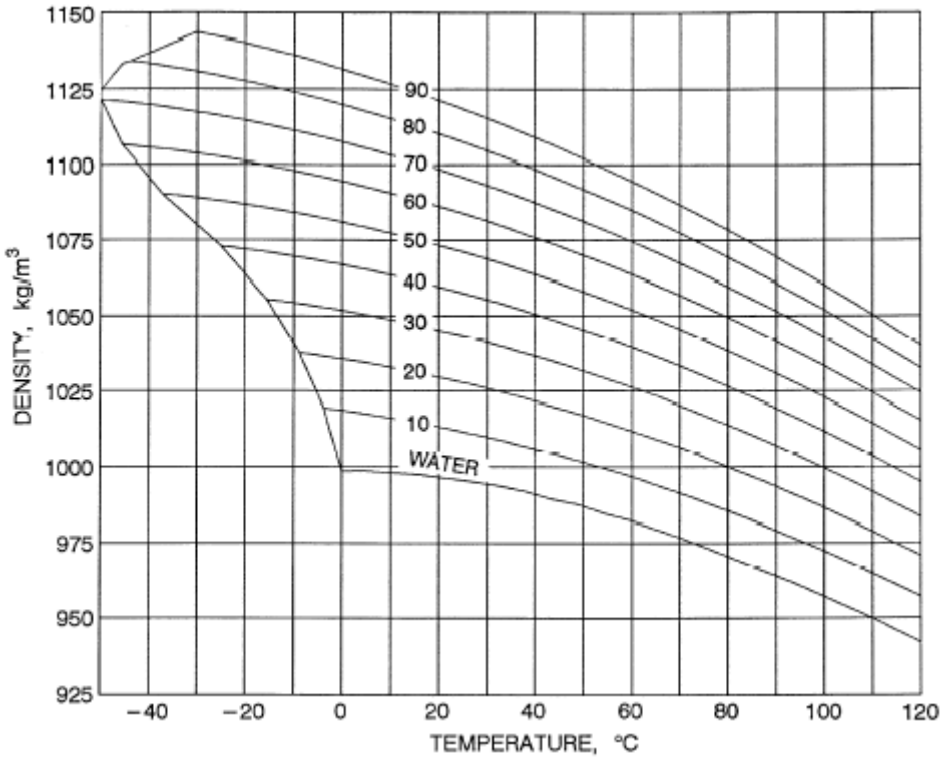


Figure A.1. Density of aqueous solutions of ethylene glycol (vol. %)

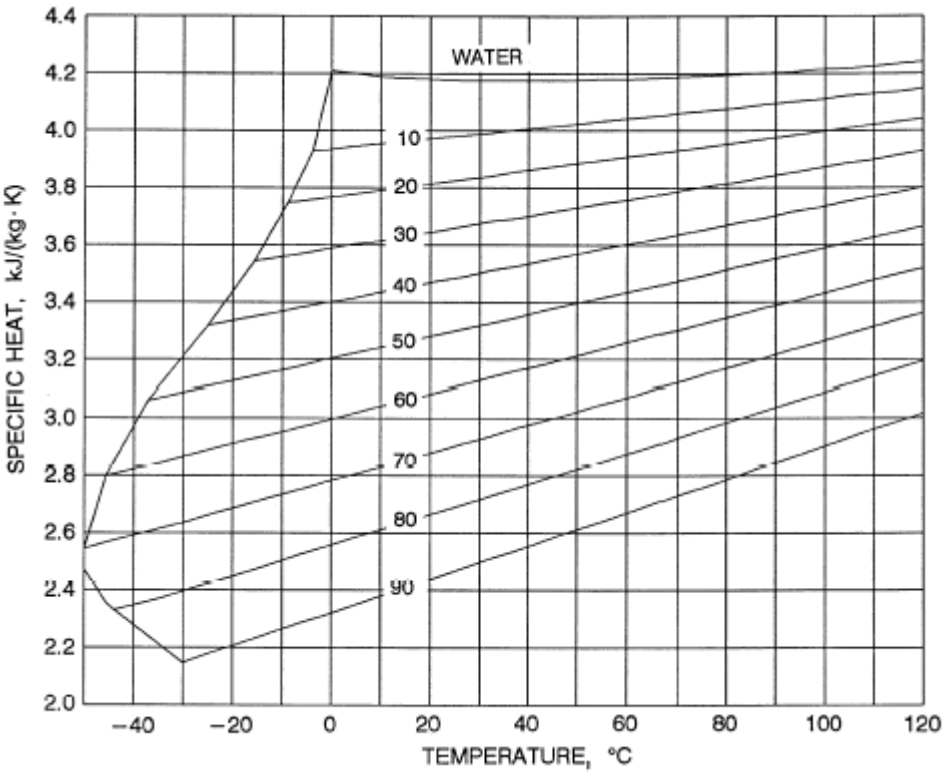


Figure A.2. Specific heat of aqueous solutions of ethylene glycol (vol. %)

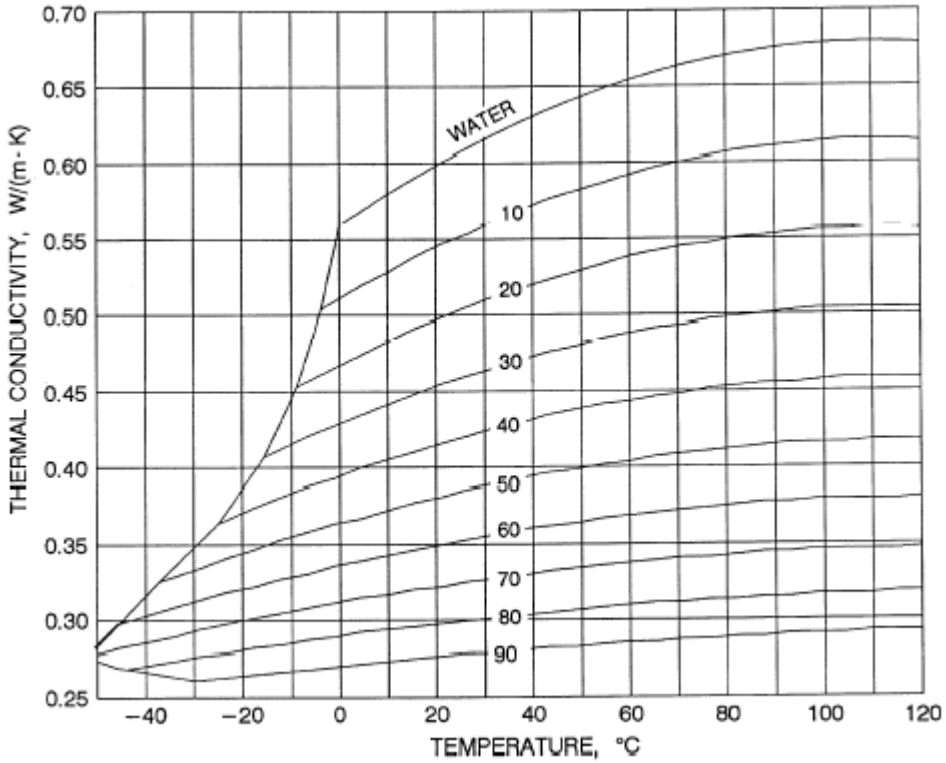


Figure A.3. Thermal conductivity of aqueous solutions of ethylene glycol (vol. %)

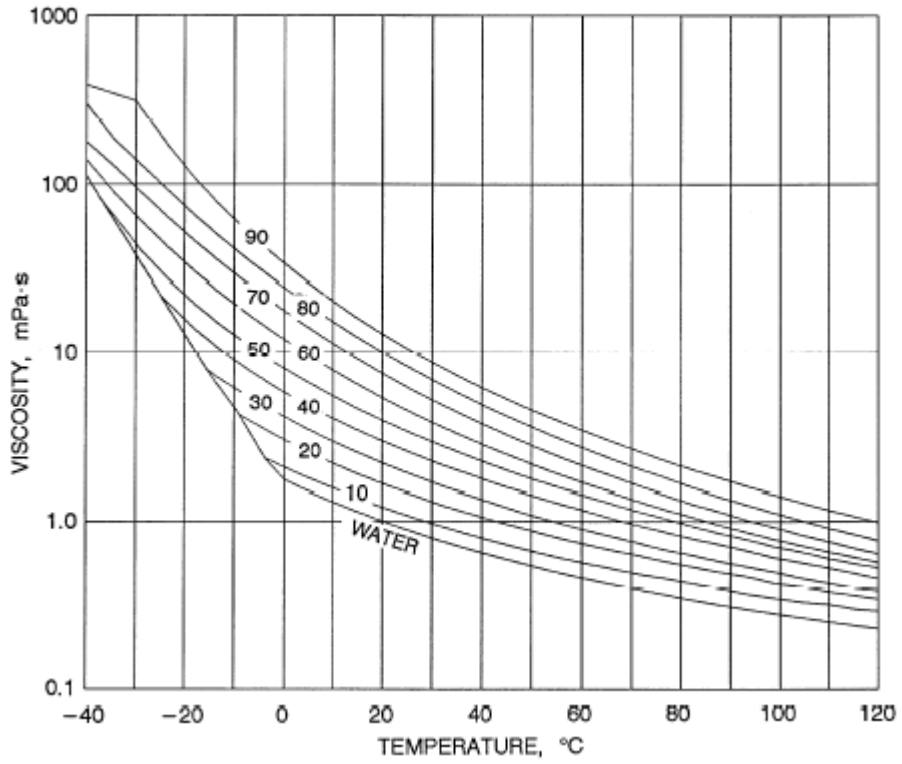


Figure A.4. Viscosity of aqueous solutions of ethylene glycol (vol. %)